Development of Phenylethynyl Anthranilic Acid-Based Dihydroorotate Dehydrogenase Inhibitors as Potential Antiviral Agents

Dissertation

to obtain the Scientific Doctoral Degree

by

Desiree Rijono

(born in Hamburg)

presented to

the Department of Chemistry

of the Faculty of Science

at the University of Hamburg

Hamburg 2025

The presented work was compiled in the group of Prof. Dr. Chris Meier at the Institute of Organic Chemistry in the Department of Chemistry of the University of Hamburg from May 2020 until October 2025.

1st Reviewer: Prof. Dr. Chris Meier

2nd Reviewer: Prof. Dr. Ralph Holl

Date of Disputation: 16.01.2026

„Das Halbverstandene und Halberfahrene ist nicht die Vorstufe der Bildung,

sondern ihr Todfeind.“

Theodor W. Adorno 1903-1969

List of Publications & Conferences

Publications

Alberti, C.; Rijono, D.; Wehrmeister, M.; Cheung, E.; Enthaler, S.; Depolymerization of Poly(1,2-propylene carbonate) via Ring Closing Depolymerization and Methanolysis. *ChemistrySelect* **2022**, *7*, e202104004.

Alberti, C.; Damps, N.; Meißner, R. R. R.; Hofmann, M.; Rijono, D.; Enthaler, S.; Selective Degradation of End-of-Life Poly(lactide) via Alkali-Metal-Halide Catalysis. *Adv. Sustainable Syst.* **2020**, *4*, 1900081.

Patents

Meier, C.; Fohrmann, N. C.; Rijono, D.; DHODH inhibitors and their use as antiviral agents. WO 2023285371 (A1) 2022-07-11

Conferences

09/2021 5th Innovative Approaches for the Identification of Antiviral Agents Summer School, virtual meeting, oral presentation: Optimization of a Phenylethynyl Anthranilic Acid based Dihydroorotate Dehydrogenase Inhibitor Series for the Use as Antiviral Agents.

09/2022 XXVII EFMC International Symposium on Medicinal Chemistry, Nice, France, poster presentation: Phenylethynyl Anthranilic Acid based Dihydroorotate Dehydrogenase Inhibitors for the Use as Antiviral Agents.

09/2023 IX EFMC International Symposium on Advances in Synthetic and Medicinal Chemistry, Zagreb, Croatia, poster presentation: Phenylethynyl Anthranilic Acid based Dihydroorotate Dehydrogenase Inhibitors for the Use as Antiviral Agents.

06/2025 33rd GP_2A Conference & XIVth Paul Ehrlich MedChem Euro-PhD Network Meeting – COST Action OneHealthdrugs, Nantes, France, flash poster presentation: Development of Anthranilic Acid based Dihydroorotate Dehydrogenase Inhibitors for the Use as Antiviral Agents.

06/2025 CRC1648's 1st Pandemic Preparedness Symposium, Hamburg, Germany, poster presentation: Targeting cellular and viral enzymes involved in hemorrhagic fever virus replication using new small molecule broad-spectrum inhibitors.

09/2025 XII. Nucleinsäurechemietreffen, Hamburg, Germany, poster presentation: Combining DHODH Inhibitors and Pronucleotides to Block Viral Replication.

Abstract

Dihydroorotate dehydrogenase (DHODH) is a mitochondrial enzyme involved in *de novo* pyrimidine synthesis, leading to the formation of uridine monophosphate (UMP). Afterwards, UMP is converted to other pyrimidine nucleotides needed for the biosynthesis of RNA and DNA. Large amounts of natural nucleotides are necessary during a viral infection. Blocking DHODH with small synthetic molecules should result in a depletion of pyrimidines in the nucleotide pool. An advantage of inhibiting essential cellular enzymes is the lower risk of resistance development. In combination therapy, DHODH inhibitors have the potential to enhance the effectiveness of viral RNA polymerase-targeting nucleoside analogs by reducing the competition with cellular pyrimidine nucleotides for their incorporation into the viral RNA. Different series of DHODH inhibitors based on anthranilic acids have been developed by the group of C. MEIER, showing antiviral activity against a broad range of RNA viruses, including viruses from the families *Arenaviridae*, *Nairoviridae*, *Flaviviridae* and *Filoviridae*.

This work aims to conduct an optimization campaign with selected compounds from the phenylethynyl anthranilic acid series, especially focusing on enzymatic stability and aqueous solubility. The newly synthesized compounds were investigated for their physicochemical properties and inhibitory potency against human DHODH (hDHODH). Furthermore, antiviral activities were assessed against several hemorrhagic fever viruses and other RNA viruses. Promising candidates for further development as therapeutic agents have emerged from this work. They are not only potent hDHODH inhibitors but also demonstrate nanomolar broad-spectrum antiviral activity *in vitro* and improved pharmacokinetic properties.

Überblick

Dihydroorotat-Dehydrogenase ist ein mitochondriales Enzym, das an der Pyrimidin-*de novo*-Synthese beteiligt ist. Als Produkt wird Uridinmonophosphat erhalten, welches anschließend zu den weiteren Pyrimidinnucleotiden umgewandelt wird. Diese sind essentielle Bausteine für die Biosynthese von RNA und DNA. Während einer Virusinfektion steigt der Bedarf an natürlichen Nucleotiden in der Zelle erheblich. Eine Inhibition der DHODH durch kleine synthetische Moleküle kann zu einer Reduzierung der zellulären Pyrimidinnucleotid-Konzentration führen. Ein wesentlicher Vorteil der Inhibition essentieller zellulärer Enzyme besteht in der geringeren Wahrscheinlichkeit einer Resistenzentwicklung. Im Rahmen einer Kombinationstherapie haben DHODH-Inhibitoren das Potenzial die Wirksamkeit von auf virale RNA-Polymerase abzielenden Nucleosidanaloga zu erhöhen. Dies beruht darauf, dass weniger natürlich vorkommende Pyrimidinnucleotide mit den Nucleosidanaloga um den Einbau in die virale RNA konkurrieren. Die Arbeitsgruppe von C. MEIER hat verschiedene Serien von DHODH-Inhibitoren auf Basis von Anthranilsäuren entwickelt, die eine antivirale Aktivität gegenüber einer Vielzahl an RNA-Viren, darunter Viren der Familien *Arenaviridae*, *Nairoviridae*, *Flaviviridae* und *Filoviridae*, aufweisen.

Ziel dieser Arbeit war es, ausgewählte Verbindungen aus der Phenylethynyl-Anthranilsäure-Serie im Hinblick auf ihre enzymatische Stabilität und wässrige Löslichkeit zu optimieren. Die neu synthetisierten Verbindungen wurden hinsichtlich ihrer physikochemischen Eigenschaften sowie ihrer hemmenden Wirkung gegenüber der humanen DHODH untersucht. Darüber hinaus wurden die antiviralen Aktivitäten gegen verschiedene hämorrhagische Fieberviren und andere RNA-Viren bestimmt. Aus dieser Arbeit gingen vielversprechende Kandidaten für die Weiterentwicklung als therapeutische Wirkstoffe hervor. Sie sind nicht nur potente hDHODH-Inhibitoren, sondern zeigen zudem eine nanomolare, breit wirksame antivirale Aktivität *in vitro* sowie verbesserte pharmakokinetische Eigenschaften.

List of Abbreviations

ADE	antibody dependent enhancement
ADME	absorption, distribution, metabolism, elimination
AHF	Alkhurma hemorrhagic fever
AML	acute myeloid leukemia
ArHF	Argentine hemorrhagic fever
AT	atom transfer
ATCase	aspartate transcarbamylase
ATP	adenosine triphosphate
BCS	Biopharmaceutical Classification System
BHF	Bolivian hemorrhagic fever
BHK cells	baby hamster kidney cells
n-BuLi	n-butyllithium
CAD	carbamoyl phosphate synthase II, aspartate transcarbamylase, dihydroorotase
calc.	calculated
cat.	catalytic
CC_{50}	half maximal cytotoxic concentration
CCHF	Crimean-Congo hemorrhagic fever
CCHFV	Crimean-Congo hemorrhagic fever virus
CHF	Chapare hemorrhagic fever
CHIKV	chikungunya virus
CoQ_1	Coenzyme Q1 (ubiquinone-1)
CoQ_{10}	Coenzyme Q10 (ubiquinone-10)
COVID-19	Coronavirus disease 2019
CPSase2	carbamoyl phosphate synthase II
CTP	cytidine triphosphate
CYP	cytochrome P450

d	doublet (NMR)
dd	doublet of doublets (NMR)
DAAs	direct acting antivirals
DAD	diode array detection
DCPIP	2,6-dichlorophenolindophenol
dCTP	deoxycytidine triphosphate
DENV	Dengue virus
DHO	dihydroorotate
DHOase	dihydroorotase
DHODH	dihydroorotate dehydrogenase
DMF	*N,N*-dimethylformamide
DMSO	dimethyl sulfoxide
DNA	deoxyribonucleic acid
EBOV	Ebola virus (Zaire ebolavirus)
EC	European Commission
EC_{50}	half maximal effective concentration
e.g.	for example
EMA	European Medicines Agency
eq.	equivalents
ER	endoplasmic reticulum
ESCRT	endosomal sorting complex required for transport
ESI	electron spray ionization
ETC	electron transport chain
EU	European Union
EVD	Ebola virus disease
Fa	human absorption value
FDA	U.S. Food and Drug Administration
FLD	fluorescence detector

FMN	flavin mononucleotide
FMNH2	dihydroflavin mononucleotide
GP	glycoprotein
HAZV	Hazara virus
HBV	hepatitis B virus
HCPS	Hantavirus cardiopulmonary syndrome
HCV	hepatitis C virus
HDAs	host-directed antiviral agents
hDHODH	human dihydroorotate dehydrogenase
HF	hemorrhagic fever
HFRS	hemorrhagic fever with renal syndrome
HGPRT	hypoxanthine-guanine phosphoribosyl-transferase
HIV	human immunodeficiency virus
HPLC	high performance liquid chromatography
HPS	Hantavirus Pulmonary Syndrome
IAV	influenza A virus
IC_{50}	half maximal inhibitory concentration
IMM	inner mitochondrial membrane
IMPDH	inosine monophosphate dehydrogenase
J	coupling (NMR)
kin. sol.	kinetic solubility
L	L protein (RNA-dependent RNA polymerase)
LASV	Lassa virus
LF	Lassa Fever
LHF	Lujo hemorrhagic fever
m	multiplet (NMR)
mRNA	messenger RNA
MS	mass spectrometry

MVD	Marburg virus disease
MW	molecular weight
m/z	mass/charge ratio
NADPH	nicotinamide adenine dinucleotide phosphate (reduced form)
n.d.	not detected
NIS	*N*-iodosuccinimide
NMR	nuclear magnetic resonance
NP	nucleoprotein
NPC1	receptor Niemann-Pick C1
ODCase	orotidine-5'-phosphate decarboxylase
OHF	Omsk hemorrhagic fever
OMP	orotidine monophosphate
OPRTase	orotate phosphoribosyltransferase
ORO	orotate
PAMPA	parallel artificial membrane permeability assay
PB	phosphate buffer
PBS	phosphate buffered saline
PDB	Protein Data Bank
P_e	effective permeability
PEG	polyethylenglycol
PHAC	Public Health Agency of Canada
PK	pharmacokinetic
PMS	progressive multiple sclerosis
PRPP	5-phosphoribosyl-1-pyrophosphate
PVDF	polyvinylidene fluoride
q	quartet
quant.	quantitative
RdRp	RNA-dependent RNA polymerase

R_f	retention time
Rib-1-P	ribose-1-phosphate
RMS	relapsing multiple sclerosis
RNA	ribonucleic acid
RNP	ribonucleoprotein
RRMS	relapsing-remitting multiple sclerosis
rt	room temperature
RVF	Rift valley fever
rVSV	recombinant vesicular stomatis virus
s	singlet
SAR	structure-activity relationship
SARS-CoV-2	Severe acute respiratory syndrome coronavirus 2
sept	septet
SET	single electron transfer
sext	sextet
SHF	Sabia hemorrhagic fever
SNV	Sin Nombre virus
STAB	sodium triacetoxyborohydride
t	triplet (NMR)
TBAF	tetrabutylammonium fluoride
TFA	trifluoroacetic acid
THF	tetrahydrofuran
TLC	thin layer chromatography
TMS	trimethylsilyl
TOSV	Toscana virus
TTP	thymidine triphosphate
UCK2	uridine-cytidine kinase 2
UDP	uridine diphosphate

UMP	uridine monophosphate
UMPS	uridine monophosphate synthase
UPase	uridine phosphorylase
UPRTase	uracil phosphoribosyltransferase
U.S.	United States
UTP	uridine triphosphate
UV/Vis	ultraviolet/visible
VeHF	Venezuelan hemorrhagic fever
VHF	viral hemorrhagic fever
VP24	secondary matrix protein
VP30	transcriptional activator
VP35	RNA-dependent RNA polymerase factor
VP40	matrix protein
v/v	volume per volume
YFV	Yellow fever virus
w/v	weight per volume
WHO	World Health Organization

Table of Contents

1. Introduction

In recent decades, there have been recurring outbreaks of newly emerging or re-emerging viral diseases, some of which have reached epidemic or even pandemic proportions. Notable examples of severe outbreaks with high mortality rates include SARS (Severe Acute Respiratory Syndrome) in 2002[1], swine flu in 2009[2], MERS (Middle East Respiratory Syndrome) in 2012[1], Ebola virus disease in 2014[2], and COVID-19 (Coronavirus disease 2019) in 2020.[3] Although significant progress has been made in antiviral research, existing therapies for viral infections are often insufficient.[4,5] Therefore, the discovery of new active compounds and the development of effective treatment strategies remain key priorities in current pharmaceutical research.

The World Health Organization (WHO) has published a list of diseases and pathogens that are given high priority for research and development in public health.[6] These are considered to pose the greatest threat because of their potential to cause epidemics and the current lack or insufficiency of effective preventive or therapeutic measures. Out of the eleven diseases listed, seven are capable of causing a clinical syndrome known as viral hemorrhagic fever (VHF). This syndrome is marked by symptoms such as fever, increased vascular permeability, reduced plasma volume, abnormalities in blood coagulation, and varying levels of hemorrhage.[7,8] Viruses that cause this type of clinical syndrome are referred to as hemorrhagic fever (HF) viruses. Due to growing globalization and climate-induced migration of vectors, the risk of HF viruses, originally found in Africa, Asia, or South America, spreading to Europe is increasing.[9,10]

The previous approach to combating viral infections focused on the development of virus-specific therapeutics.[1,2] These therapeutics have the advantage of achieving low toxicity by selectively inhibiting unique viral enzymes. However, the development of agents targeting individual viruses is time-consuming and costly, which poses a major problem especially in the case of newly emerging viruses. In addition, the inhibition of viral enzymes can rapidly lead to the development of drug resistance, a consequence of the high mutation rates in many viruses.[11,12] Since viral replication depends not only on viral enzymes but also on host cell factors, targeting cellular enzymes has emerged as an attractive alternative strategy for inhibiting virus replication. Many viruses exploit the same host cell factors, indicating that drugs targeting these cellular components could potentially act as broad-spectrum antivirals. A disadvantage of this approach is the interference with the host cell's metabolism, which may result in undesirable toxicity.[13] It is therefore crucial to identify and inhibit those cellular enzymes that are essential for viral replication, but not for cell growth. In this context, the enzyme dihydroorotate dehydrogenase has recently proven to be a particularly promising cellular target.[14,15]

In the group of C. MEIER, different series of hDHODH inhibitors based on anthranilic acids have been developed that demonstrate antiviral activity against a wide spectrum of RNA viruses, including HF viruses. This work aimed to optimize two lead structures from the phenylethynyl anthranilic acid series, focusing particularly on enhancing enzymatic stability and aqueous solubility, while maintaining antiviral activity.

2. Background

2.1. Viral hemorrhagic fever

The term viral hemorrhagic fever describes a group of febrile illnesses with symptoms, including a fall in blood pressure and coagulation abnormalities, which, in severe cases, can lead to shock and uncontrolled bleeding.[16] Endemic outbreaks of VHFs occur worldwide (Figure 1) and are often associated with high morbidity and mortality rates, with improved outcomes for patients when supportive therapy is started early. Treatment of VHF mainly consists of basic medical care, as only a few VHF drugs with limited clinical data on efficacy are available.[17]

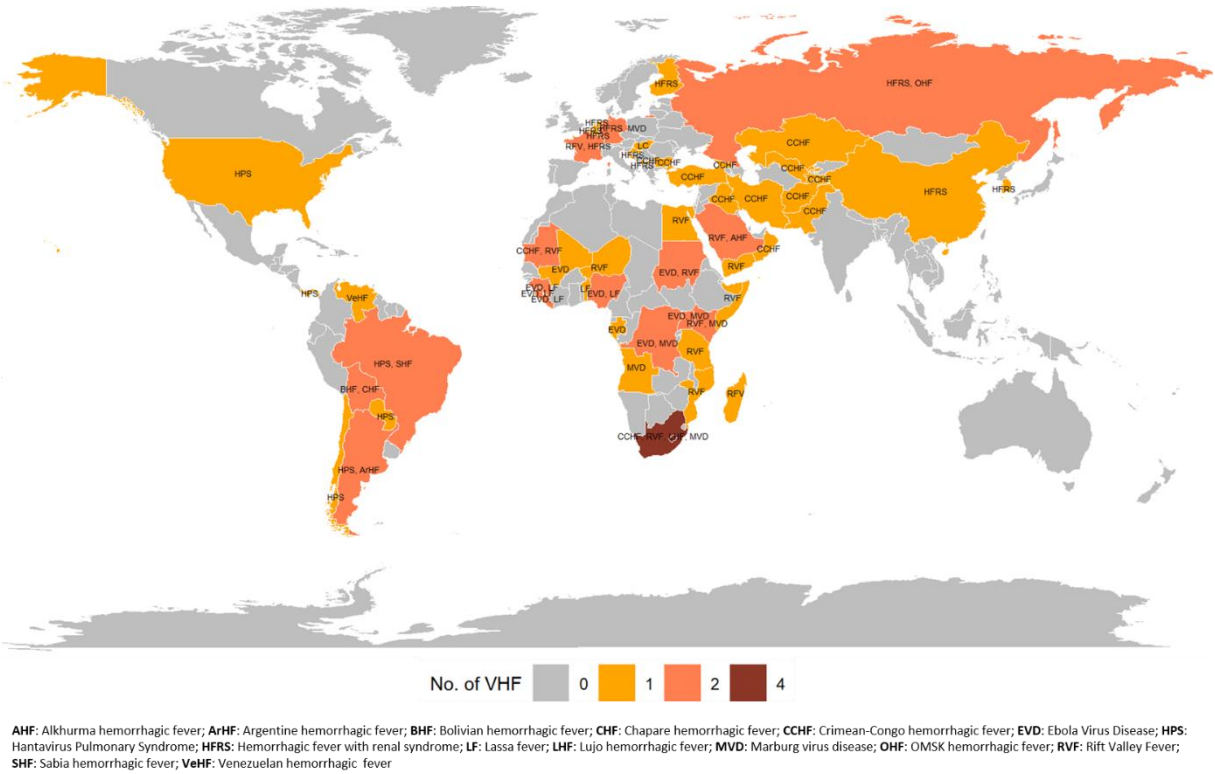

AHF: Alkhurma hemorrhagic fever; **ArHF**: Argentine hemorrhagic fever; **BHF**: Bolivian hemorrhagic fever; **CHF**: Chapare hemorrhagic fever; **CCHF**: Crimean-Congo hemorrhagic fever; **EVD**: Ebola Virus Disease; **HPS**: Hantavirus Pulmonary Syndrome; **HFRS**: Hemorrhagic fever with renal syndrome; **LF**: Lassa fever; **LHF**: Lujo hemorrhagic fever; **MVD**: Marburg virus disease; **OHF**: OMSK hemorrhagic fever; **RVF**: Rift Valley Fever; **SHF**: Sabia hemorrhagic fever; **VeHF**: Venezuelan hemorrhagic fever

Figure 1: Outbreaks of VHF. Number of outbreaks is defined by color with at least one outbreak reported by country and name of disease is described by acronyms.[17]

VHFs are caused by highly infectious RNA viruses from seven taxonomic families: *Arenaviridae, Hantaviridae, Nairoviridae, Phenuiviridae, Filoviridae, Paramyxoviridae, and Flaviviridae*.[18] However, it should be noted that not all viruses within these families are hemorrhagic fever viruses. An overview of common VHF-causing viruses, their families, geographic distribution, and reservoir hosts is shown in the table at the end of this section (see page 5).[19] Known examples of HF viruses responsible for major outbreaks with high mortality rates in-

clude Sin Nombre virus (SNV), Ebola (EBOV), Dengue (DENV), and Yellow fever virus (YFV).[17] The Ebola outbreak from 2014 to 2016 in West Afrika represents one of the most severe global health threats in recent history, with more than 28000 infections and 11000 deaths.[7] Another severe outbreak of an HF virus occurred in 2024 in Brazil and other Latin American countries. From January to June 2024, Brazil reported approximately six million cases of DENV infections and 4000 deaths, representing the greatest dengue epidemic to date.[20]

HF viruses are mainly zoonotic and infect arthropods and/or rodents, whereas human infection is considered an accidental event resulting from contact with the infected animal or its excrements. After infection, multiple HF viruses are transmitted from human to human through contact with infected body fluids (e.g. blood, excreta, saliva).[18,19] Especially in developing countries, where adequate hygienic standards cannot be maintained, the risk of human-to-human transmission and disease resurgence is extremely high. The geographical distribution of each disease reflects that of its reservoir species, and outbreaks occur in geographically confined areas.[21] However, climate change and increased globalization favor the spread of vectors to other regions and the evolution of new pathogens.[22] This phenomenon has already been observed for YFV in Brazil, where the Asian tiger mosquito emerged as a new species due to economic changes. Viral adaptation to the Asian tiger mosquito, which led to increased vectorial capacity, resulted in outbreaks in cities where control measures had been effectively maintained for nearly 70 years.[19,23]

Another risk is the spread of tick species into new geographic areas. Crimean-Congo hemorrhagic fever (CCHF) is the most widespread tick-borne viral disease and was previously confined to parts of Africa, Asia as well as eastern and southern Europe. However, it has expanded rapidly into the eastern Mediterranean region in recent years.[19,24] Regarding rodents, infection rates are correlated to the rodent population densities, which are affected by food availability and climatic conditions. For example, heavy rainfall related to El Niño led to increased food resources for rodents and a 20-fold rise in rodent populations in the southwestern United States in 1992/1993, thereby increasing the risk of an SNV infection. This led to an outbreak of Hantavirus cardiopulmonary syndrome (HCPS) in 1993/1994.[19,25]

These incidents show how external factors, including higher temperatures, changing precipitation patterns, and human behavior, can have an impact on the epidemiology of vector- and rodent-borne VHFs. The climate change-driven spread of these diseases warrants further investigation, and the findings should be incorporated into future climate adaptation measures.[26]

Table: Common hemorrhagic fever viruses.

Virus Family	Virus Genus	Virus Species	Disease	Geographic Distribution	Reservoir Host
Arenaviridae	Mammarenavirus (New world)	Junin virus	Argentinian HF	Argentina	Mouse (*Calomys masculinus)*
		Chapare virus	Chapare HF	Bolivia	Unknown rodent
	Mammarenavirus (Old world)	Lassa virus	Lassa fever	West Africa	Mouse (*Mastomys natalensis*)
		Lujo virus	Lujo HF	Zambia, South Africa	Unknown rodent
Hantaviridae	Orthohantavirus	Sin Nombre orthohantavirus	Hantavirus cardiopulmonary syndrome (HCPS)	The Americas	Mouse (*Peromyscus maniculatus*)
		Puumala orthohantavirus	Hemorrhagic fever with renal syndrome (HFRS)	Eastern Asia, Balkans, Europe	Mouse (*Clethrionomys glareolus*)
		Hantaan orthohantavirus	Hemorrhagic fever with renal syndrome (HFRS)	Eastern Asia, Balkans, Europe	Mouse (*Apodemus agrarius chejuensis*)
Nairovirdae	Orthonairovirus	Crimean-Congo HF orthonairovirus	Crimean Congo HF	Africa, Balkans, Middle East, Asia	Tick (*Hyalomma*) and livestock animals
Phenuiviridae	Phlebovirus	Rift Valley fever phlebovirus	Rift valley fever (RVF)	Sub-Saharan Africa, Arabian Peninsula	Livestock animals and several mosquitos (*Aedes* and *Culex)*
Filoviridae	Orthoebolavirus	Zaire ebolavirus	Ebola virus disease (EVD)	Central and West Africa	Most likely fruit bats
	Orthomarburgvirus	Marburg marburgvirus	Marburg virus disease (MVD)	Central and South Africa	Most likely fruit bats (*Rousettus aegyptiacus*)
Paramyxoviridae	Henipavirus	Nipah virus	Nipah virus disease	South and Southeast Asia	Pig, bat (*Pteropus*)
Flaviviridae	Orthoflavivirus	Yellow fever virus	Yellow fever	Tropical Africa, South America	Primates and mosquitos (*Aedes*, *Haemagogus)*
		Dengue virus	Dengue fever	worldwide	Mosquitos (*Aedes)*

2.1.1. Ebola virus replication cycle

VHF is caused by infection with any of at least 30 viruses from seven different taxonomic families, all of which share the characteristic of possessing an enveloped single-stranded RNA genome. Flaviviruses have a monopartite RNA genome in positive polarity, whereas viruses of the other six families have monopartite or segmented RNA genomes in negative polarity.[16,18] Among all HF viruses, Zaire ebolavirus (formerly known as Ebola virus; EBOV[27]), is one of the most widely studied and will be described in detail below (Figure 2).[7]

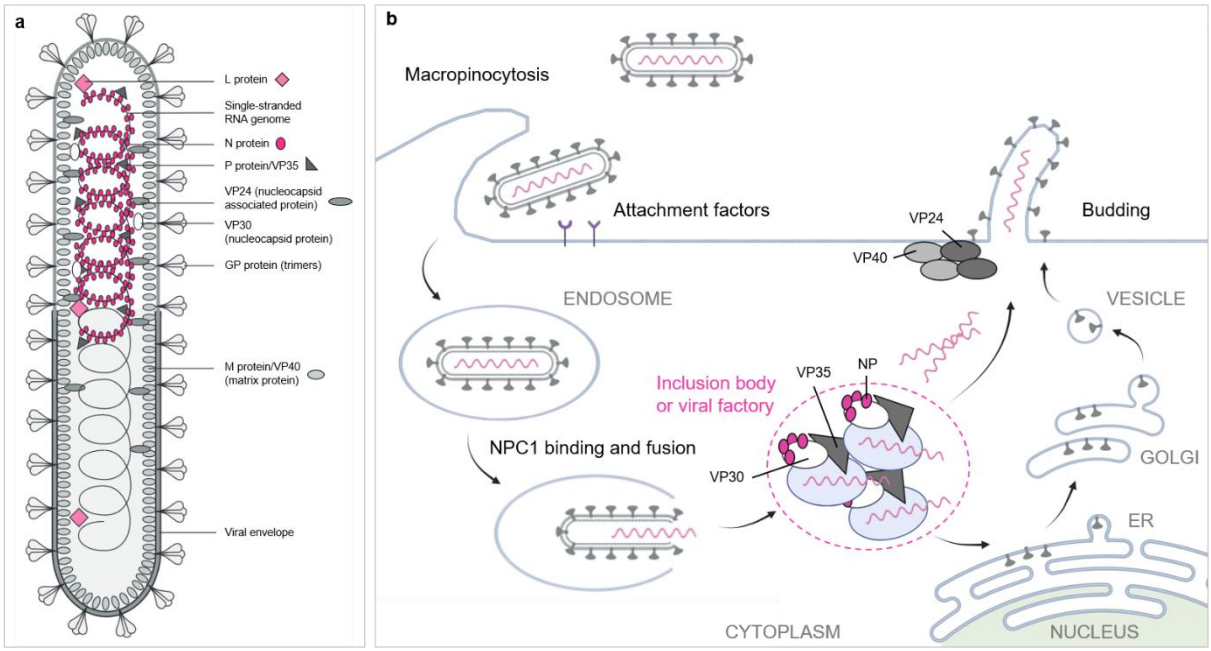

Figure 2: (a) Virion structure of EBOV.[28] (b) EBOV replication cycle.[29]

Zaire ebolavirus is one of six species belonging to the genus orthoebolavirus within the family *Filoviridae*. Like Zaire ebolavirus, the other five species are also named after the region where they were first identified: Bombali, Bundibugyo, Reston, Sudan, and Tai Forest ebolavirus.[29] The illness caused by these viruses is called Ebola virus disease (EVD).[7] They have a filamentous shape and a linear, non-segmented, single-stranded negative-sense RNA genome of approximately 19 kb nucleotides. The genome consists of seven genes encoding structural proteins, including nucleoprotein (NP), RNA-dependent RNA polymerase factor (VP35), matrix protein (VP40), glycoprotein (GP), transcriptional activator (VP30), secondary matrix protein (VP24), and the RNA-dependent RNA polymerase (L).[30,31] The NP-encapsidated genome, along with VP30, VP35, and L, form nucleocapsid structures, called ribonucleoprotein (RNP) complexes, which are the active transcription and replication complexes. The viral RNA itself is not infectious and cannot be used directly as a template for

protein synthesis.[32] The matrix proteins VP40 and VP24 are associated with nucleocapsid proteins and the inner surface of the viral envelope. Additionally, VP40 plays a crucial role in viral aggregation at the cell membrane during virion budding.[33] In EBOV, the GP gene encodes different forms of the glycoprotein: virion-associated $GP_{1,2}$, and two soluble glycoproteins, sGP and ssGP. Unlike in some other enveloped viruses, where attachment and fusion are mediated by separate proteins, in EBOV these functions are both performed by the sole surface protein $GP_{1,2}$. Specifically, the glycoprotein subunit GP_1 interacts with cellular receptors for attachment, while glycoprotein subunit GP_2 contains a fusion loop responsible for membrane fusion.[34]

The EBOV replication cycle begins with the entry of the virus particle into the host cell via macropinocytosis after $GP_{1,2}$-mediated binding to host attachment factors. The virion is taken up into an endosome, where $GP_{1,2}$ binds to the endosomal receptor Niemann-Pick C1 (NPC1) to initiate fusion of the viral and endosomal membranes. This step requires acidification of the endosome to induce the cleavage of $GP_{1,2}$ by host cathepsins and its conversion into the fusion-active form GP_{CL}. Fusion results in the release of the genome and nucleocapsid components into the cytoplasm, which then accumulate to form sites for viral replication and transcription, often referred to as inclusion bodies or viral factories. Viral mRNAs are produced through primary transcription initiated by incoming RNP complexes, which then undergo translation into proteins by host ribosomes. During primary transcription generated RNP components further support secondary transcription of viral mRNAs and replication of the genome via an intermediate, a full-length positive-sense antigenome. Newly synthesized viral RNA strands are encapsidated by RNP components and transported to budding sites at the cell membrane.[29,33] VP24, $GP_{1,2}$, and VP40 perform different roles throughout this process. VP24 likely mediates the condensation of the RNP complexes into a packaging-competent form before transport to the cell surface. $GP_{1,2}$ is synthesized in the endoplasmic reticulum (ER) as a precursor and processed along the pathway from the ER via Golgi apparatus to the cell membrane, where it interacts with VP40 to facilitate virus budding. This final step requires the support of various host factors, such as those of the endosomal sorting complex required for transport (ESCRT), and is coordinated by VP40.[29,34]

2.1.2. Medical prevention of VHFs

Clinical differentiation of VHFs from other infectious diseases is difficult due to nonspecific symptoms, and diagnosis is only possible by identifying the causative agent directly through specialized laboratory tests. After infection, early diagnosis is important not only for a better outcome for the individual patient but also for preventing an outbreak by applying appropriate clinical treatment methods and correct disease control measures, respectively.[16] Such diag-

nostic methods require medically trained personnel and have previously been restricted to large containment reference facilities, which are established in Europe and the United States but are limited in endemic areas.[19] Mobile laboratories have been employed in regions without a strong public health system as a response during outbreaks. In the last decade, features of mobile laboratories have evolved, and today self-reliant vehicles equipped with the latest innovative diagnostic devices and biocontainment systems are used. For example, the EVD outbreak in 2014 in West Africa has led to significant progress, and methods including on-site real-time sequencing, real-time serology, and ecological sampling were established. However, sufficient capacity is often not available at the beginning of an outbreak, and many challenges are associated with the setup and operation of a mobile laboratory.[35,36]

Regarding prevention through active immunization, only a few VHF vaccines are in regular use in humans.[16,19] Among the safest and most efficacious vaccines ever developed is the live attenuated YF vaccine 17D, first introduced in the 1930s and now sold under the brand names YF-VAX® and Stamaril®. Usually, only mild side effects are observed following vaccination, and one dose is considered sufficient to provide lifelong protection. Despite the availability of a vaccine, coverage remains insufficient in many countries in South America and Africa to achieve herd immunity and prevent outbreaks. Vaccination campaigns are often hindered by limited in-country vaccine supplies, challenges in timely requests to access emergency stockpiles, and problems with vaccine delivery.[37–39]

Approved vaccines for another orthoflavivirus are Dengvaxia® and Qdenga®, two live attenuated tetravalent vaccines targeting four strains of DENV.[40] Dengvaxia® was first introduced in 2015 and approved in the EU in 2018.[41,42] Generally, people who experience a secondary dengue infection are at higher risk of severe disease, most likely due to a phenomenon called antibody-dependent enhancement (ADE), in which cross-reacting antibodies form immune complexes instead of neutralizing the virus. The application of Dengvaxia® may also increase the risk of severe disease in individuals without a previous dengue infection and is limited to those residing in endemic regions with a history of dengue fever.[40,43] Qdenga® was approved by the European Commission (EC) in 2022 and has been commercially available in Germany since 2023. It may also be used in people who have not been previously infected.[42,44] The only successfully applied mammarenavirus vaccine is the live attenuated vaccine Candid #1, which is licensed only in Argentina for the prevention of Junin virus infections.[16,19,45] There are other vaccines licensed in only one country but not approved by the FDA or EC, including inactivated vaccines against CCHF orthonairovirus (CCHFV) and hantavirus infections, used in Bulgaria and South Korea, respectively.[19,46,47]

A major milestone for public health was the development of a safe and effective Ebola vaccine, rVSV-ZEBOV (sold under the brand name ERVEBO®), a replication-competent, re-

combinant vesicular stomatis virus (rVSV)-vectored vaccine for protection against the species Zaire ebolavirus. This vaccine was originally developed at least a decade before the severe EBOV outbreak in 2014 by the National Microbiology Lab at the Public Health Agency of Canada (PHAC) in collaboration with the US Army for biodefence purposes.[48] ERVEBO® was approved by the EC and FDA at the end of 2019, and since then, several countries in Africa have also licensed the vaccine.[49] In addition, the EMA granted marketing authorization in 2020 for two separate vaccines, Zabdeno® and Mvabea®, each following a two-dose regimen.[50,51] Zabdeno® is a replication-competent, recombinant human adenovirus type 26-vectored vaccine that is administered first, and Mvabea® is a recombinant, in human cells non-replicating vaccine based on a modified Vaccinia Ankara - Bavarian Nordic (MVA-BN) filovirus, given approximately eight weeks later as a second dose.[52] Compared to ERVEBO®, the Zabdeno®/Mvabea® vaccine regimen is not suitable for immediate outbreak response, as two doses must be given at specific time intervals, and is intended for prophylactic purposes in individuals at imminent risk of Ebola exposure, such as health care workers in outbreak areas.[53]

2.1.3. Treatment of VHFs

There is currently no adequate supply of available VHF vaccines to prevent outbreaks in most high-risk areas, and research on antiviral drugs is therefore of fundamental importance to respond effectively to future outbreaks.[54] At present, no specific treatment methods exist for VHFs, except for EVD caused by the species Zaire ebolavirus.[18] The FDA approved two antibody therapeutics for the treatment of Zaire ebolavirus infections in late 2020. Inmazeb® is a mixture of three monoclonal antibodies, and Ebanga® is a single monoclonal antibody, both targeting the glycoprotein on the surface of the EBOV particle and preventing the virus from entering the cell. Both therapeutics were evaluated in a randomized clinical control trial conducted during the 2018 EBOV outbreak in the Democratic Republic of the Congo.[18,19,55] For other infections, including Junin, Lassa, and Hantavirus infections, convalescent plasma therapy has proven effective in improving disease progression and reducing case fatality rates. This therapy involves the use of blood plasma containing neutralizing antibodies from an individual who has recovered from the infection to provide passive immunization for a currently infected patient.[16,19]

Regarding small-molecule antiviral agents, nucleoside analogs have been tested and found to be effective against some HF viruses.[56] Along with supportive medical care, most VHF patients are treated with the guanosine/adenosine analog ribavirin **1** (Figure 3).[17,18] The drug was discovered in the 1970s and was first approved by the FDA in 1986 for the use against respiratory syncytial virus (RSV) infections. Later, ribavirin **1** was also approved in combina-

tion with other agents for the treatment of hepatitis C virus (HCV) infection.[57] Since then, ribavirin **1** has been shown to have *in vitro* activity against a variety of RNA viruses and proven useful for the treatment of various viral infections in off-label therapy.[58] In the case of Lassa fever, the option of convalescent plasma therapy was largely abandoned and replaced by treatment with ribavirin **1**, as decreased mortality has been observed when the drug was administered before day 7 of illness.[16,59] Ribavirin **1** might also be beneficial for the treatment of other members of the arena- and hantavirus families, but it is not active against several filo- and flaviviruses.[60]

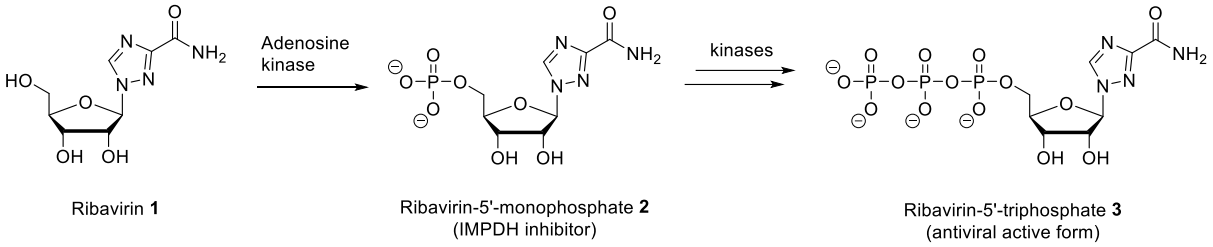

Figure 3: Activation mechanism of nucleoside analog ribavirin **1**.[61]

The antiviral activity of ribavirin **1** likely comprises multiple mechanisms of action, either virus- or host-targeted, each requiring the compound to be activated in the cell through phosphorylation by different kinases. One virus-targeted effect is the inhibition of the viral polymerase via incorporation of its 5'-triphosphate form **3**, while one host-targeted effect is the inhibition of the cell's inosine monophosphate dehydrogenase (IMPDH) by its 5'-monophosphate form **2**. IMPDH inhibition leads to a depletion of intracellular guanine nucleotide pools, which are crucial for DNA and RNA synthesis.[61,62] Additionally, ribavirin **1** can induce lethal mutagenesis, an antiviral strategy that artificially increases the mutation rate in the viral genome to the point where the viral population dies out, by incorporating nucleoside analogs with ambiguous base pairing capacity. Once incorporated into the viral RNA, base pairing can occur equally with uridine and cytosine nucleotides, leading to accumulation of viral genetic material with unfavorable mutations, e.g. genetic information necessary for survival is no longer present.[61,63] Beyond its broad-spectrum antiviral activity, ribavirin **1** is poorly selective, resulting in undesirable toxicities and side effects, such as severe anemia. Therefore, alternative drugs for the treatment of VHFs need to be investigated.[61]

Another small molecule inhibitor that exhibits *in vitro* and *in vivo* antiviral activity against a broad spectrum of HF viruses is the pyrazinamide derivative favipiravir **4** (Figure 4).[58] It was initially discovered as a selective and potent inhibitor of the RNA-dependent RNA polymer-

ase (RdRp) of influenza virus and was approved in Japan in 2014 for the treatment of novel or re-emerging influenza strains unresponsive to current medicines.[64]

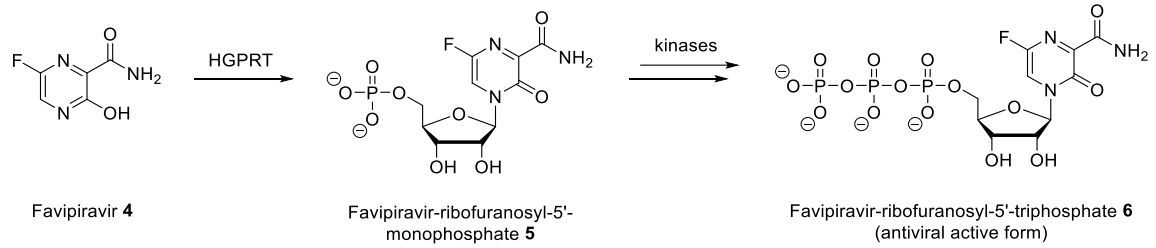

Figure 4: Activation mechanism of pyrazinamide derivative favipiravir **4**.[61]

Inside the cell, favipravir **4** resembles the nucleobases adenine or guanine and is directly converted to the appropriate nucleoside monophosphate **5** by hypoxanthine-guanine phosphoribosyl-transferase (HGPRT), an important enzyme of the purine nucleotide salvage pathway. This mechanism bypasses the first phosphorylation that is often the rate limiting step in the activation of nucleoside analogs. After phosphorylation to its 5'-triphosphate form **6**, the nucleotide is incorporated into the viral RNA by the viral RdRp, leading to chain termination and/or lethal mutagenesis.[61,65] Favipiravir **4** does not appear to cause acute toxicities comparable to ribavirin **1** and is generally well tolerated in humans. However, the drug is contraindicated for application in pregnant women, as teratogenic and embryotoxic effects have been observed in animal studies.[65] During the large Ebola outbreak in West Africa in 2014, the WHO recommended favipiravir **4** as a suitable drug for EVD research, and a multicenter, non-randomzied trial was conducted in Guinea, in which all patients received favipiravir **4** alongside standard medical care. Unfortunately, the strong antiviral effect observed *in vivo* did not translate into clinical success in humans, and additional clinical trials for other HF viruses have not been reported.[61,66] The reduced efficacy is likely due to the compound's rapid renal elimination, as it is easily hydroxylated by aldehyde oxidase, resulting in a short half-life of 2.5 to 5 h. A high percentage of molecules entering the body is eliminated before they can be intracellularly converted to their bioactive form. Therefore, strategies to increase the half-life and potency in humans of favipiravir **4** need to be developed.[61]

Remdesivir **7** is also a well-known broad-spectrum antiviral that was approved by the FDA in 2020 for the treatment of COVID-19 patients (Figure 5).[67,61] The compound was developed by the US pharmaceutical company Gilead Science as a candidate for the treatment of viral hepatitis and RSV infections and was later selected for investigation in a chemical library screening for antiviral activity against RNA viruses with pandemic potential, including coronaviruses and filoviruses.[68] The screening was conducted in collaboration with the U.S.

Centers for Disease Control and Prevention and the U.S. Army Medical Research Institute of Infectious Diseases in 2016 and was prompted by the large Ebola outbreak that occurred in West Africa. Subsequently, research focused on the development of remdesivir **7** as a drug for EBOV infections, as a potent *in vitro* activity had been identified during screening.[69,70] The expectation that remdesivir **7** would have antiviral effects against EBOV was supported by *in vivo* studies completed in rhesus monkeys, in which the animals were experimentally infected via parenteral administration of EBOV and then treated with the drug. The infection resulted in death after a clinical course similar to that observed in humans, however, a 12-day treatment with remdesivir **7** demonstrated significant suppression of EBOV, with survival rates ranging from 33% to 100%, depending on the dose administered.[68,69]

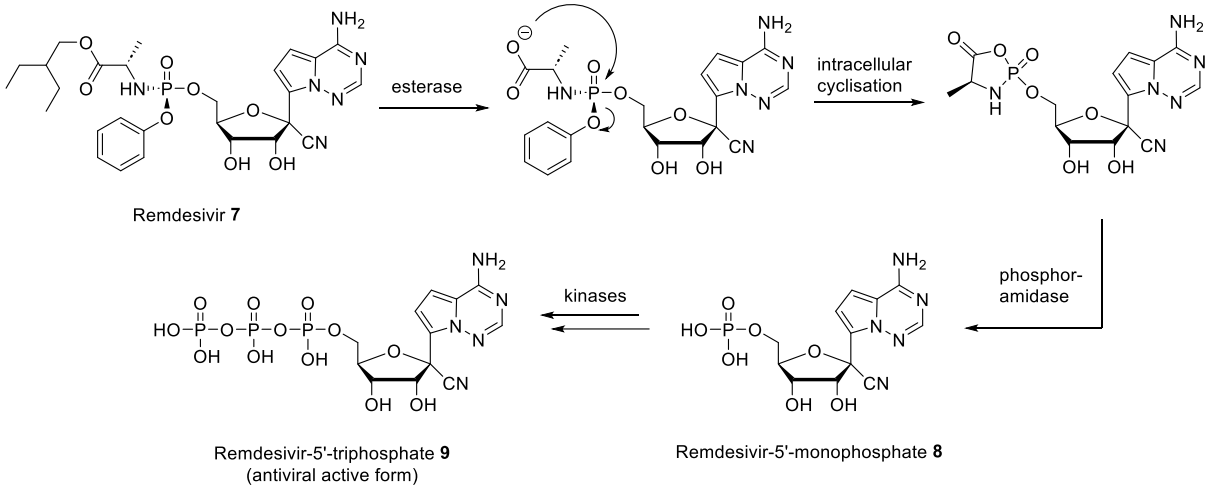

Figure 5: Activation mechanism of ProTide remdesivir **7**. [61]

Remdesivir **7** is a nucleotide prodrug with a phosphoramidate modification that enables passive diffusion into the cell and delivery of the nucleoside monophosphate **8** after enzymatic cleavage of the masking units. The first phosphorylation step is bypassed, and only two further conversions by host kinases are required to produce the active 5'-triphosphate form **9**.[61,71] Remdesivir triphosphate **9** competes with natural adenosine triphosphate (ATP) present in the cell for incorporation into viral RNA and induces delayed chain termination at position i + 5 for EBOV or i + 3 for SARS-CoV-2.[69] The affinity of remdesivir **7** for human RNA polymerase II and human mitochondrial RNA polymerase is low, which contributes to a favorable safety profile. In phase I clinical trials, the compound was found to be well tolerated and did not cause dose-limiting toxicities.[68] The efficacy of remdesivir **7** was evaluated in a phase II/III randomized control trial during an EVD outbreak in the Democratic Republic of Congo in 2018, but no significant benefit was observed compared to the two antibody thera-

peutics discussed earlier, Inmazeb® (REGN-EB3) and Ebanga® (mAb114).[72,73] Further clinical development of remdesivir **7** was not pursued until the outbreak of COVID-19.[74]

2.1.4. Identification of new hit compounds inhibiting HF viruses

The worldwide spread of HF viruses and the limited efficacy of currently available VHF drugs highlight the growing need to identify new druggable targets and antiviral compounds. G. QUERAT and co-workers conducted a high throughput screening of a chemical library against Toscana virus (TOSV), a representative of the *Phenuiviridae* family, to address this need. Three hit compounds (**10**-**12**) containing an anthranilic acid motif were identified, exhibiting activity in the micromolar to nanomolar range (Figure 6). These hits were used by the group of C. MEIER to initiate a structure-activity relationship (SAR) study aimed at identifying a promising lead structure for drug development.[75] At the outset of this project, the target enzyme was unknown, and structural modifications were performed to optimize lipophilicity, flexibility and number of sites for hydrogen bonding. Compound **13** has emerged from the hit to lead stage and was selected as a lead structure due to its low nanomolar antiviral activity *in vitro* against several HF viruses, including Lassa (IC_{50} = 5 nM) and Ebola virus (IC_{50} = 2 nM).

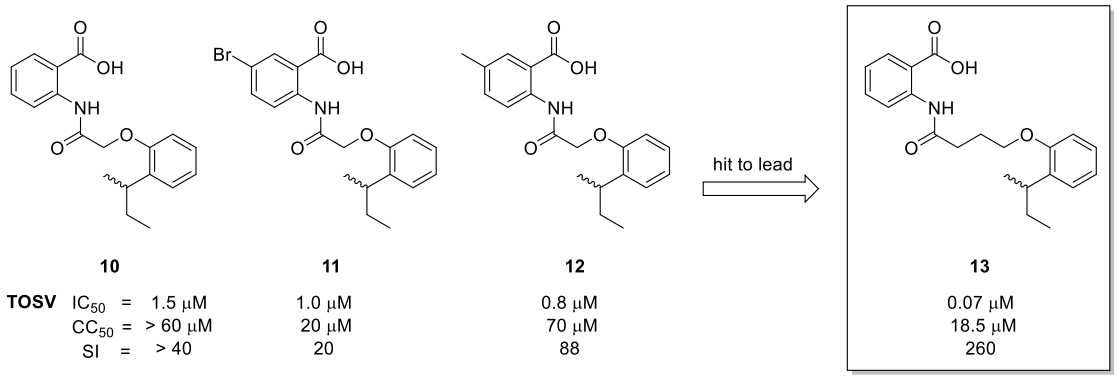

Figure 6: Hit compounds **10-12** derived from the high throughput screening and identified lead compound **13** used in ongoing optimization campaign.

Using biochemical and biocomputational analytical methods, the target enzyme was later identified as human dihydroorotate dehydrogenase (hDHODH), a host enzyme involved in the *de novo* biosynthesis of pyrimidine nucleotides. The lead structure demonstrates a strong inhibitory potency against isolated recombinant hDHODH (IC_{50} = 17 nM), which correlates with its broad-spectrum antiviral activity. Based on the lead compound **13**, a lead optimization campaign was initiated by the group of C. MEIER.

2.2. Pyrimidine nucleotide biosynthesis as target for antiviral therapy

Hundreds of viruses are known to cause human disease, but antiviral drugs have been approved for fewer than a dozen.[1,76] Most approved antivirals are designed to target unique viral enzymes, typically proteases and polymerases, thereby following the “one drug-one bug” approach. Such direct-acting antivirals (DAAs) have proven successful in the treatment of several virus infections, e.g. human immunodeficiency virus (HIV), hepatitis B virus (HBV), HCV, influenza virus and SARS-CoV-2, and are generally considered safe for human use because they act selectively against a viral factor.[1,77] However, this approach has major limitations, including a narrow spectrum of coverage, a lengthy development period, and high investment costs. Due to these limitations, DAAs cannot be readily deployed to treat newly emerging viruses and are not suitable for immediate outbreak response. Additionally, administration of DAAs often leads to the emergence of drug-resistant virus variants and a consequent loss of efficacy. Therefore, alternative drugs with new mechanism of action and broad-spectrum antiviral activity must be explored.[1,77,78]

Besides viral enzymes, cellular factors are also necessary for successful virus replication and hence represent potential targets for antiviral drug development. Viruses within the same family often need to hijack the same host proteins and/or pathways to complete their replication, and targeting these host proteins can lead to the development of host-directed antiviral agents (HDAs) with broad-spectrum efficacy, providing a “one drug-multiple bugs” solution. To avoid cell toxicities, HDAs must target host factors that are essential for viral replication but dispensable for normal host cell functions.[77–79] Compared to DAAs, HDAs offer a higher barrier to resistance development, and drug design can occur before the emergence of a new virus. HDAs that can be directly applied may be beneficial in preventing outbreaks by slowing initial viral spread. Currently, few HDAs have been validated in preclinical or clinical studies, and even fewer have been approved by the FDA or EC. Only about one-tenth of all approved antivirals target host factors, and half of these are interferon-related biologics.[80]

Host pathways that are considered potential antiviral targets include lipid metabolism, protein synthesis, protein folding, and nucleotide metabolism.[81] For the biosynthesis of DNA and RNA, nucleotides are essential building blocks and are composed of purines (adenine and guanine) and pyrimidines (thymine, uracil and cytosine).[82] Viruses require large amounts of nucleotides provided by the host cell to replicate efficiently and depend on upregulated nucleotide synthesis via the *de novo* pathway.[15,83] In resting cells, the demand for nucleotides is mainly covered by the salvage pathway, in which nucleotide metabolites are recycled from DNA/RNA degradation or obtained through uptake from the blood stream.[83–86] As previously mentioned, ribavirin **1** is an inhibitor of IMPDH, an enzyme involved in the *de novo* biosynthesis of guanine nucleotides, which induces depletion of intracellular guanine nucleotide

pools. In recent years, the *de novo* biosynthesis of pyrimidine nucleotides has also been extensively studied as a target for antiviral therapy.[81,83,87]

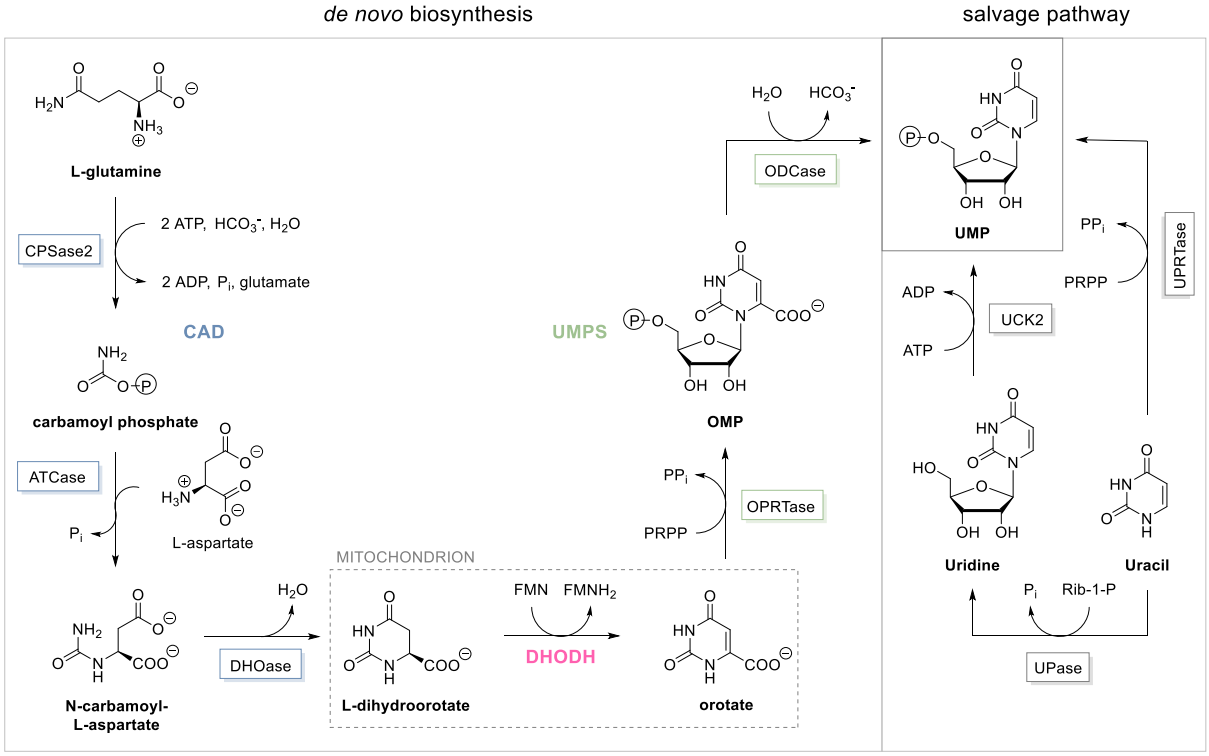

Figure 7: *De novo* biosynthesis and salvage pathway of UMP.

In the *de novo* pathway, uridine monophosphate (UMP) is synthesized from simple molecules and is subsequently converted into all other pyrimidine nucleotides. The *de novo* synthesis of UMP consists of six steps catalyzed by three proteins (Figure 7).[88] The first three steps are initiated by the CAD protein, which contains three enzymatic domains: carbamoyl phosphate synthase II (CPSase2), aspartate transcarbamylase (ATCase), and dihydroorotase (DHOase). Initially, the starting materials L-glutamine and bicarbonate are converted into carbamoyl phosphate by CPSase2, consuming two molecules of ATP. Next, ATCase catalyzes the reaction of carbamoyl phosphate with aspartate to form carbamoyl aspartate, which is then converted into dihydroorotate by DHOase. In the fourth step, the mitochondrial enzyme DHODH oxidizes dihydroorotate into orotate by transferring two electrons to the mitochondrial respiratory chain, using flavin mononucleotide (FMN) and ubiquinone as co-factors. This is the only mitochondrial step, whereas all other steps occur in the cytosol around the mitochondria. The last two steps are catalyzed by the bifunctional protein uridine monophosphate synthase (UMPS), which contains two enzymatic domains: orotate phosphoribosyltransferase (OPRTase) and orotidine-5'-phosphate decarboxylase (ODCase). OPRTase catalyzes the conversion of orotate into orotidine monophosphate (OMP) by transferring a

phosphoribosyl group from co-substrate 5-phosphoribosyl-1-pyrophosphate (PRPP). Finally, ODCase converts OMP into UMP through decarboxylation. UMP serves as the precursor for the synthesis of uridine triphosphate (UTP), cytidine triphosphate (CTP), thymidine triphosphate (TTP) and deoxycytidine triphosphate (dCTP), all of which are substrates for polymerases during DNA/RNA replication.[15,81,83,84]

In contrast, UMP can be obtained through salvage pathways that recover appropriate nucleotide metabolites from the catabolic degradation of nucleic acids or from extracellular nucleosides transported into the cell via specific channels and pumps.[81,83] Uridine is salvaged by uridine-cytidine kinase 2 (UCK2), which phosphorylates the nucleoside into UMP. The free nucleobase uracil can also be salvaged either through uridine phosphorylase (UPase), which catalyzes the reaction of the nucleobase and ribose-1-phosphate (Rib-1-P) to form uridine, or via uracil phosphoribosyltransferase (UPRTase), which converts the nucleobase and phosphoribosyl pyrophosphate (PRPP) directly into UMP.[89]

As discussed above, the salvage pathway of UMP is energetically favored by resting cells, whereas viruses are highly dependent on the *de novo* biosynthesis for an adequate supply of pyrimidine nucleotides. This difference makes the *de novo* biosynthesis of UMP a very attractive target for antiviral drug discovery. In this pathway, DHODH catalyzes the rate-limiting step, the oxidation of dihydroorotate to orotate, and is consequently considered the most promising target to inhibit the *de novo* pathway.[81,90]

2.3. Dihydroorotate Dehydrogenase

DHODHs from different organisms can be divided into two major classes, which vary in cofactor content, oligomeric state, subcellular localization, and membrane association. Human DHODH belongs to the monomeric membrane-associated class 2 DHODHs, which can also be found in Gram-negative bacteria and other eukaryotes. In contrast, DHODHs of class 1 are oligomeric protein complexes located in the cytosol and are mainly found in Gram-positive bacteria.[91,92]

Human DHODH consists of a large C-terminal domain and a small N-terminal domain connected by an extended loop (Figure 8). The C-terminal domain has an α/β barrel fold composed of eight parallel β strands (pink), enclosed by eight α helices (light green). There are two antiparallel β strands at the bottom of the barrel and three antiparallel β strands at the top of the barrel (cyan), with the latter forming the proximal redox site. Located close to this redox site, a catalytic loop is involved in the opening mechanism that regulates access of the substrate and release of the product. The small N-terminal domain contains two α helices (violet) connected by a short loop. One of the α helices of the N-terminal domain is connect-

ed to the bottom of the α/β barrel of the C-terminal domain by an extended loop (red). The N-terminal domain is specific to DHODHs of class 2 and mediates association with the membrane via a hydrophobic transmembrane sequence. In humans, DHODH is located on the outer surface of the inner mitochondrial membrane (IMM).[91,93,94]

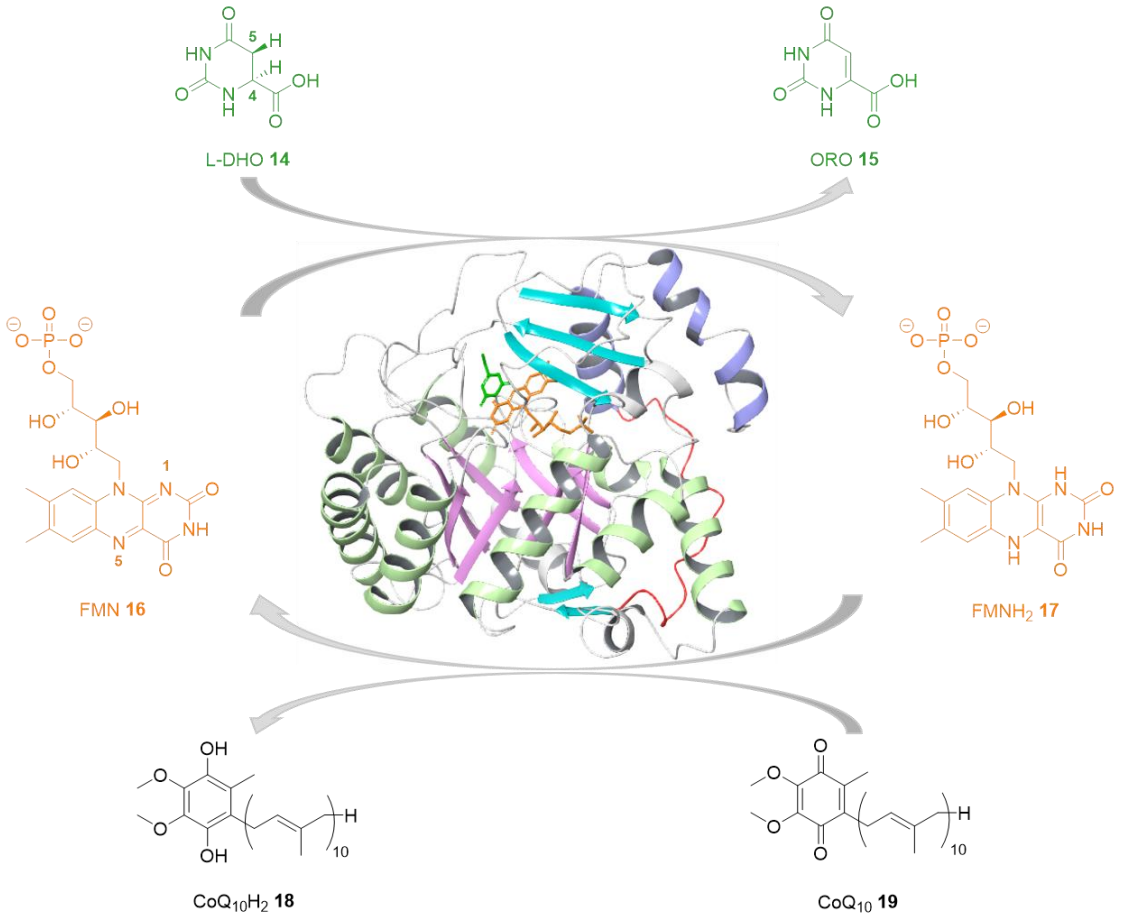

Figure 8: Enzymatic reaction catalyzed by hDHODH (crystal structure PDB code: 2PRM).

DHODH catalyzes the fourth and rate-limiting step of the *de novo* pyrimidine nucleoside biosynthesis pathway: the oxidation of L-dihydroorotate **14** (L-DHO, green) to orotate **15** (ORO), and the reduction of FMN **16** (orange) to dihydroflavin mononucleotide **17** ($FMNH_2$). The cofactor FMN **16** is tightly bound and located beneath the short loop of the N-terminal domain, which is near the binding site of the substrate L-DHO **14**. In the active site of class 2 DHODHs, a serine residue mediates the stereospecific oxidation of L-DHO **14** and abstracts a proton from the C5 atom of L-DHO **14**. ORO **15** is ultimately generated through direct hydride transfer from the C4 position of L-DHO **14** to the N5 position of FMN **16**, resulting in the formation of a double bond between the C5 and C4 atoms. During the reduction of FMN **16** to

$FMNH_2$ **17**, the formation of the second N-H bond at the N1 position is most likely mediated by a conserved lysine residue that acts as a proton donor.[93,94]

Regeneration of FMN **16** is essential for continued DHODH catalysis, for which human DHODH uses ubiquinone **19**, also known as coenzyme Q_{10} (CoQ_{10}), as an oxidant. Ubiquinone **19** is supplied by the mitochondrial electron transport chain (ETC) and utilizes a tunnel formed by the N-terminal domain to reach the binding cavity of $FMNH_2$ **17**. In this second redox reaction, $FMNH_2$ **17** is reoxidized to FMN **16**, and ubiquinone **19** is reduced to ubiquinol **18** ($CoQ_{10}H_2$). After successful electron transfer, ubiquinol **18** exits the enzyme along the same path and is released into the IMM, where it is again available for processes of the mitochondrial ETC.[91,94]

2.3.1. Known hDHODH inhibitors

A selection of known hDHODH inhibitors approved by the FDA or in clinical trials is shown in Figure 9. The most well-known hDHODH inhibitors previously described are brequinar **20** and leflunomide **21** (prodrug of active compound teriflunomide **22**). Brequinar **20** was initially developed as an anticancer agent in the 1990s and was later discovered to be one of the most potent hDHODH inhibitors, with an IC_{50} value of 1.8 nM.[95] The *de novo* synthesis of pyrimidines is crucial not only for viruses to replicate efficiently but also for rapidly proliferating cells, such as cancer cells and T cells of the immune system.[96] Despite its strong inhibitory potency against hDHODH, brequinar **20** failed in multiple clinical trials with cancer patients due to a limited therapeutic window and toxic effects at clinically relevant doses.[96,97] Leflunomide **21** and teriflunomide **22** are immunomodulatory agents that have been approved by the FDA for the treatment of rheumatoid arthritis (1998) and multiple sclerosis (2012), respectively.[96] Upon oral administration, leflunomide **21** is converted into its active metabolite, teriflunomide **22**, via an isoxazole ring-opening reaction.[98] Unfortunately, both compounds can cause severe side effects, such as diarrhea, alopecia, neutropenia, and elevated liver enzyme levels.[99] Liver toxicity associated with teriflunomide treatment is linked to its long plasma half-life of two weeks.[85] Moreover, teriflunomide **22** is a less potent hDHODH inhibitor than brequinar **20**, with an IC_{50} value of approximately 600 nM in the isolated enzyme.[100,101]

In recent years, DHODH inhibitors have gained increasing interest in the field of antiviral therapy and have been shown to be active against various RNA viruses *in vitro* and *in vivo*. For example, antiviral effects of brequinar **20** were observed for Zika, Influenza, Ebola and SARS-CoV-2 viruses. Brequinar's safety profile and anti-SARS-CoV-2 response were even evaluated in a phase I/II clinical trial in 2020 (NCT04425252), and published results indicate that brequinar was well tolerated but did not provide any clinical benefit in COVID-19 pa-

tients.[101] Another highly potent inhibitor of SARS-CoV-2 replication is the DHODH inhibitor emvododstat **23** (PTC299), which also possesses the ability to suppress the production of a subset of proinflammatory cytokines and thereby attenuate a cytokine storm.[102] Compared to brequinar **20** and leflunomide **21**, the inhibitory potency of emvododstat **23** is lower in recombinant DHODH with an IC_{50} value of approximately 1 µM, but similar when purified mitochondria are used as the DHODH source, with an IC_{50} value of about 20 nM.[103] Emvododstat **23** was originally developed in 2016 as a potential anticancer agent and was tested in a phase II clinical study in patients with Kaposi's sarcoma but failed due to a low response rate.[104] However, emvododstat **23** was repurposed and investigated in a phase II/III trial in patients with COVID-19 infection. The clinical trial started in 2020, but was terminated, likely due to a lack of observed improvement compared to the control group.[102]

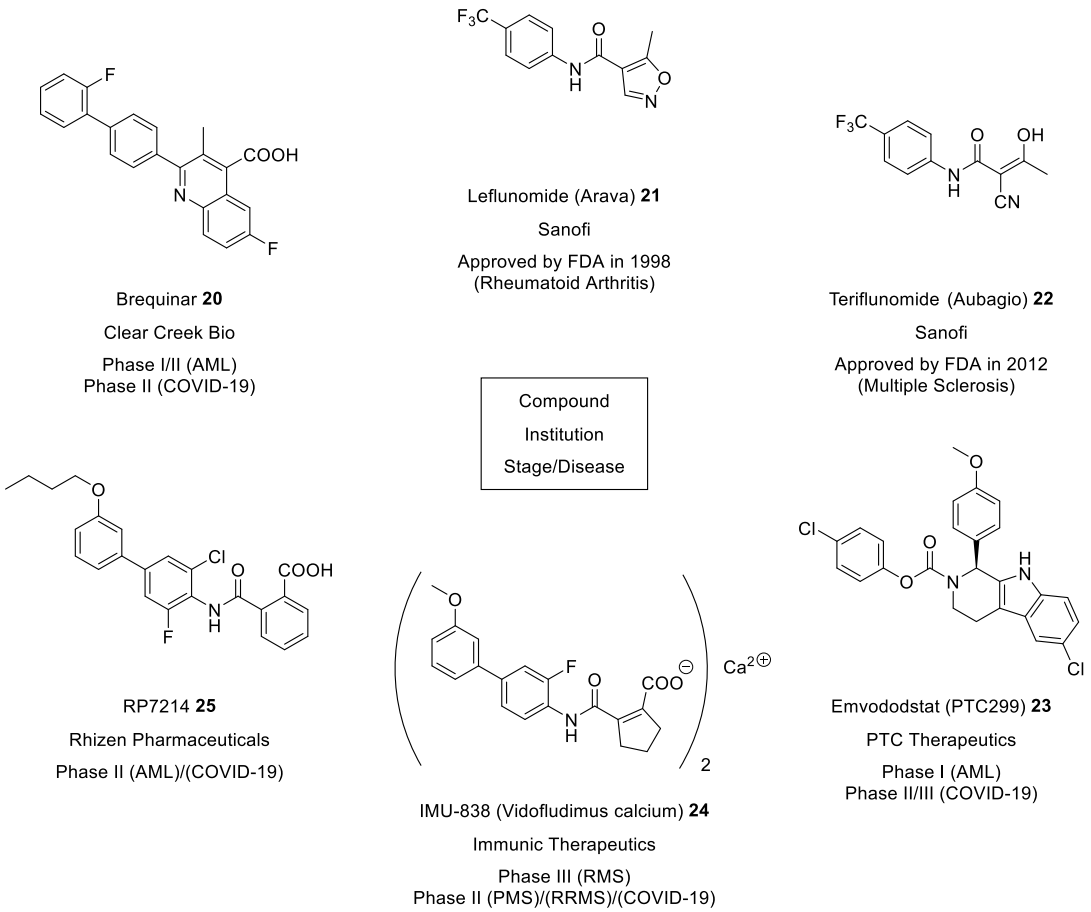

Figure 9: Selection of known hDHODH inhibitors approved by the FDA or in clinical trials.

There are two other DHODH inhibitors in phase II clinical development for COVID-19 infections: the calcium carboxylate analog of vidofludimus (IMU-838 **24**) and RP7214 **25**. Vidofludimus and RP7214 **25** are able to inhibit hDHODH, with IC_{50} values of 134 nM[105] and 8 nM[106], respectively. Originally, vidofludimus was extensively investigated for its anti-

inflammatory effects in *in vivo* studies, which led to several clinical trials in patients with multiple sclerosis.[107,101] The drug has also demonstrated antiviral activity against various viruses, including Epstein-Barr virus, hepatitis C virus, and SARS-CoV-2.[87,108] A first phase II clinical trial in 2020 (NCT04379271) showed that IMU-838 **24** is well tolerated in patients with COVID-19 infection and that it exhibits antiviral effects while preserving the humoral response to SARS-CoV-2. However, further studies are necessary to confirm its clinical efficacy.[108] Another phase II clinical trial conducted in 2020 (NCT04516915) used IMU-838 **24** in combination with the antiviral oseltamivir to treat COVID-19 patients, but results are not yet available. RP7214 **25** has also recently completed a phase II clinical trial in COVID-19 patients (NCT05007236). According to a preprint published by Rhizen Pharmaceuticals, it showed a favorable safety profile and a statistically significant reduction in viral load during early disease stages and in unvaccinated patients. RP7214 **25** may be beneficial in preventing severe disease in vulnerable populations, but further clinical development is warranted.[109]

2.3.2. Structural ligand features

Most discovered DHODH inhibitors are amphiphilic compounds containing a large lipophilic part and a small hydrophilic part.[96] Moreover, they often share one or more common motifs with brequinar **20**, such as a biphenyl motif, a quinoline or naphthalene moiety, and/or a carboxylic acid group attached to an aromatic ring. These inhibitors are specifically designed to bind at the same site where the co-substrate ubiquinone **19** interacts (Figure 10a). By occupying this binding site, they prevent ubiquinone **19** from accessing the redox center, thereby inhibiting the regeneration of FMN **16** and ultimately halting DHODH catalytic activity.[85,101]

As illustrated by brequinar analog **20A** in Figure 10b, the nonpolar side chains of the two N-terminal α-helices form a hydrophobic entrance. The biphenyl group of brequinar analog **20A** fits ideally into this part of the tunnel, enabling hydrophobic contacts with side chains of several amino acids, including Met43, Ala59, Leu68, and Pro364. The tunnel narrows towards the inner subsite, which contains various charged and polar side chains, such as Gln47, His56, Tyr356, Thr360, and Arg136. Side chains of Val134 and Val143 form a small hydrophobic patch that caps the narrow end of the tunnel. Target specificity and inhibitor affinity are primarily determined by interactions within the inner subsite. The carboxylate group of brequinar analog **20A** strongly interacts with the side chains of Arg136 and Gln47 via salt bridges and hydrogen bonds, respectively. Additionally, the carboxylate can form a hydrogen bond with a buried water molecule, which, in turn, forms a further hydrogen bond with the side chain of Thr360. Stacking interactions between the quinoline ring system of brequinar analog **20A** and the imidazole ring of His56 further contribute to a high binding affinity.[93,94,98]

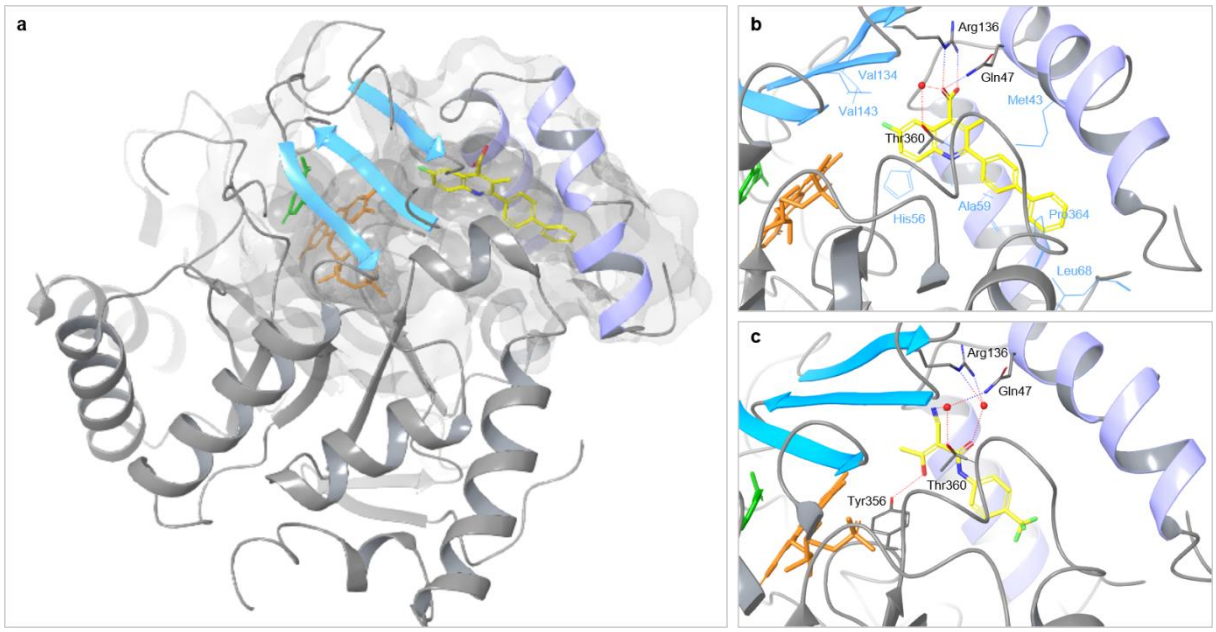

Figure 10: (a) Crystal structure of hDHODH in complex with brequinar analog **20A** (yellow). Binding-motif of (b) brequinar **20A** (PDB: 1D3G) and (c) teriflunomide **22** (PDB: 1D3H) in the lipophilic tunnel.

Compared to brequinar analog **20A**, teriflunomide **22** forms fewer hydrophobic interactions at the entrance of the tunnel (Figure 10c), primarily due to the smaller size of its lipophilic residue. This reduced hydrophobic contact area may influence its binding affinity and specificity. In the inner subsite, the deprotonated enolic hydroxy group of teriflunomide **22** interacts with the side chain of Tyr356 via a hydrogen bond. In addition, several hydrogen bonds are established between the isonitrile and carboxylic acid groups of teriflunomide **22** and the side chains of amino acids such as Thr360, Gln47, and Arg136. These interactions are mediated by two tightly bound water molecules, serving as molecular bridges that enhance the overall stability of the inhibitor within the active site.[94,98]

2.3.3. Phenylethynyl anthranilic acid based DHODH inhibitors

Following the identification of hDHODH as the molecular target for compound **13**, the group of C. MEIER dedicated efforts to developing additional lead structures featuring an anthranilic acid motif, as illustrated in Figure 11. Lead structure **13** from series 1, identified through a high-throughput screening targeting Toscana virus, exhibited moderate lipophilicity and good membrane permeability, although it demonstrated poor metabolic stability. In this series, N. C. LAUBACH designed a promising drug candidate with favorable pharmacokinetic properties and broad-spectrum antiviral activity in the nanomolar range.[110] However, the synthetic route was complex, which limited further structural optimization.

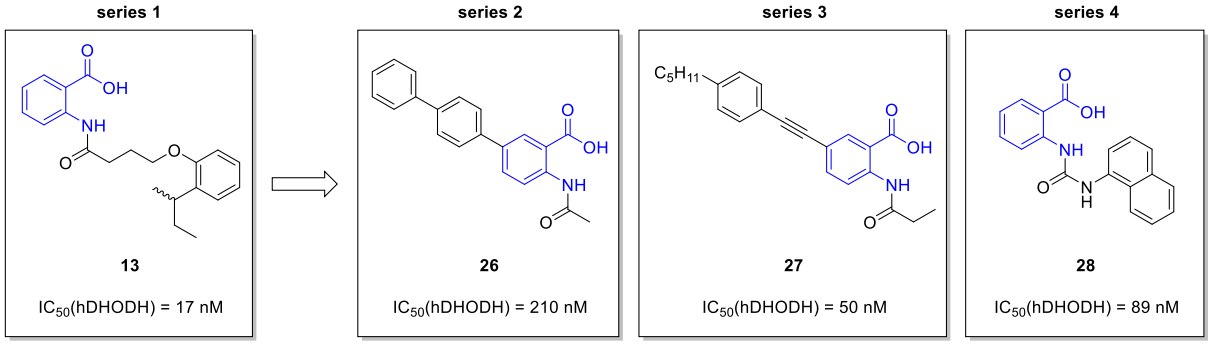

Figure 11: DHODH inhibitor series based on anthranilic acids.

Based on available literature and virtual screenings conducted by the group of C. MEIER, three novel series have been identified. The inhibitory potential of the 2-aminobenzoate core scaffold against hDHODH was also explored by I. FRITZON[85] and co-workers, who reported that the biphenyl anthranilic acid derivative **26** exhibited high potency in isolated hDHODH, with an IC_{50} value of 210 nM. As a result, the biphenyl anthranilic acid derivative **26** was selected by the group of C. MEIER as a lead structure for further optimization. However, this compound **26** demonstrated poor aqueous solubility and poor metabolic stability. To address these issues, an optimization campaign was recently initiated by M. WINKLER.[111]

Another lead structure identified by N. C. LAUBACH is the naphthyl-bearing anthranilic acid derivative **28**, which already exhibits favorable pharmacokinetic properties. This compound demonstrates potent activity against hDHODH (IC_{50} = 89 nM), along with high metabolic stability, suitable lipophilicity, and good membrane permeability. Its compact structure and straightforward synthetic route provide a solid foundation for future pharmacokinetically guided optimization and drug development efforts.[110]

This dissertation focuses on optimizing the phenylethynyl anthranilic acid series. The lead structure **27**, developed by M. WINKLER[111] in the group of C. MEIER, was inspired by previous work by I. FRITZON *et al*.[85,112] and formed the basis for subsequent optimization efforts. This compound demonstrates exceptional potency as a hDHODH inhibitor, with an IC_{50} value of 50 nM in the isolated enzyme. Additionally, it shows markedly enhanced antiviral activity against Toscana and Hazara viruses (HAZV) compared to the lead structure **13** from series 1, achieving IC_{50} values of 10.5 nM and 8 nM, respectively (Figure 12).

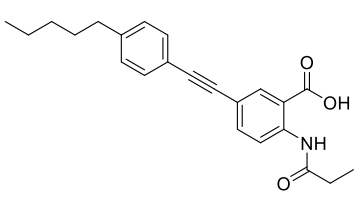

27

ANTIVIRAL DATA

IC_{50} (TOSV)	10.5 nM
IC_{50} (HAZV)	8 nM
CC_{50} (Vero E6)	8 µM
SI	760 (Tosc)
	1000 (Haz)

ADME DATA

Solubility in PBS pH 7.4 (µM)	18 ± 6
log D (PBS pH 7.4/octanol)	4.6 ± 0.3
Permeability (PAMPA) 16 h passage in %	24
Hepatic microsome stability remaining at 1 h in %	70 ± 3
Plasma stability remaining at 2 h in %	114 ± 5

Figure 12: Antiviral and ADME data of phenylethynyl anthranilic acid **27**.

Compound **12** exhibited a low CC_{50} value of 8 µM in Vero cells. However, the calculated ratios between cytotoxicity and antiviral activity for Toscana virus (SI = 760) and Hazara virus (SI = 1000) greatly exceed the suggested SI value of at least 10. Nevertheless, the compound's high lipophilicity limits its oral bioavailability, and its amide group is prone to enzymatic cleavage by amidases. Fortunately, a straightforward synthetic route provides numerous derivatization possibilities to address these disadvantages and facilitate the identification of a drug candidate with suitable pharmacokinetic properties.

3. Objectives

This work aims to conduct an optimization campaign with selected compounds of the phenylethynyl anthranilic acid series to improve their physicochemical properties, particularly regarding aqueous solubility and enzymatic stability, without compromising their hDHODH potency and antiviral activity. For this campaign, compounds MW-577 **29** and MW-BG-22 **30** were chosen as lead structures, with one carrying a butyl group and the other a cyclohexyl group as the terminal aromatic residue (Figure 13). Both compounds proved more active against Toscana and Hazara viruses than **27**, the first compound developed in the phenylethynyl series, with IC_{50} values below 6 nM. A short synthesis route should enable rapid access to a wide variety of new derivatives, facilitating initial structure-activity relationship studies. The strategy was to modify the core structure stepwise at different positions and analyze the resulting changes in physicochemical properties and inhibitory activity on isolated hDHODH. The primary objective of the optimization campaign was to discover a highly potent compound with favorable pharmacokinetic characteristics suitable for advancement as a potential drug candidate.

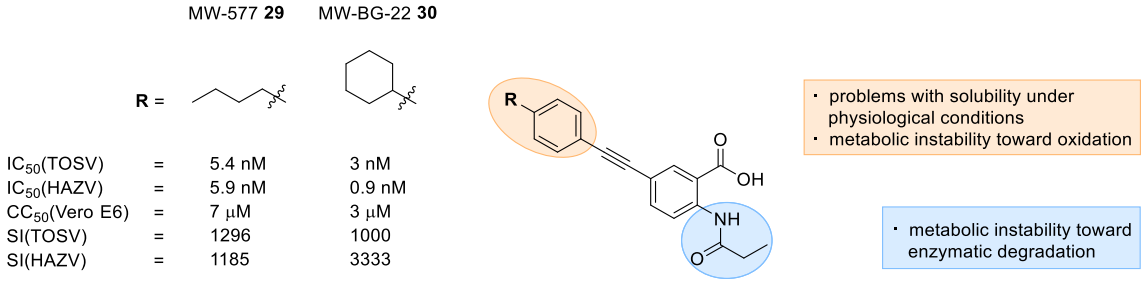

Figure 13: Antiviral data of lead compounds MW-577 **29** and MW-BG-22 **30**.

The first part of this thesis investigates the pharmacokinetic properties of lead structures **29** and **30**, including the kinetic aqueous solubility, lipophilicity, membrane permeability and metabolic stability. For this purpose, established assays were employed and slightly adapted to match the characteristics of phenylethynyl anthranilic acid compounds. To compare the hDHODH potencies of the lead structures with those of newly synthesized derivatives, the percentage hDHODH inhibition was determined at specific inhibitor concentrations. In addition, this work aims to demonstrate the broad-spectrum activity potential of the lead compounds **29** and **30** by assessing their efficacy in cell-based assays against different hemorrhagic fever viruses, such as YFV, DENV, CCHFV, and EBOV.

The second aim of this thesis was to deliver a wide range of derivatives based on both lead structures **29** and **30** (Figure 14) and to evaluate their hDHODH inhibition potential and phys-

icochemical properties. Since most drugs are designed to penetrate biological membranes, sufficient lipophilicity is required, however, excessive lipophilicity can lead to poor aqueous solubility that limits suitability for oral administration.[113] In this context, the big lipophilic *para*-substituted phenylethynyl moiety of **29** and **30** may cause solubility issues under physiological conditions. Therefore, the terminal alkyl chain should be replaced with more polar groups, such as morpholine, piperidine, or propylamine. Highly lipophilic compounds can also be more vulnerable to oxidation processes by cytochrome P450 enzymes (CYP).[114] To mitigate this, fluorine atoms can be used to substitute carbon-bound hydrogen atoms, as their electron-withdrawing effect impedes CYP-catalyzed hydroxylation at the aromatic ring or alkyl chain.[115] Docking simulations further revealed that the enzyme pocket, where the phenylethynyl moiety interacts, provides enough space to introduce small substituents (e.g. acetoxy, trifluoromethyl, and methoxy) on the aromatic ring to potentially improve binding affinity. The amide group is another functional group prone to enzymatic degradation, therefore, more stable functions such as urea should be considered, or the entire anthranilic acid part should be replaced by bicyclic compounds, e.g. benzimidazole.

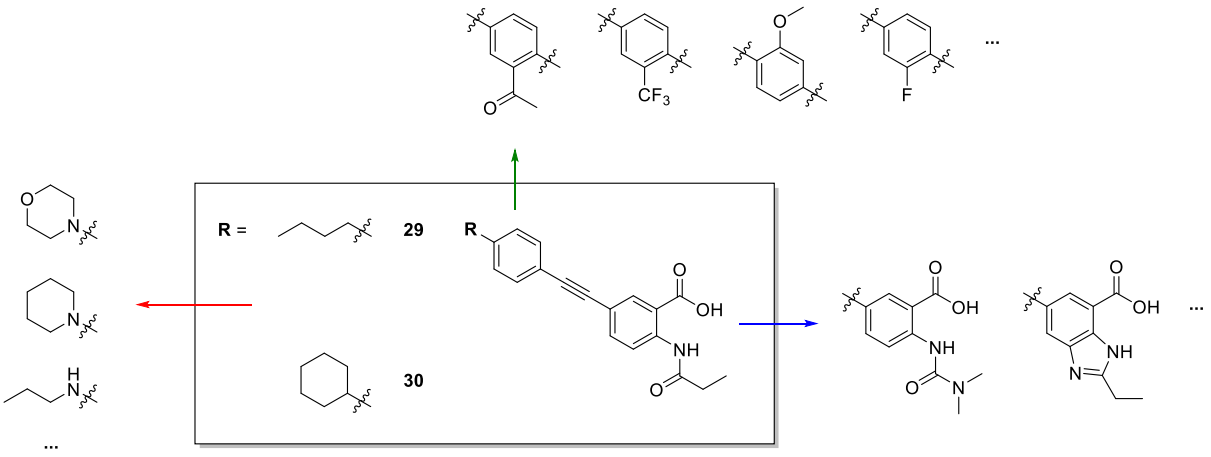

Figure 14: Possible modifications for lead structures **29** and **30**.

Finally, hDHODH inhibitors should be synthesized, incorporating the modifications from the previous optimization campaign that improved physicochemical properties while preserving binding affinity. These final compounds should also be evaluated for their physicochemical properties, hDHODH potency, and antiviral activity. The aim is to use these findings to identify a compound suitable for *in vivo* validation and potential progression into the development of a therapeutic drug.

4. Results and Discussion

4.1. Pharmacokinetic characterization of MW-577 29 and MW-BG-22 30

In drug development, investigation of the compounds' pharmacokinetic (PK) properties is essential for lead identification and during further lead optimization. Preclinical PK characterization include the assessment of the compound's absorption, distribution, metabolism, and elimination (ADME). A high efficacy requires a rapid absorption, well distribution, minimal metabolic degradation, and slow elimination of the drug.[116,117] There are various relatively rapid and cost-effective *in vitro* assays established that can be applied to predict the bioavailability of a compound. Lead optimization aims to improve the ADME properties of a lead compound while maintaining its potency toward the target enzyme, however, sometimes compounds with lower *in vitro* potencies but better ADME properties can be more efficacious *in vivo*.[117] The first aim of this thesis was to investigate the ADME properties of lead compounds MW-577 **29** and MW-BG-22 **30** and use these results to start an optimization campaign.

4.1.1. Solubility

Oral administration is the most common route of drug delivery due to its ease of application, high patient adherence, cost-effectiveness, and ease of dosage adjustment.[118] The absorption of a drug by passive diffusion is proportional to the concentration gradient between the intestinal lumen and the blood, which depends on the drug's solubility.[119] Drugs with a poor aqueous solubility have a slower absorption rate, which can result in inadequate and variable bioavailability. Solubility is the most important parameter for orally administered drugs to adjust a defined concentration in systemic circulation. If a drug has a poor aqueous solubility, higher doses are often required to reach the therapeutic plasma concentrations after oral ingestion.[118] Moreover, crystallization and acute toxicity can occur due to high concentrations of poorly soluble drug molecules in organisms. [119]

Both lead compounds MW-577 **29** and MW-BG-22 **30** were investigated for their kinetic solubility in PBS buffer (pH 7.4). Compared to the thermodynamic solubility, measurement of the kinetic solubility is faster and well suited for high throughput screening methods.[120] For this purpose, a 10 mM DMSO stock solution of the test substance was prepared and diluted with PBS buffer (50-fold), yielding a final compound concentration of 200 µM and a DMSO concentration of 2%. The samples were prepared in triplicate and incubated for 24 h at room temperature (~25 °C). The appearance of precipitate was then monitored by measuring the residual compound concentration in the supernatant after 24 h using UV/Vis spectroscopy. Calibration curves for quantification needed to be prepared separately (Figure 15). Kinetic

solubilities were calculated using equation 1 (see experimental part 6.2.1). It should be mentioned that the addition of a co-solvent (DMSO) affects the solubility and values may vary with the assay conditions.[121] Phenylpropanoic acid was used as a reference substance, which has moderate solubility in water. For phenylpropanoic acid (MW = 150 g/mol), a kinetic solubility of 111 ± 2 µM was determined, which is equivalent to a concentration of 17 ± 1 µg/mL. This value agrees well with the value of 111 ± 3 µM reported in the literature.[122]

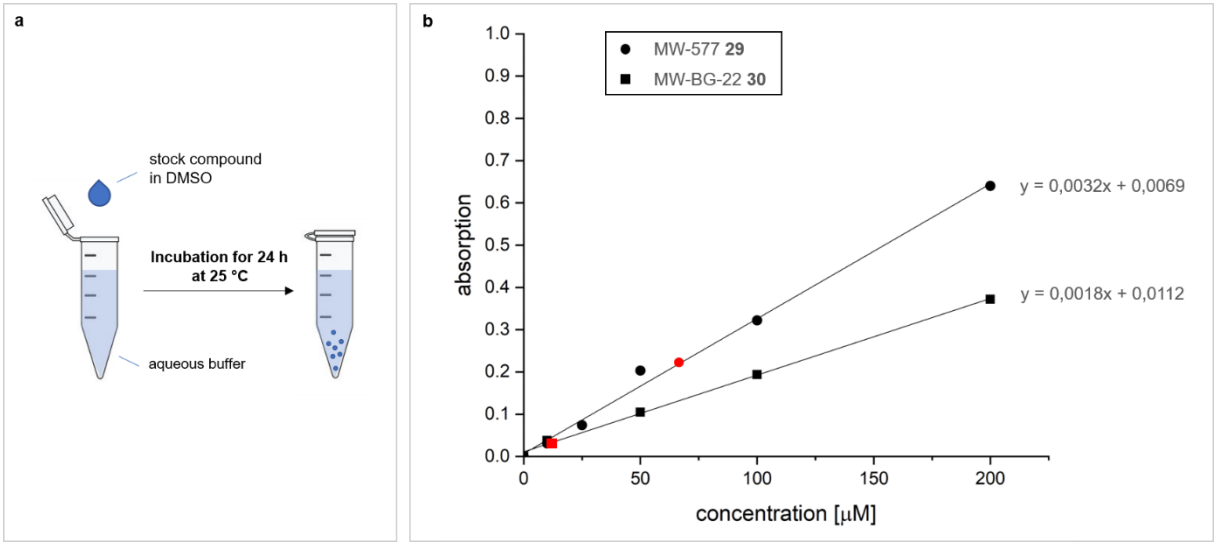

Figure 15: (a) Setup for kinetic solubility assay. (b) Calibration curves and determined kinetic solubility (highlighted in red) for lead compounds **29** and **30**.

According to solubility guidelines discussed in a publication of R. GUHA *et al*.[123], values of <10 µg/mL indicate a low solubility, values of 10-60 µg/mL a moderate solubility and values of >60 µg/mL a high solubility. The kinetic solubility of MW-577 **29** (MW = 349 g/mol) was determined to 65 ± 2 µM, which corresponds to a concentration of 22 ± 1 µg/mL. For MW-BG-22 **30** (M = 375 g/mol) a kinetic solubility of 12 ± 3 µM was determined, which is equivalent to a concentration of 4.5 µg/mL. Thus, kinetic solubility was only moderate for MW-577 **29** and low for MW-BG-22 **30**.

4.1.2. Lipophilicity

Lipophilicity is another important parameter in drug discovery that has a big impact on the ADME properties of a compound.[124] A good aqueous solubility is desirable for the oral administration of a drug, but sufficient lipophilicity is also required since most drugs need to penetrate lipid membranes to reach the target tissue.[113] Such druggable targets are primarily

surrounded by an aqueous environment and have binding sites that consist of at least one hydrophobic region, which is why lipophilicity also plays a critical role in target selectivity and potency. The binding of lipophilic ligands to hydrophobic protein binding sites is driven by more favorable hydrophobic interactions that are formed between the protein and the ligand than those formed between the protein and solvating water molecules found in the pocket.[125] On the other hand, an excessive lipophilicity may result in low solubility, rapid metabolic turnover by CYP enzymes and higher risk of toxicities.[114,126]

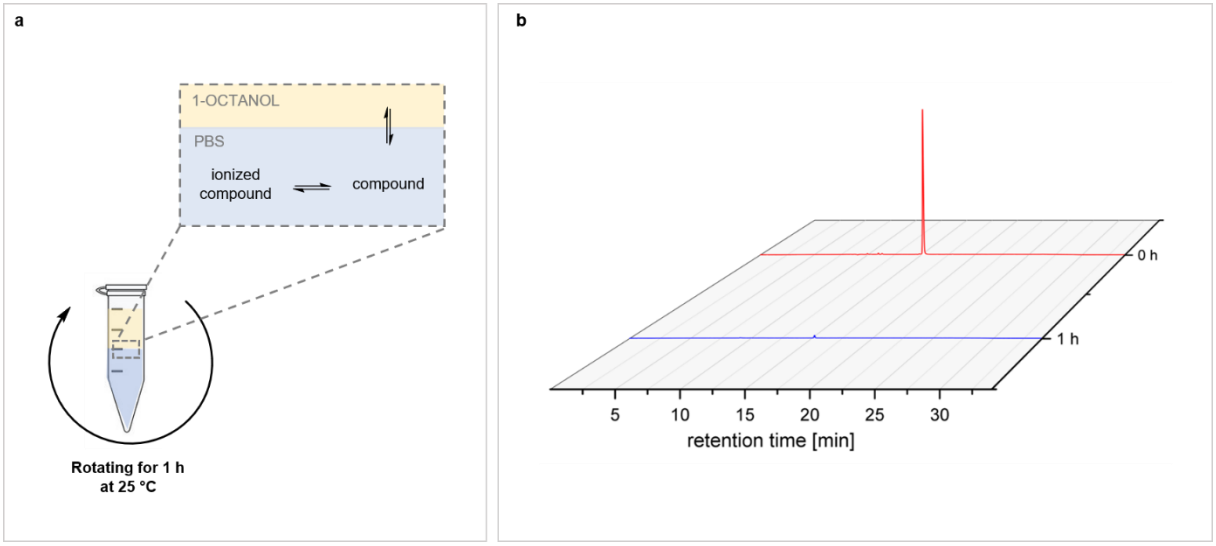

Figure 16: (a) Setup for logD assay. (b) HPLC-chromatograms of MW-BG-22 **30** in PBS recorded before and after shaking with 1-octanol for 1 h.

The lipophilicity of MW-577 **29** and MW-BG-22 **30** were measured as the distribution between 1-octanol and PBS buffer (pH 7.4) using the well-known shake-flask method, as shown in Figure 16. The result is expressed as the 10-base logarithm of the distribution coefficient (logD). It is defined as the ratio of the concentration of the compound's ionized and non-ionized forms in the organic and aqueous phases at a determined concentration.[127] As the core scaffold of both lead compounds **29** and **30** contains ionizable groups, measurement of logD was chosen over logP (octanol/water participation), which is the common measure for lipophilicity but for neutral compounds only. For this purpose, a 10 mM DMSO stock of the test substance was prepared and diluted with PBS buffer (50-fold), resulting in a final compound concentration of 200 µM and a DMSO concentration of 2%. 1-Octanol was then added to the samples. All samples were prepared in triplicate and shaken for 1 h at room temperature (~25 °C). The decrease in compound concentration was measured for the aqueous phase by high performance liquid chromatography (HPLC) analysis. LogD values were calculated using equation 2 (see experimental part 6.2.2). Caffeine was used as a ref-

erence compound and a logD value of -0.069 ± 0.005 was calculated. This value agrees well with the value of -0.07 reported in the literature.[128]

Unfortunately, the lower detection limit was reached with MW-577 **29** and MW-BG-22 **30** (Figure 16), leaving too little compound in the aqueous phase to determine the logD accurately. The lowest limit of detection depends not only on the applied procedure and detection technique but also on the sensitivity and absorptivity of the compound. In this case, only a logD value higher than 3.3 could be determined for MW-577 **29** and MW-BG-22 **30**. LogP and logD values are negative for hydrophilic and positive for lipophilic compounds. In drug discovery, a logP range between 2 and 4 or a logD value at pH = 7.4 between 1 and 3 is suggested to obtain optimal ADME properties.[129] But these ranges depend on the molecular weight, acid/base properties and/or the desired mode of action of the drug and might be even narrower. Although no accurate determination is possible for both lead compounds **29** and **30** with this procedure, the result indicates a high lipophilicity with a logD > 3, which is not in the suggested logD range. Such highly lipophilic compounds tend to accumulate in fatty tissues and may not reach their target.[124] However, since hDHODH inhibitors have to reach the inner mitochondrial membrane to enter the enzyme pocket, a comparably high lipophilicity is required. A logD > 2.5 is suggested by M. LOLLI for translation of potent *in vitro* activity into substantial *in vivo* efficacy. Nonetheless, as previously mentioned, excessive lipophilicity can lead to adverse ADME properties, which has led M. LOLLI and other researchers to explore alternative strategies aimed at improving *in vivo* efficacy.[130]

4.1.3. Permeability

Besides aqueous solubility, permeability is another key property that contributes to a successful transport across the gastrointestinal membrane and distribution of the drug to the intended target organs and cells.[131] In eukaryotes, a drug can pass through membranes by two different transport modes: active transport or passive diffusion. Active transport is an energy-requiring process that involves transport proteins to move a drug across a membrane against a concentration gradient. In contrast, passive diffusion is a process, in which a drug crosses the membrane according to the concentration gradient from a higher drug concentration to a lower concentration until equilibrium is reached. This mode of passage requires neither help of proteins nor cellular energy to realize the movement across the membrane and is predominant for most drugs. The process of passive diffusion is determined by the combination and fine balance of properties in the molecular scaffold, including lipophilicity, molecular weight, and measures of molecular polarity.[113,132]

Assessment of membrane permeability is an important procedure in the early stages of the drug discovery process, as a poor permeability of a drug intended to target intracellular sites

will result in low efficacy. There are several *in vitro* assays that have been developed to predict the membrane permeability. One common and simple method is the parallel artificial membrane permeability assay (PAMPA), which is also cost-effective and well-suited for high-throughput screening. PAMPA allows for the determination of a compound's diffusion ability from a donor compartment into an acceptor compartment across a membrane filter that supports an artificial membrane. The artificial membrane can be composed of different phospholipids and may vary among experiments. PAMPA does not contain any active transporter and is designed to give an indication of a drug's passive transcellular permeability (Figure 17).[131]

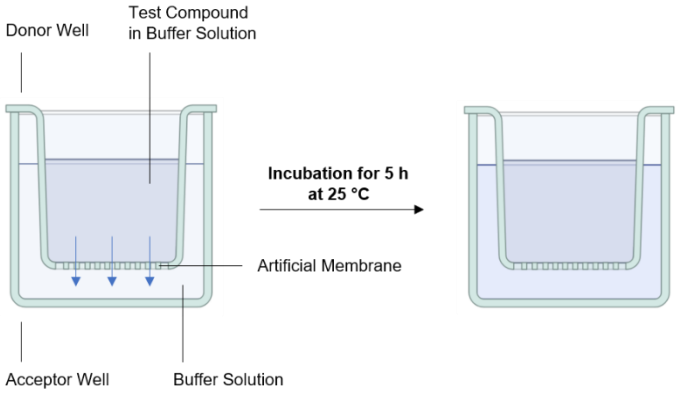

Figure 17: Setup for PAMPA.

The PAMPA was performed following a protocol published by Merck[133], from which the supplies for the assay were also purchased. Therefore, a donor plate with a polyvinylidene fluoride (PVDF) membrane filter pretreated with L-α-phosphatidylcholine was used. The effective permeability (P_e) was calculated using equation 3 (see experimental part 6.2.3). Using testosterone as the reference compound, a P_e value of $(16.5 \pm 5.17) \cdot 10^{-6}$ cm/s was obtained. This is comparable to the literature value of approximately $15.8 \cdot 10^{-6}$ cm/s.[133] The classification into low, moderate, and high solubility depends on the PAMPA setup used. According to a publication by J.GOSCIANSKA[134], in this conventional PAMPA method, solubility is classified as follows: $P_e < 0.1 \cdot 10^{-6}$ cm/s indicates low permeability, $0.1 \cdot 10^{-6}$ to $1 \cdot 10^{-6}$ cm/s indicates medium permeability, and $> 1 \cdot 10^{-6}$ cm/s indicates high permeability. In Table 1, selected P_e values of well-known active compounds are presented, along with their corresponding human absorption values (Fa). The Biopharmaceutical Classification System (BCS) categorizes compounds with human oral absorption exceeding 90% as highly permeable. Values are cited from X. CHEN *et al.*[135].

Table 1: Human absorption and P_e values of well-known active compounds.

Compound	Fa [%]	PAMPA P_e [$\cdot 10^{-6}$ cm/s]
Sulfasalazine	13	0.00 ± 0.00
Acyclovir	16	0.04 ± 0.01
Famotidine	40	0.06 ± 0.00
Terbutaline	60	0.05 ± 0.05
Timolol	90	0.61 ± 0.06
Ibuprofen	95	2.40 ± 0.38
Caffeine	100	1.20 ± 0.10
Nicotine	100	10.47 ± 1.57

In order to determine the permeability of MW-577 **29** and MW-BG-22 **30**, a 10 mM DMSO stock of the test substance was prepared and diluted with PBS buffer (50-fold), yielding a final compound concentration of 200 µM and a DMSO concentration of 2%. The drug-containing donor solution was added in triplicate to wells of the donor plate. Subsequently, the donor plate was placed into the PBS-filled acceptor plate and covered with a lid. Due to the poor solubility of the two lead structures in PBS buffer, an incubation time of 5 h was chosen instead of 16 h. After incubation for 5 h at room temperature (~25 °C), UV/Vis absorption was measured for each well of the acceptor solutions and for previously prepared drug solutions at the theoretical equilibrium. Partial precipitation could be observed for both compounds during the experiment, which may result in deviations of the measured values from the actual permeability. However, MW-577 **29** and MW-BG-22 **30** demonstrated high membrane permeability, with P_e values of $(12.8 \pm 1.69)\cdot 10^{-6}$ and $(4.39 \pm 0.293)\cdot 10^{-6}$ cm/s, respectively.

4.1.4. Metabolic stability

After uptake into the body, most drugs undergo metabolism by various enzymes, resulting in reduced concentrations of active species before reaching the target tissue. This phenomenon is called first-pass effect. This applies in particular to orally administered drugs that pass directly to the liver, which is the main site of metabolism in the body. However, drug metabolism can also occur in other tissues (e.g. kidney, skin, gastrointestinal tract), and some drugs that are administered by a different route (e.g. injection, inhalation) still undergo first-pass

metabolism.[136,137] The purpose of metabolism is to modify foreign compounds so that they are more easily excreted by the body. Polar compounds will be quickly excreted by the kidneys, whereas lipophilic compounds must first be transformed into more polar metabolites to be eliminated successfully. Metabolizing enzymes are able to add polar groups/molecules or to reveal masked polar groups already present in the structure. Such reactions can be classified into phase I, phase II, and in some cases, phase III reactions.[138]

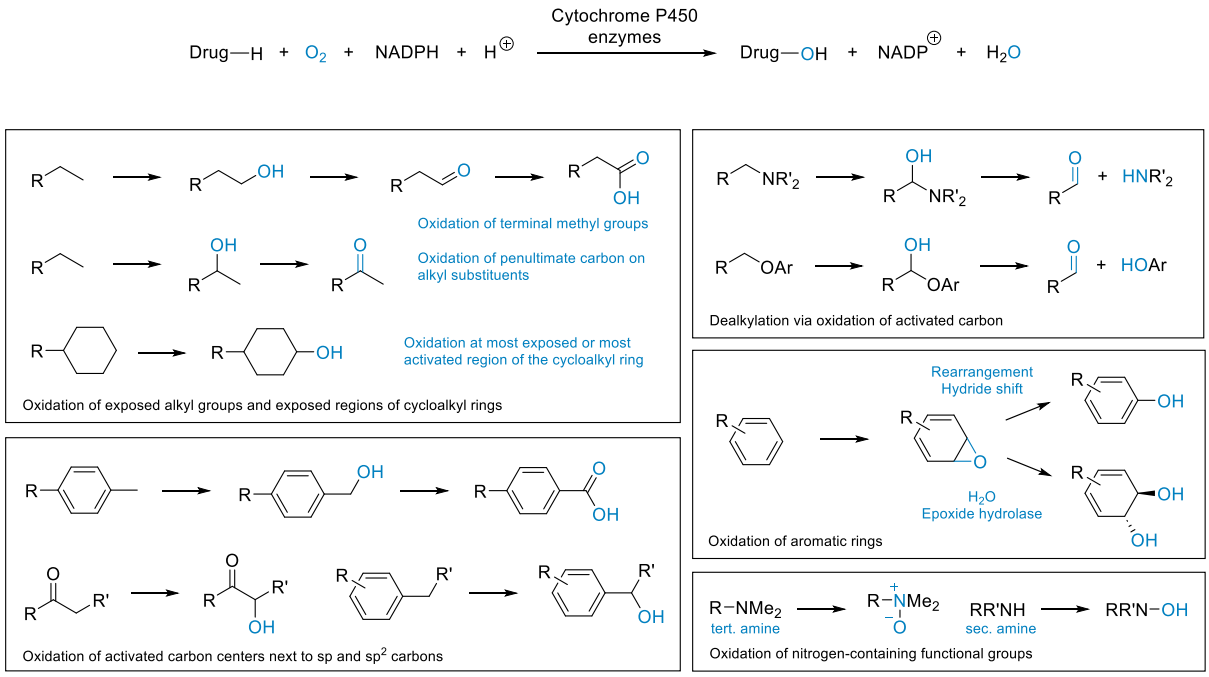

Figure 18: Stoichiometry of oxidation by Cytochrome P450 enzymes and selection of common reactions.[138]

Phase I reactions are functionalizing reactions and include oxidation, reduction, and hydrolysis. Enzymes that are members of the cytochrome P450 family are the most important enzymes in phase I metabolism and are involved in the oxidation of most drugs. Such enzymes have a heme-iron center as active site and mainly function as monooxygenases. In a monooxygenase reaction, cytochrome P450 enzymes utilize molecular oxygen to introduce one oxygen atom into the drug while the other atom is reduced to water, using NADPH (the reduced form of nicotinamide adenine dinucleotide phosphate) as a cofactor (Figure 18). They are responsible for the oxidation of carbon, nitrogen, phosphorus, sulfur, and other atoms.[138–140] Oxidation of carbon can occur if a functional group contains an exposed or activated carbon atom, such as a terminal or penultimate carbon atom on an alkyl chain, the most exposed region of a cycloalkyl ring, an activated carbon atom next to a sp^2 or sp carbon center, an activated carbon atom next to a heteroatom, or a carbon atom in an aromatic ring. Such carbon atoms are hydroxylated to form alcohols and may be further oxidized to form

aldehydes/ketones and carboxylic acids. There are several other oxidative enzymes that play a role in drug metabolism, including flavin-containing monooxygenases, monoamine oxidases, alcohol dehydrogenases, and aldehyde dehydrogenases. In phase I drug metabolism, reductive reactions involving aldehyde, ketone, azo, and nitro groups may also occur, but these are less common than oxidative reactions. Cytochrome P450 enzymes can catalyze reactions in both directions and are responsible for catalyzing some of these reductive reactions. Another common reaction in phase I drug metabolism is the hydrolysis of esters and amides, catalyzed by esterases and peptidases, respectively.[138]

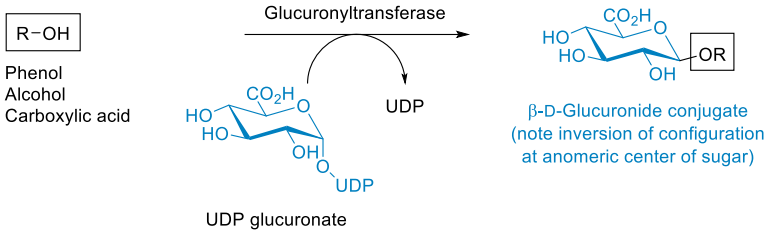

Figure 19: Glucuronidation of alcohols, phenols, and carboxylic acids. [138]

Phase II reactions are conjugation reactions and include methylation, acetylation, sulfation, glucuronidation, and glycine or glutathione conjugation. Generally, polar endogenous molecules are attached to the parent drug or a phase I metabolite, a process that usually leads to increased hydrophilicity and inactivation of the drug.[137] Such reactions are catalyzed by different transferase enzymes found in various organs, such as the liver, bile, kidneys, gastrointestinal tract, lungs, and skin.[139] Glucuronidation is the most common conjugation reaction, in which primarily phenols, alcohols, hydroxylamines, and carboxylic acids react with UDP-glucuronate to form *O*-glucuronides, catalyzed by glucuronyltransferase (Figure 19).[138] Phase II drug conjugates can undergo further metabolism and transporter-mediated excretion from the cells, which is a process also referred to as phase III metabolism.[139]

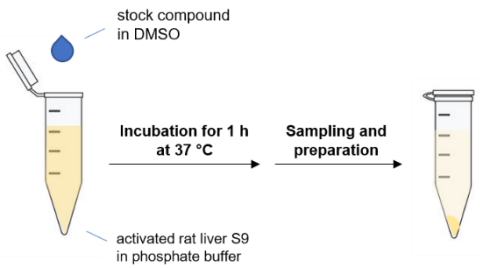

Figure 20: Setup for rat liver S9 stability assay.

There are several *in vitro* assays that have been developed to predict metabolic stability, which is defined as the percentage of parent drug remaining after a certain time interval in the presence of a metabolically active test system. Assessment of metabolic stability is effective in excluding candidates with unfavorable properties in the early stage of drug discovery. Various systems have been applied, including recombinant enzymes, liver microsomes, liver S9 fractions, and hepatocytes.[141,142] In order to determine the metabolic stability of MW-577 **29** and MW-BG-22 **30**, a metabolic stability assay was performed using rat S9 fractions as the source for metabolizing enzymes. S9 fraction is the supernatant obtained after centrifugation of liver homogenate at 9000 g.[143] Unlike liver microsomes, which contain phase I enzymes, S9 fractions include both microsomal and cytosolic components, with the latter containing phase II enzymes. Cell-free systems such as S9 fractions have certain limitations, including enzyme inactivation during preparation, which can lead to variability in enzyme activity, as well as the need to add cofactors during incubation. In contrast, metabolically competent cells like hepatocytes do not require exogenous cofactors and offer a more comprehensive overview of a drug's metabolic profile. However, in comparison to S9 fractions, whole-cell systems tend to be more complex and expensive.[141]

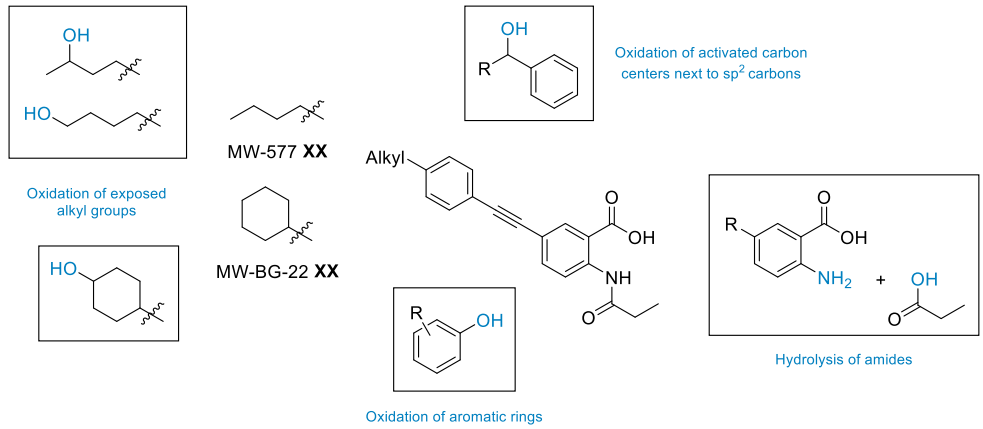

Figure 21: Possible phase I metabolic reactions of MW-577 **29** and MW-BG-22 **30**.

To assess metabolic stability, the phase I metabolism of MW-577 **29** and MW-BG-22 **30** was evaluated using rat S9 fraction. The alkyl groups and aromatic rings of both compounds are prone to oxidation by cytochrome P450 enzymes, whereas the amide groups undergo hydrolysis by peptidases (Figure 21). To measure metabolic stability, rat S9 fraction was first activated by adding magnesium chloride and NADPH in phosphate buffer and then incubated at 37 °C. The experiment was then started by the addition of the test substance dissolved in DMSO. Aliquots were taken after 0 and 1 h and prepared to be analyzed by HPLC. The metabolic stability was calculated using equation 4 (see experimental part 6.2.4). The samples

were prepared in triplicate and another aliquot was sampled after 3 h for the graphical representation of the compound's metabolic conversion. 7-Ethoxycoumarin was used as a reference substance and metabolic stability was calculated to 75 ± 8%. Depending on the assay conditions reported in the literature, different values can be found, e.g. 50-65% in a study from J. D. MANNA *et al.*[144] and approximately 80% in a study from G. C. FORTI *et al.*[145]. It is also important to note that the enzyme composition in the rat S9 fraction can vary.[146] The measured value falls within this range. The recorded fluorescent chromatograms of MW-BG-22 **30** are shown in Figure 22 as an example.

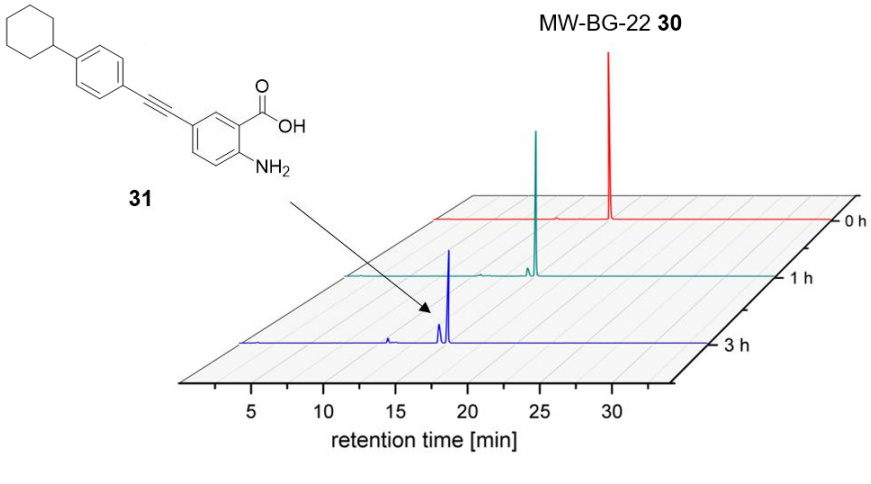

Figure 22: HPLC-chromatograms of MW-BG-22 **30** recorded after incubation for 0, 1 and 3 h in rat S9 fraction.

The chromatograms obtained for MW-BG-22 **30** show the decrease in compound concentration and formation of metabolite **31**, which refers to the corresponding amine. The metabolite **31** was identified by co-injection and comparison of the retention times. MW-BG-22 **30** exhibited a metabolic stability of 73 ± 6%. MW-577 **29** showed a similar metabolism profile like MW-BG-22 **30** in rat S9 fraction, although a low metabolic stability of 32 ± 6% was observed and an increased formation of the corresponding amine could be detected. The alkyl substituents may influence steric hindrance, electronic properties, and lipophilicity, thereby affecting the binding affinity to hydrolytic enzymes and subsequently impacting the rate of enzymatic hydrolysis.

The metabolic stability of a drug should be high enough to achieve sufficient *in vivo* exposure levels, however, excessive metabolic stability can lead to unwanted adverse reactions, toxicities, and drug interactions, as the drug remains in the body for longer periods.[147] It should be mentioned that *in vitro* preparations with subcellular fractions may underpredict *in vivo* metabolizing enzyme activities.[148] Moreover, only phase I metabolism was investigated in this

experiment. Previous studies conducted by the group of C. MEIER indicated a loss of activity for other phenylethynyl anthranilic acid derivatives after the cleavage of the amide group.[111] Therefore, a stabilization of this moiety was aimed for MW-577 **29** and MW-BG-22 **30**.

4.2. Human DHODH activity of MW-577 29 and MW-BG-22 30

The inhibitory potential of MW-577 **29** and MW-BG-22 **30** against human DHODH was investigated using a modified protocol developed by N. C. LAUBACH, which was based on the method established by H. MUNIER-LEHMANN *et al.*[149]. The enzyme assay was performed at pH 8.0 and 25 °C. For this purpose, the enzyme (35 nM) was added to a solution consisting of substrate L-DHO (100 µM), cofactor ubiquinone-1 (CoQ_1, 25 µM), the inhibitor (varying concentrations), and redox dye 2,6-dichlorophenolindophenol (DCPIP, 60 µM) in Tris-HCl/Triton X-100 buffer. DHODH activity was determined by monitoring the decrease in DCPIP absorbance at 600 nm with a spectrometer.

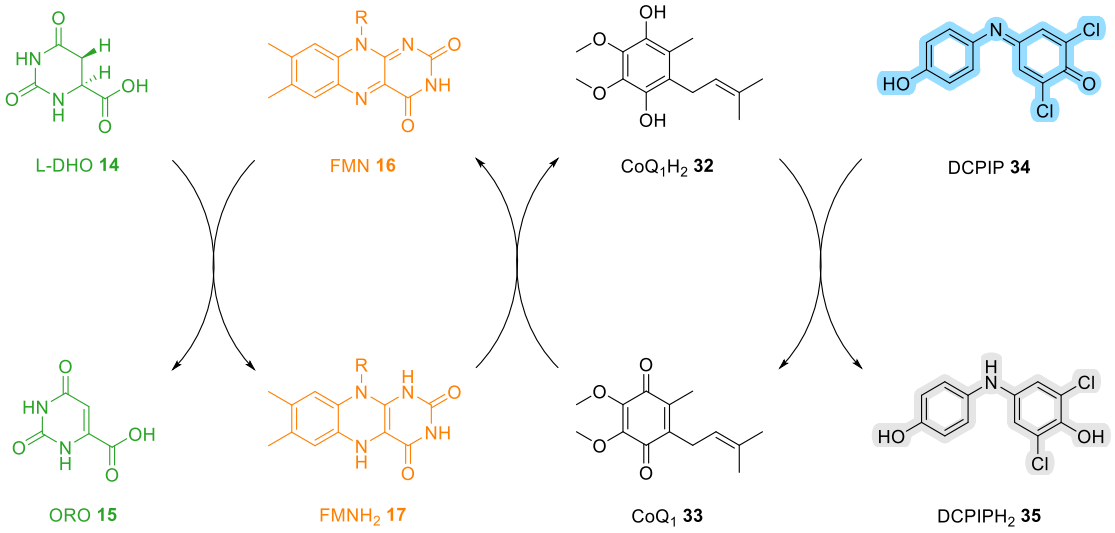

Figure 23: Redox cycle of DHODH with DCPIP reduction introduced.[150]

The blue redox dye DCPIP **34** has a maximum absorption at 600 nm and becomes colorless upon reduction.[151] This occurs when DCPIP **34** is introduced into the redox cycle of DHODH, where the substrate L-DHO **14** is converted to ORO **15** using FMN **16** and CoQ_1 **33** as redox partners (Figure 23). If an inhibitor prevents CoQ_1 **33** from accessing its binding site, the redox cycle is interrupted, and DCPIP **34** is not reduced to its colorless form **35**.

To obtain a preliminary approximation of the inhibitory potency on isolated hDHODH, the percentage inhibition of hDHODH at a certain concentration was determined. A low concentration of 50 nM was chosen because MW-577 **29** and MW-BG-22 **30** both exhibited antiviral

activities against Toscana and Hazara virus in the nanomolar range in previously conducted cell-based assays. The decrease in DCPIP absorbance at 600 nm was measured over a period of 25 min, during which a linear range was observed for the first 200 sec before it transitioned into a flattening curve (Figure 24). The percentage DHODH inhibition can be determined from the negative slope of the initial linear range and by comparing it with the slope obtained when no inhibitor is added. The decrease rate of the absorbance curve is lower for more potent inhibitors.

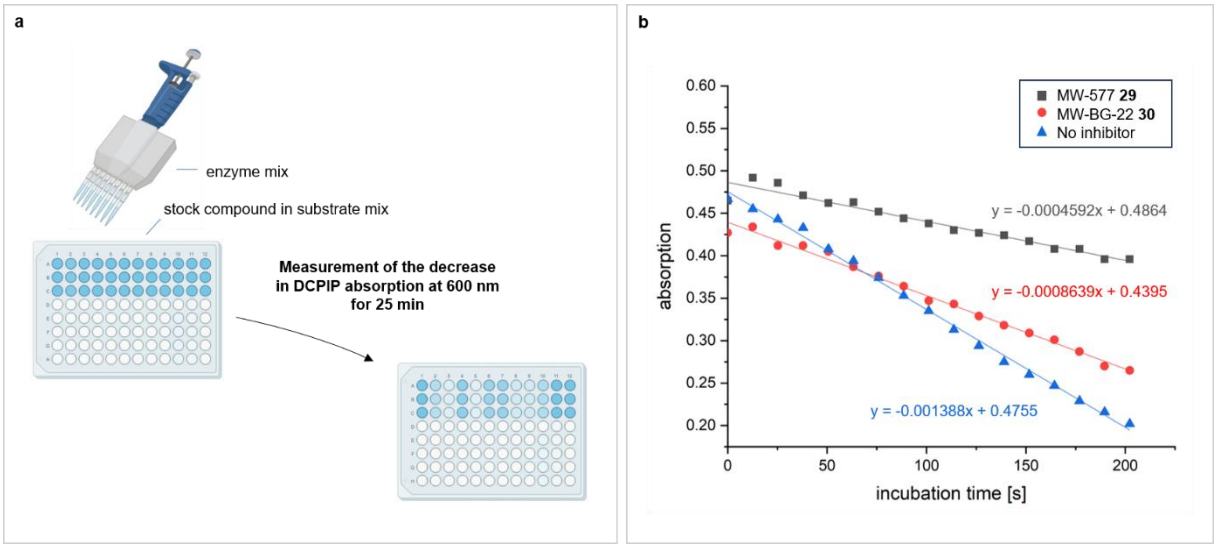

Figure 24: (a) Setup for DHODH assay (b) DCPIP absorbance curves obtained when MW-577 **29** and MW-BG-22 **30** are added.

At a concentration of 50 nM, the hDHODH inhibition potencies of MW-577 **29** and MW-BG-22 **30** were determined to be 62 ± 4% and 39 ± 3%, respectively. These results indicate that both lead structures are highly potent hDHODH inhibitors. A hDHODH inhibition of 50% at an inhibitor concentration of 50 nM corresponds to an IC_{50} value of 50 nM. Therefore, a high inhibition potency below 50 nM is expected for MW-BG-22 **30**. For comparison, Brequinar **20**, another highly potent hDHODH inhibitor with an IC_{50} value of approximately 2 nM, demonstrated a hDHODH inhibition potency of 88 ± 2% in the assay.

4.3. Antiviral activities of MW-577 29 and MW-BG-22 30

MW-577 **29** and MW-BG-22 **30** were tested for their antiviral activities against various HF viruses in cell-based assays. Antiviral data for TOSV and HAZV in Vero cells were provided by G. QUERAT *et al.* (Aix-Marseille University), for LASV and CCHFV in Vero cells by L. OESTEREICH *et al.* (Bernhard Nocht Institute for Tropical Medicine, Hamburg), for YFV and DENV

in Huh-7 cells by R. BARTENSCHLAGER *et al.* (University Hospital Heidelberg) and for EBOV in Vero cells by T. HOENEN *et al.* (Friedrich-Loeffler-Institut, Riems). The determined EC_{50} values are presented in Table 2.

Table 2: Anti-HFV-data of MW-577 **29** and MW-BG-22 **30**.

Compound	EC_{50} **TOSV** (Vero)	EC_{50} **HAZV** (Vero)	EC_{50} **LASV** (Vero)	EC_{50} **CCHFV** (Vero)	EC_{50} **YFV** (Huh-7)	EC_{50} **DENV** (Huh-7)	EC_{50} **EBOV** (Vero)
MW-577 **29**	5.9 nM	5.4 nM	n.d.	n.d.	27.8 nM	10.9 nM	32 nM
MW-BG-22 **30**	3 nM	0.9 nM	9.8 nM	26.6 nM	< 2.5 nM	< 2.5 nM	19 nM

MW-577 **29** and MW-BG-22 **30** were selected as lead structures due to the high antiviral activities determined for TOSV and HAZV (≤ 10 nM). MW-BG-22 **30** was further tested against two other viruses of the order *Hareavirales*, the mammarenavirus LASV and orthonairovirus CCHFV, for which EC_{50} values of 9.8 nM and 26.6 nM were determined, respectively. Furthermore, MW-BG-22 **30** exhibited high antiviral activities of < 2.5 nM against the orthoflaviviruses YFV and DENV. In contrast, MW-577 **29** was less active against YFV and DENV but still demonstrated notable antiviral activities of 27.8 nM and 10.9 nM, respectively. Both compounds were also tested against EBOV, which belongs to the family *Filoviridae*. MW-577 **29** exhibited an antiviral activity of 19 nM, while MW-BG-22 **30** showed an antiviral activity of 32 nM. Overall, high antiviral activities against a broad range of HF viruses were observed for MW-577 **29** and MW-BG-22 **30**.

Table 3: Additional antiviral and toxicity data of MW-577 **29** and MW-BG-22 **30**.

Compound	EC_{50} **HCV** (Vero)	EC_{50} **CHIKV** (BHK)	CC_{50} **Vero**	CC_{50} **Huh-7**	CC_{50} **BHK**
MW-577 **29**	11.7 nM	n.d.	7 μM	> 50 μM	n.d.
MW-BG-22 **30**	7 nM	5.8 nM	7 μM	43 μM	> 100 μM

In addition, MW-577 **29** and MW-BG-22 **30** were tested for their antiviral activity against HCV in Vero cells by B. KÜMMERER *et al.* from University Hospital Bonn. HCV also belongs to the family *Flaviviridae*, like YFV and DENV, but does not cause symptoms typical for VHFs. MW-577 **29** and MW-BG-22 **30** exhibited high antiviral activities against HCV, with values of

11.7 nM and 7 nM, respectively (Table 3). MW-BG-22 **30** was further tested against the alphavirus CHIKV (Chikungunya virus) by B. KÜMMERER *et al.* in BHK cells, for which an EC_{50} value of 5.8 nM was determined. These data support the hypothesis that DHODH inhibitors provide broad-spectrum antiviral activity *in vitro*.

The toxicity of MW-577 **29** and MW-BG-22 **30** in the different cell lines was also evaluated (Table 3). In Vero cells, a comparably low CC_{50} value of 7 µM was determined for both compounds, however, the ratio between CC_{50} and EC_{50} values greatly exceeds the suggested value of 10. The lowest SI in Vero cells was calculated for MW-BG-22 **30** when infected with CCHFV and was found to be greater than 250. Furthermore, MW-577 **29** and MW-BG-22 **30** showed low cytotoxicity in Huh-7 cells, with CC_{50} values of approximately 50 µM, while MW-BG-22 **30** also exhibited low toxicity in BHK cells, with a CC_{50} value > 100 µM.

4.4. Lead optimization

The second aim of this thesis was to modify the lead structures MW-577 **29** and MW-BG-22 **30** in a rational structure-based drug design approach. Knowledge of the three-dimensional structure of DHODH was applied to propose substituents with appropriate electronic properties that complement the shape of the enzyme pocket. Substituents were chosen that were predicted to improve the physicochemical properties of the compound, especially aqueous solubility and enzymatic stability, while preserving high binding affinity. Newly synthesized derivatives were evaluated for their physicochemical properties and hDHODH inhibition potential using the assays discussed in the previous chapters (4.1 and 4.2). A selection of the most potent compounds was further tested in cell-based assays against HF and other RNA viruses.

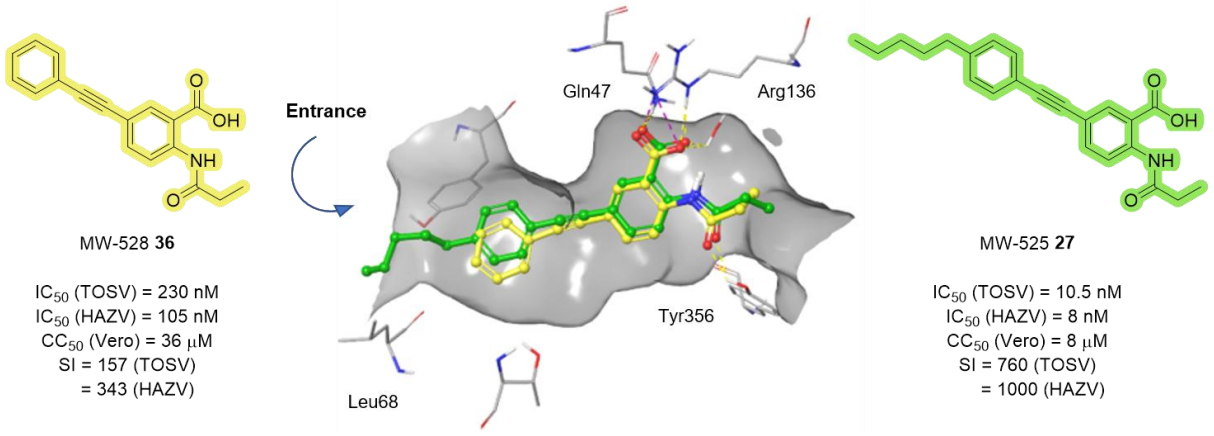

Figure 25: Binding-motif of MW-528 **36** (yellow) in the lipophilic tunnel of hDHODH overlaid with docking pose of MW-525 **27** (green).

The identification of potential drug candidates was conducted by performing docking simulation on the X-ray structure of recombinant hDHODH in complex with phenylethynyl anthranilic acid derivative MW-528 **36**. Initially, it was intended to prepare an X-ray structure of the enzyme co-crystallized with MW-525 **27**, however, the compound is likely too hydrophobic, and its long alkyl chain may be too flexible for successful co-crystallization. Figure 25 shows the binding site for MW-528 **36** in the crystal complex with hDHODH overlaid with the proposed binding mode of MW-525 **27** from the docking simulation experiment. X-ray and docking data were both kindly provided by N. C. LAUBACH. The binding motif of MW-528 **36** is similar to that of brequinar **20**, as both compounds feature a carboxylate group that forms a salt bridge with Arg136 and hydrogen bonds with Gln47, as well as a buried water molecule that, in turn, interacts with Thr360 (not shown) via another hydrogen bond. Unlike brequinar **20**, the carbonyl oxygen of the amide group forms an additional hydrogen bond with the side chain of Tyr356, which likely contributes to the high binding affinity of the phenylethynyl anthranilic acid compound class. Compared to MW-528 **36**, the additional alkyl chain in MW-525 **27** allows hydrophobic interactions with non-polar side chains at the entrance of the pocket. This enhancement might improve binding affinity, leading to better antiviral activities in cell-based assays. For example, MW-528 **36** is 20-fold less active against TOSV than MW-525 **27**. In the hydrophobic entrance, Leu68 interacts with the alkyl chain of MW-525 **27** and pushes the aromatic ring slightly upward, which enables more optimal interactions with Arg136 and Gln47.

4.4.1. Modification of the terminal alkyl group

In the first optimization cycle, polar groups should be introduced to the terminal alkyl groups of MW-577 **29** and MW-BG-22 **30** to enhance the aqueous solubility. In the best case, the high binding affinity should remain unchanged or even improve due to the formation of additional interactions between the newly introduced polar group and the side chains of amino acids in the binding pocket. Polar groups that should be introduced to the structure of MW-577 **29** include amines, ketones, amides and polyethylenglycol (PEG) groups.

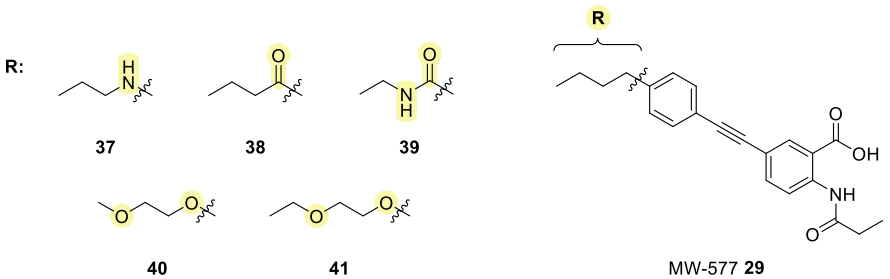

Figure 26: Synthesized derivatives (**37**-**41**) of MW-577 **29** during optimization cycle 1.

Derivatives of MW-577 **29** that were selected for synthesis in the first optimization cycle are shown in Figure 26. The synthesis procedures for all derivatives are detailed in section 4.5 at the end of this chapter. In this section 4.4, the obtained data regarding physicochemical properties, hDHODH inhibition potential, and antiviral activities are discussed.

All derivatives of MW-577 **29** (**37**-**41**) were investigated for their kinetic solubility in PBS (pH 7.4) and hDHODH inhibition potential using the assays described previously. The respective data are listed in Table 4. All modifications led to increased aqueous solubility, with values of about 190 µM for derivatives **37**, **38** and **41**, and ≥200 µM for derivatives **39** and **40**. The modified compounds are at least 2-fold more soluble in PBS (pH 7.4) compared to lead compound **29**, which exhibited a kinetic solubility of 65 ± 2 µM.

Analysis of the percentage hDHODH inhibition at an inhibitor concentration of 50 nM showed that the inhibition potency of amine derivative **37** is comparable to that of MW-577 **29**, with a value of about 68%, whereas all other derivatives **38**-**41** are slightly less potent, with values ranging from 41% to 48%. Nevertheless, all derivatives of MW-577 **29** (**37**-**41**) are strong hDHODH inhibitors and should exhibit potencies in the nanomolar range.

Table 4: Data for kinetic solubility and hDHODH inhibition of MW-577 **29** and analogs **37**-**41**.

Compound	29	37	38	39	40	41
Kin. Sol. in PBS pH 7.4 [µM]	65 ± 2	195 ± 5	187 ± 8	≥ 200	≥ 200	187 ± 6
% hDHODH inhibition at 50 nM	62 ± 4	68 ± 6	48 ± 3	41 ± 3	41 ± 4	46 ± 4

Amino functional groups are present in many drugs and can act either as hydrogen bond acceptors or hydrogen bond donors. The lone electron pair available at the nitrogen atom can function as a hydrogen bond acceptor, while the N-H groups of primary and secondary amines serve as hydrogen bond donors. In the case of aromatic amines, the lone electron pair interacts with the aromatic ring, which indicates that the aromatic amine can only act as a hydrogen bond donor.[138] According to the proposed binding mode of **37** from the docking simulation experiment (Figure 27a), the amino group forms a hydrogen bond with the hydroxyl group of Tyr38. Additionally, the aromatic ring of **37** is involved in van der Waals interactions with the aromatic ring of Tyr38.

The formation of additional bonds contributing to high binding affinity was also proposed for the amide group in derivative **39** (Figure 27b). According to docking simulation experiments, the amide group interacts with side chains of Tyr38 and Leu68 via hydrogen bonds. Like **37**, the aromatic ring of amide derivative **39** is involved in van der Waals interactions with the

aromatic ring of Tyr38. However, in comparison to lead structure **29**, a decrease in inhibition potency was observed.

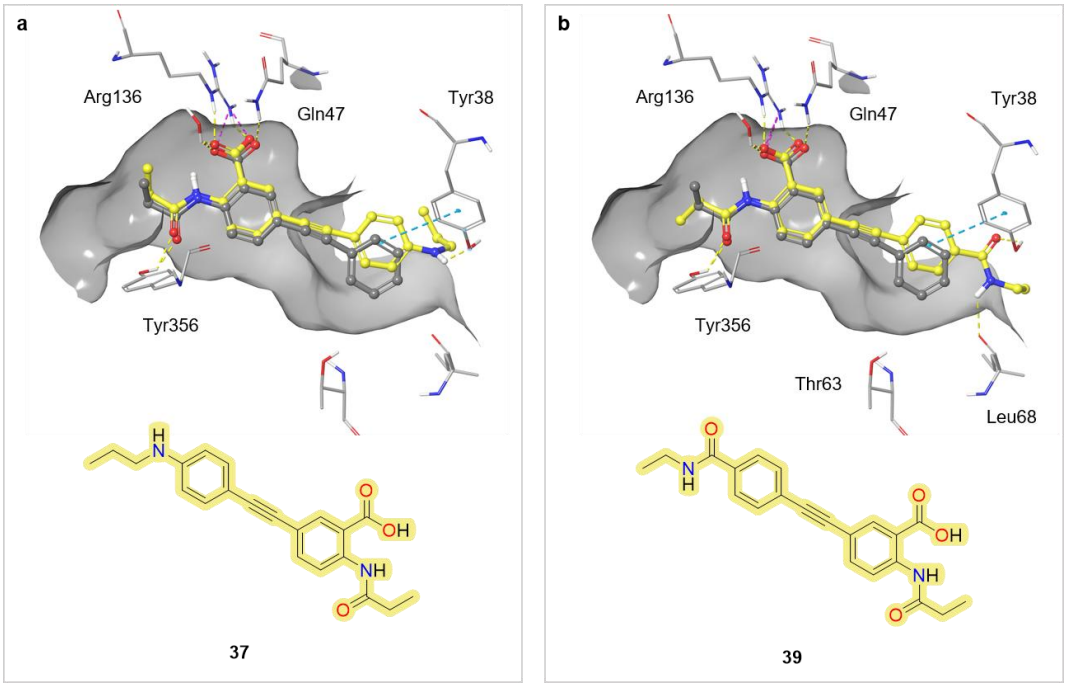

Figure 27: Binding-motif of MW-528 **36** (grey) in the lipophilic tunnel of hDHODH overlaid with docking pose (yellow) of **37** (a) and **39** (b).

In collaboration with J. NEYTS *et al.* from the Rega Institute in Leuven, analogs **37** and **39** were tested against YFV in Huh-7 cells (Table 5). A high antiviral activity of <19.5 nM and low cytotoxicity of 78.5 µM were observed for amine analog **37**. Although amide analog **39** is also a potent hDHODH inhibitor, it was 580-fold less active, with an EC_{50} value of 11.3 µM. With a P_e value of $(0.608 \pm 0.158) \cdot 10^{-6}$, amide analog **39** exhibited only moderate permeability in PAMPA and was about 2.5-fold less permeable than amine analog **37**, for which a P_e value of $(1.60 \pm 0.417) \cdot 10^{-6}$ was determined. Furthermore, the amide group of **39** is prone to metabolism by amidases, potentially leading to cleavage before the compound reaches the target tissue.

Table 5: Anti-YFV and toxicity data provided by J. NEYTS *et al.*.

Compound	37	39
EC_{50} **YFV** (Huh-7) [µM]	< 0.0195	11.3
CC_{50} **Huh-7** [µM]	78.5	> 100

Due to the high antiviral activity determined for YFV, further antiviral assays were performed with amine analog **37** by our previously mentioned collaborators (chapter 4.3). Antiviral data are shown in Table 6. Compound **37** was again tested against YFV, revealing an antiviral activity in the similarly low nanomolar range of 25 nM. Other HF viruses that were investigated are DENV and EBOV, for which EC_{50} values of 16 nM and 6 nM were determined, respectively. In addition, **37** was tested against HCV and CHIKV, yielding EC_{50} values of 5.2 nM and 14.7 nM, respectively. Antiviral data obtained for analog **37** are comparable to those for lead compound MW-577 **29**. Amine analog **37** exhibited low cytotoxicity in Huh-7 cells, with a CC_{50} value of > 50 µM. The maximum concentration measured in Vero cells was 4 µM, and since no cytotoxic effects were observed, the CC_{50} could be significantly higher. Nevertheless, even at this low concentration, the suggested SI value of 10 would still be substantially exceeded.

Table 6: Antiviral and toxicity data of **37**.

Compound	EC_{50} **YFV** (Huh-7)	EC_{50} **DENV** (Huh-7)	EC_{50} **EBOV** (Vero)	EC_{50} **HCV** (Huh-7)	EC_{50} **CHIKV** (BHK)	CC_{50} **Vero**	CC_{50} **Huh-7**
37	25 nM	16 nM	6 nM	5.2 nM	14.7 nM	> 4 µM	> 50 µM

Amine analog **37** was additionally investigated for its PK properties (Table 7). With a molecular weight of 350 g/mol, the determined kinetic solubility of 195 ± 5 µM corresponds to a concentration of 68 ± 2 µg/mL, indicating high solubility. In contrast, lead compound **29** had a 3-fold lower solubility, with a concentration of 22 ± 1 µg/mL. A higher aqueous solubility often correlates with a lower logD value and lower permeability. For amine analog **37**, a logD value of 2.10 and a P_e value of $(1.60 \pm 0.417) \cdot 10^{-6}$ were determined.

Table 7: PK data of lead structure **29** and propylamine analog **37**.

Compound	**29**	**37**
Kin. Sol. in PBS pH 7.4 [µM]	65 ± 2	195 ± 5
Kin. Sol. in PBS pH 7.4 [µg/mL]	22 ± 1	68 ± 2
LogD (PBS pH 7.4/ octanol)	≥ 3.3	2.10 ± 0.09
PAMPA P_e [cm/s]	$(12.8 \pm 1.69) \cdot 10^{-6}$	$(1.60 \pm 0.417) \cdot 10^{-6}$

The amine modification in **37** resulted in a significant increase in aqueous solubility, while hDHODH inhibition potency and antiviral activities have remained roughly unchanged compared to lead structure MW-577 **29**. Furthermore, **37** demonstrated high membrane permeability in PAMPA. Therefore, the amine moiety was deemed as a suitable modification for the continued development of a drug candidate.

Regarding the alkyl modification of MW-BG-22 **30**, seven derivatives (**42**-**48**) were selected for synthesis in the first optimization cycle (Figure 28). To enhance polarity and aqueous solubility, the cyclohexyl substituent was replaced by more polar functional groups, including various nitrogen, oxygen, and sulfur-containing heterocycles such as piperidine and morpholine.

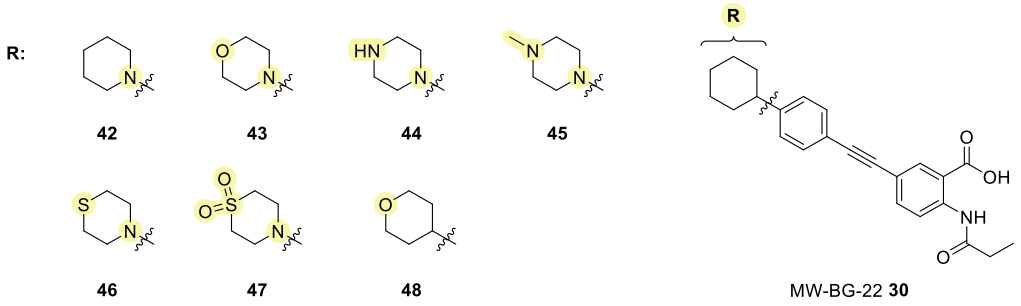

Figure 28: Synthesized derivatives (**42**-**48**) of MW-BG-22 **30** during optimization cycle 1.

Data obtained for analogs **42**-**48** from the kinetic solubility and hDHODH inhibition assay are listed in Table 8. Except for piperazine derivatives **44** and **45**, as well as thiomorpholine derivative **46**, all other modifications again led to a significant increase in aqueous solubility. Piperazine derivative **44** is 3-fold, thiomorpholine derivative **46** is 6-fold, and compounds **42**, **43**, **47**, and **48** are at least 15-fold more soluble in PBS (pH 7.4) than lead structure MW-BG-22 **30**. The kinetic solubility assay could not be carried out with piperazine analog **45**, since it was not soluble under the assay conditions used.

Table 8: Data for kinetic solubility and hDHODH inhibition of MW-BG-22 **30** and analogs **42**-**48**.

Compound	30	42	43	44	45	46	47	48
Kin. Sol. in PBS pH 7.4 [µM]	12 ± 3	187 ± 6	184 ± 1	41 ± 7	n.d.	75 ± 6	≥ 200	≥ 200
% hDHODH inhibition at 50 nM	39 ± 3	41 ± 5	55 ± 4	20 ± 4	28 ± 5	48 ± 5	16 ± 7	57 ± 3

Analysis of the percentage hDHODH inhibition at an inhibitor concentration of 50 nM revealed that both piperazine analogs (**44**, **45**) and thiomorpholine dioxide analog **47** are less potent than MW-BG-22 **30**, with inhibition values around 20%. In contrast to the cyclohexyl group of MW-BG-22 **30**, the six-membered heterocycles of analogs **44**, **45**, and **47** offer a high polar surface area, which may not align with the lipophilic character at the entrance of the tunnel. Piperidine analog **42** shows comparable potency to MW-BG-22 **30**, demonstrating a hDHODH inhibition rate of approximately 40%. Notably, for all other analogs, an increase in inhibition potency was observed. Morpholine analog **43** and tetrahydropyran analog **48** exhibited the strongest potential for hDHODH inhibition, achieving values around 60%.

Table 9: Anti-YFV and toxicity data provided by J. NEYTS *et al.*.

Compound	**42**	**43**	**44**	**45**	**47**
EC_{50} **YFV** (Huh-7) [µM]	0.072	0.401	1.5	1.7	14.3
CC_{50} **Huh-7** [µM]	> 100	> 100	> 100	> 100	> 100

Anti-YFV data were provided by J. NEYTS *et al.* for compounds **42**-**45** and **47**, as detailed in Table 9. Compounds **44**, **45** and **47**, which showed relatively poor results in the enzyme assay, also exhibited low antiviral activities against YFV with EC_{50} values > 1 µM. In contrast, piperidine analog **42** demonstrated a strong antiviral activity, with an EC_{50} value of 72 nM. While morpholine analog **43** is a more potent inhibitor of hDHODH, with an EC_{50} value of 401 nM, it is 6-fold less active against YFV compared to piperidine analog **42**. Notably, all compounds showed low cytotoxicity (≥ 100 µM).

Table 10: Antiviral and toxicity data of **42** and **43**.

Compound	EC_{50} **YFV** (Huh-7)	EC_{50} **DENV** (Huh-7)	EC_{50} **EBOV** (Vero)	EC_{50} **HCV** (Huh-7)	EC_{50} **CHIKV** (Huh-7)	CC_{50} **Vero**	CC_{50} **Huh-7**
42	62.4 nM	31.1 nM	n.d.	25 nM	n.d.	n.d.	> 50 µM
43	610 nM	159 nM	166 nM	323 nM	271 nM	> 4 µM	> 100 µM

Additional antiviral data were obtained for piperidine **42** and morpholine analog **43**, as listed in Table 10. Both compounds **42** and **43** were tested against DENV, HCV, and, once again, YFV. Piperidine analog **42** exhibited high antiviral activities, with EC_{50} values ranging from 25 to 62 nM, whereas morpholine analog **43** demonstrated moderate activity, with values be-

tween 159 and 610 nM. Compound **43** was further tested against EBOV and CHIKV, showing moderate antiviral activities of 166 nM and 271 nM, respectively.

Although piperidine analog **42** and morpholine analog **43** demonstrate comparable potencies against hDHODH, a significant disparity exists in their antiviral activities. To explore the factors contributing to this observation, both compounds were investigated for their PK properties (Table 11). While their kinetic solubility is identical, they differ in terms of lipophilicity and membrane permeability. The determined concentration of 70 µg/mL is 15 times higher than for MW-BG-22 **30**, indicating high solubility. In comparison to MW-BG-22 **30**, piperidine analog **42** and morpholine analog **43** both exhibited lower lipophilicity, with logD values of 2.70 and 1.13, respectively. The difference in antiviral activity may be attributed to the observation that piperidine analog **42** was about 20 times more permeable in PAMPA than morpholine analog **43**, with P_e values of $(10.7 \pm 0.704) \cdot 10^{-6}$ and $(0.505 \pm 0.357) \cdot 10^{-6}$, respectively.

Table 11: PK data of MW-BG-22 **30**, piperidine analog **42** and morpholine analog **43**.

Compound	30	42	43
Kin. Sol. in PBS pH 7.4 [µM]	12 ± 3	187 ± 6	184 ± 1
Kin. Sol. in PBS pH 7.4 [µg/mL]	4.5 ± 1	70 ± 2	70 ± 1
LogD (PBS pH 7.4/ octanol)	≥ 3.3	2.70 ± 0.06	1.13 ± 0.09
PAMPA P_e [cm/s]	$(4.39 \pm 0.293) \cdot 10^{-6}$	$(10.7 \pm 0.704) \cdot 10^{-6}$	$(0.505 \pm 0.357) \cdot 10^{-6}$

The incorporation of piperidine and morpholine modifications in compounds **42** and **43**, respectively, resulted in a significant enhancement of aqueous solubility compared to the lead structure MW-BG-22 **30**, while preserving strong potency against hDHODH. Although both modified compounds demonstrate lower activity in cell-based antiviral assays relative to MW-BG-22 **30**, their improved aqueous solubility is crucial for oral administration. This property suggests that *in vivo* efficacy may be enhanced despite the lower *in vitro* potencies observed. Consequently, the piperidine and morpholine moieties were selected for further development of potential drug candidates.

Among the modifications selected to thus far, the propylamine and piperidine moiety feature exposed aliphatic carbon atoms that are prone to oxidation by CYP enzymes.[138] During aliphatic oxidation, a hydrogen atom is abstracted from the exposed or activated carbon atom, leading to the formation of a radical species, which is subsequently oxidized to an alcohol.[152] To mitigate oxidative metabolism, fluorine substitution at the metabolic labile site is common-

ly employed. Given the significant electronegativity difference between carbon and fluorine, the C-F bond is recognized as one of the strongest bonds in organic chemistry. Additional benefits of fluorine substitution include the modulation of the compound's acidity, lipophilicity and hydrogen bonding capacity. The strong inductive effect of fluorine alters electron distribution, which can impact adjacent acidic or basic centers and, consequently, the overall pK_a of a molecule.[153,115]

Fluorine substitution is a widely used strategy in medicinal chemistry for modulating the lipophilicity of a compound. While aromatic fluorination typically increases lipophilicity, fluorination of aliphatic systems can result in decreased lipophilicity.[153] Additionally, fluorination is increasingly utilized to enhance a compound's binding affinity for target proteins. The alteration of electron distribution through fluorine substitution influences the polarity of other functional groups that interact with the side chains of amino acids in the binding pocket. Furthermore, fluorine atoms can also interact directly with the protein, e.g. by acting as hydrogen bond acceptors.[115]

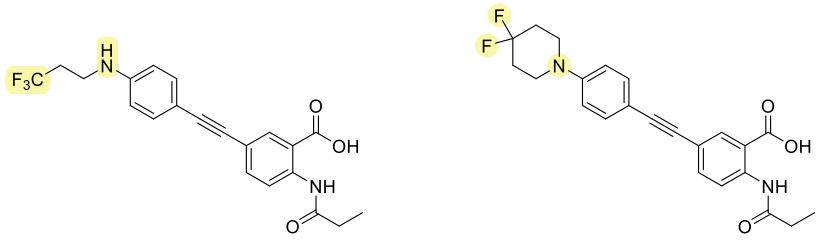

49 **50**

Figure 29: Fluorinated compounds **49** and **50** from optimization cycle 1.

The fluorination of the exposed carbon atoms in the alkyl groups of **37** and **42** should yield the fluorinated analogs **49** and **50** (Figure 29). The determined PK data is shown in Table 12, along with data from the hDHODH inhibition assay. In this case, aliphatic fluorination of **37** and **42** did not result in a decrease in kinetic solubility in PBS buffer. In fact, no precipitation was observed during the kinetic solubility assay after 24 h, with solubility rising from 68 ± 2 to ≥ 80 µg/mL for the amine analogs (**37** and **49**) and from 70 ± 2 to ≥ 82 µg/mL for the piperidine analogs (**42** and **50**). This increase in solubility correlates with a decrease in logD values for both fluorinated compounds, dropping from 2.10 to 1.96 for **49** and from 2.70 to 2.46 for **50**. Additionally, the permeability of the fluorinated amine compound **49** was assessed using PAMPA, revealing that permeability also slightly decreased with fluorination. The fluorinated compound **49** exhibited a P_e value of $(0.996 \pm 0.0620) \cdot 10^{-6}$ cm/s, while its non-

fluorinated analog **37** showed a permeability approximately twice as high, with a P_e value of $(1.60 \pm 0.417) \cdot 10^{-6}$ cm/s.

Analysis of the percentage hDHODH inhibition at an inhibitor concentration of 50 nM revealed that the inhibition potency remained unchanged following aliphatic fluorination of compounds **37** and **42**. The propylamine compound **37** and its fluorinated analog **49** exhibited a hDHODH inhibition of approximately 70%, whereas the piperidine compound **42** and its fluorinated analog **50** showed inhibition in the range of 45-50%.

Table 12: PK and hDHODH inhibition data of fluorinated compounds **49** and **50**.

Compound	49	50
Kin. Sol. in PBS pH 7.4 [µM]	≥ 200	≥ 200
Kin. Sol. in PBS pH 7.4 [µg/mL]	≥ 80	≥ 82
LogD (PBS pH 7.4/ octanol)	1.96 ± 0.12	2.46 ± 0.07
PAMPA P_e [cm/s]	$(0.996 \pm 0.0620) \cdot 10^{-6}$	n.d.
% hDHODH inhibition at 50 nM	70 ± 8	50 ± 5

Aliphatic fluorination of the exposed carbon atoms in compounds **37** and **42** resulted in an increased aqueous solubility while maintaining a high binding affinity towards hDHODH. Furthermore, fluorination of these exposed carbon atoms, which are susceptible to metabolic attack, can prevent oxidative metabolism by CYP and enhance the compound's stability. Although antiviral data are lacking, both fluorine modifications were considered for the further development process.

Two additional compounds, the bicyclic derivatives **51** and **52** shown in Figure 30, were synthesized during the first optimization cycle. These derivatives are derived from the structure of the propylamine compound **37**.

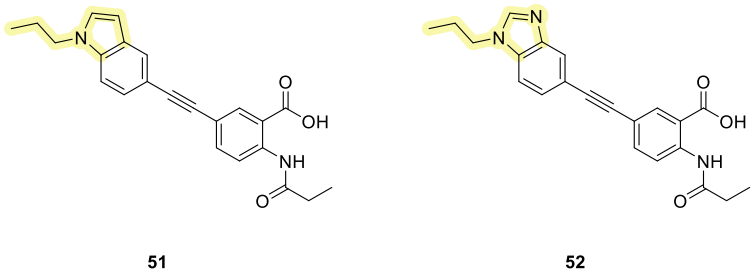

51 52

Figure 30: Bicyclic compounds **51** and **52** from optimization cycle 1.

Replacing the propylamine moiety in compound **37** with an indole or benzimidazole scaffold is expected to enhance the ligand's rigidity. The strategy of rigidification is commonly employed in medicinal chemistry to reduce side effects and improve binding affinity. Among the numerous conformations that flexible ligands can adopt, only one conformation typically triggers the proper function of the protein. It is possible that the other conformations may bind to other proteins, resulting in undesirable biological responses. By reducing the number of potential conformations, the molecule is more likely to exist in the active conformation, thereby binding more readily to the target protein while minimizing binding to other proteins.[138]

Regarding the thermodynamics of binding, a flexible ligand must become more ordered to adopt the active conformation during the binding process, which results in a decrease in entropy. In other words, if the ligand is already in its active conformation, there is no loss of entropy. However, synthesizing rigidified structures may be more complex, and it is uncertain whether rigidification will preserve the active conformation.[138]

The primary challenge in designing rigidified ligands is ensuring that their shape fits perfectly into the binding site of the target protein, as the ability to adopt different conformations that may bind is minimized. This challenge is further complicated if a target protein is prone to mutations that alter the shape of the binding site.[138] Measuring the inhibition potency of the rigidified compounds **51** and **52** in the enzymatic assay should provide valuable insights into their binding affinity compared to the amine compound **37**.

Table 13: Kinetic solubility and hDHODH inhibition data of **37** and its bicyclic derivatives **51** and **52**.

Compound	37	51	52
Kin. Sol. in PBS pH 7.4 [µM]	195 ± 5	≥ 200	190 ± 5
Kin. Sol. in PBS pH 7.4 [µg/mL]	68 ± 2	≥ 74	71 ± 2
% hDHODH inhibition at 50 nM	68 ± 6	70 ± 8	47 ± 3

Data obtained for the bicyclic compounds (**51** and **52**) from the kinetic solubility and hDHODH inhibition assay are listed in Table 13. Both bicyclic compounds exhibited high kinetic solubility in PBS buffer, with concentrations greater than 70 µg/mL, similar to the parent amine compound **37**. In contrast, the lead structure **29** was 3-fold less soluble, with a concentration of 22 ± 1 µg/mL. In terms of hDHODH inhibition potential, indole **51** demonstrated comparable potency to propylamine compound **37**, showing an inhibition value of approximately 70%, whereas benzimidazole **52** exhibited a lower potency of 47%. Unfortunately, antiviral data are lacking to assess whether the bicyclic rings in compounds **51** and **52** repre-

sent promising modifications for further development. However, based on the available data, the indole modification appears more suitable for drug candidate development than the benzimidazole modification.

4.4.2. Modification of the aromatic ring

In the second cycle of the optimization campaign, functional groups should be introduced to the aromatic ring to either adjust lipophilicity or to enhance binding affinity. Modifications were focused on morpholine compound **43**, as the synthetic access to appropriate analogs is less labor-intensive and the physicochemical properties are more suitable for *in vitro* assays compared to the lead structures MW-577 **29** and MW-BG-22 **30**. The derivatives of morpholine compound **43** selected for synthesis in the second optimization cycle are shown in Figure 31.

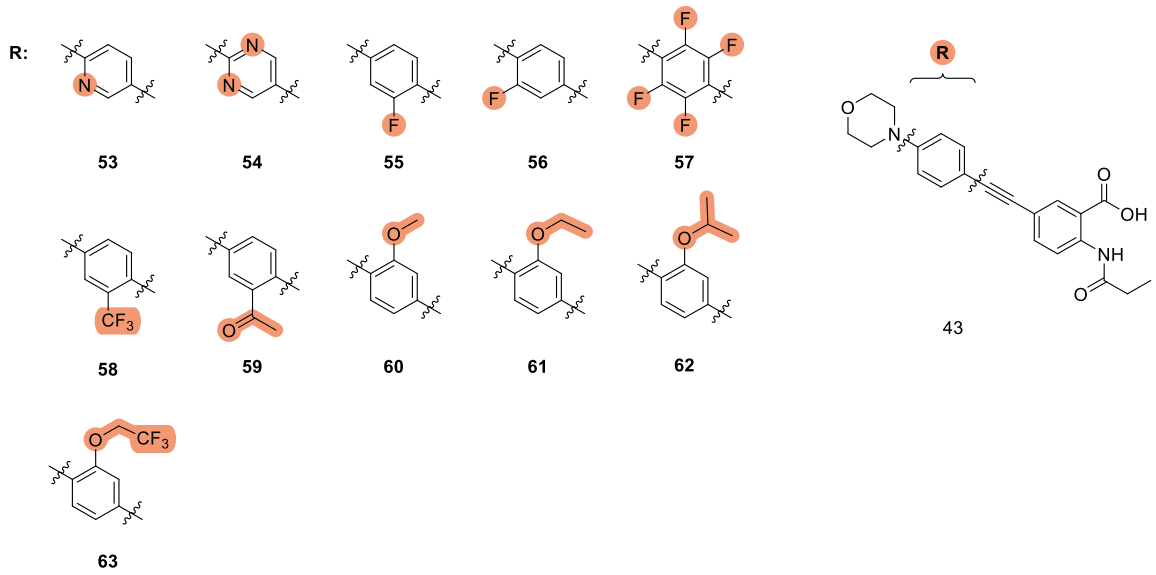

Figure 31: Synthesized derivatives (**53**-**63**) of **43** during optimization cycle 2.

The isosteric replacement of an aromatic methylene group with nitrogen is a common strategy in medicinal chemistry to modify a compound's hydrogen bonding capacity and increase its polarity. Furthermore, the introduction of nitrogen into the aromatic ring offers additional vectors for target binding.[154] Nitrogen atoms should be introduced into the aromatic ring of compound **43** to give the analogs **53** and **54**. In contrast, aromatic fluorination of **43** was performed to further enhance its lipophilicity. Two mono-fluorinated (**55** and **56**) and one tetra-fluorinated compound (**57**) were synthesized.

Kinetic solubility and hDHODH inhibition data obtained for the pyridine (**53**), pyrimidine (**54**), and fluorinated analogs (**55**-**57**) are listed in Table 14. With ≥ 200 µM, the pyrimidine analog **53** exhibited higher kinetic solubility than the parent morpholine compound **43**. Unfortunately, the kinetic solubility assay could not be performed with pyrimidine analog **54**, as it was not soluble under the present assay conditions. As anticipated, an increase in lipophilicity was observed for the fluorinated analogs **55**-**57**. Monofluorination of morpholine compound **43** to analogs **55** and **56** resulted in a decrease in kinetic solubility from 184 µM to 128 µM and 160 µM, respectively, while tetrafluorination of compound **43** to analog **57** led to an even greater reduction to 27 µM.

Table 14: Solubility and hDHODH inhibition data of morpholine compound **43** and analogs **53**-**63**.

Compound	43	53	54	55	56	57
Kin. Sol. in PBS pH 7.4 [µM]	184 ± 1	≥ 200	n.d.	128 ± 8	160 ± 5	27 ± 2
% hDHODH inhibition at 50 nM	55 ± 4	30 ± 6	33 ± 4	57 ± 4	47 ± 2	49 ± 5

At an inhibitor concentration of 50 nM, both the pyridine (**53**) and pyrimidine analogs (**54**) exhibited hDHODH inhibition of approximately 30%. Therefore, these aromatic nitrogen-containing compounds are less potent than the parent morpholine derivative **43**. For the analogs **55**-**57**, inhibition levels of approximately 50% were observed, similar to the parent morpholine derivative **43**, which likely indicates that their binding affinity remained largely unchanged.

Docking simulation experiments revealed that the binding pocket provides space for small substituents on the aromatic ring in *ortho* position relative to the ethynyl group. Figure 32 illustrates the proposed binding modes of two structures obtained from these experiments. The introduction of a trifluoromethyl (CF_3) group into a ligand is an increasingly common strategy used in medicinal chemistry to enhance protein-ligand interactions and adjust lipophilicity. In contrast to methyl groups, CF_3 exhibits substantially higher electronegativity due to its strong electron-withdrawing effect.[155] Changes in electron distribution, particularly in small ligands, can significantly impact binding interactions with surrounding amino acids in the binding pocket.[153] CF_3 should be introduced to the structure of **43** to give analog **58**. Another structure emerging from the docking studies is analog **59**, which bears an additional acetyl group at the aromatic ring compared to morpholine compound **43**. According to the proposed binding mode, the acetyl group forms an additional hydrogen bond with Thr63.

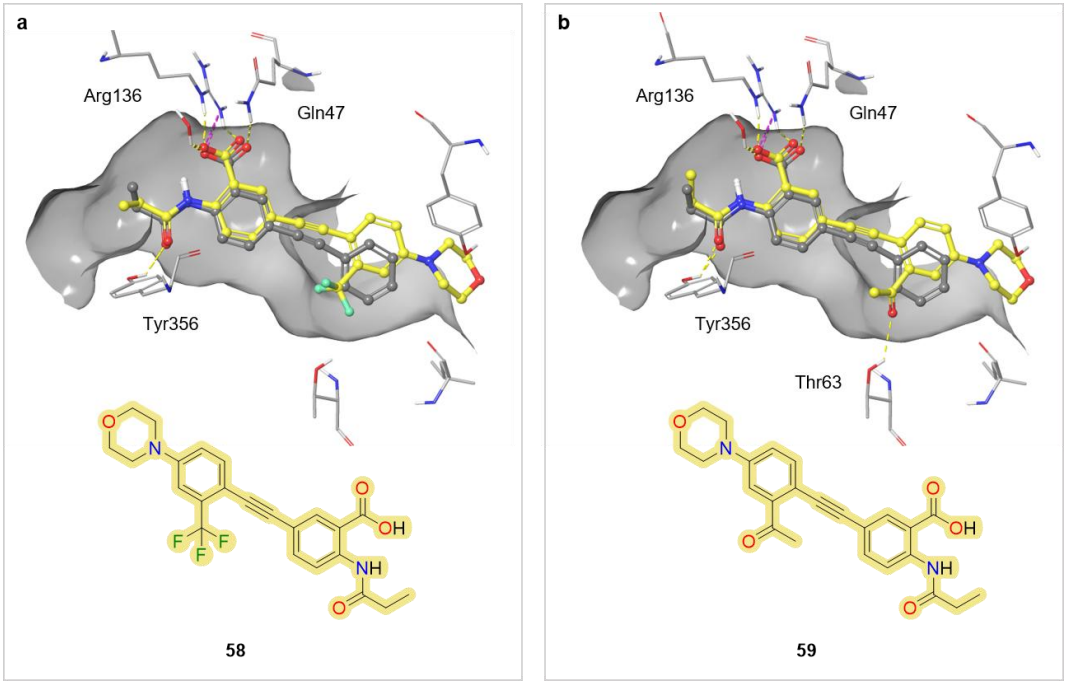

Figure 32: Binding-motif of MW-528 **36** (grey) in the lipophilic tunnel of hDHODH overlaid with docking pose (yellow) of **58** (a) and **59** (b).

Kinetic solubility and hDHODH inhibition data obtained for analogs **58** and **59** are presented in Table 15. The additional CF_3 group in analog **58** resulted in a 6-fold decrease in kinetic solubility, reducing it to 31 µM, while the acetyl analog **59** maintained a high kinetic solubility of 173 µM. Regarding hDHODH inhibition at an inhibitor concentration of 50 nM, the trifluoromethyl analog **58** showed comparable potency to the parent morpholine compound **43**, whereas acetyl analog **59** exhibited a significant decrease in potency, dropping from 55% to 17%.

Table 15: Kinetic solubility and hDHODH inhibition data of analogs **58**-**63**.

Compound	58	59	60	61	62	63
Kin. Sol. in PBS pH 7.4 [µM]	31 ± 4	173 ± 4	≥ 200	≥ 200	≥ 200	≥ 200
% hDHODH inhibition at 50 nM	59 ± 6	17 ± 3	70 ± 5	49 ± 2	23 ± 6	35 ± 6

Figure 33 shows the structure of known DHODH inhibitor BAY 242234 **64** and its interactions in the binding pocket. This orally bioavailable DHODH inhibitor demonstrates efficacy in treating various subtypes of acute myeloid leukemia (AML).[156] One interesting structural feature of BAY 242234 **64** is the 1,1,1-trifluoropropan-2-yl substituent, which points towards the pocket entrance. This substituent contributes to the extensive hydrophobic interactions observed at the lipophilic entrance of the pocket. Inspired by the structure of BAY 242234 **64**,

different alkoxy groups were introduced into the aromatic ring of compound **43** in the *ortho* position relative to the morpholine substituent, resulting in analogs **60**-**63**.

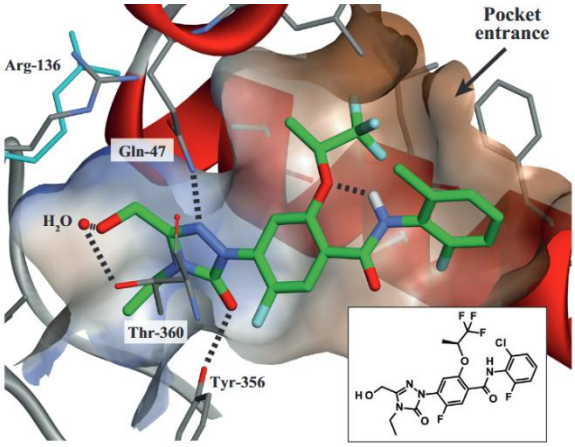

Figure 33: Protein-ligand interactions of known DHODH inhibitor BAY 2402234 **64** (green) in the ubiquinone pocket of DHODH.[156]

Data obtained for alkoxy analogs **60**-**63** from the kinetic solubility and hDHODH inhibition assay are also listed in Table 15. Compared to the morpholine compound **43**, all analogs exhibited a higher kinetic solubility of ≥ 200 µM. Differences in kinetic solubility may be observed at higher concentrations due to the varying lengths of alkyl chains in analogs **60**-**62** and the introduction of fluorine in compound **63**. However, there are notable variations in the determined hDHODH inhibition potencies. The methoxy modification in analog **60** resulted in an increase of inhibition potency from 55% to 70%, whereas the other analogs **61**-**63** exhibited lower potencies ranging from 23% to 49%. The bulkier the substituent, the lower the potency. Additionally, the ethoxy compound **61** demonstrated greater potency compared to its fluorinated analog **63**.

Table 16: Anti-YFV and toxicity data provided by J. NEYTS *et al*..

Compound	53	54	55	57	58	59
EC_{50} **YFV** (Huh-7) [µM]	1.1	1.5	0.136	0.454	< 0.0195	1.1
CC_{50} **Huh-7** [µM]	> 100	> 100	> 100	> 100	47.7	> 100

Anti-YFV data were provided by J. Neyts *et al.* for analogs **53**-**55** and **57**-**59**, as shown in Table 16. Analogs that exhibited only moderate inhibition potencies towards hDHODH also showed moderate antiviral activities above 1 µM, including the pyridine (**53**), pyrimidine (**54**),

and acetyl analogs (**59**). The introduction of fluorine in analog **55** resulted in a 3-fold increase in antiviral activity compared to the parent morpholine compound **43**, improving from 401 nM to 136 nM. In contrast, tetrafluorinated analog **57** showed only moderate antiviral activity at 454 nM. The highest antiviral activity was observed for the trifluoromethyl analog **58**, with an EC_{50} value of < 19.5 nM. All compounds exhibited low cytotoxicity in Huh-7 cells.

Table 17: Antiviral and toxicity data of **55** and **58**.

Compound	EC_{50} **YFV** (Huh-7)	EC_{50} **DENV** (Huh-7)	EC_{50} **EBOV** (Vero)	EC_{50} **HCV** (Huh-7)	CC_{50} **Vero**	CC_{50} **Huh-7**
55	204 nM	75.7 nM	123 nM	66 nM	< 4 µM	> 50 µM
58	41.3 nM	23.3 nM	18 nM	7.5 nM	< 4 µM	> 50 µM

The most potent compounds, the fluorine analog **55** and the trifluoromethyl analog **58**, were further tested against DENV, EBOV, HCV and, once again, YFV (Table 17). Compared to the morpholine compound **43**, both analogs showed higher antiviral activities against all tested virus strains. The fluorine analog **55** exhibited an increase in antiviral activity by factors ranging from 1.3 to 4.9, resulting in EC_{50} values between 66 and 204 nM. In contrast, the trifluoromethyl analog **58** showed an increase by factors of 6.9 to 43, yielding EC_{50} values between 7.5 and 41 nM. To investigate the factors that might explain the significant differences in antiviral activities, despite both compounds exhibiting similarly high inhibition potencies on the isolated enzyme, their physicochemical properties were analyzed (Table 18).

Table 18: PK data of morpholine compound **43** and analogs **55** and **58**.

Compound	**43**	**55**	**58**
Kin. Sol. in PBS pH 7.4 [µM]	184 ± 1	128 ± 8	31 ± 4
Kin. Sol. in PBS pH 7.4 [µg/mL]	70 ± 1	51 ± 3	14 ± 2
LogD (PBS pH 7.4/ octanol)	1.13 ± 0.09	1.54 ± 0.02	2.42 ± 0.04
PAMPA P_e [cm/s]	$(0.505 \pm 0.357) \cdot 10^{-6}$	$(0.984 \pm 0.0449) \cdot 10^{-6}$	$(1.35 \pm 0.131) \cdot 10^{-6}$

With a logD value of 2.42, trifluoromethyl analog **58** exhibited greater lipophilicity than the fluorine analog **55** (logD = 1.54), which is associated with increased membrane permeability. Compared to the morpholine compound **43**, the fluorine analog **55** is 2-fold more permeable,

while the trifluoromethyl analog **58** demonstrates a 3-fold increase in permeability. At the same time, a decrease in kinetic solubility was observed. The fluorine analog **55** exhibited moderate kinetic solubility, with a concentration of 51 µg/mL, while the trifluoromethyl analog **58** showed low kinetic solubility at 14 µg/mL. Considering their similar enzyme activity and the enhanced antiviral efficacy of the trifluoromethyl analog **58**, both functional groups were chosen for further development, as each offers distinct advantages, such as a better solubility profile with the fluorine group and improved membrane permeability with the trifluoromethyl group.

4.4.3. Modification of the amide group

In the third optimization cycle, stabilization of the amide bond should be achieved by steric shielding or isosteric replacement. The amide functional group in the lead structures MW-577 **29** and MW-BG-22 **30** suffers from poor metabolic stability due to rapid degradation by amidases. For a successful approach, the new analogs must retain the biological activities of their parent compounds while also altering their susceptibility to metabolic degradation. The derivatives of MW-BG-22 **30** that were selected for synthesis are shown in Figure 34.

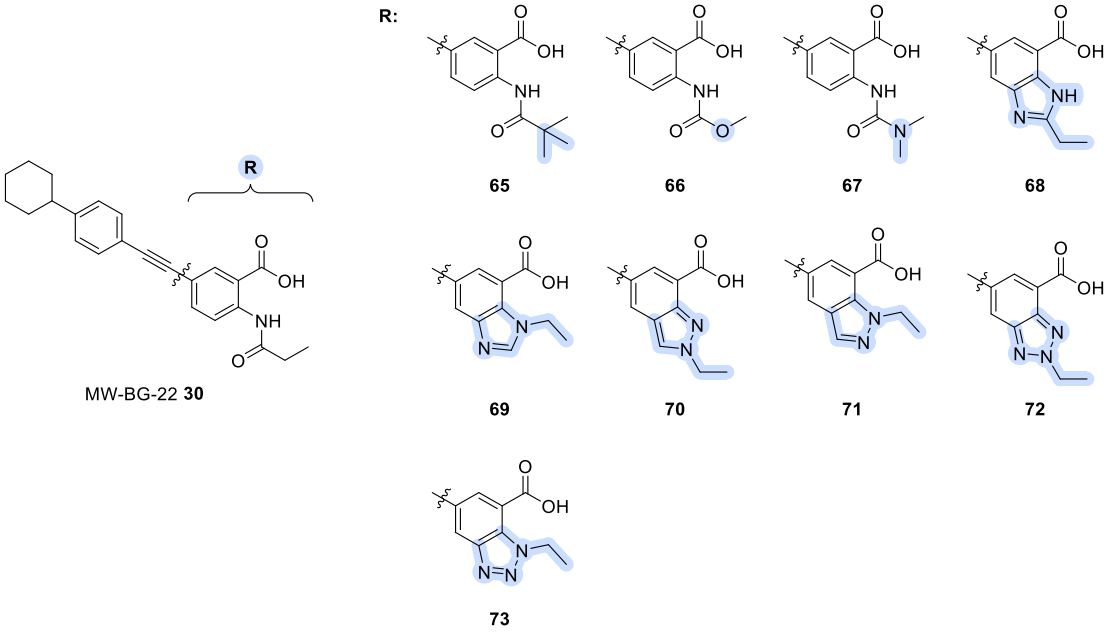

Figure 34: Synthesized derivatives (**65**-**73**) of MW-BG-22 **30** during optimization cycle 3.

A common strategy for protecting a labile functional group involves introducing a steric shield that prevents nucleophiles or enzymes from accessing the site of attack. Typically, this is achieved by adding a bulky alkyl group near the vulnerable functional group.[138] In a first ap-

proach, two methyl groups were incorporated into the propionamide moiety of MW-BG-22 **30** to yield the pivalamide analog **65**.

In another common strategy, electronic stabilization of a labile group is achieved by using a bioisostere. Bioisosteres can exhibit similar physical and chemical properties, such as size and valency, but possess different electronic characteristics that enhance metabolic stability. Importantly, it is crucial to retain the biological activity of the original compound. To date, various amide bioisosteres have been identified, including classical bioisosteres, such as urea, amidine, sulfonamide, thioamide, carbamate, and non-classical bioisosteres, such as imidazole, 1,2,3-triazole, tetrazole and oxadiazole.[157]

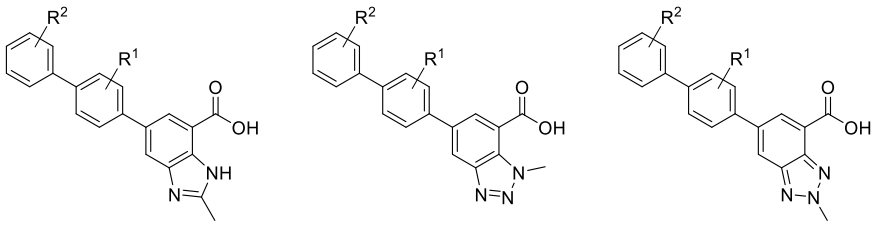

Figure 35: hDHODH inhibitors based on a benzimidazole and benzotriazole scaffold.

In a second approach, the amide group in MW-BG-22 **30** was replaced with classical bioisosteres to yield analogs **66**-**67**, as well as with nonclassical bioisosteres to give analogs **68**-**73**. This strategy of isosteric replacement with non-classical bioisosteres, including benzimidazole and benzotriazole, has already been successfully applied to the biphenyl anthranilic acid class, as demonstrated in previous studies by S. THUNUGUNTLA.[158] From these investigations, three promising scaffolds (Figure 35) have emerged, demonstrating high inhibition potency against hDHODH in micro- and nanomolar range. Therefore, it is desirable to extend these findings to the phenylethynyl anthranilic acid class.

Phase I metabolic stability was assessed for all synthesized analogs using rat S9 fraction (see chapter 4.1.4). Figure 36 shows the recorded fluorescent chromatograms of the lead structure MW-BG-22 **30** and, as an example, urea analog **67**. A significant decrease in compound concentration was observed for MW-BG-22 **30**, while the urea analog **67** remained largely intact after an incubation period of 3 h. Except for indazole **70**, all other analogs showed a metabolism profile similar to that of the urea analog **67**.

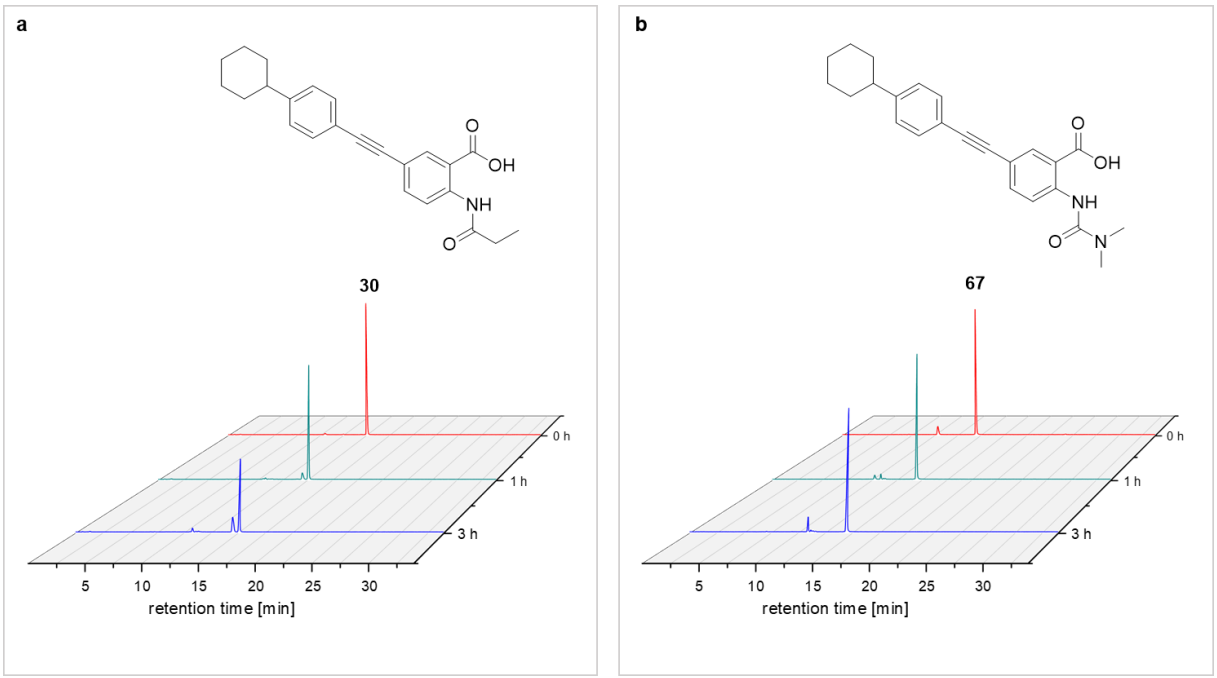

Figure 36: HPLC-chromatograms of MW-BG-22 **30** (a) and urea analog **67** (b) recorded after incubation for 0, 1 and 3 h in rat S9 fraction.

Metabolic stability and hDHODH inhibition data obtained for analogs **65**-**67** and **68**-**73** are listed in Table 19 and Table 20, respectively. The steric shielding and replacement of the amide group in MW-BG-22 **30** with the selected classical bioisosteres resulted in a notable increase in metabolic stability from 73% to over 90%. The carbamate and urea groups demonstrate greater resistance to hydrolysis compared to the amide group, as the additional heteroatom donates electron density to the electrophilic center. While indazole **70** exhibited a metabolic stability of 67%, indicating decreased stability relative to MW-BG-22 **30**, all other bicyclic analogs showed elevated metabolic stabilities ranging from 85% to 93%.

Table 19: Data for metabolic stability in S9 fractions and hDHODH inhibition of MW-BG-22 **30** and analogs **65**-**67**.

Compound	30	65	66	67
S9 stability after 1 h in PB pH 7.4 [%]	73 ± 6	97 ± 1	91 ± 1	91 ± 1
% hDHODH inhibition at 200 nM	75 ± 2	23 ± 3	42 ± 4	37 ± 3

In the hDHODH inhibition assay, a higher inhibitor concentration of 200 nM was employed, as the inhibition potency values for analogs **65**-**73** were anticipated to be substantially lower than those of the lead structure **30**. All modifications led to a significant decrease in inhibition potency. A decrease from 75% to 23%, representing a factor of 3, was observed for

pivalamide **65**, whereas carbamate **66** and urea **67** were half as potent as MW-BG-22 **30**, with values of 42% and 37%, respectively. Among the bicyclic compounds, benzotriazole **73** exhibited the highest inhibition potency at 24%. The benzimidazole analogs **68** and **69** were slightly less potent, with values of 12-13%, while the other benzotriazole regioisomer **72** and both indazole analogs (**70**, **71**) were barely active in the enzyme assay, showing an inhibition potency of only 2-5%

Table 20: Data for metabolic stability in S9 fractions and DHODH inhibition of analogs **68**-**73**.

Compound	68	69	70	71	72	73
S9 stability after 1 h in PB pH 7.4 [%]	86 ± 3	91 ± 1	67 ± 7	93 ± 2	90 ± 6	85 ± 7
% hDHODH inhibition at 200 nM	12 ± 3	13 ± 4	2 ± 1	5 ± 2	4 ± 2	24 ± 1

Anti-YFV data were provided by J. NEYTS *et al.* for urea **67**, benzimidzaole **68**, and benzotriazoles **72** and **73** (Table 21). The measured antiviral activities were found to correlate broadly with the hDHODH inhibition potential. Benzotriazole **72**, which showed little inhibition potential towards hDHODH, exhibited a low antiviral activity of 7.8 µM. Benzimidazole **68** and benzotriazole **73** had moderate antiviral activities of 282 nM and 459 nM, respectively. Notably, urea **67** showed high antiviral activity at 63 nM, making it the most potent hDHODH inhibitor among these four compounds.

Table 21: Anti-YFV and toxicity data provided by J. NEYTS *et al*..

Compound	30	67	68	72	73
EC_{50} **YFV** (Huh-7) [µM]	< 0.0195	0.063	0.282	7.8	0.459
CC_{50} **Huh-7** [µM]	43	42	59	40	42

Further antiviral assays were conducted with urea **67** and benzimidazole **68** (Table 22). Urea **67** showed greater antiviral activity against all tested viral strains, with the exception of CHIKV. While urea **67** exhibited antiviral effects in the nanomolar range, benzimidazole **68** demonstrated micromolar EC_{50} values. Additionally, urea **67** was tested against EBOV, for which a moderate antiviral activity of 264 nM was observed. Both compounds showed low cytotoxicity in Huh-7 cells.

Table 22: Antiviral and toxicity data of **67** and **68**.

Compound	EC_{50} **YFV** (Huh-7)	EC_{50} **DENV** (Huh-7)	EC_{50} **EBOV** (Vero)	EC_{50} **HCV** (Huh-7)	EC_{50} **CHIKV** (Huh-7)	CC_{50} **Vero**	CC_{50} **Huh-7**
67	240 nM	23.9 nM	264 nM	19 nM	129 nM	> 4 µM	> 100 µM
68	~ 2 µM	454 nM	n.d.	~ 1 µM	70.2 nM	n.d.	> 100 µM

Compared to MW-BG-22 **30**, urea compound **67** exhibited a slight decrease in hDHODH inhibition potency and antiviral activity, however, the bioisosteric replacement of the amide group resulted in a significant increase in metabolic stability. Since the compound is less metabolized, more active molecules may reach the target site, potentially making them more effective *in vivo* despite lower *in vitro* potency than those with poor metabolic stability. Thus, the urea functional group was considered a suitable modification for the continued development of a drug candidate.

4.4.4. Target compounds

In the final optimization cycle, the selected modifications should be combined to create potent hDHODH inhibitors with improved physicochemical properties. As shown in Figure 37, these modifications have been carefully chosen from previous optimization cycles. Utilizing these modifications, ten distinct target compounds can be designed that incorporate a urea group as a replacement for the amide, an additional fluorine or trifluoromethyl substituent on the aromatic ring, and one of five selected amines in place of the alkyl chain.

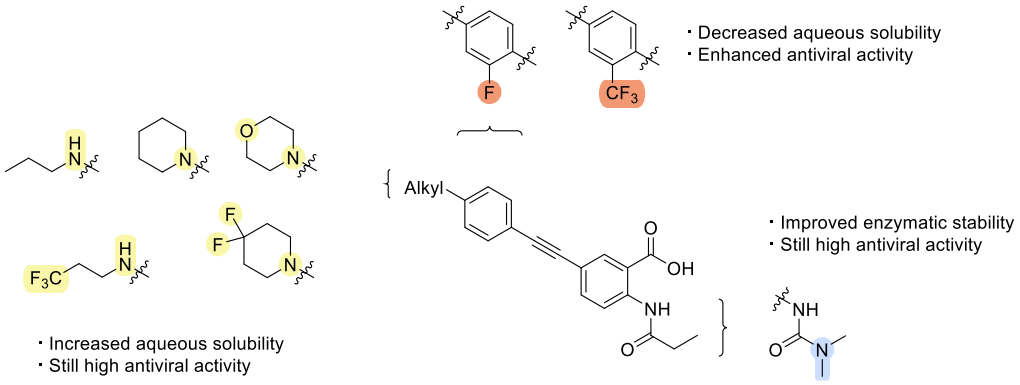

Figure 37: Selected modifications from the previous optimization cycles.

Of the ten possible structures evaluated in the previous optimization campaign, six target compounds were selected based on their straightforward and rapid synthetic accessibility, as well as their predicted high activity against hDHODH and various RNA viruses. These include all five fluorine derivatives and one trifluoromethyl analog (Figure 38).

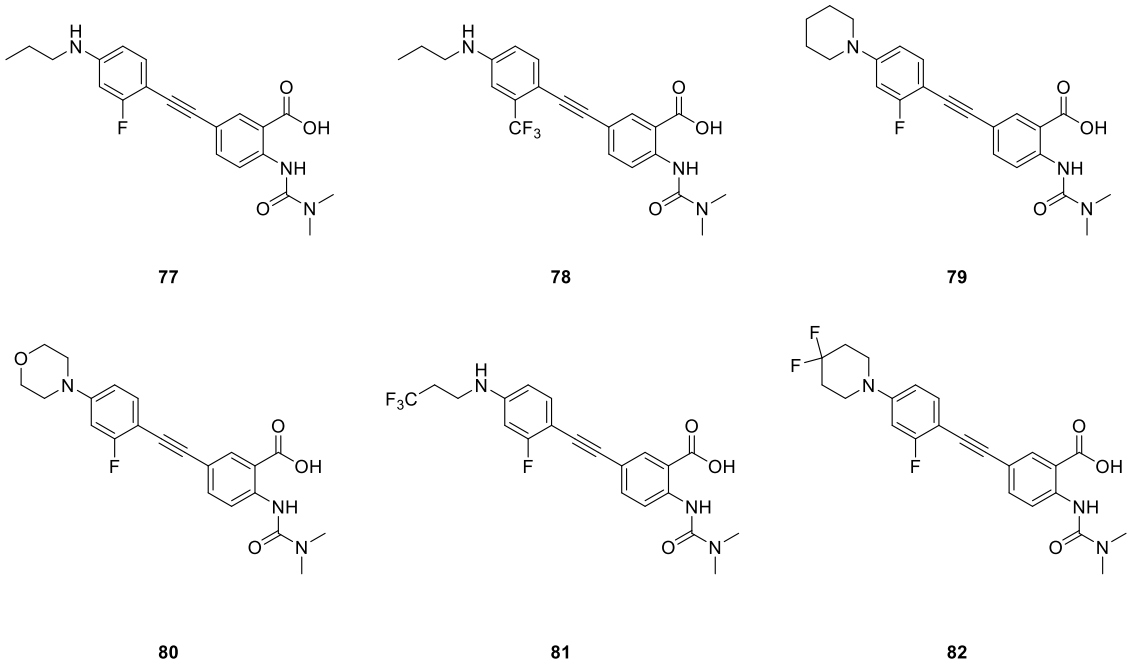

Figure 38: Synthesized target compounds **77**-**82**.

The hDHODH inhibition and PK data obtained for target compounds **77**-**79** and **80**-**82** are summarized in Table 23 and Table 24, respectively. At an inhibitor concentration of 50 nM, hDHODH inhibition potency of approximately 50% was observed for all target compounds containing a terminal propylamine moiety (**77**, **78** and **81**). The difluoropiperidine analog **82** demonstrated a moderate inhibition potency of 31%, whereas the piperidine analog **79** and morpholine analog **80** were significantly less potent, with a value of 15%.

Complete characterization of the physicochemical properties was conducted for the most potent hDHODH inhibitors **77**, **78** and **81**. The trifluoromethyl analog **78** exhibited high lipophilicity (logD ≥ 2.88) and high membrane permeability (P_e = (6.28 ± 1.88)·10^{-6}), but showed poor kinetic solubility (13 ± 2 µg/mL). With 73% stability in S9 fraction, it was 2-fold higher than that of lead structure MW-577 **29**. In contrast, the fluorine analog **77** demonstrated lower lipophilicity (logD = 1.82) and membrane permeability (P_e = (0.824 ± 0.368)·10^{-6}) but achieved 5-fold higher solubility (67 ± 4 µg/mL). Additionally, it showed enhanced stability in the S9 fraction, reaching 91%. The trifluoropropylamine analog **81** was comparably hydrophilic (logD = 1.02) and exhibited the highest kinetic solubility (≥ 87 µg/mL) among the three

compounds tested. Additionally, **81** demonstrated high membrane permeability (P_e = (1.92 ± 0.445)·10^{-6}) and significant metabolic stability of 96%.

Table 23: PK and hDHODH inhibition data of target compounds **77**-**82**.

Compound	77	78	79
Kin. Sol. in PBS pH 7.4 [µM]	175 ± 10	31 ± 4	83 ± 6
Kin. Sol. in PBS pH 7.4 [µg/mL]	67 ± 4	13 ± 2	34 ± 2
LogD (PBS pH 7.4/ octanol)	1.82 ± 0.03	≥ 2.88	1.86 ± 0.01
PAMPA P_e [cm/s]	(0.824 ± 0.368)·10^{-6}	(6.28 ± 0.188)·10^{-6}	n.d.
S9 stability (PB pH 7.4/ 1 h) [%]	90.6 ± 1.2	72.8 ± 3.4	n.d.
% hDHODH inhibition at 50 nM	46 ± 0	50 ± 5	17 ± 6

Table 24: PK and hDHODH inhibition data of target compounds **77**-**82**.

Compound	80	81	82
Kin. Sol. in PBS pH 7.4 [µM]	≥ 200	≥ 200	19 ± 3
Kin. Sol. in PBS pH 7.4 [µg/mL]	≥ 82	≥ 87	8 ± 2
LogD (PBS pH 7.4/ octanol)	1.26 ± 0.02	1.02 ± 0.04	1.63 ± 0.08
PAMPA P_e [cm/s]	n.d.	(1.92 ± 0.445)·10^{-6}	n.d.
S9 stability (PB pH 7.4/ 1 h) [%]	n.d.	95.5 ± 3.2	n.d.
% hDHODH inhibition at 50 nM	14 ± 4	53 ± 0	31 ± 2

The target compounds **77**-**82** were tested in cell-based assays against HF-viruses, including YFV, DENV and EBOV, and the hepacivirus HCV (Table 25). The morpholine analog **80**, which showed limited inhibition potential in the enzyme assay, exhibited only a micromolar antiviral effect against the tested virus strains. In contrast, compounds **79** and **82** showed significant antiviral activities in the three-digit nanomolar range. Notably, the most potent hDHODH inhibitors **77**, **78** and **81** also showed the lowest EC_{50} values in the antiviral assays. The comparatively high lipophilicity and membrane permeability of **78** likely contributed to its remarkable antiviral activity of approximately 10 nM against all tested virus strains. Compounds **77** and **81** exhibited only slightly reduced efficacies in the antiviral assays, with EC_{50} values of up to 25 nM and 60 nM, respectively. All compounds demonstrated low cytotoxicity in Huh-7 cells.

Table 25: Antiviral and toxicity data of target compounds **77**-**82**.

Compound	EC_{50} **YFV** (Huh-7)	EC_{50} **DENV** (Huh-7)	EC_{50} **EBOV** (Vero)	EC_{50} **HCV** (Huh-7)	CC_{50} **Vero**	CC_{50} **Huh-7**
77	25 nM	16 nM	17 nM	5.2 nM	> 4 µM	> 50 µM
78	13.5 nM	9.1 nM	9 nM	4.4 nM	> 4 µM	> 50 µM
79	210 nM	90.2 nM	n.d.	127 nM	n.d.	> 50 µM
80	1831 nM	1554 nM	n.d.	1055 nM	n.d.	> 50 µM
81	60.4 nM	34.5 nM	n.d.	17.7 nM	n.d.	> 50 µM
82	324 nM	158 nM	n.d.	69.5 nM	n.d.	> 50 µM

77, **78** and **81** have emerged from the last optimization cycle as potent hDHODH inhibitors with nanomolar broad-spectrum antiviral activity *in vitro*. The highest antiviral activities were observed for the trifluoromethyl compound **78**, which demonstrated enhanced metabolic stability compared to the lead structure MW-577 **29**. However, there was no improvement in aqueous solubility. The fluorine analog **77** and trifluoropropylamine analog **81** exhibited both high kinetic solubility in PBS buffer and exceptional metabolic stability, representing a substantial improvement over the lead structures MW-577 **29** and MW-BG-22 **30**. Additionally, both compounds also demonstrated acceptable membrane permeability. These two analogs have shown encouraging preliminary results and establish a new basis for the ongoing development of a therapeutic agent. They are both currently being tested for their pharmacological behavior *in vivo* by K. ROX at the Helmholtz Centre for Infection Research in Braunschweig.

During the first two optimization cycles, additional functional groups were identified that also contributed to an increase in kinetic solubility and resulted in comparable hDHODH activity, however, antiviral data were lacking for these compounds. These include ketone **38**, PEG analogs **40** and **41**, tetrahydropyran **48**, indole **51**, and methoxy analog **60**. They are planned to be tested for their antiviral activity, and based on the results, further target compounds will be designed. A further suggestion is to introduce a second fluorine substituent on the aromatic ring of fluorine analog **77** to further enhance lipophilicity and permeability, although it might result in decreased solubility.

4.5. Synthesis

The synthesis route for preparing the hDHODH inhibitors is depicted in Figure 39. Phenylethynyl anthranilic acid derivatives (**83**) should be obtained through saponification of the coupled product (**84**), which results from the SONOGASHIRA coupling reaction involving the appropriate halogen-substituted anthranilic acid derivative (**86**) and alkyne (**85**). As these building blocks were not commercially available, they had to be synthesized as well. For the anthranilic acid derivatives (**86**), synthesis was achieved in up to two steps using different reactions. Alkynes (**85**) were obtained by deprotection of the corresponding trimethylsilyl (TMS)-protected alkyne (**87**), which was previously prepared via a SONOGASHIRA coupling reaction of the appropriate aryl halide (**88**) with TMS-acetylene. The aryl halides (**88**) were synthesized through various methods, including ULLMANN-GOLDBERG coupling, BUCHWALD-HARTWIG coupling, MICHAEL addition, and reductive amination.

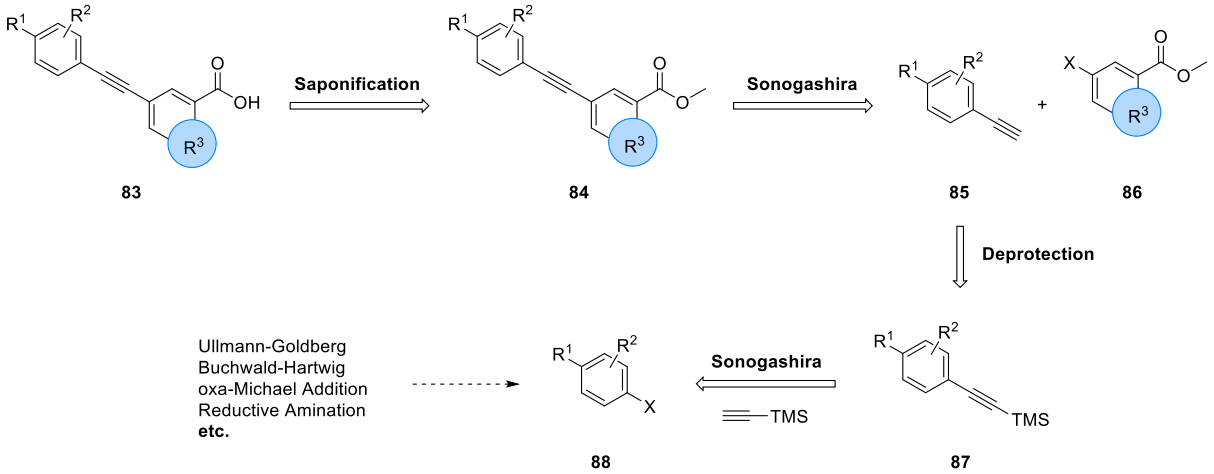

Figure 39: Retrosynthetic analysis for the preparation of phenylethynyl anthranilic acid derivatives.

4.5.1. Syntheses of anthranilic acid building blocks

For the synthesis of the hDHODH inhibitors from optimization cycle 1 and 2, methyl 5-iodo-2-propionamidobenzoate **90** was required as a building block for the SONOGASHIRA coupling reaction with the appropriate alkynes (Figure 40). While its bromine analog (provided by M. WINKLER) was utilized in previous studies, the use of aryl iodide **90** resulted in higher reaction rates under milder conditions. This compound was synthesized via acylation of methyl anthranilate **89** with propionyl chloride in acetone in the presence of potassium carbonate.[159] Propionyl chloride was added to the mixture at 0 °C, and the reaction was stirred for 2 h at room temperature. Quenching the reaction with water followed by aqueous work-up afforded anthranilic acid building block **90** in quantitative yield.

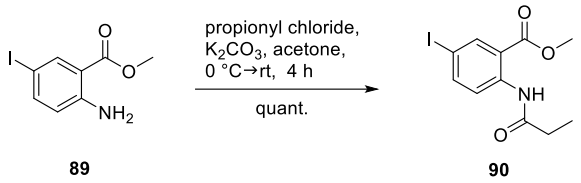

Figure 40: Synthesis of anthranilic acid building block **90** by acylation of methyl anthranilate **89**.

In optimization cycle 3, the stabilization of the amide group was targeted through bioisosteric replacement. Figure 41 shows analogs of MW-BG-22 **30**, in which the propyl amide group has been replaced with classical bioisosteres. The urea analog **67** was obtained from previous work,[160] whereas the other two compounds (**65** and **66**) should be synthesized using anthranilic acid derivatives **91** and **92** as building blocks. Both building blocks were provided by M. WINKLER.

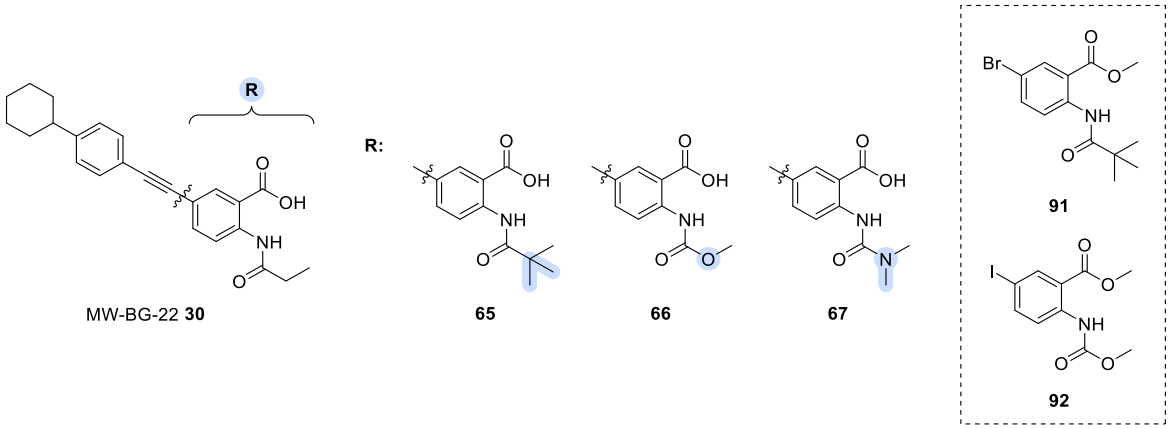

Figure 41: Analogs (**65**-**67**) of MW-BG-22 **30** and anthranilic acid derivatives (**91** and **92**) required for their synthesis.

Figure 42 shows analogs of MW-BG-22 **30**, in which the propyl amide group has been replaced by nonclassical bioisosteres. The benzimidazole (**68**) and benzotriazole (**72**) analogs were synthesized in previous work.[160] The synthesis of the remaining four compounds (**69**-**71**, **73**) required anthranilic acid derivatives **93**-**96** as building blocks. The preparation of these derivatives is described below. The benzotriazole building block **96** was also obtained from prior work.[160]

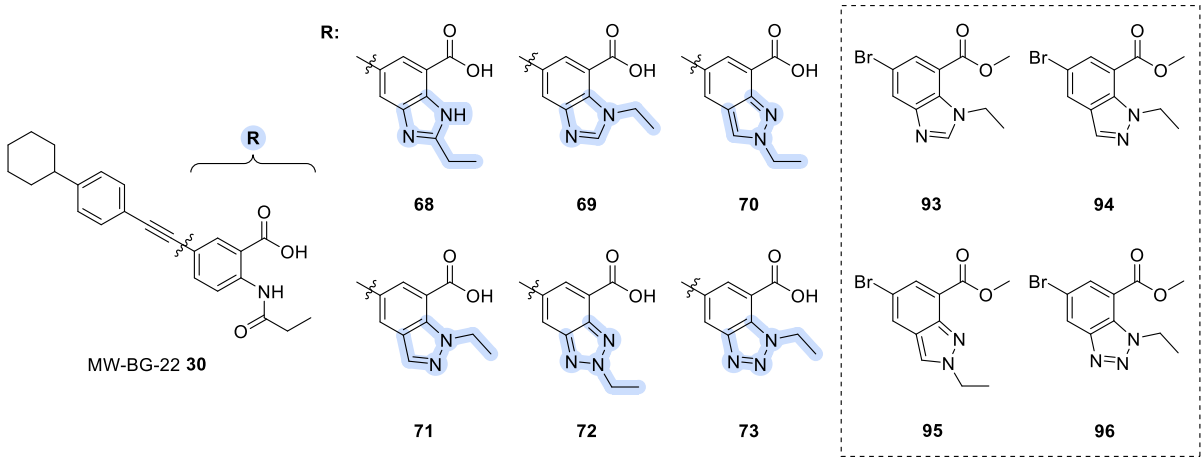

Figure 42: Analogs (**68**-**73**) of MW-BG-22 **30** and anthranilic acid derivatives (**93**-**96**) required for their synthesis.

Building block **93** should be prepared by conversion of diamine **97** with trimethyl orthoformate into benzimidazole **98**, followed by alkylation with ethyl iodide (Figure 43). In the first step, diamine **97** was dissolved in trimethyl orthoformate with the addition of one drop of sulfuric acid, and the resulting mixture was stirred for 30 min at room temperature.[161] The precipitated solid was collected by filtration and subsequently washed with water. Purification by column chromatography afforded benzimidazole **93** in a yield of 61%.

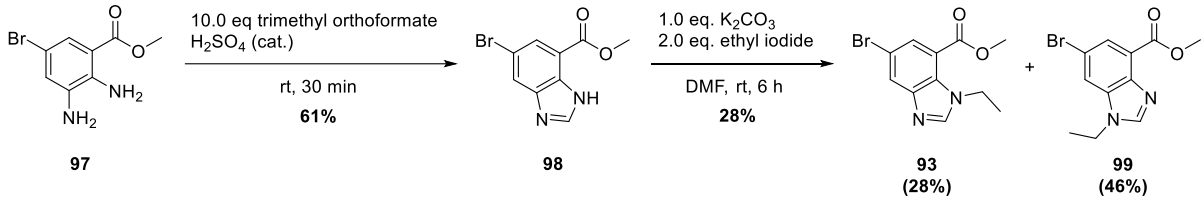

Figure 43: Synthesis of **93** by conversion of diamine **97** into benzimidazole **98** followed by alkylation.

In the second step, ethyl iodide was added to a mixture of benzimidazole **98** and potassium carbonate in dimethylformamide.[158] After stirring for 6 h at room temperature, the reaction mixture was quenched with water. The precipitated solid was obtained by filtration, and the product was further separated from regioisomer **99** via column chromatography. Building block **93** was isolated in a yield of 28%.

The two building blocks **94** and **95** should be synthesized from indazole **100** also via alkylation with ethyl iodide (Figure 44), using the same conditions as described for previous reaction. The regioisomers **94** and **95** were isolated in yields of 28% and 38%, respectively.

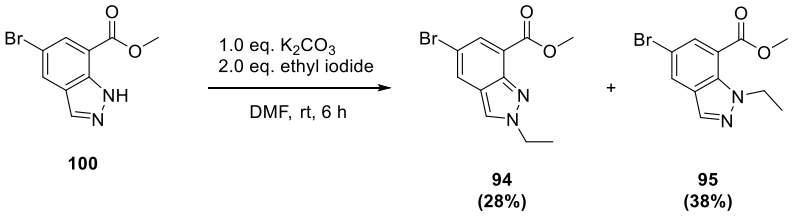

Figure 44: Synthesis of **94** and **95** by alkylation of indazole **100**.

At this stage, all necessary anthranilic acid building blocks for the synthesis of the target compounds had been prepared and were available for the subsequent SONOGASHIRA coupling with the alkyne building blocks.

4.5.2. Syntheses of alkyne building blocks

Syntheses of aryl halides

The analogs of MW-577 **29** examined in this study are shown in Figure 45. Amine (**37**) and amide (**39**) analogs were obtained from previous work,[160] while the remaining four compounds (**38**, **40**, **41**, **49**) needed to be synthesized. Therefore, the aryl halides **101**-**104** were required as starting materials, but only three (**101**-**103**) of them were commercially available. The synthesis of aryl halide **104** is described below.

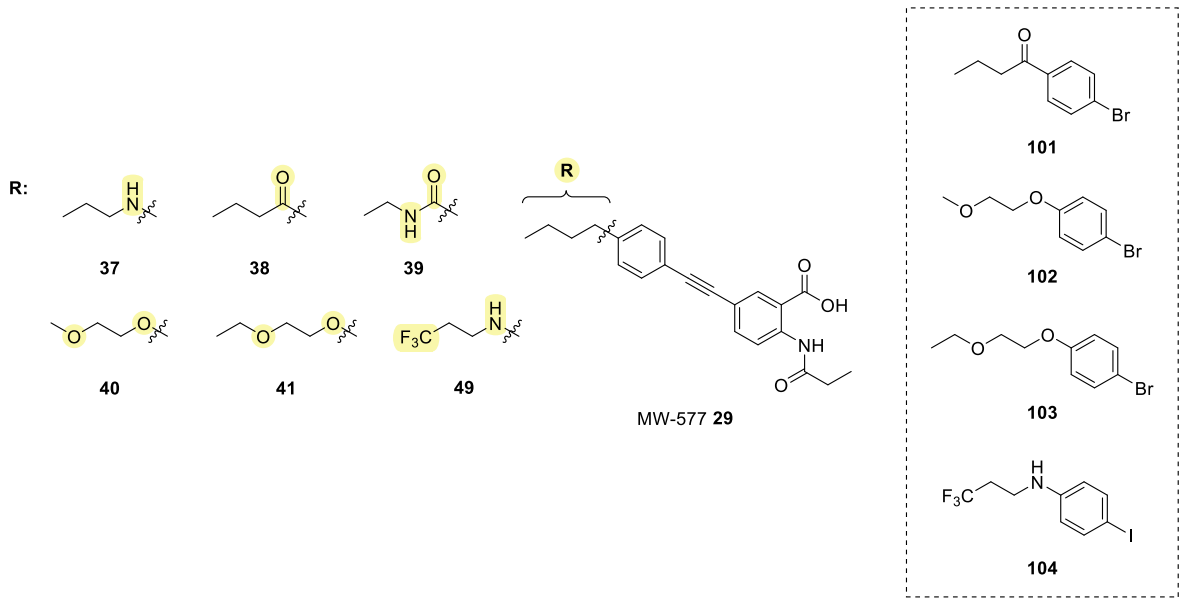

Figure 45: Analogs (**37**-**41**, **49**) of MW-577 **29** and aryl halides (**101**-**102**) required for their synthesis.

For the synthesis of aryl halide **104**, direct reductive amination was applied using 4-iodoaniline **105** and propionaldehyde **106** as starting materials, with sodium triacetoxyborohydride (STAB) serving as the reducing agent (Figure 47). In this method, the amine and the

aldehyde form an imine intermediate that immediately reacts with the reducing agent to yield the secondary amine (Figure 46). STAB is commonly used in reductive aminations and is preferred over sodium borohydride because it acts as a more selective and milder reducing agent. Its gentle nature can be attributed to the electron-withdrawing inductive effect of the acetoxy groups, which results in decreased electron density on the hydride.[162,163]

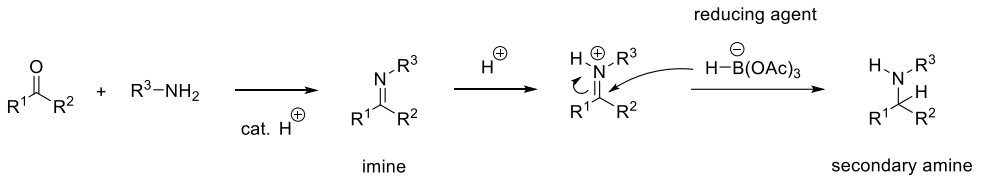

Figure 46: Mechanism for the reductive amination using STAB.

Aryl halide **104** was synthesized following a protocol of J. CHEN *et al.*[164]. Propionaldehyde **106** was added to 4-iodoaniline **105** in the presence of acetic acid in dichloromethane at 0 °C. The mixture was treated with STAB and allowed to warm to room temperature. After aqueous workup and purification via column chromatography, **104** was obtained with a moderate yield of 40%. Highly reactive aldehydes react again with the secondary amine leading to the formation of an iminium ion which is immediately reduced to the tertiary amine. This secondary reaction was also observed for aryl halide **104** via TLC.

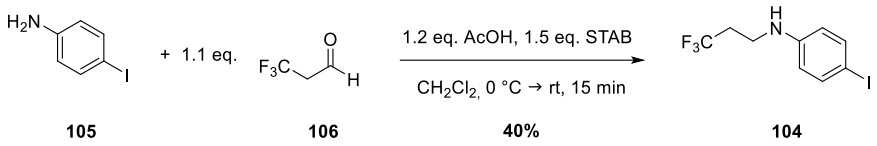

Figure 47: Synthesis of aryl halide **104** by reductive amination of 4-iodoanaline **105**.

For the synthesis of the two bicyclic compounds **51** and **52**, the aryl halides **107** and **108** shown in Figure 48 were required. These compounds should be synthesized by alkylation of the appropriate indole **109** and benzimidazole **110** under basic conditions.

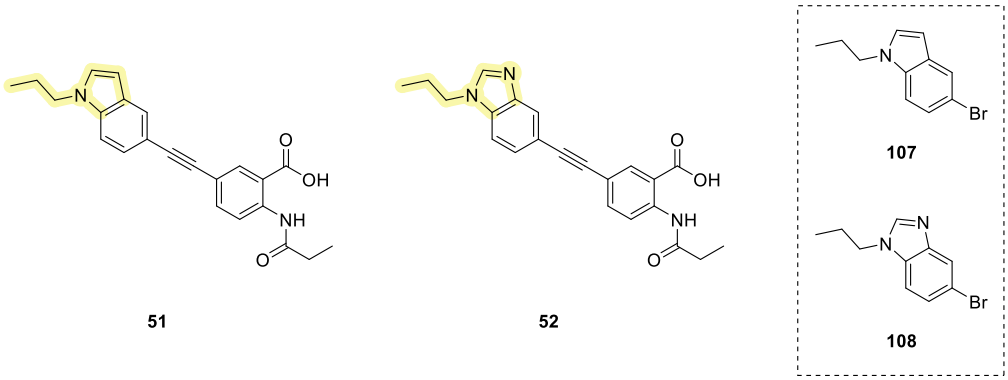

Figure 48: Required aryl halides **107** and **108** for the synthesis of target compounds **51** and **52**.

Alkylation of indole **109** (Figure 49) and benzimidazole **110** (Figure 50) was performed with bromopropane in the presence of cesium carbonate in dimethylformamide for 2 h at 100 °C. During the reaction, cesium bromide precipitated and had to be removed prior to aqueous workup of the reaction mixture. Purification by column chromatography provided indole compound **107** as a pure product with a yield of 67%, whereas benzimidazole compound **108** could only be obtained as a 1:1 mixture with its regioisomer **111**.

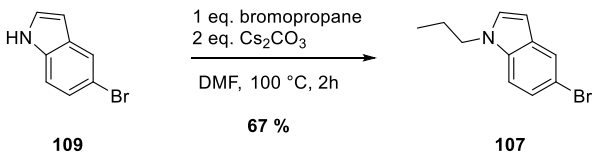

Figure 49: Synthesis of aryl halide **107** by alkylation of indole **109**.

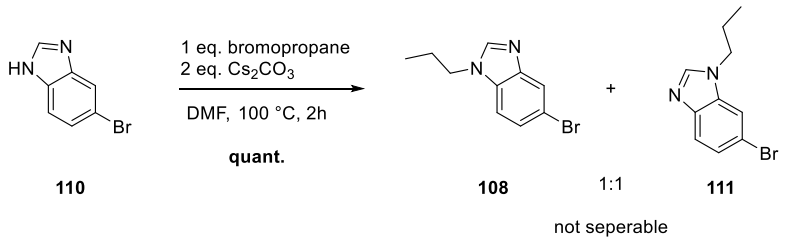

Figure 50: Synthesis of aryl halide **108** by alkylation of benzimidazole **110**.

The analogs of MW-BG-22 **30** investigated in this study are presented in Figure 51. Morpholine analog **43** was provided from previous work,[160] whereas all other analogs (**42**, **44**-**48**, **50**) needed to be synthesized first. The aryl halides (**112**-**118**) required for their synthesis are also shown in Figure 51. Of these, only 1-(4-iodophenyl)piperazine **113** was commercially available. The synthesis of the remaining aryl halides (**112**, **114**-**118**) is described below.

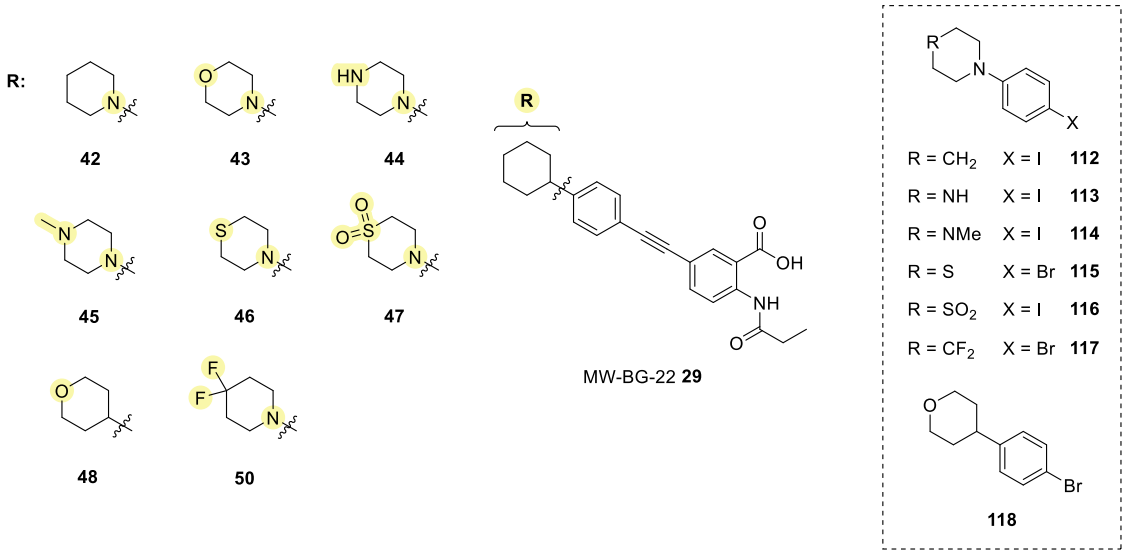

Figure 51: Analogs (**42**-**48**, **50**) of MW-BG-22 **30** and aryl halides (**112**-**118**) required for their synthesis.

The ULLMANN-GOLDBERG reaction is a copper-catalyzed cross-coupling reaction of an aryl halide with a nucleophile in the presence of a base, leading to the formation of aryl ethers, thioethers, nitriles, or amines (Figure 52).[165]

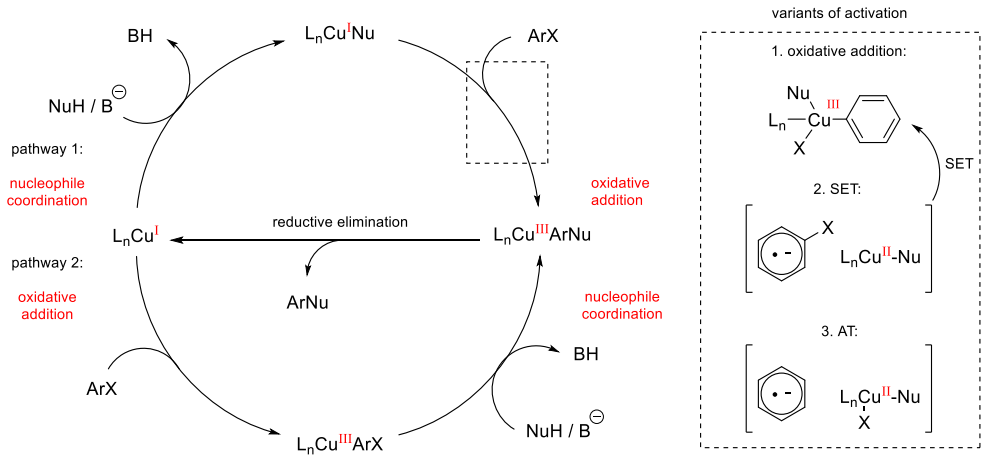

Figure 52: Proposed mechanism for the Ullmann-Goldberg coupling reaction involving the formation of an aryl-Cu(III)-Nu species.[166]

Although first described in the early 20th century, some aspects of the mechanism are still not fully understood, including the identity and oxidation state of the active copper complex and the activation process of the aryl halide. Two different pathways have been proposed. One involves activation of the aryl halide followed by the coordination of the deprotonated nucleophile (pathway 2), with the coupling product released after subsequent reductive elimination.

However, it is generally assumed that the coordination of the nucleophile occurs prior to the activation of the aryl halide (pathway 1). Three main modes of activation are discussed. The most widely proposed mechanism involves oxidative addition to form an aryl-copper(III) intermediate. Other potential activation modes include single electron transfer (SET) and atom transfer (AT), which involve the formation of an aryl radical species and a copper(II) complex.[166,167]

The reaction rate depends on the choice of aryl halide (Figure 53). The reactivity order (ArI > ArBr >> ArCl) correlates with the leaving group ability of halides (I > Br > Cl), and higher reactivity is observed with aryl halides bearing electron-withdrawing groups. Additionally, sterically demanding substituents decrease the reaction rate.[168]

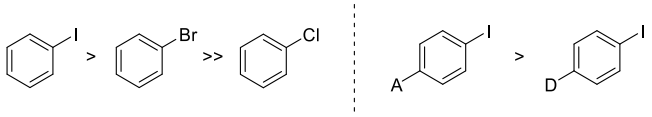

Figure 53: Relative reaction rates of different aryl halides.

ULLMANN-GOLDBERG coupling reactions were performed according to the protocol of C. DELDAELE *et al.*[169] (Figure 54 and Table 26). Therefore, potassium carbonate and a catalyst system consisting of copper(I)iodide (20 mol-%) and L-proline (40 mol-%) were added to the appropriate aryl halide dissolved in DMSO. The resulting mixture was treated with the appropriate amine and stirred for 20-24 h at room temperature or at 50 °C. In contrast to 1-bromo-4-iodobenzene **119**, a higher temperature was required for the conversion of 1,4-diiodobenzene **120**, as the second iodine substituent exerts a lower electron-withdrawing effect than bromine. Additionally, more equivalents of the amine were needed. After a basic workup, the crude product was purified by column chromatography. The aryl bromides **115** and **117** were obtained in moderate yields of 39% and 35%, whereas the ULLMANN-GOLDBERG coupling of 1,4-diiodobenzene **120** under modified conditions afforded aryl iodides **112** and **114** in higher yields of 53% and 56%.

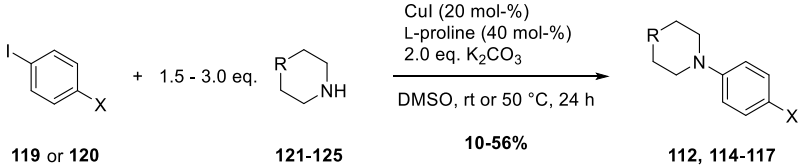

Figure 54: Synthesis of aryl halides **112**, **114**-**117** by ULLMANN-GOLDBERG coupling of **119** or **120** with amines **121**-**125**.

Table 26: Starting materials used for the synthesis of **112**, **114**-**117** and the corresponding yields.

Aryl halide		Amine		Product		Yield
120	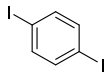	**121**		**112**	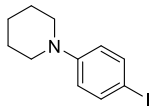	53%
120	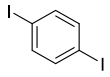	**122**		**114**	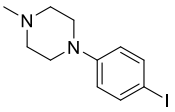	56%
119	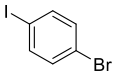	**123**		**115**	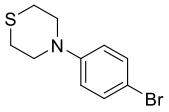	39%
120	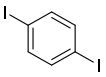	**124**	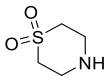	**116**	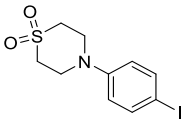	10%
119	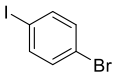	**125**	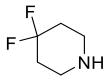	**117**	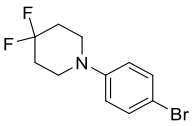	35%

In a first approach, aryl iodide **116** was also synthesized via ULLMANN-GOLDBERG coupling of 1,4-diiodobenzene **120** with thiomorpholine-1,1-dioxide **124**, but only a bad yield of 10% was achieved due to low conversion, even at higher temperatures and with increased equivalents of amine **124**. Therefore, **116** was synthesized using a second approach based on a oxa-MICHAEL addition reaction between 4-iodoanaline **105** and divinyl sulfone **126** (Figure 55).[170] Both compounds were dissolved in water and treated with glycerol and boric acid under reflux for 20 h. The resulting solid was separated from the supernatant by decantation and redissolved in dichloromethane for aqueous workup. After purification by column chromatography, aryl iodide **116** was obtained with a significantly improved yield of 57%.

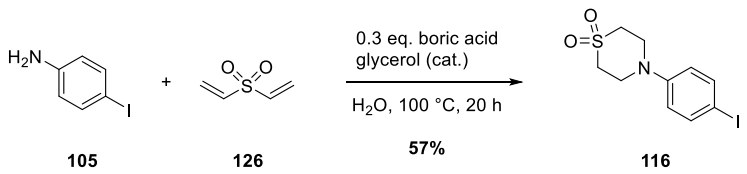

Figure 55: Synthesis of aryl iodide **116** by Michael addition of aniline **105** and divinyl sulfone **126**.

Aryl bromide **118** should be prepared via an *n*-butyllithium-mediated coupling of 1-bromo-4-iodobenzene **119** with ketone **127**, followed by deoxygenation (Figure 56).[171] Therefore, *n*-butyllithium was added to a solution of both starting materials in THF at -78 °C over a period of 15 min. The resulting mixture was allowed to warm to room temperature and stirred for a total of 3 h before being quenched with aqueous ammonium chloride solution. After aqueous work up, purification by column chromatography provided alcohol **128** in a yield of 50%. The hydroxy group in **128** was subsequently removed afterwards by deoxygenation using triethylsilane and trifluoroacetic acid (TFA). To a solution of alcohol **128** and triethylsilane in dichloromethane, TFA was added at -78 °C over a period of 30 min. The mixture was then allowed to warm to room temperature and stirred for a total of 3.5 h before being quenched with aqueous sodium hydroxide solution. Aqueous work up and following purification by column chromatography afforded aryl bromide **118** in a yield of 73%.

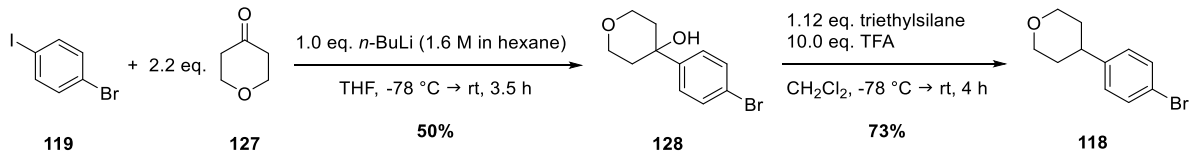

Figure 56: Synthesis of aryl bromide **118** by coupling of **119** and **127** followed by deoxygenation.

Figure 57 shows several analogs of morpholine compound **43** that were to be synthesized. The required aryl halides **129**-**135** were not commercially available and needed to be prepared. The syntheses of the aryl halides **129**-**135** are described below.

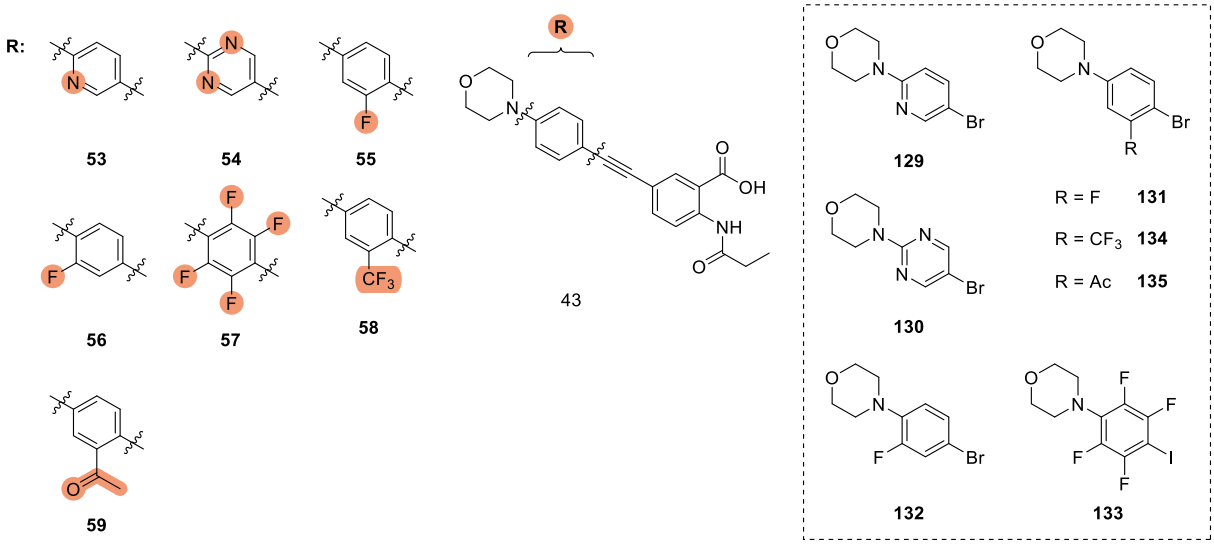

Figure 57: Analogs (**53**-**59**) of **43** and aryl halides (**129**-**135**) required for their synthesis.

Aryl morpholine compounds **129**-**135** should be prepared analogously to **112**, **114**-**117** by ULLMANN-GOLDBERG coupling of the appropriate aryl halide (**136**-**139**) with morpholine (Figure 58 and Table 27). In contrast to 1-bromo-4-iodobenzene **119**, more electron deficient aryl bromides (**136**-**139**) were used in this series of ULLMANN-GOLDBERG coupling reactions leading to better conversions.

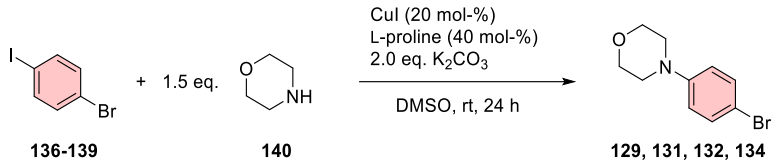

Figure 58: Synthesis of aryl halides **129**, **131**, **132**, and **134** by ULLMANN-GOLDBERG coupling of **136**-**139** with morpholine **140**.

In the case of coupling products **129**, **131** and **134**, high yields ranging between 57 and 76% were achieved. However, the coupling of 4-bromo-2-fluoro-1-iodobenzene **138** with morpholine **140** to obtain product **132** resulted in a significantly lower yield of 13%. Dehalogenation of the used aryl halide is a common side reaction occurring during ULLMANN-GOLDBERG couplings. Monitoring via TLC indicated that **138** was more likely converted into the side product 1-bromo-3-fluorobenzene than the desired coupling product **132**.

Table 27: Starting materials used for the synthesis of **129**-**134** and the corresponding yields.

Starting material		Product		Yield
136	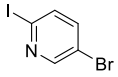	**129**	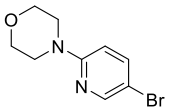	76%
137	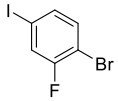	**131**	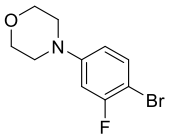	57%
138	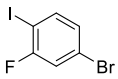	**132**	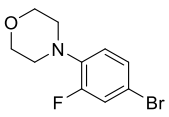	13%
139	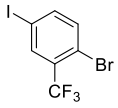	**134**	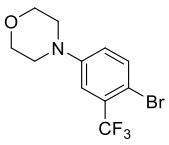	71%

For the synthesis of aryl morpholine compound **135** via ULLMANN-GOLDBERG coupling, aryl bromide **142** was required (Figure 59). The compound was not commercially available and needed to be synthesized. This should be achieved by iodination of 2'-bromoacetophenone **141**.

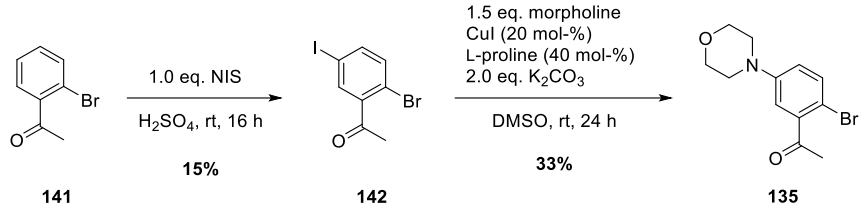

Figure 59: Synthesis of **135** by iodination of 2'-bromoacetophenone **141** and following Ullmann-Goldberg coupling with morpholine.

In combination with strong and more concentrated acids, *N*-iodosuccinimide (NIS) has been shown to be an efficient iodination agent for electron-deficient, deactivated aromatic compounds like **141**.[172] The bromine and the acetyl substituent in **141** both withdraw electron density from the aromatic ring, which decreases the reaction rate. The reaction is highly regioselective and occurs at the 3' and 5' positions of the aromatic ring due to the +M effect of the bromine and the -M effect of the acetyl substituent (Figure 60).

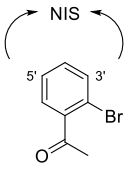

Figure 60: Possible positions for the electrophilic aromatic substitution.

The iodination was performed following a protocol from J. J. DRESSLER *et al.*[173]. An ice-cold mixture of 2'-bromoacetophenone **141** in concentrated sulfuric acid was treated with NIS and stirred for 16 h at room temperature. After aqueous workup, the two regioisomers were separated by column chromatography. The desired regioisomer **142** was obtained in a yield of 15%. Complete conversion of the starting material **141** was not achieved, and separation of the regioisomers was complicated due to their similar retention times during column chromatography. The following ULLMANN-GOLDBERG coupling reaction of 2'-bromoacetophenone **142** with morpholine finally gave aryl bromide **135** in a yield of 33%.

Tetrafluorinated morpholine compound **133** should be synthesized by nucleophilic aromatic substitution (S_NAr) of iodopentafluorobenzene **143** with morpholine **140** (Figure 61). Therefore, both starting materials were stirred in triethylamine at 150 °C for 1 h.[174] The reaction order (ArF > ArCl > ArBr > ArI) of S_NAr reactions is contrary to the typical leaving group ability of halides (I > Br > Cl > F).[175,176] The fluorine substituents in the *ortho* and *para* positions relative to the iodine substituent are activated for substitutions due to resonance effects.[177] After purification by column chromatography, the desired *para*-substituted product **133** was obtained in a yield of 68%. The formation of the *ortho*-product was observed via TLC only in trace amounts.

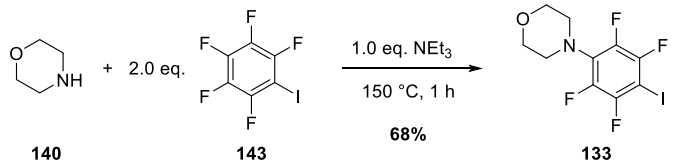

Figure 61: Synthesis of **133** by S_NAr of iodopentafluorobenzene **143** with morpholine **140**.

Figure 62 shows further analogs (**60**-**63**) of morpholine compound **43** that should be synthesized, including the aryl halides (**144**-**147**) necessary for the synthesis. The methods for synthesizing the required aryl halides **144**-**147** are detailed below.

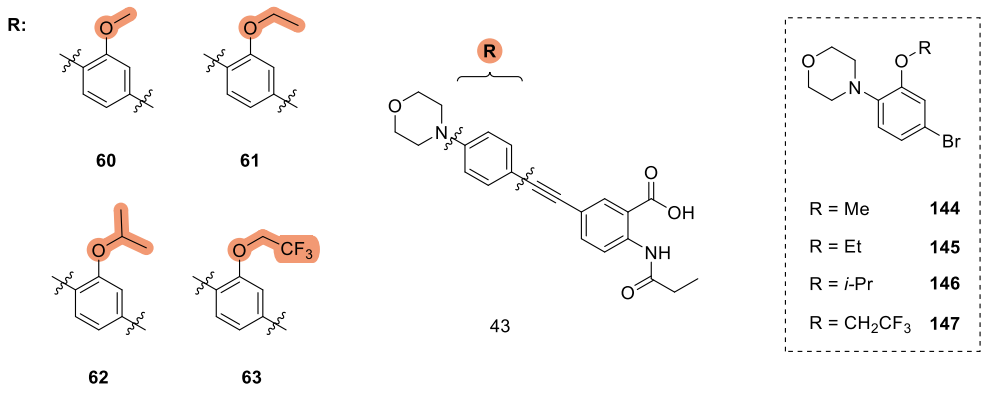

Figure 62: Analogs (**60**-**63**) of **43** and aryl halides (**144**-**147**) required for their synthesis.

The aryloxy compounds **144**-**147** should be obtained by BUCHWALD-HARTWIG coupling of the appropriate aryl iodide (**149**-**152**) with morpholine (Figure 63). Only the methoxy compound **149** was commercially available, whereas all other aryl iodides (**150**-**152**) needed to be synthesized. The ethoxy and isopropoxy compounds (**150** and **151**) should be prepared by alkylation of phenol **148**. Therefore, 5-bromo-2-iodophenol **148** was dissolved in acetone

and treated with potassium carbonate and the appropriate alkyl iodide. The mixture was stirred at room temperature for 16 h. Purification by column chromatography gave the ethoxy (**150**) and isopropoxy compounds (**151**) in yields of 88 and 84%, respectively.

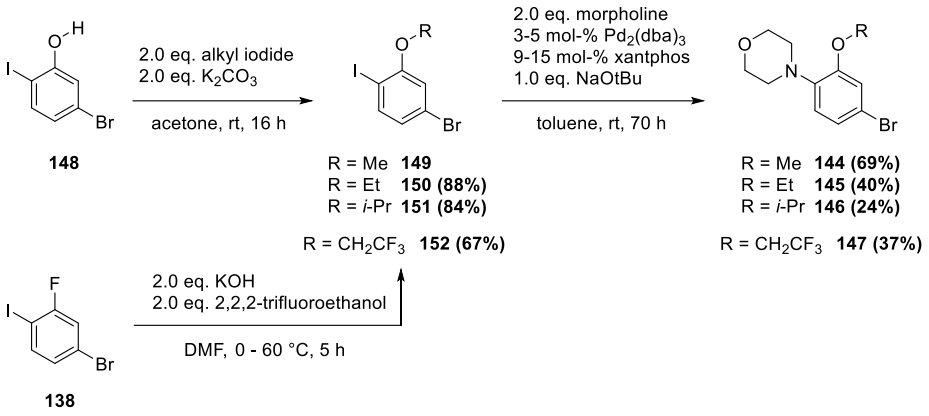

Figure 63: Synthesis of **144**-**147** starting from **148** and **138**.

The trifluoroethoxy compound **152** should be synthesized in a S_NAr reaction using 4-bromo-2-fluoro-1-iodobenzene **138** and 2,2,2-trifluoroethanol as starting materials.[178] To an ice-cold suspension of aryl fluoride **138** and potassium hydroxide in dimethylformamide, 2,2,2-trifluoroethanol was added dropwise. The reaction mixture was stirred at 60 °C for 5 h and then quenched with water. Purification by column chromatography afforded the trifluoroethoxy compound **152** in a yield of 67%.

A following BUCHWALD-HARTWIG coupling of the appropriate aryl iodides (**149**-**151**) with morpholine should then afford the aryloxy compounds **144**-**147**. In this Pd-catalyzed cross-coupling reaction new C-N or C-O bonds are formed between aryl halides or triflates and amines or alcohols in the presence of a stoichiometric amount of base.[179] The first Pd-catalyzed C-N bond formation was reported by T. MIGITA and co-workers in 1983 between aryl bromides and aminostannanes. More than a decade later, STEPHEN L. BUCHWALD and JOHN F. HARTWIG independently reported first an improved protocol for this reaction (1994) and later a tin-free Pd-catalyzed coupling of aryl bromides with amines (1995), now known as the BUCHWALD-HARTWIG amination. The mechanism of the BUCHWALD-HARTWIG amination has been thoroughly investigated throughout its development and varies depending on the nature of the ligand and substrate. Two pathways for the BUCHWALD-HARTWIG amination are shown in Figure 64. The first step is the oxidative addition of the aryl halide to the palladium(0) catalyst. In the second step, a palladium(II) aryl amine species is formed either by coordination of the amine and direct displacement of the halide (path A) or via a palladium(II)

alkoxide intermediate formed by base complexation (path B). Finally, the arylamine is released through reductive elimination.[179,180]

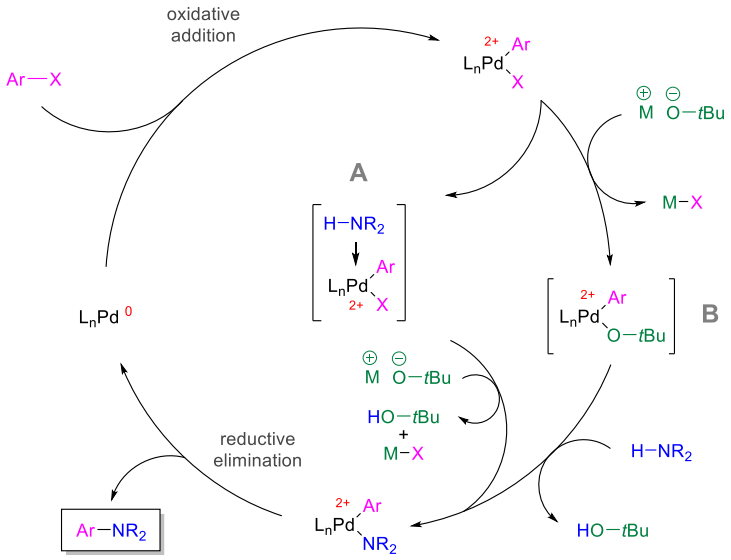

Figure 64: Catalytic cycles proposed for BUCHWALD-HARTWIG amination reactions.[179]

BUCHWALD-HARTWIG coupling reactions were performed according to a protocol from P. Blencowe *et al.*[181]. Morpholine, sodium *tert*-butoxide and a catalyst system consisting of tris(dibenzylidene-acetone)dipalladium(0) (3-5 mol-%) and xantphos (9-15 mol-%) were added to the appropriate aryl iodide (**149**-**152**) dissolved in toluene (Figure 63). Due to observed displacement of the bromine substituent at higher temperatures, rather than the desired substitution of the iodine, the mixture was stirred at room temperature for an extended period of 70 h. Aqueous work up and purification by column chromatography provided the aryloxy compounds **144**-**147**. Lower conversion was observed for compounds with bulkier alkoxy groups, probably due to steric hindrance. The methoxy compound **144** was isolated in a yield of 69%, whereas only a yield of 24% was obtained for the isopropoxy compound **146**. The coupling reaction yielded the ethoxy (**145**) and trifluoroethoxy compounds (**147**) in moderate yields of 40% and 37%, respectively.

For the synthesis of the final hDHODH inhibitors **77**-**82**, the aryl halides **153**-**157** shown in Figure 65 were required. They should be synthesized either by reductive amination or ULLMANN-GOLDBERG coupling reaction using the same reaction conditions described above.

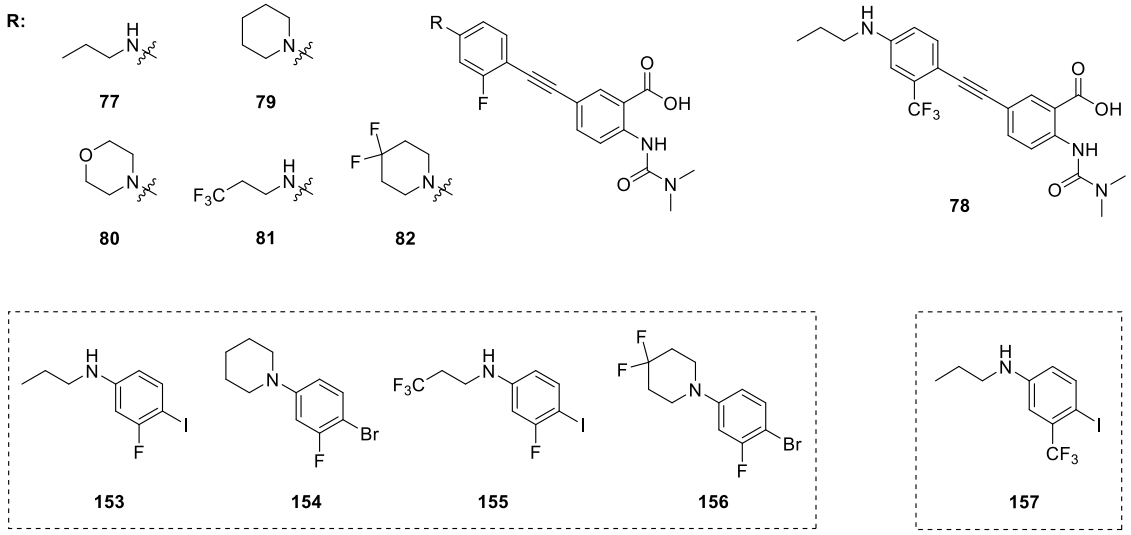

Figure 65: Required aryl halides **153**-**157** for the synthesis of the final DHODH inhibitors **77**-**82**.

Aryl halides **153, 155** and **157** were prepared analogously to **104** by reductive amination of anilines **158** and **159** with aldehydes **160** and **106** (Figure 66). In contrast to 4-iodoaniline **105**, the formation of the tertiary amine as a side reaction was notably less prevalent when using the more electron-deficient anilines **158** and **159** for the preparation of aryl halides **153, 155** and **157**. Fluorine analogs **153** and **155** were isolated in yields of 63% and 69%, whereas an even higher yield of 89% was achieved for trifluoromethyl analog **157**.

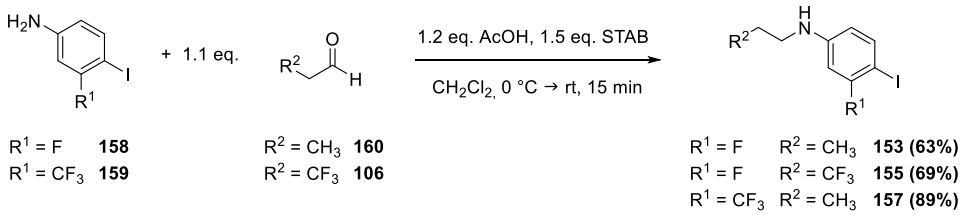

Figure 66: Synthesis of aryl halides **153**, **155** and **157** by reductive amination of anilines **158** and**159** with aldehydes **160** and **106**.

The ULLMANN-GOLDBERG reaction should also be applied for the coupling of 4-bromo-2-fluoro-1-iodobenzene **137** with amines **121** and **161** to give aryl halides **154** and **156**. The aryl halides **154** and **156** were obtained in yields of 39% and 57%, respectively (Figure 67).

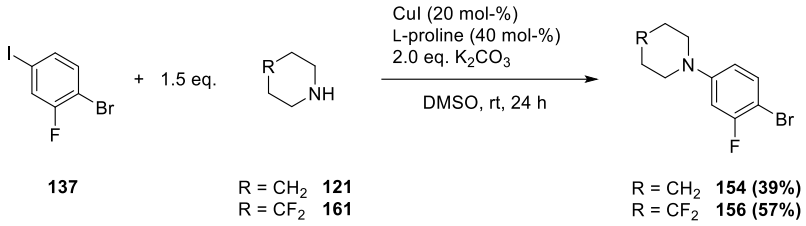

Figure 67: Synthesis of aryl halides **154** and **156** by ULLMANN-GOLDBERG coupling of **137** with amines **121** and **161**.

All aryl halides were successfully synthesized, with yields ranging from moderate to good, and should be used in the subsequent synthesis steps to obtain the alkyne building blocks required for the preparation of target compounds.

Syntheses of alkynes

The alkyne building blocks should be synthesized by SONOGASHIRA coupling of the appropriate aryl halide with trimethylsilylacetylene and following cleavage of the silyl ether. The mechanism of the SONOGASHIRA cross-coupling reaction is not yet fully elucidated. As depicted in Figure 68, it is assumed that the mechanism is divided into two independent catalytic cycles.[182]

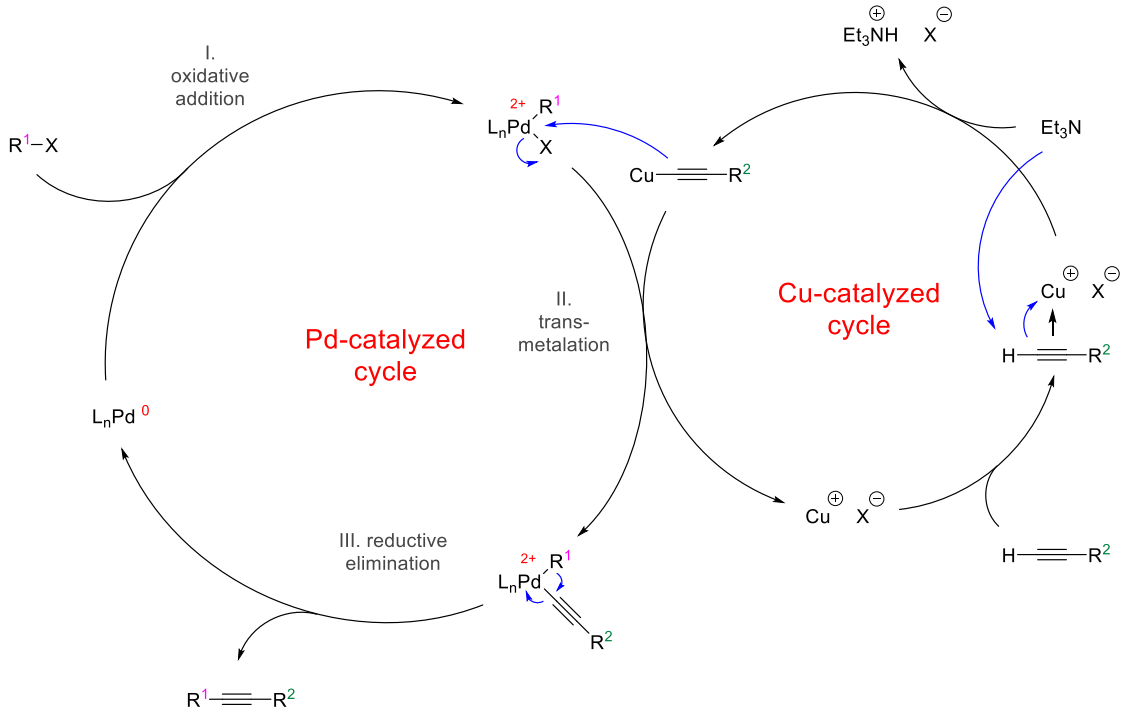

Figure 68: Catalytic cycles proposed for SONOGASHIRA cross-coupling reactions.[182]

The initial step of the palladium cycle involves the oxidative addition of an aryl, heteroaryl, or vinyl halide to the palladium(0) catalyst, resulting in the formation of a palladium(II) complex. In the following rate-limiting transmetalation step, a copper acetylide transfers its organic group to the palladium(II) complex. The copper acetylide involved in the transmetalation is formed in the copper cycle by deprotonation of a terminal alkyne using a tertiary amine as base and in the presence of a copper(I) salt. Finally, an unsymmetrical alkyne is released as the coupled product through reductive elimination and the palladium(0) catalyst is regenerated. The two substituents must adopt cis-orientation to get in close vicinity for reductive elimination, suggesting that a trans/cis isomerization may be integrated into the mechanism. [182]

After obtaining the TMS-protected alkyne, the silyl ether should be cleaved using methanolate as the nucleophile. The mechanism is shown in Figure 69. Silicon has a strong affinity for electronegative atoms such as oxygen, fluorine, and chlorine. Sterically hindered silyl groups (e.g. tetrabutylsilyl) are cleaved under harsher reaction conditions with fluoride sources, such as tetra-*n*-butylammonium fluoride (TBAF) or hydrofluoric acid, whereas cleavage of TMS can be achieved simply by treatment with methanol. The nucleophile attacks the silicon atom of the silyl group, resulting in the formation of a pentavalent anion, and subsequent decomposition releases the free alkyne.[163,183]

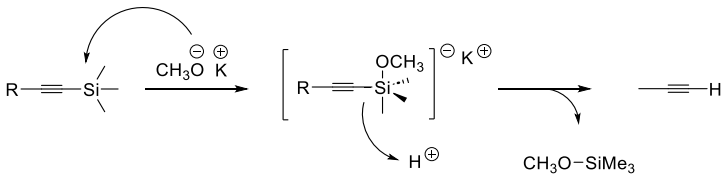

Figure 69: Mechanism for the cleavage of the TMS protecting group.

SONOGASHIRA coupling reactions were performed according to a protocol of T. INOUCHI *et al*.[184] (Figure 70). Tetrakis(triphenylphosphine)palladium(0) ($Pd(PPh_3)_4$) and TMS acetylene were added to a mixture of the appropriate aryl halide and copper iodide in triethylamine and THF. The mixture was then stirred for 20-24 h at room temperature or 70 °C. In contrast to aryl iodides, higher temperatures are needed for the conversion of aryl bromides. Aqueous work up and purification via column chromatography afforded the TMS-protected alkynes. Due to similar retention times of the starting material and the product, complete conversion is necessary for purification via column chromatography. The cleavage of the TMS protecting group was then carried out with potassium carbonate in methanol at room temperature for 2-4 h.[185] The free alkynes were obtained after removal of potassium carbonate followed by aqueous work up. Due to their instability, the alkynes were used in the next reaction step without further purification. Sufficient purity could be observed with NMR spectroscopy.

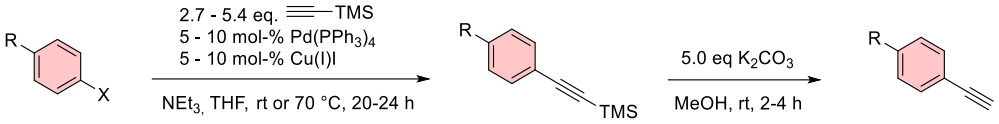

Figure 70: Synthesis of required alkyne building blocks by SONOGASHIRA coupling of the appropriate aryl halide with TMS-acetylene and following cleavage of the TMS protecting group.

Table 28 and Table 29 present the yields from the synthesis of the TMS-protected alkynes (**162**-**167**, **174**-**180**) and free alkynes (**168**-**173**, **181**-**187**) from the first optimization cycle. All TMS-protected alkynes were synthesized with moderate to good yields. For the 1-methyl-piperazine analog **176**, incomplete conversion of the starting material required preparative TLC as an additional purification step. Only a lower yield of 32% was obtained for the benzimidazole analog **167**. In the previous reaction, starting material **108** could not be separated from its regioisomer, so a 1:1 mixture was used for the SONOGASHIRA coupling with TMS acetylene. Fortunately, column chromatography enabled successful separation at this stage.

Table 28: Yields obtained from the synthesis of the TMS-protected alkynes **162**-**167** and free alkynes **168**-**173** during optimization cycle 1.

Aryl halide		TMS-protected alkyne		Yield	Alkyne		Yield
101	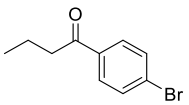	**162**	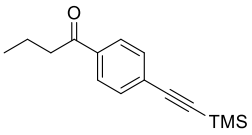	76%	**168**	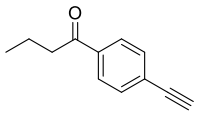	56%
102	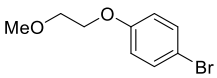	**163**	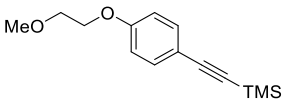	82%	**169**	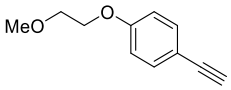	88%
103	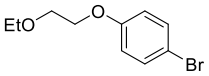	**164**	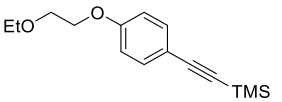	81%	**170**	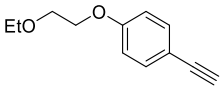	62%
104	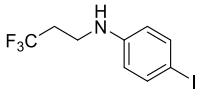	**165**	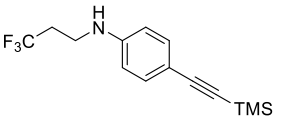	61%	**171**	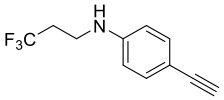	80%
107	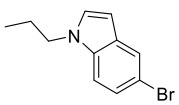	**166**	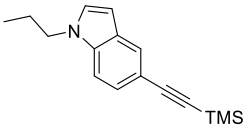	61%	**172**	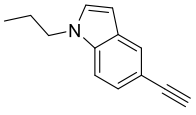	76%

108	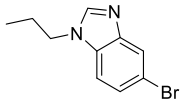 (regioisomeric mixture)	**167**	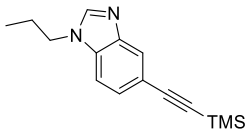	32%	**173**	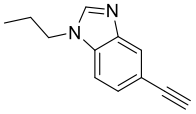	96%

The alkyne building blocks **168**-**173** and **181**-**187** were also synthesized successfully in moderate to good yields. Alkynes are the most acidic of hydrocarbons and can be deprotonated even by milder nitrogen bases (e.g. ammonia), which is useful for the subsequent SONOGASHIRA coupling reaction. However, decomposition and dimerization were also observed during aqueous work up, particularly for electron deficient phenylacetylenes. This instability is one reason why the alkynes were not further purified via column chromatography.

Table 29: Yields obtained from the synthesis of the TMS-protected alkynes **174**-**180** and free alkynes **181**-**187** during optimization cycle 1.

Aryl halide		TMS-protected alkyne		Yield	Alkyne		Yield
112	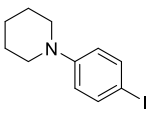	**174**	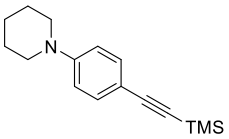	81%	**181**	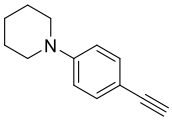	69%
113	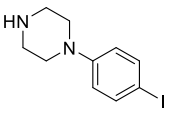	**175**	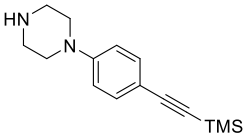	57%	**182**	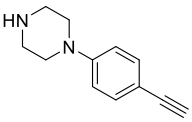	73%
114	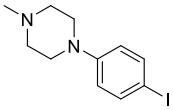	**176**	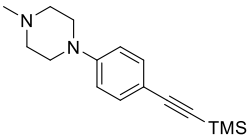	88%	**183**	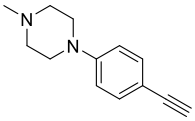	91%
115	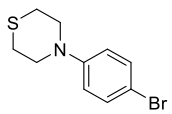	**177**	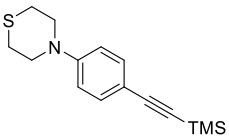	78%	**184**	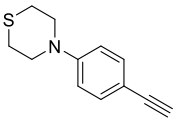	75%
116	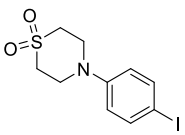	**178**	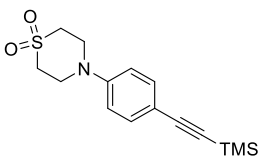	76%	**185**	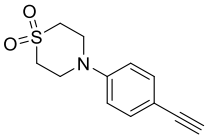	77%
118	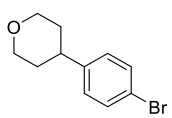	**179**	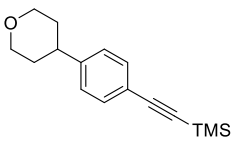	93%	**186**	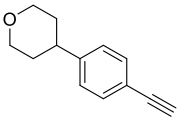	80%

117	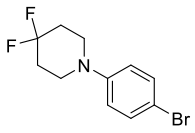	**180**	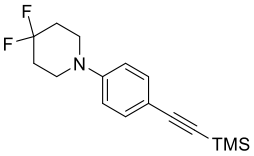	77%	**187**	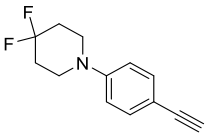	73%

The yields from the synthesis of the TMS-protected alkynes (**188**-**194**, **202-205**) and free alkynes (**195**-**201**, **206-209**) from the second optimization cycle are summarized in Table 30 and Table 31. Moderate to good yields were also obtained in the synthesis of TMS-protected alkynes **188**-**194** and **202-205**. However, the coupling of TMS-acetylene with trifluoromethyl analog **134** afforded TMS-protected alkyne **193** in a low yield of only 26%. This low yield may be attributed to steric hindrance during the oxidative addition of Pd(0) to aryl bromide **134**, caused by the neighboring trifluoromethyl group, even though its electron-withdrawing properties should favor the reaction. The reaction was quenched after 24 h due to stagnating conversion of the starting material, and preparative TLC was additionally required for purification of the product.

Table 30: Yields obtained from the synthesis of the TMS-protected alkynes **188**-**194** and free alkynes **195**-**201** during optimization cycle 2.

Aryl halide		TMS-protected alkyne		Yield	Alkyne		Yield
129	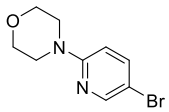	**188**	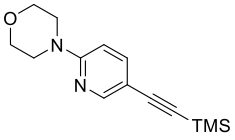	94%	**195**	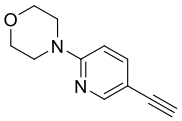	63%
130	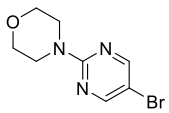	**189**	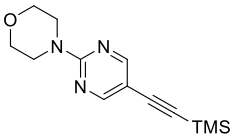	82%	**196**	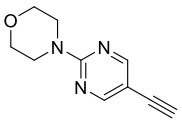	88%
131	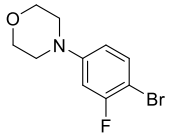	**190**	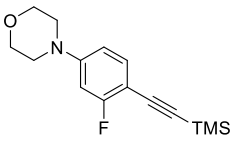	65%	**197**	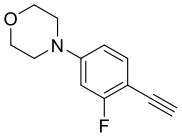	52%
132	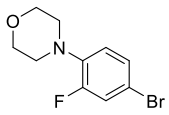	**191**	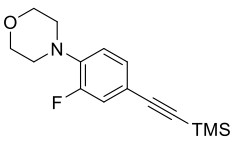	74%	**198**	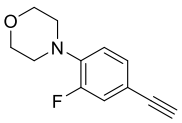	81%
133	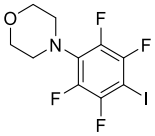	**192**	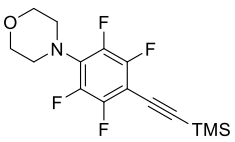	70%	**199**	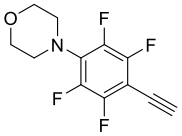	n.d.

134	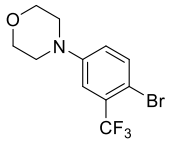	**193**	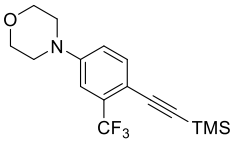	26%	**200**	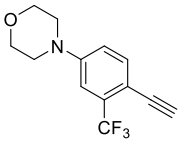	86%
135	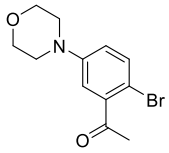	**194**	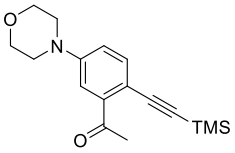	81%	**201**	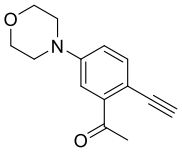	n.d.

Deprotection of the TMS-protected alkynes **188**-**194** and **202**-**205** afforded the alkyne building blocks **195**-**201** and **206**-**209** also in moderate to good yields. For the electron-deficient phenylethynyl compounds **199** and **201**, decomposition occurred during aqueous workup, leading to the decision to skip this step and directly utilize the crude product in the subsequent SONOGASHIRA coupling reaction.

Table 31: Yields obtained from the synthesis of the TMS-protected alkynes **202**-**205** and free alkynes **206**-**209** during optimization cycle 2.

Aryl halide		TMS-protected alkyne		Yield	Alkyne		Yield
144	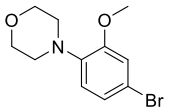	**202**	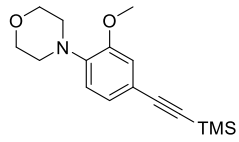	82%	**206**	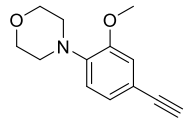	87%
145	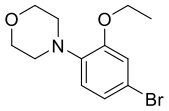	**203**	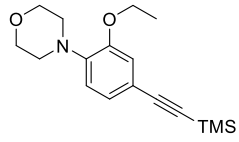	68%	**207**	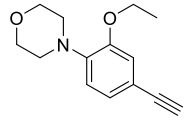	87%
146	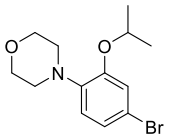	**204**	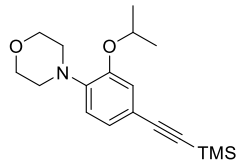	82%	**208**	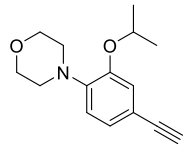	90%
147	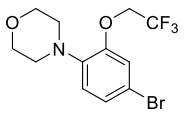	**205**	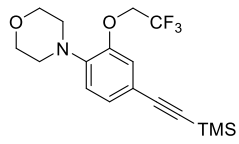	92%	**209**	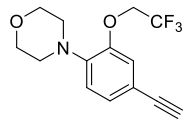	85%

In the third optimization cycle, the synthesis of the target compounds required alkyne **212** (Table 32). TMS-protected alkyne **211** was obtained in a yield of 84% and following deprotection provided alkyne **212** in a yield of 88%.

Table 32: Yields obtained from the synthesis of the TMS-protected alkyne **211** and free alkyne **212** during optimization cycle 3.

Aryl halide		TMS-protected alkyne		Yield	Alkyne		Yield
210	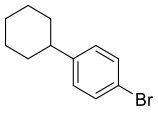	**211**	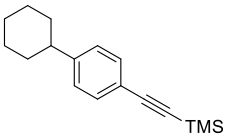	84%	**212**	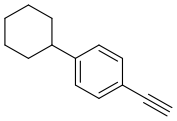	88%

Table 33 presents the yields obtained from the synthesis of both TMS-protected alkynes (**213**-**217**) and free alkynes (**218**-**222**) required for the preparation of the final DHODH inhibitors **77**-**82**. Moderate to good yields were consistently achieved in both reactions. However, after aqueous workup, the purity of alkyne **218** was inadequate, necessitating an additional purification step via column chromatography. Unfortunately, dimerization of alkyne **218** occurred during this process, resulting in a reduced yield of only 29% for the desired product.

Table 33: Yields obtained from the synthesis of the TMS-protected alkynes **213**-**217** and free alkynes **218-222** required for the preparation of the final hDHODH inhibitors **77**-**82**.

Aryl halide		TMS-protected alkyne		Yield	Alkyne		Yield
153	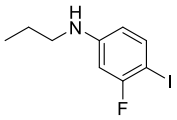	**213**	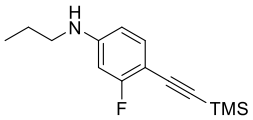	76%	**218**	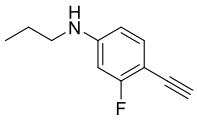	29%
157	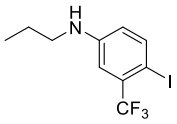	**214**	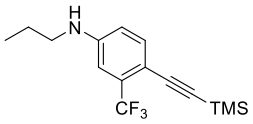	85%	**219**	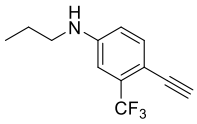	97%
154	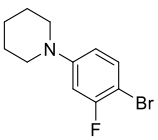	**215**	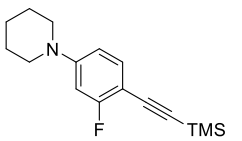	85%	**220**	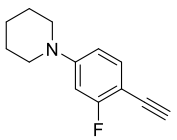	79%
155	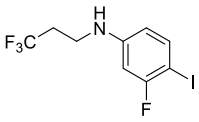	**216**	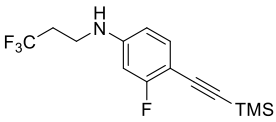	56%	**221**	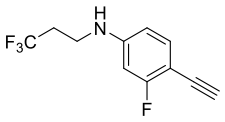	89%
156	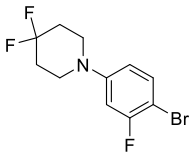	**217**	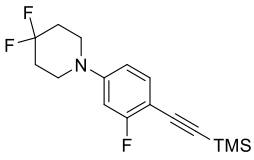	84%	**222**	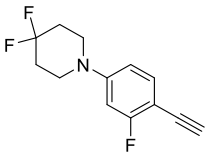	82%

All alkyne building blocks were synthesized successfully in up to four reaction steps, achieving mostly good yields. In the following SONOGASHIRA reaction, these building blocks should be coupled with an anthranilic acid derivative. Finally, saponification of the coupled product should yield the desired hDHODH inhibitors.

4.5.3. Syntheses of target compounds

For the following SONOGASHIRA coupling, the same reaction conditions as described in chapter 4.5.2 were used, with varying equivalents of the alkyne building blocks (Figure 71). Therefore, a mixture of the appropriate anthranilic acid derivative and copper iodide in tetrahydrofuran and triethylamine was treated with $Pd(PPh_3)_4$ and the appropriate alkyne. The reaction was carried out at room temperature and with 1.1 equiv. of the alkyne building block when using aryl iodides as staring materials. In contrast, a higher temperature of 70 °C and up to 3.0 equivalents of the alkyne building block were required for the conversion of aryl bromides. After stirring for 18-24 h, the crude product was purified by column chromatography.

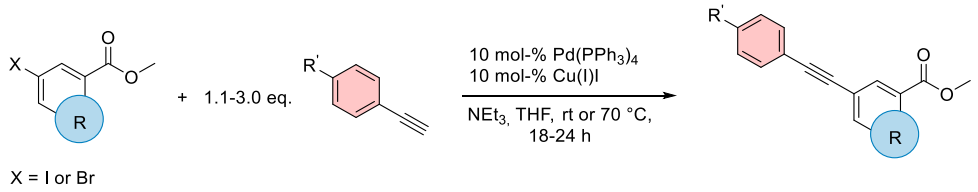

Figure 71: Reaction conditions for SONOGASHIRA couplings of previously synthesized anthranilic acid derivatives and alkyne building blocks.

The yields obtained from the synthesis of the coupled products are presented in Table 34 to Table 39, categorized by optimization cycle. All coupled products were successfully synthesized in moderate to good yields, except for tetrafluorinated analog **240** and acetyl analog **242** from optimization cycle 2, as well as benzimidazole **249** from optimization cycle 3. Alkynes **199** and **201** could not be purified due to their instability and were utilized as crude products in the synthesis of **240** and **242**, resulting in yields of only 12% and 20%, respectively (Table 36). In contrast to the other bicyclic compounds, the conversion of the benzimidazole building block **93** stagnated after 24 hours, even with the addition of more equivalents, resulting in a yield of only 34% for benzimidazole analog **249** (Table 38). Urea compound **259**, required as building block for the synthesis of the final hDHODH inhibitors **77**-**82**, was provided from previous work.[160] Coupling with the respective alkynes (**197**, **218**-**222**) allowed for the successful synthesis of intermediates **253**-**258** in good yields (Table 39).

Table 34: Yields obtained from the synthesis of the methyl esters **223**-**228** during optimization cycle 1.

Aryl halide		Alkyne		Product		Yield
90	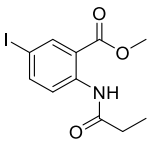	**168**	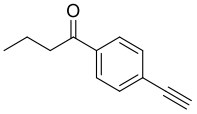	**223**	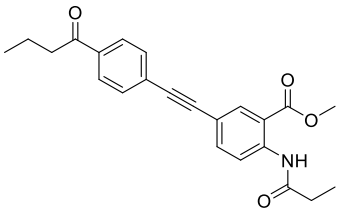	87%
90	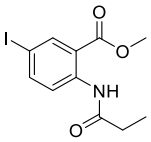	**169**	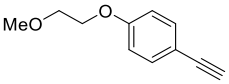	**224**	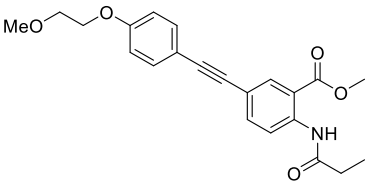	91%
90	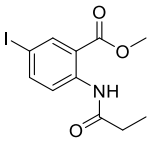	**170**	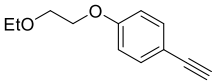	**225**	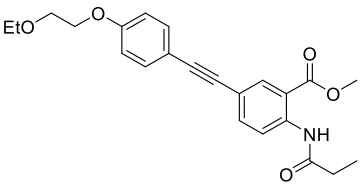	81%
90	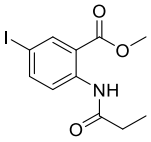	**171**	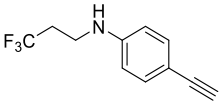	**226**	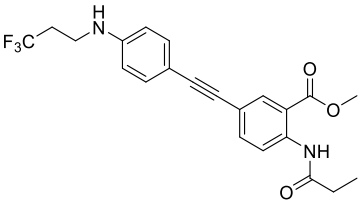	93%
90	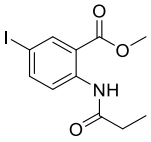	**172**	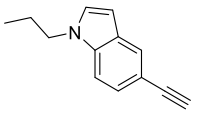	**227**	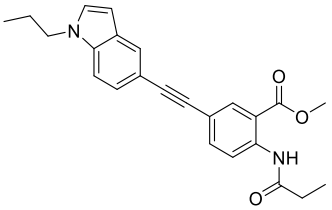	56%
90	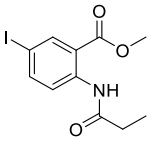	**173**	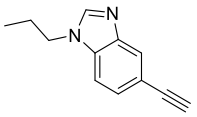	**228**	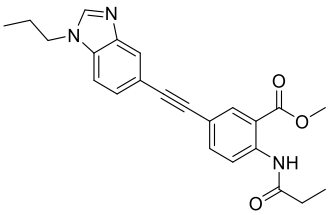	100%

Table 35: Yields obtained from the synthesis of the methyl esters **229**-**235** during optimization cycle 1.

Aryl halide		Alkyne		Product		Yield
90	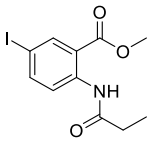	**181**	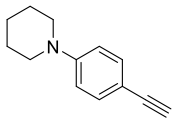	**229**	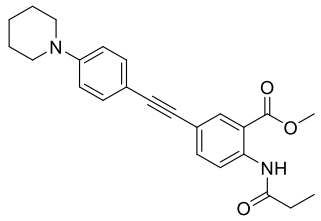	93%
90	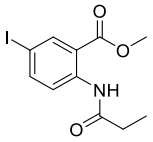	**182**	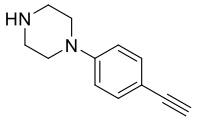	**230**	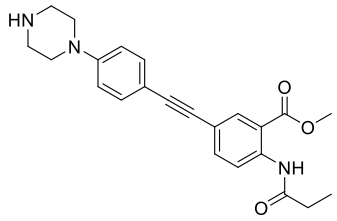	96%
90	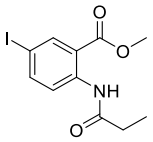	**183**	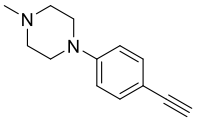	**231**	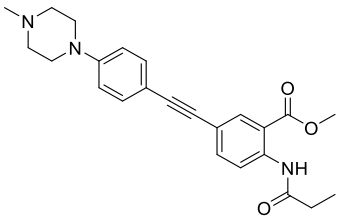	93%
90	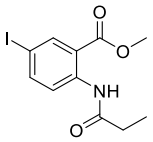	**184**	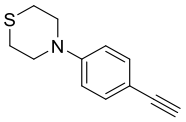	**232**	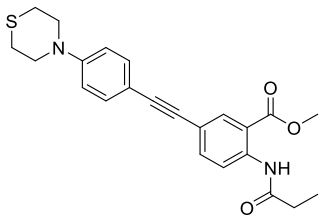	86%
90	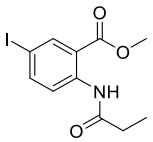	**185**	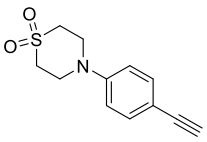	**233**	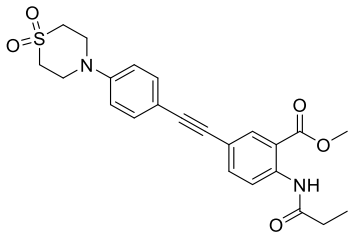	65%
90	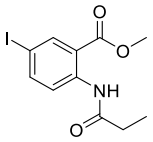	**186**	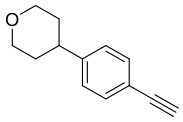	**234**	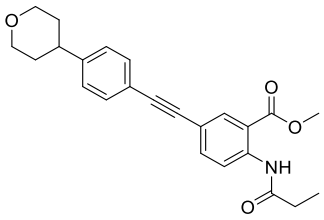	82%

90	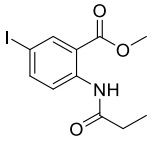	**187**	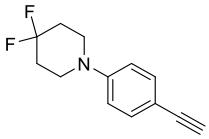	**235**	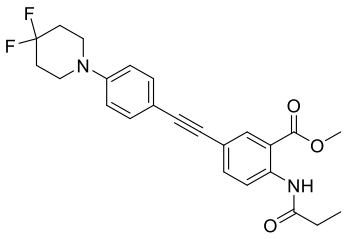	82%

Table 36: Yields obtained from the synthesis of the methyl esters **236**-**242** during optimization cycle 2.

Aryl halide		Alkyne		Product		Yield
90	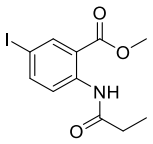	**195**	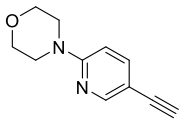	**236**	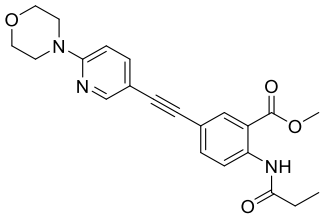	84%
90	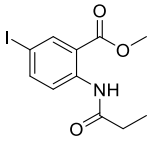	**196**	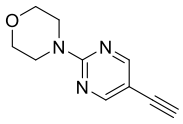	**237**	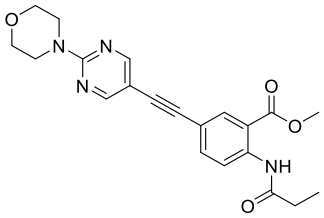	98%
90	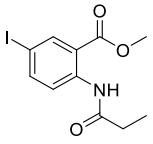	**197**	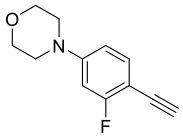	**238**	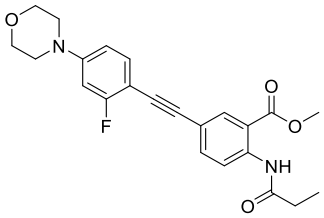	84%
90	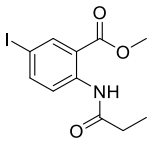	**198**	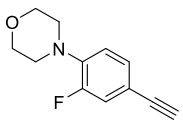	**239**	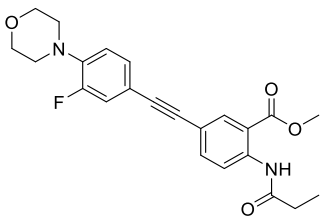	77%
90	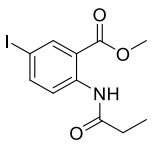	**199**	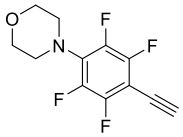	**240**	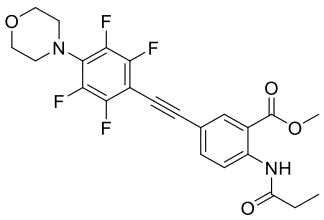	12%

90	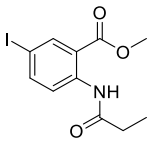	**200**	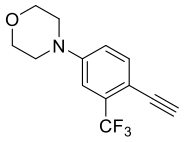	**241**	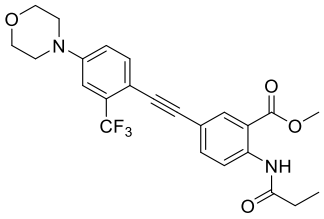	100%
90	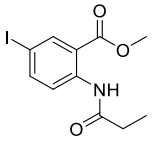	**201**	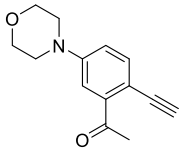	**242**	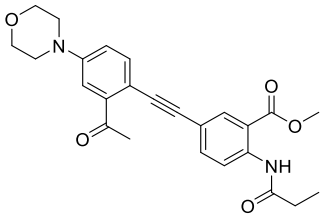	20%

Table 37: Yields obtained from the synthesis of the methyl esters **243**-**246** during optimization cycle 2.

Building block 1		Building block 2		Product		Yield
90	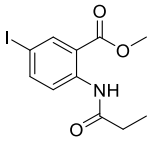	**206**	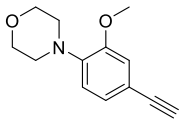	**243**	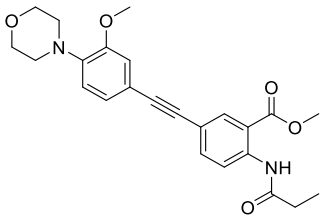	93%
90	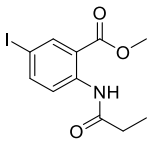	**207**	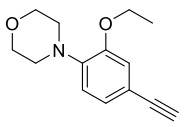	**244**	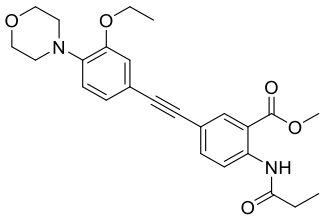	89%
90	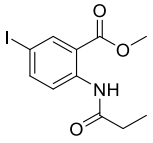	**208**	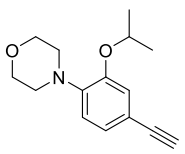	**245**	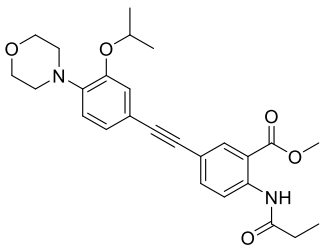	77%
90	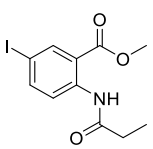	**209**	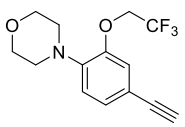	**246**	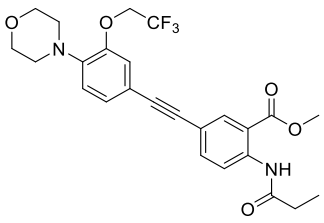	62%

Table 38: Yields obtained from the synthesis of the methyl esters **247**-**252** during optimization cycle 3.

Building block 1		Building block 2		Product		Yield
91	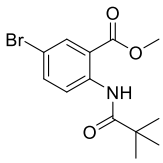	**212**	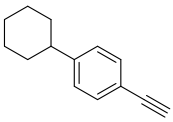	**247**	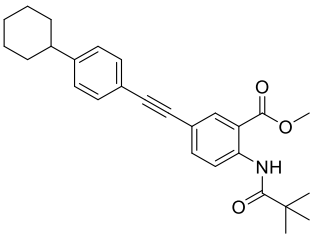	63%
92	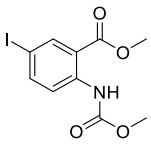	**212**	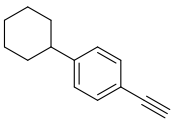	**248**	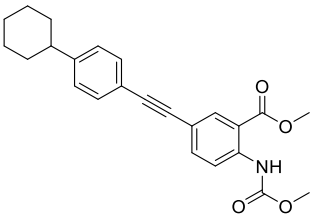	89%
93	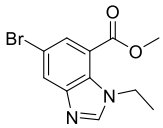	**212**	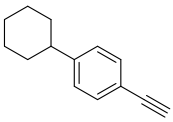	**249**	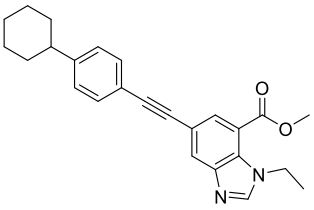	34%
94	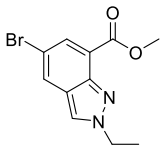	**212**	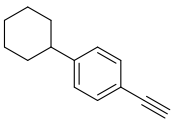	**250**	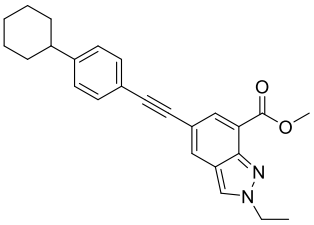	68%
95	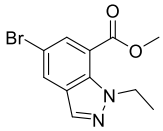	**212**	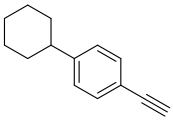	**251**	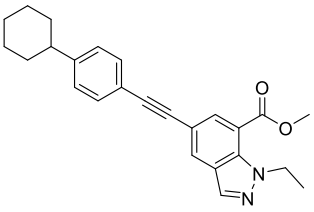	67%
96	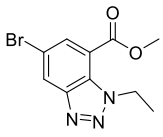	**212**	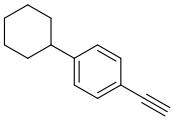	**252**	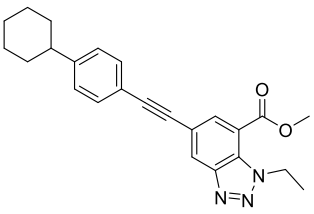	90%

Table 39: Yields obtained for the synthesis of the methyl esters **253**-**258** which are the precursors of the final DHODH inhibitors **77**-**82**.

Aryl halide		Alkyne		Product		Yield
259	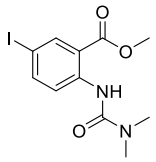	**218**	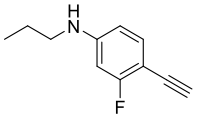	**253**	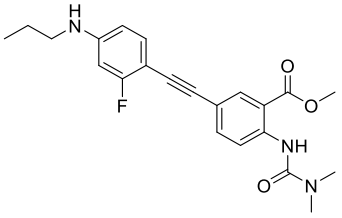	83%
259	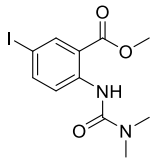	**219**	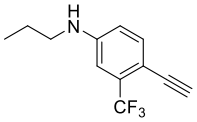	**254**	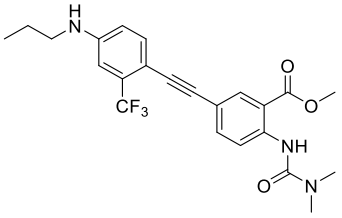	61%
259	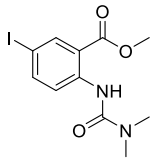	**220**	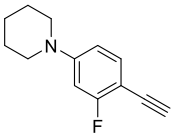	**255**	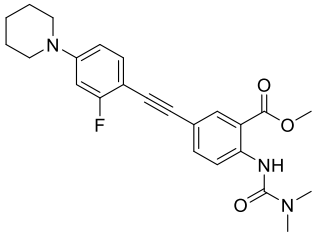	100%
259	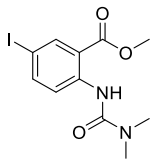	**197**	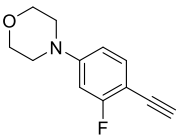	**256**	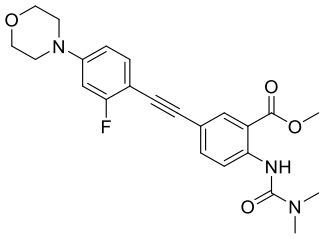	97%
259	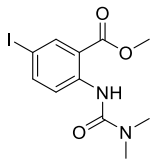	**221**	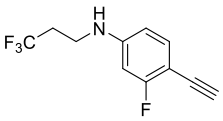	**257**	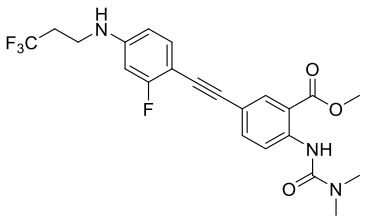	69%
259	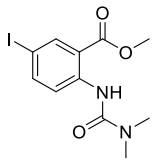	**222**	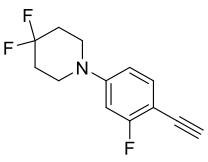	**258**	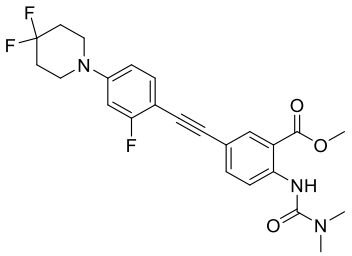	62%

The saponification of the coupled products **223**-**258** was carried out in tetrahydrofuran with the addition of 1 M aqueous NaOH (Figure 72). The reaction was stirred for up to 24 h at room temperature. The hDHODH inhibitors were obtained through precipitation in an acidic solution.

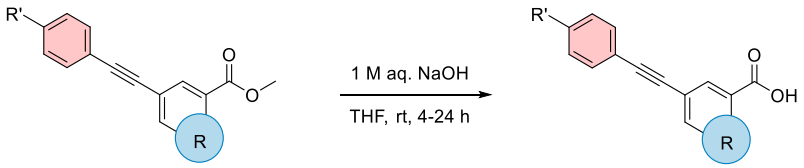

Figure 72: Saponification of methyl esters **223-258** as the final step in synthesizing the hDHODH inhibitors.

The hDHODH inhibitors obtained from the saponification are shown in Table 40 to Table 45, along with their corresponding yields for each optimization cycle. Most target compounds were successfully isolated in good yields. However, only small quantities of methyl esters **228** and **242** were available for saponification, making isolation by precipitation and filtration challenging, which resulted in a low yield of 29% for target compounds **52** and **59**.

Table 40: Yields obtained from the synthesis of target compounds **38**, **40**, **41**, **49**, **51** and **52** during optimization cycle 1.

Methyl ester		Target compound		Yield
223	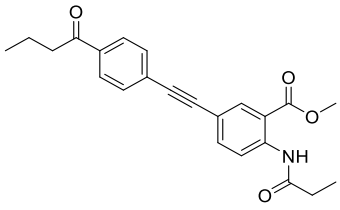	**38**	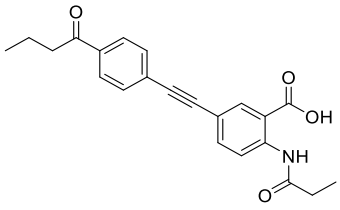	96%
224	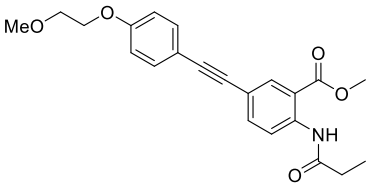	**40**	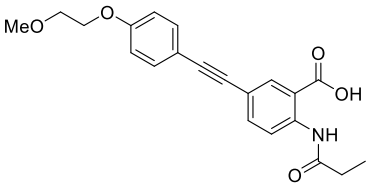	97%
225	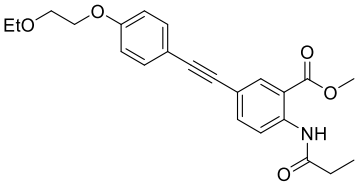	**41**	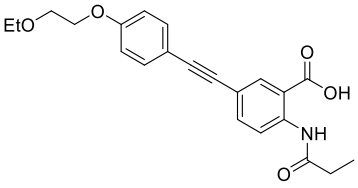	82%

226	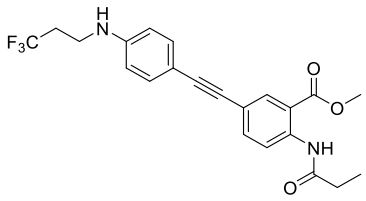	**49**	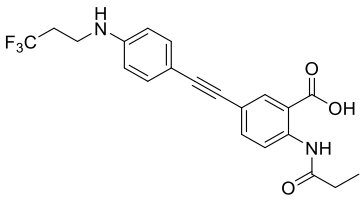	70%
227	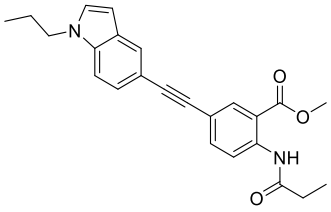	**51**	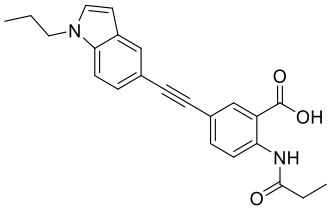	56%
228	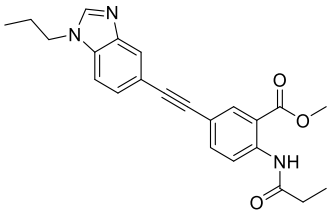	**52**	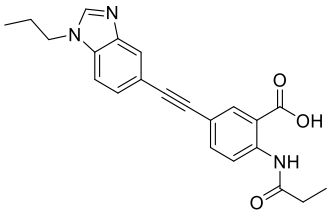	29%

Table 41: Yields obtained from the synthesis of target compounds **42**, **44**-**48** and **50** during optimization cycle 1.

Methyl ester		Target compound		Yield
229	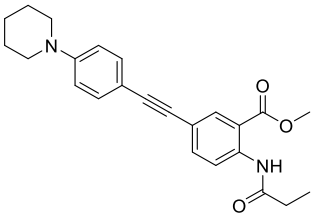	**42**	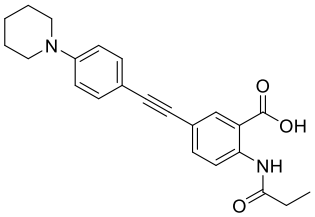	100%
230	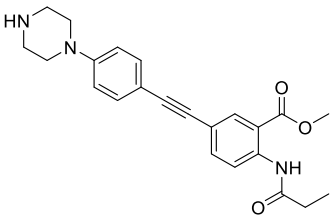	**44**	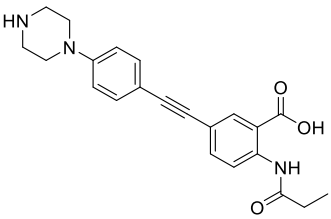	74%
231	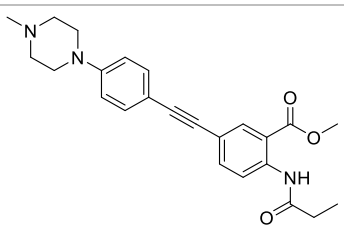	**45**	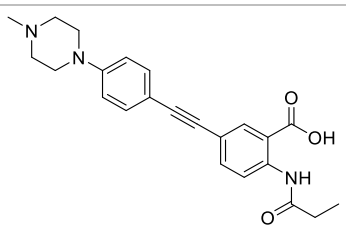	54%

232	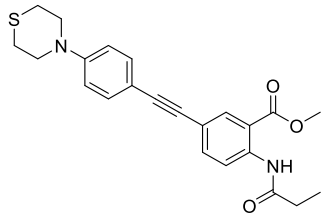	**46**	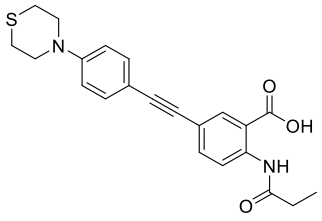	92%
233	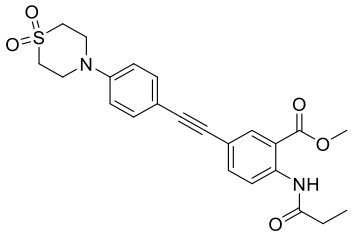	**47**	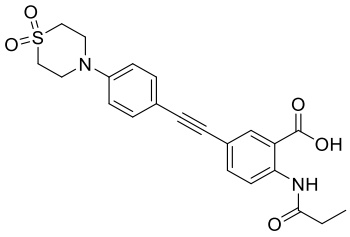	80%
234	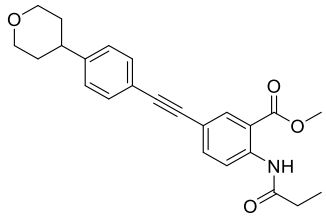	**48**	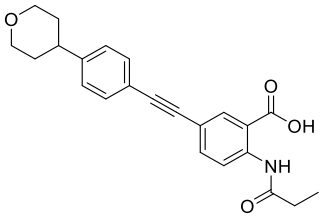	88%
235	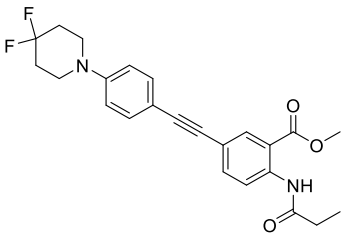	**50**	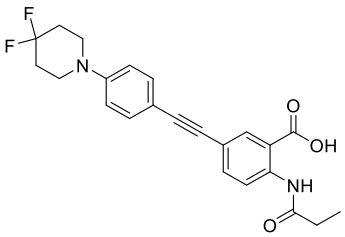	73%

Table 42: Yields obtained from the synthesis of target compounds **53**-**59** during optimization cycle 2.

Methyl ester		Target compound		Yield
236	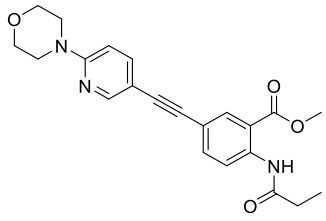	**53**	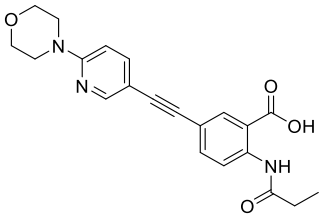	79%
237	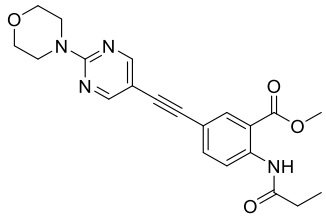	**54**	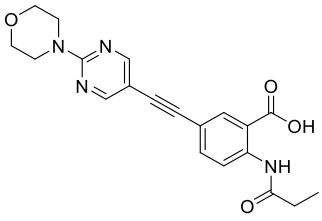	94%

238	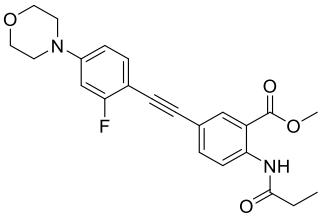	**55**	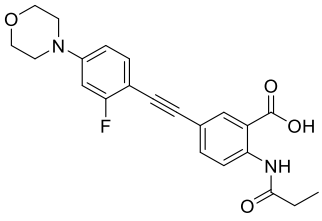	81%
239	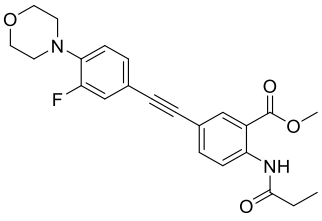	**56**	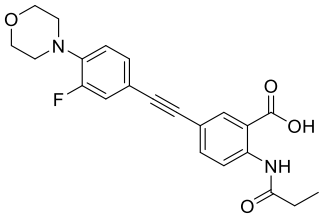	85%
240	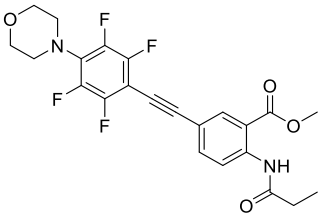	**57**	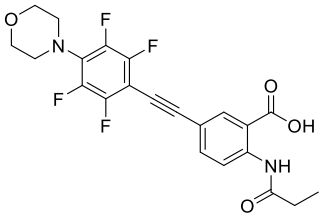	58%
241	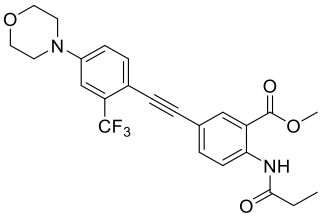	**58**	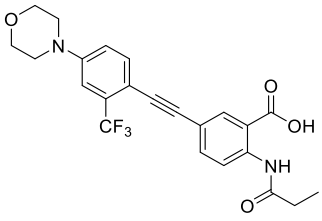	95%
242	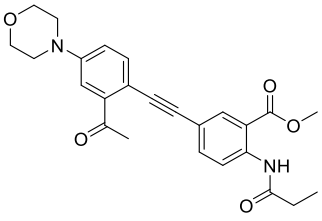	**59**	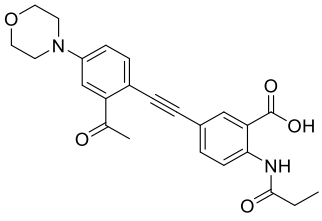	29%

Table 43: Yields obtained from the synthesis of target compounds **60**-**63** during optimization cycle 2.

Methyl ester		Target compound		Yield
243	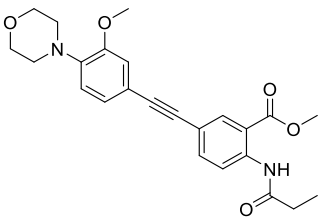	**60**	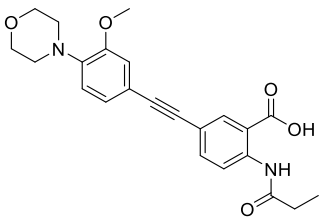	71%

244	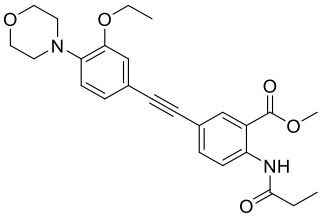	**61**	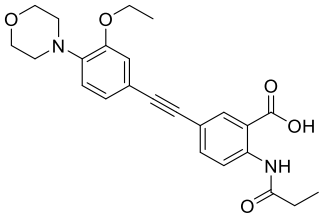	80%
245	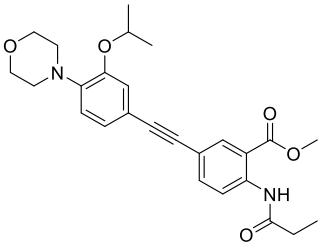	**62**	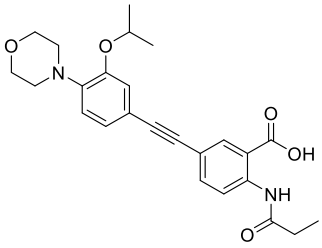	95%
246	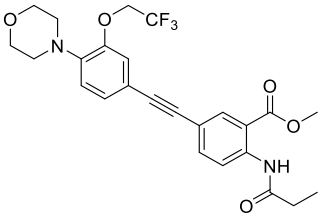	**63**	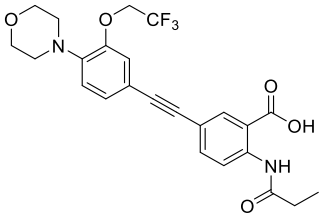	98%

Table 44: Yields obtained from the synthesis of target compounds **65**, **66**, **69-71** and **73** during optimization cycle 3.

Methyl ester		Target compound		Yield
247	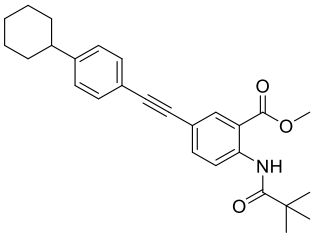	**65**	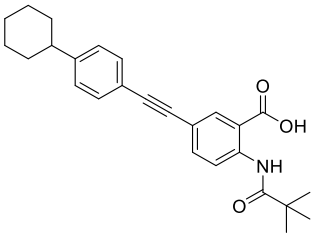	75%
248	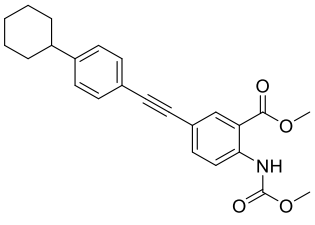	**66**	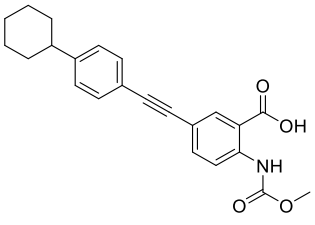	98%
249	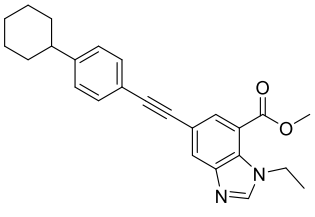	**69**	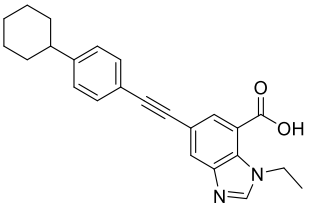	87%

250	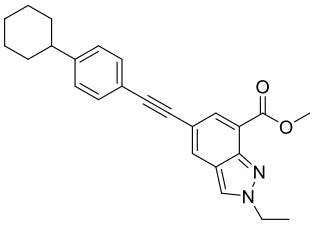	**70**	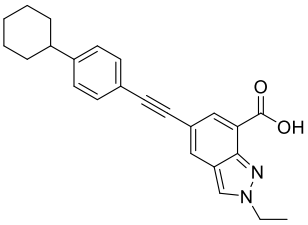	87%
251	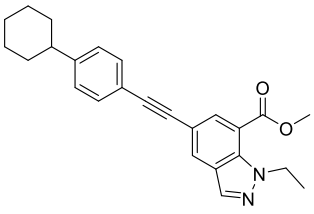	**71**	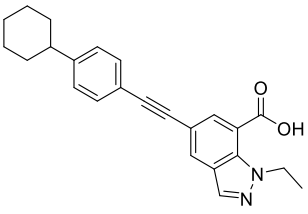	86%
252	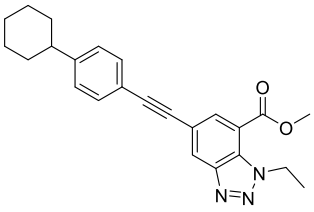	**73**	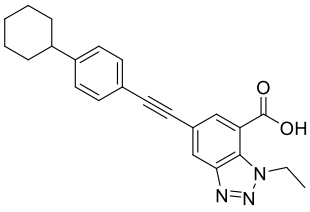	86%

Table 45: Yields obtained from the synthesis of final hDHODH inhibitors **77**-**82**.

Methyl ester		Target compound		Yield
253	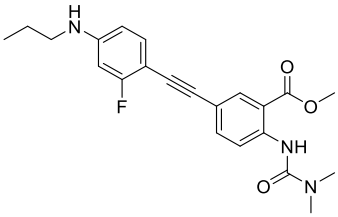	**77**	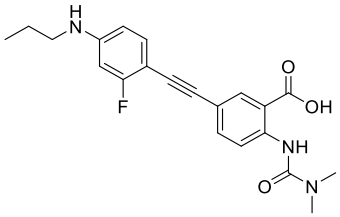	95%
254	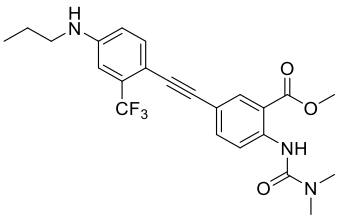	**78**	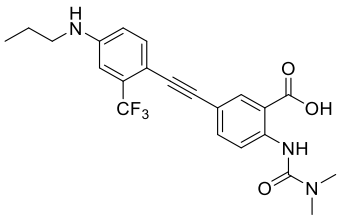	79%
255	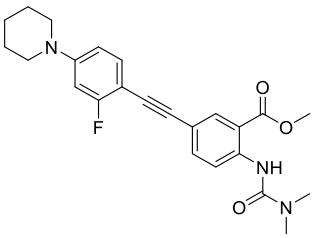	**79**	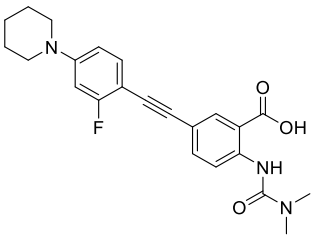	93%

256	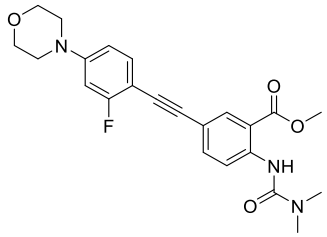	**80**	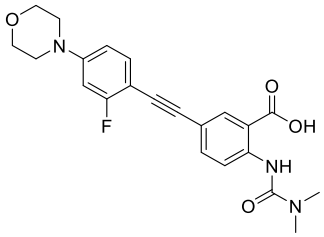	77%
257	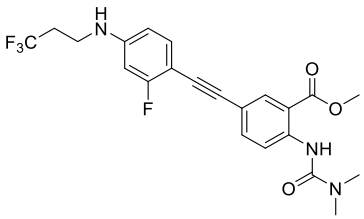	**81**	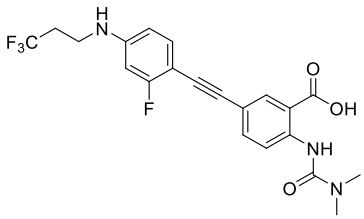	55%
258	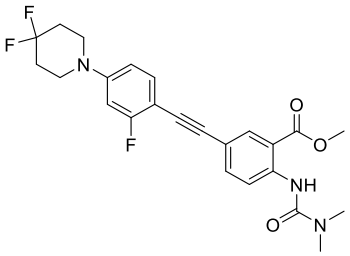	**82**	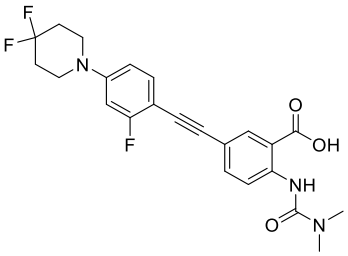	62%

A short synthesis route (4 to 6 steps) provided rapid access to a wide variety of phenylethynyl anthranilic acid based hDHODH inhibitors. All target compounds were successfully synthesized, predominantly in moderate to good yields, and subsequently investigated for their physicochemical properties, as well as their activities in the isolated enzyme and against various RNA viruses in cell-based assays.

5. Outlook

In addition to the compounds already described in chapter 2.3.1, several hDHODH inhibitors with remarkable antiviral *in vitro* activities have been developed over the past decades. Noteworthy examples include RYL-634 **260** and RYL687 **261**, S312 **262** and S416 **263**, as well as MEDS433 **264** (Figure 73).[101] RYL-634 **260** was identified through phenotypic screening of a biarylquinolone library targeting HCV-GFP. It exhibited potent activity at low nanomolar concentrations against various RNA viruses, including DENV, ZIKV, and HIV, with submicromolar efficacy against MERS-CoV and CHIKV.[186] RYL-634 **260** was also shown to be effective against EBOV, leading to the development of derivatives such as RYL-687 **261**, which exhibited enhanced potency with an EC_{50} value of 7.4 nM against EBOV.[187] S312 **262** and S416 **263** were identified through structure-based virtual screening targeting hDHODH, with IC_{50} values of 29.2 nM and 7.5 nM respectively. Both demonstrated broad antiviral activity *in vitro*, with S416 **263** showing particularly strong efficacy against various human RNA viruses, including influenza A virus (IAV), EBOV, ZIKV, and SARS-CoV-2.[188] MEDS433 **264** is a highly potent hDHODH inhibitor with a distinctive 2-hydroxypyrazolo[1,5-*a*]pyridine scaffold, exhibiting an IC_{50} value of 1.2 nM.[189] It displays broad antiviral effects *in vitro*, effectively inhibiting herpesviruses, coronaviruses and influenza viruses at low nanomolar concentrations, indicating its promise as a broad-spectrum antiviral agent.[101]

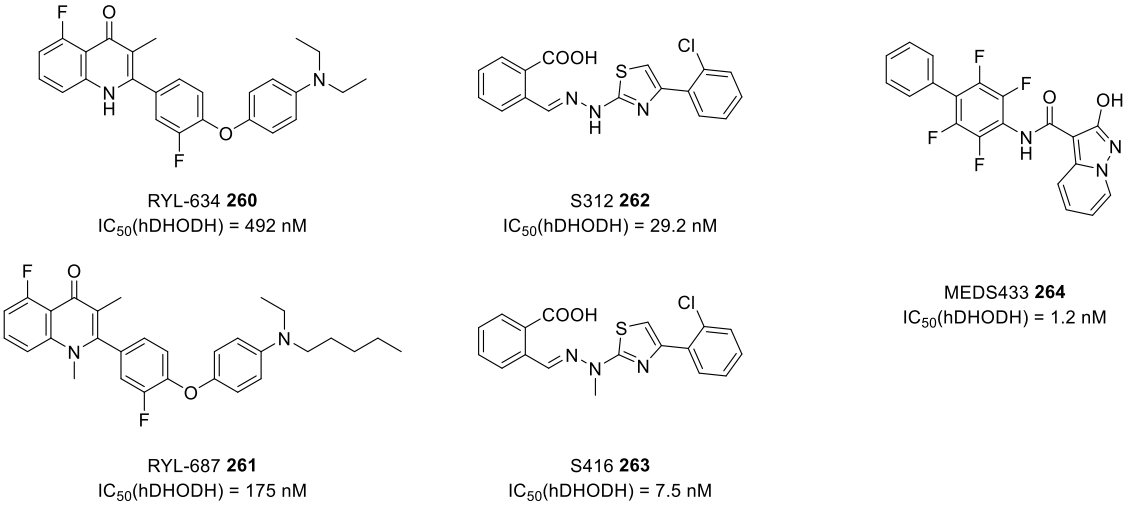

Figure 73: Selection of hDHODH inhibitors (**260**-**264**) with antiviral broad-spectrum activity.

Although hDHODH inhibitors show strong *in vitro* antiviral activity, *in vivo* studies and clinical trials reveal limited direct antiviral effects, likely due to metabolic compensation via the pyrimidine salvage pathway. This bypass seems to maintain sufficient pyrimidine levels for viral replication, reducing the inhibitors' efficacy as monotherapy. Therefore, combination strate-

gies targeting multiple pathways are crucial to realizing their full therapeutic potential.[101] *In vitro* studies demonstrate strong synergy between hDHODH inhibitors and nucleoside analogs (Figure 74), such as MEDS433 **264** with acyclovir **265** against HSV-1[190], and combinations like remdesivir **7** with IMU-838 **24**[191], brequinar **20**, or BAY240234 **64**[192] against SARS-CoV-2. Similar effects are seen with molnupiravir **267** and combinations involving brequinar **20**, IMU-838 **24**, BAY240234 **64**, or teriflunomide **22**.[192,193] Additionally, MEDS433 **264** and *N*4-hydroxycytidine **266** synergistically suppress influenza A virus replication.[194] Recent research also suggests that hDHODH inhibitors enhance the antiviral activity of the pyrimidine analog 4′-fluorouridine **268** against various RNA viruses, including IAV, SARS-CoV-2, EBOV, and henipaviruses.[195]

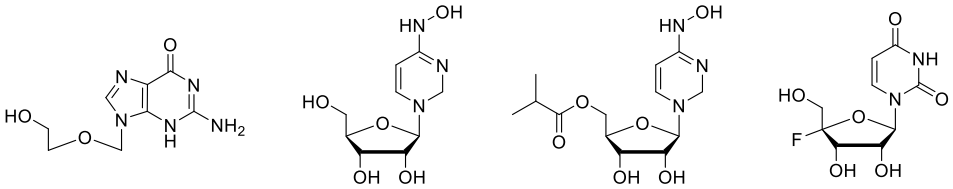

Figure 74: Nucleoside analogs **265**-**268** for which a synergistic effect with DHODH inhibitors has been demonstrated.

Building on the *in vitro* evidence of synergistic antiviral effects between hDHODH inhibitors and nucleoside analogs, recent studies demonstrate that this combination also shows efficacy *in vivo*. For example, in animal models of SARS-CoV-2 infection, co-administration of molnupiravir with hDHODH inhibitors such as brequinar **20** and teriflunomide **22** significantly reduced viral loads and lung inflammation. Although not fully synergistic, these results are promising and suggest that such combinations have the potential to significantly enhance COVID-19 treatment strategies.[101,192,193]

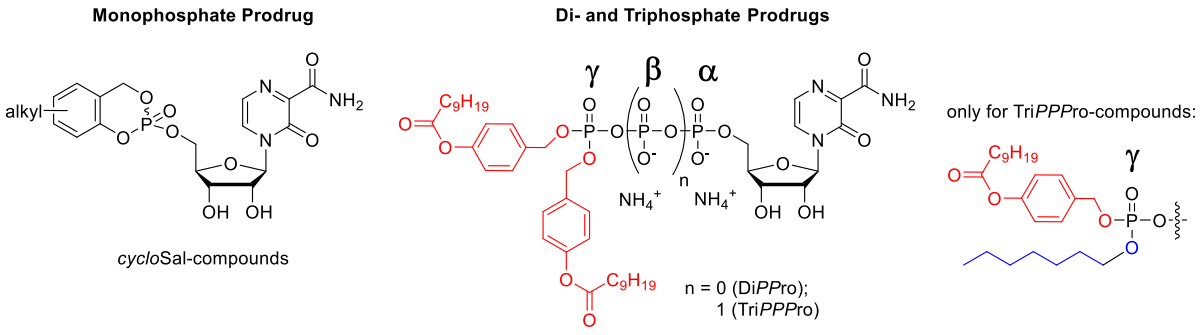

Figure 75: Prodrug technologies developed for the intracellular delivery of different nucleotides.

While several nucleoside analogues are available for treating various viral infections in clinical practice, their widespread use is often limited. This is primarily because these compounds must be effectively taken up by cells, undergo stepwise phosphorylation into their active triphosphate forms by different kinases, and effectively inhibit the target viral polymerase. Over the past decades, the working group of C. MEIER has developed innovative prodrug strategies for nucleoside analogs, including mono- (*cyclo*Sal-approach), di- (Di*PP*ro-approach), and triphosphate (Tri*PPP*ro-approach) prodrugs (Figure 75). It has been demonstrated that the corresponding nucleotide is effectively delivered into cells via passive diffusion of the prodrug, followed by chemical or enzymatic cleavage of its masking groups. Tri*PPP*ro compounds enable complete bypass of phosphorylation steps, directly forming the active triphosphate that interacts with viral polymerases.[196]

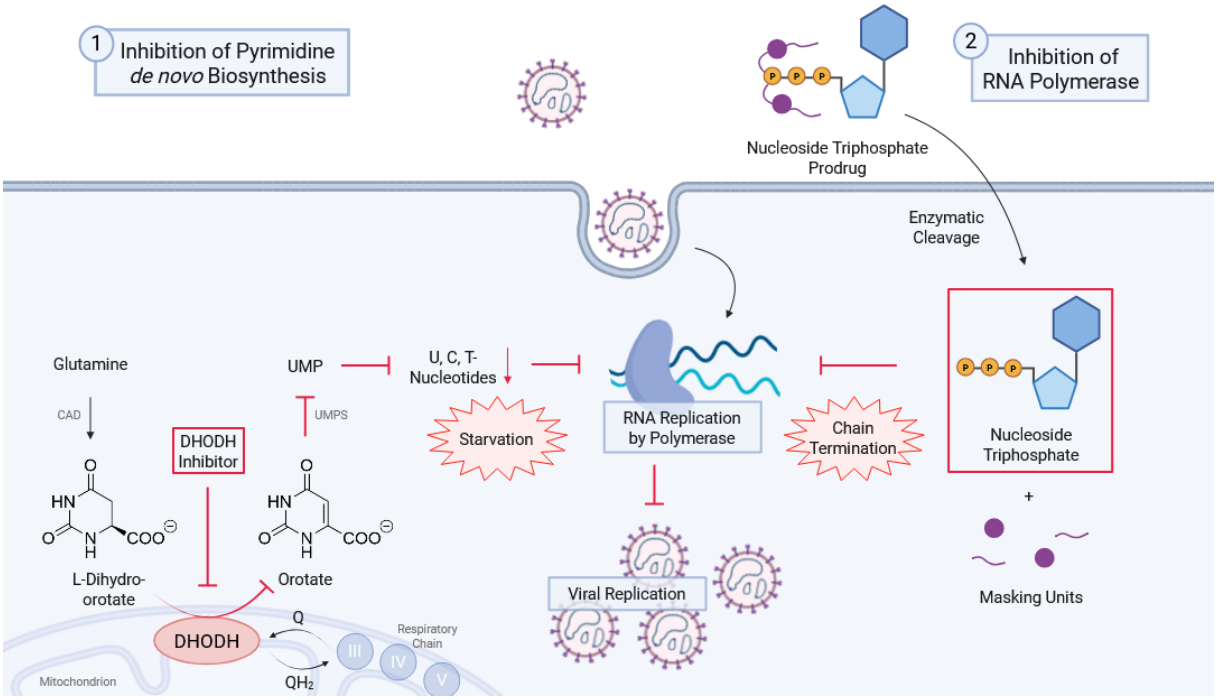

Figure 76: A combinational approach involving hDHODH inhibitors and pronucleotides.

Future research could involve a combination of hDHODH inhibitors and prodrugs of antivirally active pyrimidine nucleoside analogs (Figure 76). On one hand, prodrug technology enhances the bioavailability of the active nucleoside triphosphate, while on the other hand, competition with natural pyrimidine nucleotides for incorporation is minimized by reducing pyrimidine pools through the use of hDHODH inhibitors. A synergistic effect is expected from this combination, potentially leading to improved antiviral efficacy. Corresponding tests are already being planned in collaboration with T. HOENEN and A. GROSETH.

6. Experimental part

6.1. General

6.1.1. Solvents and buffers

Solvents

Acetone	C_3H_6O; bp.: 56 °C; distilled before use
Acetonitrile	C_2H_3N; bp.: 81 °C; HiPerSolv CHROMANORM®, HPLC grade
Chloroform	$CHCl_3$; bp.: 62 °C; deuterated: Euriso-Top D007H for spectroscopic use
Dichloromethane	CH_2Cl_2; bp.: 40 °C; distilled before use
Diethyl ether	$C_4H_{10}O$; bp.: 35 °C, distilled and stored over sodium hydroxide
N,N-Dimethylformamide	C_3H_6O; bp.: 153 °C; anhydrous: Acros Organics, molecular sieve (4 Å)
Dimethyl sulfoxide	C_2H_6OS; bp.: 189 °C; anhydrous: Acros Organics, molecular sieve (4 Å); deuterated: Deutero 009507 for spectroscopic use
Ethyl acetate	$C_4H_8O_2$; bp.: 77 °C; distilled before use
Methanol	CH_4O; bp.: 65 °C; distilled before use
Petroleum ether 50-70	Sdp.: 50-70 °C; distilled before use
Tetrahydrofuran	C_4H_8O; bp.: 66 °C; VWR chemicals, HPLC grade; anhydrous: Acros Organics, molecular sieve (4 Å)
Toluene	C_7H_8; bp.: 111 °C; anhydrous: Acros Organics, molecular sieve (4 Å)
Water, deionized ultrapure	Sartorius Aurium® pro unit (Sartopore 0.2 µm, UV)

Buffers

Phosphate buffered saline	Sigma-Aldrich: Cat. No. P4474, pH 7.4
Phosphate buffer 0.5 M	Sodium dihydrogen phosphate (28.6 g, 238 mmol) and disodium hydrogen phosphate (37.1 g, 262 mmol) in ul-

	trapure water (1 L), pH 7.4 was set using diluted phosphoric acid or 1 M aq. sodium hydroxide solution
Enzyme assay buffer	Trizma® hydrochloride (7.88 g, 50 mmol) and Triton™ X-100 (1 mL, 0.1% v/v) in ultrapure water (1 L), pH 8.0 was set using hydrochloric acid

6.1.2. Chromatography

Thin-layer chromatography was conducted using silica gel-coated aluminum plates with a fluorescence indicator (Macherey-Nagel ALUGRAM® Xtra Sil G/UV254, layer thickness 0.2 mm). UV-active compounds were visualized under a UV lamp at 254 nm. Additionally, the plates were stained with a vanillin reagent (5 g vanillin, 900 mL methanol, 100 mL acetic acid, and 35 mL concentrated sulfuric acid) and heated to enhance visualization of the compounds.

Column chromatography was carried out using silica gel MN 60 M (0.04-0.063 mm, 230-400 mesh) obtained from Macherey-Nagel.

High-performance liquid chromatography was performed on an Agilent 1260 Infinity II (1260 quat. pump, 1260 autosampler, multicolumn thermostat 20 °C, DAD and FLD detector), using an EC 125/3 Nucleodur 100-5 C18ec column/ EC 4/3 Nucleodur 100-5 C18ec pre-column system supplied by Macherey-Nagel.

Method 1: CH_3CN gradient in 2 mM tetrabutylammonium acetate buffer (pH 6); 5-80%; 0-20 min; flow 1 ml/min.

Method 2: CH_3CN + 0.1 v% formic acid gradient in ultrapure water + 0.1 v% formic acid; 5-80%; 0-20 min; flow 1 ml/min.

6.1.3. Spectroscopy/Spectrometry

Nuclear magnetic resonance spectroscopy (NMR) spectra were recorded by the NMR service at the Institute of Organic Chemistry at the University of Hamburg at room temperature. MestReNova software was used for the analysis of the NMR spectra.

^{1}H-NMR: Bruker FourierHD (300 MHz), Bruker Avance I, II, III (400 MHz), Bruker Avance I (500 MHz) und Bruker Avance III HD (600 MHz). The spectra were acquired over a chemical shift range of 0 to 14 ppm.

^{13}C-NMR: Bruker Avance I, II, III (101 MHz), Bruker Avance I (126 MHz) und Bruker Avance III HD (151 MHz). The spectra were acquired over a chemical shift range of -10 to 200 ppm.

^{19}F-NMR: Bruker Avance III HD (565 MHz). The spectra were acquired over a chemical shift range of -200 to 100 ppm.

2D NMR spectra (H,H-COSY, HSQC, HMBC) were acquired for all compounds. The chemical shifts of solvent signals were calibrated to 7.26 ppm (^{1}H) and 77.10 ppm (^{13}C) for $CDCl_3$, and to 2.50 ppm (^{1}H) and 39.52 ppm (^{13}C) for DMSO-d_6.

Infrared (IR) spectra were recorded using an ALPHA FT-IR spectrometer from Bruker at room temperature in a measurement range of 400–4000 cm^{-1}.

Mass spectrometry (MS) was performed by the MS service at Institute of Organic Chemistry at the University of Hamburg on an Agilent 6224 ESI-TOF spectrometer (ESI spectra) and a Thermo Scientific ISQ LT EI spectrometer (EI spectra) at 25 °C.

Ultraviolet/ visible spectrophotometry (UV/Vis) was performed on a peqlab NanoDrop 2000c microvolume spectrophotometer and a Berthold TriStar2 LB 942 microplate reader (plates: Greiner, 96 well, polystyrene, transparent (655101); software: ICE) at 25 °C.

Fluorescence spectrophotometry was performed on a Berthold TriStar2 LB 942 microplate reader (plates: Thermo Scientific, 96 well, polystyrene, black (237108); software: ICE) at 25 °C.

6.1.4. Further Devices

For metabolism studies, samples were incubated using a CellMedia thermo shaker (basic) and centrifuged with an Eppendorf centrifuge 5418 R.

6.2. Biochemical assays

6.2.1. Kinetic solubility

6 µL of a 10 mM DMSO stock solution of the test substance were diluted with 294 µL PBS buffer to achieve a final compound concentration of 200 µM and a DMSO concentration of 2%. The samples were prepared in triplicate and incubated at room temperature (~25 °C) for 24 h. Subsequently, the residual compound concentration in the supernatant was determined using UV/Vis spectroscopy (NanoDrop). Calibration curves for quantification were prepared separately.

Kinetic solubilities (x) were obtained using the following equation:

$$x = \frac{y-b}{m} \qquad (1)$$

y: Absorption measured for an aliquot of 2 µL

b: y-intercept

m: Slope

6.2.2. Lipophilicity (logD)

To minimize potential phase separation issues and ensure consistent partitioning behavior during the assay, octanol and PBS were pre-saturated with each other prior to the experiment. 20 µL of a 10 mM DMSO stock solution of the test substance were diluted with 980 µL saturated PBS buffer to achieve a final compound concentration of 200 µM and a DMSO concentration of 2%. Three samples were prepared by adding 300 µL of the compound solution and overlaying each with 300 µL of saturated octanol. The mixtures were vortexed for 1 min and then continuously stirred on a rotator at 180 rpm for 1 hour at room temperature (~25 °C). Afterwards, the PBS phase was carefully aspirated into a syringe and transferred to a new vial. Subsequently, 20 µL aliquots of each PBS phase, as well as the initial 200 µM compound solution, were injected into the HPLC system for analysis (method 1, DAD λ_{max}).

Distribution coefficients (logD) were obtained using the following equation:

$$\mathrm{logD} = \log\left(\frac{A_0 - A_1}{A1}\right) \qquad (2)$$

A_0: Integral of the compound peak in the chromatogram obtained for the initial 200 µM compound solution

A_1: Integral of the compound peak in the chromatogram obtained for the aqueous phase after the experiment

6.2.3. Permeability (PAMPA)

The assay was performed using 96-well collection (MATRNPS50) and filter (MAIPNTR10) plates obtained from Merck Millipore. Prior to the experiment, the PVDF membrane in each well of the filter plate was treated with 5 µL of a 1% solution (w/v) of L-α-phosphatidylcholine in dodecane. 20 µL of a 10 mM DMSO stock solution of the test substance were diluted with 980 µL of PBS buffer to achieve a final compound concentration of 200 µM and a DMSO concentration of 2%. An aliquot of 150 µL of the drug-containing donor solution was added in triplicate to wells of the filter (donor) plate. Subsequently, the donor plate was placed into the collection (acceptor) plate filled with 300 µL of PBS buffer and covered with a lid. After incubation for 5 h at room temperature (~25 °C), UV/Vis absorption was measured using a microplate reader for 250 µL of each well of the acceptor solutions and for previously prepared drug solutions at the theoretical equilibrium.

Membrane permeabilities (P_e) were obtained using the following equation:

$$P_e = -\ln\left(1 - \frac{c_{acc}(t)}{c_{eq}}\right) \cdot C \qquad (3)$$

$C_{acc}(t)$: Absorption (λ_{max}) measured for an aliquot of 250 µL of the acceptor solution taken after time t (5 h)

c_{eq}: Absorption (λ_{max}) measured for an aliquot of 250 µL of the drug solution at the theoretical equilibrium

C: Measurement constant: $C = \frac{V_D \cdot V_A}{(V_D + V_A) \cdot A \cdot t}$

A: Filter area (0.3 cm^2)

V_D: Volume donor well (0.15 mL)

V_A: Volume acceptor well (0.3 mL)

6.2.4. Metabolic stability (rat S9 fraction)

First, the phase I metabolic enzymes in the S9 fraction needed to be activated. Therefore, 30 µL of a 50 mM $MgCl_2$ solution (in PB buffer) and 30 µL of a 50 mM NADPH x 4 Na solution (in PB buffer) were added to 177 µL of PB buffer and subsequently treated with 60 µL of rat S9 fraction (Sigma-Aldrich S2067). The mixture was then incubated at 37 °C for 10 min. The experiment was initiated by the addition of 3 µL of a 10 mM DMSO stock solution of the test substance. The samples were prepared in triplicate and incubated at 37 °C. An aliquot of 50 µL was taken at 0, 1 and 3 h and added to 150 µL of ice-cooled methanol. The sample was then centrifuged at 14000 rpm and 4 °C for 10 min, followed by filtration through

CHROMAFIL® RC-20/15 MS (Macherey-Nagel) syringe filters. Subsequently, 30 µL aliquots of each sample were injected into the HPLC system for analysis (methods 1 and 2, DAD λ_{max} and FLD λ_{exc} = 300 nm, λ_{em} = 407 nm).

Metabolic stabilities (S_{S9}) were obtained using the following equation:

$$S_{s9} = \frac{A_1}{A_0} \cdot 100 \qquad (4)$$

A_1: Integral of the compound peak in the chromatogram obtained for the sample taken after 1 h of incubation

A_0: Integral of the compound peak in the chromatogram obtained for the sample without incubation

6.2.5. hDHODH inhibition

The enzyme assay was conducted using 96-well plates, with His_6-$hDHODH_{29\text{-}396}$ kindly provided by N. C. LAUBACH. Experiments were performed at pH 8.0 and 25 °C in a reaction medium containing 100 µM L-DHO, 25 µM CoQ_1, 60 µM DCPIP, 35 nM His_6-$hDHODH_{29–396}$, and either 50 nM or 200 nM of the inhibitor in Tris-HCl/Triton X-100 buffer.

To prepare the enzyme solution, His_6-$hDHODH_{29–396}$ (325 µM) was diluted to 87.5 nM with ice-cold Tris-HCl/Triton X-100 buffer. The inhibitor stock solution (10 µM in DMSO) was diluted to the desired concentrations of 500 nM or 2000 nM with the same buffer. Additionally, stock solutions of L-DHO (1000 µM in DMSO), CoQ1 (250 µM in DMSO) and DCPIP (600 µM in buffer) were prepared, combined in equal proportions, and diluted with Tris-HCl/Triton X-100 buffer (3:2 v/v) to form the substrate mixture. Aliquots of 100 µL of the substrate mixture and 20 µL of the inhibitor solution were added in triplicate to the plate wells. The reaction was initiated by simultaneously adding 80 µL of the ice-cooled enzyme solution, followed by careful mixing using a transfer pipette. hDHODH activity was determined by monitoring the decrease in DCPIP absorbance at 600 nm with a spectrometer.

Values for the percentage inhibition of hDHODH were obtained using following equation:

$$\%\ \text{inhibition (hDHODH)} = \left(1 - \frac{v_c}{v_0}\right) \cdot 100 \qquad (5)$$

v_c: Enzyme velocity determined for the linear range in the first 200 s at an inhibitor concentration c

v_0: Enzyme velocity determined for the linear range in the first 200 s without added inhibitor

6.3. Syntheses

6.3.1. General procedures

General procedure I: ULLMAN-GOLDBERG cross-coupling of aryl halides with amines

Copper iodide (20 mol%), L-proline (40 mol%), and potassium carbonate (2.0 eq.) was added to a solution of the appropriate aryl halide (1.0 eq.) in dry DMSO (2.0 mL/mmol) under nitrogen atmosphere. After stirring for 5 min at room temperature, the appropriate amine (1.5-3.0 eq.) was added dropwise, and the reaction mixture was further stirred at room temperature or 50 °C (depending on whether an aryl iodide or bromide was used) until complete conversion or a stagnation in conversion was monitored by TLC. The reaction mixture was diluted with aqueous 1 M NaOH and then extracted three times with diethyl ether. The combined organic layers were dried over anhydrous Na_2SO_4, and solvent was removed under reduced pressure. The crude product was purified by column chromatography.

General procedure II: SONOGASHIRA cross-coupling of aryl halides with TMS acetylene

A mixture of the appropriate aryl halide (1.0 eq.) and copper iodide (5-10 mol%) in triethylamine (4 mL/mmol) and THF (1.5 mL/mmol) was degassed with nitrogen for 15 min. After the addition of $Pd(PPh_3)_4$ (5-10 mol%) and TMS acetylene (2.7 eq.), the reaction mixture was stirred overnight at either room temperature or 70 °C, depending on whether an aryl iodide or bromide was used. Complete or stagnating conversion was monitored by TLC analysis. Subsequently, water was added, and the aqueous phase was extracted three times with ethyl acetate. The combined organic extracts were dried over anhydrous Na_2SO_4, and all volatiles were removed in vacuo. The residue was then purified by column chromatography.

General procedure III: Cleavage of TMS protecting group

The appropriate TMS-protected alkyne (1.0 eq.) was dissolved in methanol (8.0 mL/mmol) and treated with potassium carbonate (5.0 eq.). The reaction mixture was stirred at room temperature until complete conversion was observed by TLC. After potassium carbonate was removed by filtration, all volatiles were evaporated. The residue was redissolved in dichloromethane and washed with water. The organic phase was dried over anhydrous Na_2SO_4, and subsequent evaporation of the solvent afforded the corresponding terminal alkyne. Due to its instability and sufficient purity, the product was used without further purification.

General procedure IV: SONOGASHIRA cross-coupling of anthranilic acid derivatives with alkynes

A suspension of the appropriate anthranilic acid derivative (1.0 eq.) and copper iodide (10 mol%) in triethylamine (6 mL/mmol) and THF (5 mL/mmol) was degassed with nitrogen for 15 min. Afterwards, the appropriate alkyne (1.1-3.0 eq.) and $Pd(PPh_3)_4$ (10 mol%) were added, and the reaction mixture was stirred at room temperature (for iodoanthranilic acid) or 70 °C (for bromoanthranilic acid) under TLC monitoring. When full conversion was reached, the suspension was diluted with water and extracted three times with dichloromethane. After drying the combined organic layers over anhydrous Na_2SO_4 and removal of the solvent under reduced pressure, the crude product was purified by column chromatography.

General procedure V: Saponification of anthranilic acid methyl esters

The appropriate methyl ester (1.0 eq.) was dissolved in THF (10 mL/mmol), and after adding aqueous 1 M NaOH (4 mL/mmol), the reaction mixture was stirred overnight at room temperature. Full conversion was monitored by TLC analysis. THF was removed under reduced pressure to final volume of 1-2 mL, and a pH value of 1 was adjusted by the addition of aqueous 1.2 M HCl. After complete precipitation of the desired anthranilic acid, it was isolated by filtration, and impurities were removed by washing with water.

General procedure VI: Reductive amination

The appropriate aldehyde (1.1 eq) and glacial acetic acid (1.2 eq) were dissolved in dry dichloromethane (1 mL) and added to a cooled solution of the appropriate aniline dissolved in dry dichloromethane (2 mL/mmol) under nitrogen atmosphere. The resulting mixture was treated with STAB and stirred for 15 min at 0 °C. Subsequently, the reaction was quenched with water and extracted three times with dichloromethane. The combined organic layers were dried over Na_2SO_4, and all volatiles were removed in vacuo. The crude product was purified by column chromatography.

General procedure VII: BUCHWALD-HARTWIG cross-coupling of aryl iodides with morpholine

Morpholine (1.0-2.0 eq.), xantphos (9-15 mol%), $Pd_2(dba)_3$ (3-5 mol%) and NaOtBu (1.0 eq.) were added to a solution of the appropriate aryl iodide (1.0 eq.) in dry toluene (6 mL/mmol) under nitrogen atmosphere. After stirring at room temperature until complete or stagnating conversion of the starting material was observed by TLC, the reaction mixture was diluted with water and extracted three times with ethyl acetate. The combined organic layers were

dried over Na_2SO_4, and the solvent was then removed under reduced pressure. The residue was purified by column chromatography.

6.3.2. Syntheses of hDHODH inhibitors 29 and 30

5-((4-Butylphenyl)ethynyl)-2-propionamidobenzoic acid 29

The compound was synthesized in a previous study and was provided for use in this work.[111]

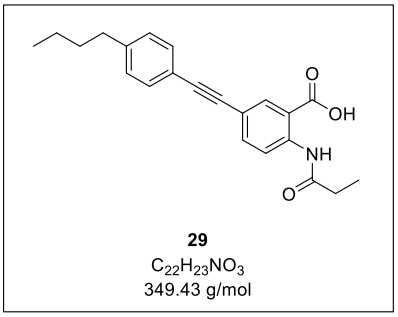

29
$C_{22}H_{23}NO_3$
349.43 g/mol

5-((4-Cyclohexylphenyl)ethynyl)-2-propionamidobenzoic acid 30

The compound was synthesized in a previous study and was provided for use in this work.[160]

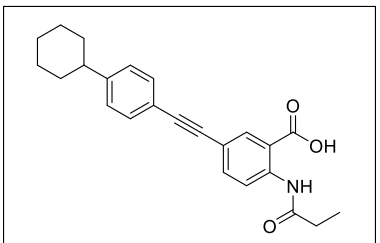

30
$C_{24}H_{25}NO_3$
375.47 g/mol

6.3.3. Syntheses of hDHODH inhibitors 37-41 (cycle 1)

2-Propionamido-5-((4-(propylamino)phenyl)ethynyl)benzoic acid 37

The compound was synthesized in a previous study and was provided for use in this work.[160]

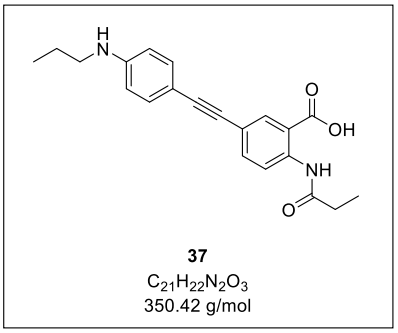

37
$C_{21}H_{22}N_2O_3$
350.42 g/mol

1-(4-((Trimethylsilyl)ethynyl)phenyl)butan-1-one 162

According to general procedure II, the reaction was performed with 1-(4-bromophenyl)butan-1-one **101** (500 mg, 2.20 mmol), copper iodide (42.0 mg, 220 µmol), $Pd(PPh_3)_4$ (255 mg, 220 µmol) and TMS acetylene (820 µL, 5.95 mmol) in triethylamine (8 mL) and THF (3 mL) at

70 °C for 19 h. The crude product was purified by column chromatography (CH_2Cl_2/PE 1:2 v/v) to yield **162** (408 mg, 1.67 mmol, 76%) as a colorless solid.

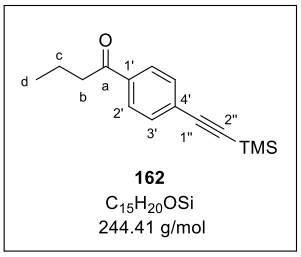

162
$C_{15}H_{20}OSi$
244.41 g/mol

^{1}H-NMR (600 MHz, $CDCl_3$): δ [ppm] = 7.88 (d, $^3J_{H,H}$ = 8.7 Hz, 2H, H-2'), 7.53 (d, $^3J_{H,H}$ = 8.7 Hz, 2H, H-3'), 2.92 (t, $^3J_{H,H}$ = 7.3 Hz, 2H, H-b), 1.76 (sext, $^3J_{H,H}$ = 7.3 Hz, 2H, H-c), 1.00 (t, $^3J_{H,H}$ = 7.3 Hz, 3H, H-d), 0.26 (s, 9H, Si(CH_3)$_3$); **^{13}C-NMR** (151 MHz, $CDCl_3$): δ [ppm] = 199.8 (C-a), 136.5 (C-1'), 132.2 (C-3'), 128.0 (C-2'), 127.9 (C-4'), 104.2 (C-1''), 98.0 (C-2''), 40.7 (C-b), 17.9 (C-c), 14.0 (C-d), −0.02 (Si(CH_3)$_3$); **ATR-IR** (neat): $\tilde{\nu}$ [cm^{-1}] = 2957, 2160, 1679, 1597, 1402, 1248, 1208, 1001, 839, 825, 755, 656; **HRMS** (ESI$^+$): m/z calc.: 245.1356 [M+H]$^+$, found: 245.1355; **R_f**: 0.25 (CH_2Cl_2/PE 1:2 v/v).

1-(4-Ethynylphenyl)butan-1-one 168

The reaction was carried out according to general procedure III with **162** (372 mg, 1.52 mmol) and potassium carbonate (1.05 g, 7.61 mmol) in methanol (12 mL) for 4 h. Alkyne **168** (146 mg, 848 mmol, 56%) was obtained as a colorless solid.

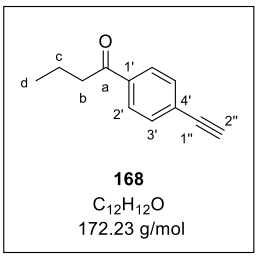

168
$C_{12}H_{12}O$
172.23 g/mol

^{1}H-NMR (500 MHz, $CDCl_3$): δ [ppm] = 7.91 (d, $^3J_{H,H}$ = 8.7 Hz, 2H, H-2'), 7.57 (d, $^3J_{H,H}$ = 8.7 Hz, 2H, H-3'), 3.24 (s, 1H, H-2''), 2.93 (t, $^3J_{H,H}$ = 7.4 Hz, 2H, H-b), 1.77 (sext, $^3J_{H,H}$ = 7.4 Hz, 2H, H-c), 1.00 (t, $^3J_{H,H}$ = 7.4 Hz, 3H, H-d); **^{13}C-NMR** (126 MHz, $CDCl_3$): δ [ppm] = 200.0 (C-a), 137.0 (C-1'), 132.4 (C-3'), 128.1 (C-2'), 126.8 (C-4'), 83.0 (C-1''), 80.3 (C-2''), 40.7 (C-b), 17.8 (C-c), 14.0 (C-d); **ATR-IR** (neat): $\tilde{\nu}$ [cm^{-1}] = 3229, 2961, 2873, 2102, 1677, 1602, 1404, 1365, 1309, 1287, 1210, 1174, 997, 898, 820, 755, 729, 682, 572; **HRMS** (ESI$^+$): m/z calc.: 173.0961 [M+H]$^+$, found: 173.0957; **R_f**: 0.20 (CH_2Cl_2/PE 1:2 v/v).

Methyl 5-((4-butyrylphenyl)ethynyl)-2-propionamidobenzoate 223

The reaction was carried out as described in general procedure IV with anthranilic acid **90** (200 mg, 600 µmol), copper iodide (11.4 mg, 60.0 µmol), Pd(PPh_3)$_4$ (69.4 mg, 60.0 µmol) and alkyne **168** (114 mg, 660 µmol) in triethylamine (4 mL) and THF (3 mL) at room temperature for 14 h. After purification by column chromatography (CH_2Cl_2 + 0.5% acetone v/v), **223** (198 mg, 525 µmol, 87%) was obtained as a yellow solid.

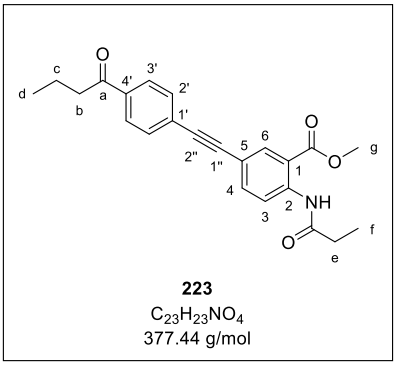

^{1}H-NMR (400 MHz, $CDCl_3$): δ [ppm] = 11.16 (s, 1H, CON*H*), 8.79 (d, $^{3}J_{H,H}$ = 8.8 Hz, 1H, H-3), 8.23 (d, $^{4}J_{H,H}$ = 2.0 Hz, 1H, H-6), 7.94 (d, $^{3}J_{H,H}$ = 8.7 Hz, 2H, H-3'), 7.69 (dd, $^{3}J_{H,H}$ = 8.8 Hz, $^{4}J_{H,H}$ = 2.0 Hz, 1H, H-4), 7.59 (d, $^{3}J_{H,H}$ = 8.7 Hz, 2H, H-2'), 3.96 (s, 3H, H-g), 2.95 (t, $^{3}J_{H,H}$ = 7.4 Hz, 2H, H-b), 2.50 (q, $^{3}J_{H,H}$ = 7.6 Hz, 2H, H-e), 1.78 (sext, $^{3}J_{H,H}$ = 7.4 Hz, 2H, H-c), 1.29 (t, $^{3}J_{H,H}$ = 7.6 Hz, 3H, H-f), 1.01 (t, $^{3}J_{H,H}$ = 7.4 Hz. 3H, H-d); **^{13}C-NMR** (101 MHz, $CDCl_3$): δ [ppm] = 199.7 (C-a), 173.1 (CON*H*), 168.3 (*C*OOMe), 142.0 (C-2), 137.7 (C-4), 136.4 (C-4'), 134.5 (C-6), 131.8 (C-2'), 128.2 (C-3'), 127.8 (C-1'), 120.5 (C-3), 116.8 (C-1), 115.0 (C-5), 91.6 (C-2''), 88.8 (C-1''), 52.7 (C-g), 40.7 (C-b), 31.9 (C-e), 17.9 (C-c), 14.0 (H-d), 9.65 (H-f); **R_f**: 0.33 (CH_2Cl_2 + 0.5% acetone v/v).

5-((4-Butyrylphenyl)ethynyl)-2-propionamidobenzoic acid 38

The reaction was performed according to general procedure V by treating methyl ester **223** (180 mg, 477 µmol) with aqueous 1.0 M NaOH (1.5 mL) in THF (5 mL) for 16 h. Precipitation in acidic solution provided target compound **38** (166 mg, 458 µmol, 96%) as a colorless solid.

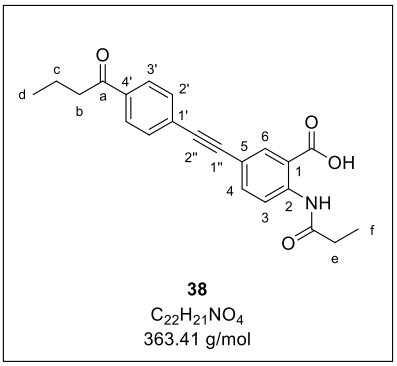

^{1}H-NMR (500 MHz, DMSO-d_6): δ [ppm] = 11.33 (s, 1H, CON*H*), 8.60 (d, $^{3}J_{H,H}$ = 8.8 Hz, 1H, H-3), 8.15 (d, $^{4}J_{H,H}$ = 2.2 Hz, 1H, H-6), 7.99 (d, $^{3}J_{H,H}$ = 8.4 Hz, 2H, H-3'), 7.78 (dd, $^{3}J_{H,H}$ = 8.8 Hz, $^{4}J_{H,H}$ = 2.2 Hz, 1H, H-4), 7.69 (d, $^{3}J_{H,H}$ = 8.4 Hz, 2H, H-2'), 3.01 (t, $^{3}J_{H,H}$ = 7.1 Hz, 2H, H-b), 2.44 (q, $^{3}J_{H,H}$ = 7.5 Hz, 2H, H-e), 1.64 (sext, $^{3}J_{H,H}$ = 7.1 Hz, 2H, H-c), 1.13 (t, $^{3}J_{H,H}$ = 7.5 Hz, 3H, H-f), 0.93 (t, $^{3}J_{H,H}$ = 7.1 Hz. 3H, H-d); **^{13}C-NMR** (126 MHz, DMSO-d_6): δ [ppm] = 199.3 (C-a), 172.2 (*C*ONH), 168.7 (*C*OOH), 141.4 (C-2), 136.6 (C-4), 136.1 (C-4'), 134.3 (C-6), 131.6 (C-2'), 128.2 (C-3'), 126.6 (C-1'), 120.0 (C-3), 116.8 (C-1), 115.4 (C-5), 91.3 (C-2''), 88.4 (C-1''), 39.8 (C-b), 30.7 (C-e), 17.1 (C-c), 13.6 (H-d), 9.22 (H-f); **ATR-IR** (neat): $\tilde{\nu}$ [cm^{-1}] = 3170, 2961, 2873, 2207, 1685, 1583, 1512, 1288, 1182, 1152, 835; **HRMS** (ESI^+): m/z calc.: 362.1398 $[M-H]^-$, found: 362.1379; **R_f**: 0.60 (CH_2Cl_2/MeOH 9:1 v/v).

5-((4-(Ethylcarbamoyl)phenyl)ethynyl)-2-propionamidobenzoic acid 39

The compound was synthesized in a previous study and was provided for use in this work.[160]

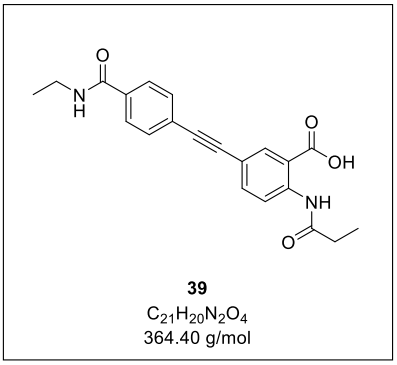

39
$C_{21}H_{20}N_2O_4$
364.40 g/mol

((4-(2-Methoxyethoxy)phenyl)ethynyl)trimethylsilane 163

As described in general procedure II, the reaction was performed with 1-bromo-4-(2-methoxyethoxy)benzene **102** (499 mg, 2.16 mmol), copper iodide (41.1 mg, 216 µmol), $Pd(PPh_3)_4$ (250 mg, 216 µmol) and TMS acetylene (810 µL, 5.83 mmol) in triethylamine (8 mL) and THF (3 mL) at 70 °C for 20 h. The crude product was purified by column chromatography (CH_2Cl_2/PE 1:1 v/v) to yield **163** (442 mg, 1.78 mmol, 82%) as a yellowish oil.

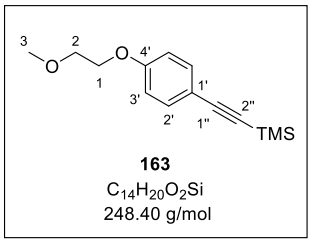

163
$C_{14}H_{20}O_2Si$
248.40 g/mol

^{1}H-NMR (500 MHz, $CDCl_3$): δ [ppm] = 7.39 (d, $^3J_{H,H}$ = 8.9 Hz, 2H, H-2'), 6.84 (d, $^3J_{H,H}$ = 8.9 Hz, 2H, H-3'), 4.17-4.09 (m, 2H, H-1), 3.77-3.71 (m, 2H, H-2), 3.45 (s, 3H, H-3), 0.23 (s, 9H, Si(CH_3)$_3$); **^{13}C-NMR** (126 MHz, $CDCl_3$): δ [ppm] = 159.1 (C-4'), 133.6 (C-2'), 115.7 (C-1'), 114.6 (C-3'), 105.3 (C-1''), 92.7 (C-2''), 71.1 (C-2), 67.4 (C-1), 59.4 (C-3), 0.20 (Si(CH_3)$_3$); **ATR-IR** (neat): $\tilde{\nu}$ [cm^{-1}] = 2926, 2880, 1601, 1505, 1247, 1173, 1126, 1060, 833; **HRMS** (ESI$^+$): m/z calc.: 218.1122 [M−OMe+H]$^+$, found: 218.2118; **R_f**: 0.35 (CH_2Cl_2/PE 1:1 v/v).

1-Ethynyl-4-(2-methoxyethoxy)benzene 169

The cleavage of the protecting group was carried out according to general procedure III by treating **163** (420 mg, 1.69 mmol) with potassium carbonate (1.17 g, 8.45 mmol) in methanol (15 mL) for 4 h. Alkyne **169** (262 mg, 1.49 mmol, 88%) was isolated as a colorless oil.

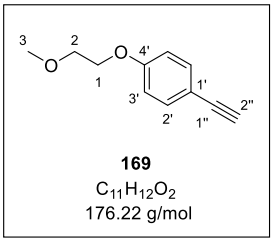

169
$C_{11}H_{12}O_2$
176.22 g/mol

^{1}H-NMR (500 MHz, $CDCl_3$): δ [ppm] = 7.42 (d, $^3J_{H,H}$ = 8.9 Hz, 2H, H-2'), 6.86 (d, $^3J_{H,H}$ = 8.9 Hz, 2H, H-3'), 4.15-4.10 (m, 2H, H-1), 3.79-3.73 (m, 2H, H-2), 3.45 (s, 3H, H-3), 2.99 (s, 1H, H-2''); **^{13}C-NMR** (126 MHz, $CDCl_3$): δ [ppm] = 159.3 (C-4'), 133.7 (C-2'), 114.7 (C-3'), 114.6 (C-1'), 83.8 (C-1''), 76.0 (C-2''), 71.0 (C-2), 67.5 (C-1), 59.4 (C-

3); **ATR-IR** (neat): $\tilde{\nu}$ [cm^{-1}] = 3285, 3249, 2926, 2887, 1604, 1505, 1286, 1244, 1171, 1124, 1057, 1032, 830, 536; **MS** (EI): m/z calc.: 176.08 $[M]^+$, found: 176.10; $\mathbf{R_f}$: 0.30 (CH_2Cl_2/PE 2:1 v/v).

Methyl 5-((4-(2-methoxyethoxy)phenyl)ethynyl)-2-propionamidobenzoate 224

The reaction was performed according to general procedure IV with anthranilic acid **90** (197 mg, 591 µmol), copper iodide (11.3 mg, 59.1 µmol), $Pd(PPh_3)_4$ (68.3 mg, 59.1 µmol) and alkyne **169** (115 mg, 651 µmol) in triethylamine (4 mL) and THF (3 mL) at room temperature for 16 h. Purification by column chromatography (CH_2Cl_2/acetone 100:1 v/v) provided **224** (204 mg, 535 µmol, 91%) as a brownish solid.

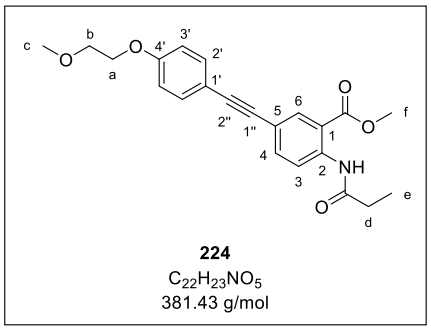

^{1}H-NMR (400 MHz, $CDCl_3$): δ [ppm] = 11.12 (s, 1H, CON*H*), 8.74 (d, $^3J_{H,H}$ = 8.8 Hz, 1H, H-3), 8.18 (d, $^4J_{H,H}$ = 2.0 Hz, 1H, H-6), 7.65 (dd, $^3J_{H,H}$ = 8.8 Hz, $^4J_{H,H}$ = 2.0 Hz, 1H, H-4), 7.44 (d, $^3J_{H,H}$ = 8.9 Hz, 2H, H-2'), 6.90 (d, $^3J_{H,H}$ = 8.9 Hz, 2H, H-3'), 4.17-4.10 (m, 2H, H-a), 3.94 (s, 3H, H-f), 3.79-3.72 (m, 2H, H-b), 3.45 (s, 3H, H-c), 2.49 (q, $^3J_{H,H}$ = 7.6 Hz, 2H, H-d), 1.28 (t, $^3J_{H,H}$ = 7.6 Hz, 3H, H-e); **^{13}C-NMR** (101 MHz, $CDCl_3$): δ [ppm] = 173.0 (*C*ONH), 168.4 (*C*OMe), 159.1 (C-4'), 141.3 (C-2), 137.4 (C-4), 134.1 (C-6), 133.1 (C-2'), 120.4 (C-3), 117.8 (C-1), 115.5 (C-1'), 114.9 (C-5), 114.8 (C-3'), 89.4 (C-2''), 87.5 (C-1''), 71.1 (C-b), 67.5 (C-a), 59.4 (C-c), 52.6 (C-f), 31.9 (C-d), 9.67 (C-e); **ATR-IR** (neat): $\tilde{\nu}$ [cm^{-1}] = 3255, 2947, 2880, 1684, 1588, 1515, 1439, 1246, 1230, 1193, 1179, 1121, 844, 830, 788, 534; **HRMS** (ESI$^+$): m/z calc.: 404.1468 $[M+Na]^+$, found: 404.1508; $\mathbf{R_f}$: 0.22 (CH_2Cl_2/acetone 100:1 v/v).

5-((4-(2-Methoxyethoxy)phenyl)ethynyl)-2-propionamidobenzoic acid 40

According to general procedure V, the saponification was carried out by treating methyl ester **224** (180 mg, 472 µmol) with aqueous 1.0 M NaOH (1.5 mL) in THF (5 mL) for 16 h. After precipitation in acidic solution, target compound **40** (168 mg, 458 µmol, 97%) was obtained as an ivory solid.

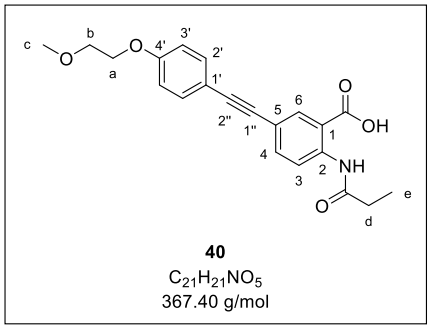

^{1}H-NMR (500 MHz, DMSO-d_6): δ [ppm] = 11.22 (s, 1H, CON*H*), 8.57 (d, $^3J_{H,H}$ = 8.8 Hz, 1H, H-3), 8.07 (d, $^4J_{H,H}$ = 2.2 Hz, 1H, H-6), 7.71 (dd, $^3J_{H,H}$ = 8.8 Hz, $^4J_{H,H}$ = 2.2 Hz, 1H, H-4), 7.49 (d, $^3J_{H,H}$ = 8.9 Hz, 2H, H-2'), 6.98 (d, $^3J_{H,H}$ = 8.9 Hz, 2H, H-3'), 4.15-4.10 (m, 2H, H-a), 3.69-3.63 (m, 2H, H-b), 3.31 (s, 3H, H-c), 2.43 (q, $^3J_{H,H}$ = 7.5 Hz, 3H, H-

d), 1.13 (t, $^3J_{H,H}$ = 7.5 Hz, 2H, H-e); **^{13}C-NMR** (126 MHz, DMSO-d_6): δ [ppm] = 172.1 (CON*H*), 168.8 (COOH), 158.8 (C-4'), 140.7 (C-2), 136.3 (C-4), 133.8 (C-6), 132.9 (C-2'), 120.0 (C-3), 116.5 (C-1), 16.5 (C-5) 114.9 (C-3'), 114.1 (C-1'), 89.2 (C-2''), 87.0 (C-1''), 70.3 (C-b), 67.1 (C-a), 58.2 (C-c), 30.7 (C-d), 9.25 (C-e); **ATR-IR** (neat): $\tilde{\nu}$ [cm^{-1}] = 3043, 2972, 2936, 2910, 1691, 1591, 1516, 1252, 1214, 1178, 1054, 833, 794; **HRMS** (ESI$^+$): m/z calc.: 366.1347 [M-H]$^-$, found: 366.1354; **R_f**: 0.53 (CH_2Cl_2/MeOH 9:1 v/v).

((4-(2-Ethoxyethoxy)phenyl)ethynyl)trimethylsilane 164

The reaction was carried out according to general procedure II with 1-bromo-4-(2-ethoxyethoxy)benzene **103** (503 mg, 2.05 mmol), copper iodide (39.1 mg, 205 µmol), $Pd(PPh_3)_4$ (237 mg, 205 µmol) and TMS acetylene (770 µL, 5.54 mmol) in triethylamine (8 mL) and THF (3 mL) at 70 °C for 20 h. Purification by column chromatography (CH_2Cl_2/PE 1:1 v/v) afforded **164** (435 mg, 1.66 mmol, 81%) as a yellow oil.

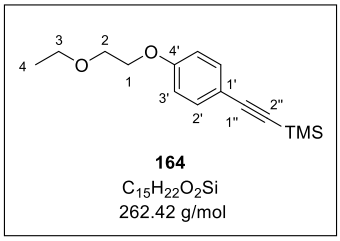

164
$C_{15}H_{22}O_2Si$
262.42 g/mol

^{1}H-NMR (600 MHz, $CDCl_3$): δ [ppm] = 7.39 (d, $^3J_{H,H}$ = 8.8 Hz, 2H, H-2'), 6.84 (d, $^3J_{H,H}$ = 8.8 Hz, 2H, H-3'), 4.13-4.09 (m, 2H, H-1), 3.79-3.77 (m, 2H, H-2), 3.59 (q, $^3J_{H,H}$ = 7.0 Hz, 2H, H-3), 1.24 (t, $^3J_{H,H}$ = 7.0 Hz, 3H, H-4), 0.23 (s, 9H, Si(*C*H$_3$)$_3$); **^{13}C-NMR** (151 MHz, $CDCl_3$): δ [ppm] = 159.2 (C-4'), 133.6 (C-2'), 115.5 (C-3'), 114.6 (C-1'), 105.3 (C-1''), 92.6 (C-2''), 69.0 (C-2), 67.6 (C-1), 67.0 (C-3), 15.3 (C-4), 0.20 (Si(*C*H$_3$)$_3$); **ATR-IR** (neat): $\tilde{\nu}$ [cm^{-1}] = 2960, 2871, 2155, 1604, 1505, 1488, 1286, 1246, 1172, 1122, 1060, 862, 831, 758; **HRMS** (ESI$^+$): m/z calc.: 285.1281 [M+Na]$^+$, found: 285.1277; **R_f**: 0.18 (CH_2Cl_2/PE 1:1 v/v).

1-(2-Ethoxyethoxy)-4-ethynylbenzene 170

The reaction was carried out as described in general procedure III by treating **164** (400 mg, 1.52 mmol) with potassium carbonate (1.05 g, 7.62 mmol) in methanol (12 mL) for 4 h. Alkyne **170** (179 mg, 943 µmol, 62%) was obtained as a yellow oil.

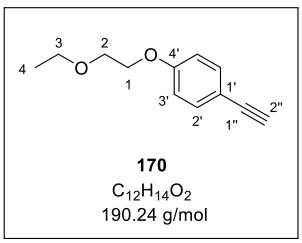

170
$C_{12}H_{14}O_2$
190.24 g/mol

^{1}H-NMR (600 MHz, $CDCl_3$): δ [ppm] = 7.41 (d, $^3J_{H,H}$ = 8.8 Hz, 2H, H-2'), 6.86 (d, $^3J_{H,H}$ = 8.8 Hz, 2H, H-3'), 4.16-4.10 (m, 2H, H-1), 3.81-3.77 (m, 2H, H-2), 3.60 (q, $^3J_{H,H}$ = 7.0 Hz, 2H, H-3), 2.99 (s, 1H, H-2''), 1.24 (t, $^3J_{H,H}$ = 7.0 Hz, 3H, H-4); **^{13}C-NMR** (151 MHz, $CDCl_3$): δ [ppm] = 159.4 (C-4'), 133.7 (C-2'), 114.8 (C-3'), 114.4 (C-1'), 83.8 (C-1''), 75.9 (C-2''), 69.0 (C-2), 67.6 (C-1), 67.0 (C-3), 15.3 (C-4); **ATR-IR** (neat): $\tilde{\nu}$ [cm^{-1}] = 3287, 2975, 2929, 2870, 2106, 1605, 1505, 1287, 1245, 1171, 1119, 1059, 830, 536; **HRMS** (ESI$^+$): m/z calc.: 191.1067 [M+H]$^+$, found: 191.1101; **R_f**: 0.14 (CH_2Cl_2/PE 1:1 v/v).

Methyl 5-((4-(2-ethoxyethoxy)phenyl)ethynyl)-2-propionamidobenzoate 225

The reaction was performed according to general procedure IV with anthranilic acid **90** (201 mg, 603 µmol), copper iodide (11.5 mg, 60.3 µmol), $Pd(PPh_3)_4$ (69.7 mg, 60.3 µmol) and alkyne **170** (126 mg, 663 µmol) in triethylamine (4 mL) and THF (3 mL) at room temperature for 18 h. The crude product was purified by column chromatography (CH_2Cl_2/acetone 100:1 v/v) to yield **225** (194 mg, 491 µmol, 81%) as a yellowish solid.

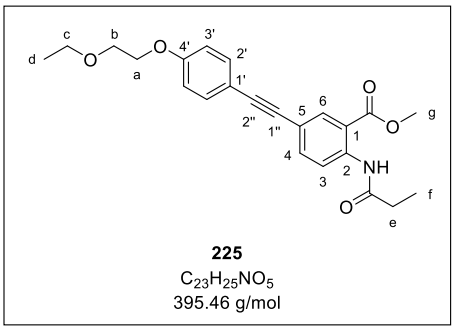

225
$C_{23}H_{25}NO_5$
395.46 g/mol

^{1}H-NMR (500 MHz, $CDCl_3$): δ [ppm] = 11.12 (s, 1H, CON*H*), 8.74 (d, $^3J_{H,H}$ = 8.8 Hz, 1H, H-3), 8.18 (d, $^4J_{H,H}$ = 2.1 Hz, 1H, H-6), 7.65 (dd, $^3J_{H,H}$ = 8.8 Hz, $^4J_{H,H}$ = 2.1 Hz, 1H, H-4), 7.44 (d, $^3J_{H,H}$ = 8.7 Hz, 2H, H-2'), 6.90 (d, $^3J_{H,H}$ = 8.7 Hz, 2H, H-3'), 4.17-4.11 (m, 2H, H-a), 3.94 (s, 3H, H-g), 3.83-3.77 (m, 2H, H-b), 3.61 (q, $^3J_{H,H}$ = 7.0 Hz, 2H, H-c), 2.49 (q, $^3J_{H,H}$ = 7.6 Hz, 2H, H-e), 1.28 (t, $^3J_{H,H}$ = 7.6 Hz, 3H, H-f), 1.25 (t, $^3J_{H,H}$ = 7.0 Hz, 3H, H-d); **^{13}C-NMR** (126 MHz, $CDCl_3$): δ [ppm] = 173.0 (*C*ONH), 168.4 (*C*OOMe), 159.2 (C-4'), 141.3 (C-2), 137.4 (C-4), 134.1 (C-6), 133.1 (C-2'), 120.4 (C-3), 117.8 (C-1), 115.4 (C-1'), 114.9 (C-5), 114.9 (C-3'), 89.5 (C-2''), 87.1 (C-1''), 69.0 (C-b), 67.7 (C-a), 67.1 (C-c), 52.6 (C-g), 31.9 (C-e), 15.3 (C-d), 9.68 (C-f); **ATR-IR** (neat): $\tilde{\nu}$ [cm^{-1}] = 3258, 2974, 2917, 1686, 1587, 1514, 1435, 1289, 1249, 1232, 1177, 1130, 1086, 834, 787; **HRMS** (ESI$^+$): m/z calc.: 396.1806 $[M+H]^+$, found: 396.1802; **R_f**: 0.30 (CH_2Cl_2/acetone 100:1 v/v).

5-((4-(2-Ethoxyethoxy)phenyl)ethynyl)-2-propionamidobenzoic acid 41

The saponification was carried out according to general procedure V with methyl ester **225** (180 mg, 455 µmol) and aqueous 1.0 M NaOH (1.5 mL) in THF (5 mL) for 16 h. Precipitation in acidic solution afforded target compound **41** (142 mg, 372 µmol, 82%) as a brownish solid.

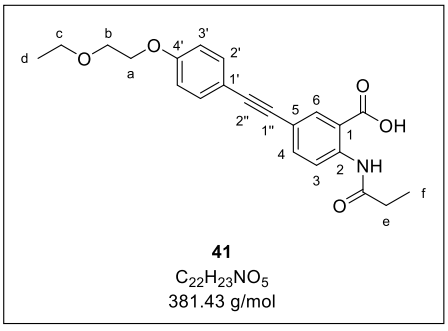

41
$C_{22}H_{23}NO_5$
381.43 g/mol

^{1}H-NMR (500 MHz, $CDCl_3$): δ [ppm] = 11.21 (s, 1H, CON*H*), 8.57 (d, $^3J_{H,H}$ = 8.8 Hz, 1H, H-3), 8.07 (d, $^4J_{H,H}$ = 2.1 Hz, 1H, H-6), 7.71 (dd, $^3J_{H,H}$ = 8.8 Hz, $^4J_{H,H}$ = 2.1 Hz, 1H, H-4), 7.49 (d, $^3J_{H,H}$ = 8.7 Hz, 2H, H-2'), 6.99 (d, $^3J_{H,H}$ = 8.7 Hz, 2H, H-3'), 4.15-4.10 (m, 2H, H-a), 3.72-3.67 (m, 2H, H-b), 3.50 (q, $^3J_{H,H}$ = 7.0 Hz, 2H, H-c), 2.43 (q, $^3J_{H,H}$ = 7.5 Hz, 2H, H-e), 1.20-1.05 (m, 6H, H-d, H-f); **^{13}C-NMR** (126 MHz, $CDCl_3$): δ [ppm] = 172.1 (*C*ONH), 168.8 (*C*OOH), 158.8 (C-4'), 140.7 (C-2), 136.3 (C-4), 133.8 (C-6), 132.9 (C-2'), 120.0 (C-3), 116.5 (C-1), 116.5 (C-5), 114.9 (C-3'), 114.1 (C-1'), 89.3 (C-2''), 86.9 (C-1''), 68.2 (C-b), 67.3 (C-a), 65.7 (C-c), 30.7 (C-e), 15.1 (C-d), 9.24 (C-f); **ATR-IR** (neat): $\tilde{\nu}$ [cm^{-1}] = 2984, 2936, 2877, 1687, 1586, 1514, 1288, 1250,

1218, 1173, 1105, 830, 795, 528; **HRMS** (ESI$^+$): m/z calc.: 380.1503 [M-H]$^-$, found: 380.1507; **R_f**: 0.54 (CH_2Cl_2/MeOH 9:1 v/v).

6.3.4. Syntheses of hDHODH inhibitors 42-48 (cycle 1)

1-(4-Iodophenyl)piperidine 112

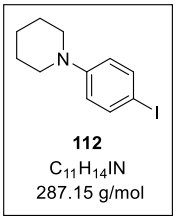

The reaction was carried out as described in general procedure I with 1,4-diiodobenzene **120** (2.00 g, 6.07 mmol), copper iodide (232 mg, 1.22 mmol), L-proline (280 mg, 2.43 mmol), potassium carbonate (1.68 g, 12.2 mmol) and piperidine (1.80 mL, 18.2 mmol) in DMSO (12 mL) for 24 h. Purification by column chromatography (PE/CH_2Cl_2 9:1 to 4:1 v/v) provided arylamine **112** (928 mg, 3.23 mmol, 53%) as a pale pink solid.

The analytical data was in accordance with those described.[197]

1-(4-((Trimethylsilyl)ethynyl)phenyl)piperidine 174

The reaction was performed according to general procedure II with 1-(4-iodophenyl)-piperidine **112** (880 mg, 3.07 mmol), copper iodide (29.2 mg, 153 µmol), $Pd(PPh_3)_4$ (177 mg, 153 µmol) and TMS acetylene (1.14 mL, 8.28 mmol) in triethylamine (12 mL) and THF (5 mL) at room temperature for 19 h. After purification by column chromatography (PE/CH_2Cl_2 3:1 v/v), TMS-protected alkyne **174** (638 mg, 2.48 mmol, 81%) was obtained as a yellowish solid.

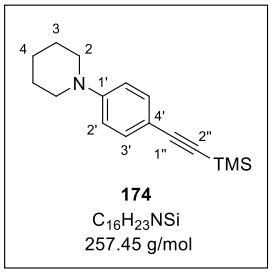

^{1}H-NMR (300 MHz, $CDCl_3$): δ [ppm] = 7.33 (d, $^3J_{H,H}$ = 8.8 Hz, 2H, H-3'), 6.80 (d, $^3J_{H,H}$ = 8.8 Hz, 2H, H-2'), 3.25-3.15 (m, 4H, H-2), 1.73-1.63 (m, 4H, H-3), 1.63-1.53 (m, 2H, H-4), 0.23 (s, 9H, Si(CH_3)$_3$); **^{13}C-NMR** (75 MHz, $CDCl_3$): δ [ppm] = 151.8 (C-1'), 133.2 (C-3'), 115.2 (C-2'), 112.4 (C-4'), 106.3 (C-1''), 91.8 (C-2''), 49.7 (C-2), 25.7 (C-3), 24.4 (C-4), 0.31 (Si(CH_3)$_3$); **ATR-IR** (neat): $\tilde{\nu}$ [cm^{-1}] = 2925, 2853, 2146, 1727, 1603, 1510, 1480, 1345, 1251, 1124, 832, 811, 758, 539; **MS** (EI): m/z calc.: 257.16 [M]$^+$, found: 257.20; **R_f**:0.60 (PE/CH_2Cl_2 2:1 v/v).

1-(4-Ethynylphenyl)piperidine 181

The cleavage of the protecting group was carried out according to general procedure III by treating compound **174** (612 mg, 2.38 mmol) with potassium carbonate (1.64 g, 11.9 mmol) in methanol (20 mL) for 4 h. Alkyne **181** (305 mg, 1.65 mmol, 69%) was isolated as a yellowish solid.

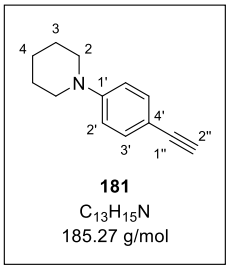

^{1}H-NMR (600 MHz, $CDCl_3$): δ [ppm] = 7.36 (d, $^3J_{H,H}$ = 8.9 Hz, 2H, H-3'), 6.82 (d, $^3J_{H,H}$ = 8.9 Hz, 2H, H-2'), 3.24-3.19 (m, 4H, H-2), 2.98 (s, 1H, H-2''), 1.72-1.65 (m, 4H, H-3), 1.62-1.57 (m, 2H, H-4); **^{13}C-NMR** (151 MHz, $CDCl_3$): δ [ppm] = 152.0 (C-1'), 133.3 (C-3'), 115.3 (C-2'), 111.2 (C-4'), 84.6 (C-1''), 75.2 (C-2''), 49.7 (C-2), 25.6 (C-3), 24.4 (C-4); **ATR-IR** (neat): $\tilde{\nu}$ [cm^{-1}] = 3296, 2940, 2923, 2853, 2824, 2095, 1604, 1508, 1247, 1223, 1123, 809, 597, 529; **MS** (EI): m/z calc.: 185.12 $[M]^+$, found: 185.10; **R_f**: 0.28 (PE/CH_2Cl_2 3:1 v/v).

Methyl 5-((4-(piperidin-1-yl)phenyl)ethynyl)-2-propionamidobenzoate 229

According to general procedure IV, the reaction was performed with anthranilic acid **90** (202 mg, 606 µmol), copper iodide (5.8 mg, 30 µmol), $Pd(PPh_3)_4$ (35 mg, 30 µmol) and alkyne **181** (169 mg, 910 µmol) in triethylamine (4 mL) and THF (3 mL) at room temperature for 2 h. Purification by column chromatography afforded **229** (219 mg, 562 µmol, 93%) as a pale orange solid.

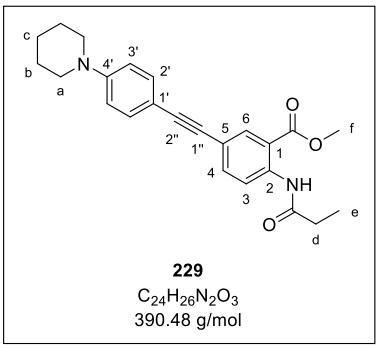

^{1}H-NMR (600 MHz, $CDCl_3$): δ [ppm] = 11.11 (s, 1H, CON*H*), 8.73 (d, $^3J_{H,H}$ = 8.8 Hz, 1H, H-3), 8.17 (d, $^4J_{H,H}$ = 2.1 Hz, 1H, H-6), 7.64 (dd, $^3J_{H,H}$ = 8.8 Hz, $^4J_{H,H}$ = 2.1 Hz, 1H, H-4), 7.39 (d, $^3J_{H,H}$ = 8.8 Hz, 2H, H-2'), 6.87 (d, $^3J_{H,H}$ = 8.8 Hz, 2H, H-3'), 3.94 (s, 3H, H-f), 3.26-3.21 (m, 4H, H-a), 2.49 (q, $^3J_{H,H}$ = 7.6 Hz, 2H, H-d), 1.72-1.66 (m, 4H, H-b), 1.64-1.57 (m, 2H, H-c), 1.28 (t, $^3J_{H,H}$ = 7.6 Hz, 3H, H-e); **^{13}C-NMR** (151 MHz, $CDCl_3$): δ [ppm] = 172.3 (*C*ONH), 168.5 (*C*OOMe), 151.1 (C-4'), 141.0 (C-2), 137.4 (C-4), 133.9 (C-6), 132.8 (C-2'), 120.4 (C-3), 118.2 (C-1), 115.4 (C-3'), 114.9 (C-5), 111.9 (C-1'), 90.4 (C-2''), 86.7 (C-1''), 52.6 (C-f), 50.0 (C-a), 31.9 (C-d), 25.7 (C-b), 24.4 (C-c), 9.70 (C-e); **ATR-IR** (neat): $\tilde{\nu}$ [cm^{-1}] = 3265, 2931, 1704, 1687, 1586, 1186, 1084, 820, 789; **HRMS** (ESI^+): m/z calc.: 391.2016 $[M+H]^+$, found: 391.2172; **R_f**: 0.47 (CH_2Cl_2/Acetone 100:1 v/v).

5-((4-(Piperidin-1-yl)phenyl)ethynyl)-2-propionamidobenzoic acid 42

The saponification was performed as described in general procedure V by treating methyl ester **229** (202 mg, 516 µmol) with aqueous 1.0 M NaOH (2 mL) in THF (5 mL) for 14 h. Precipitation in acidic solution provided target compound **42** (194 mg, 516 µmol, 100%) as a yellowish solid.

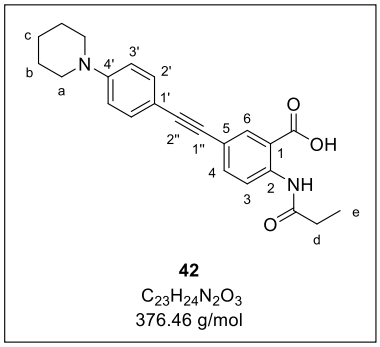

^{1}H-NMR (500 MHz, DMSO-d_6): δ [ppm] = 11.25 (s, 1H, CON*H*), 8.55 (d, $^3J_{H,H}$ = 8.7 Hz, 1H, H-3), 8.03 (d, $^4J_{H,H}$ = 2.2 Hz, 1H, H-6), 7.67 (dd, $^3J_{H,H}$ = 8.7 Hz, $^4J_{H,H}$ = 2.2 Hz, 1H, H-4), 7.35 (d, $^3J_{H,H}$ = 8.9 Hz, 2H, H-2'), 6.91 (d, $^3J_{H,H}$ = 8.9 Hz, 2H, H-3'), 3.26-3.20 (m, 4H, H-a), 2.43 (q, $^3J_{H,H}$ = 7.5 Hz, 2H, H-d), 1.63-1.52 (m, 6H, H-b, H-c), 1.13 (t, $^3J_{H,H}$ = 7.5 Hz, 3H, H-e); **^{13}C-NMR** (126 MHz, DMSO-d_6): δ [ppm] = 172.1 (*C*ONH), 168.9 (*C*OOH), 151.0 (C-4'), 140.4 (C-2), 136.0 (C-4), 133.5 (C-6), 132.4 (C-2'), 120.0 (C-3), 116.9 (C-1), 116.7 (C-5), 114.7 (C-3'), 110.2 (C-1'), 90.3 (C-2''), 86.4 (C-1''), 48.3 (C-a), 30.7 (C-d), 24.9 (C-b), 23.9 (C-c), 9.27 (C-e); **ATR-IR** (neat): $\tilde{\nu}$ [cm^{-1}] = 2929, 2201, 1706, 1579, 1506, 1291, 1212, 1123, 911, 822; **HRMS** (ESI$^+$): m/z calc.: 377.1860 [M+H]$^+$, found: 377.1882; **R_f**: 0.34 (CH_2Cl_2/MeOH 9:1 v/v).

5-((4-Morpholinophenyl)ethynyl)-2-propionamidobenzoic acid 43

The compound was synthesized in a previous study and was provided for use in this work.

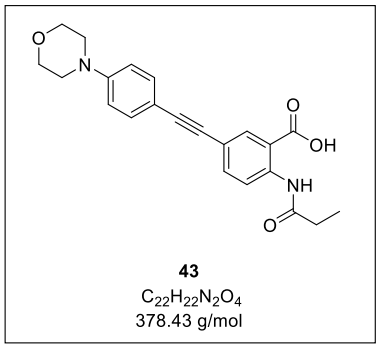

1-(4-((Trimethylsilyl)ethynyl)phenyl)piperazine 175

The reaction was carried out according to general procedure II with 1-(4-iodophenyl)-piperazine **113** (499 mg, 1.73 mmol), copper iodide (16.5 mg, 86.6 µmol), $Pd(PPh_3)_4$ (100 mg, 86.6 µmol) and TMS acetylene (650 µL, 4.68 mmol) in triethylamine (7 mL) and THF (3 mL) at room temperature for 19 h. The crude product was purified by column chromatography (CH_2Cl_2/MeOH 19:1 v/v + 1% NEt_3) to yield **175** (255 mg, 986 µmol, 57%) as a brownish solid.

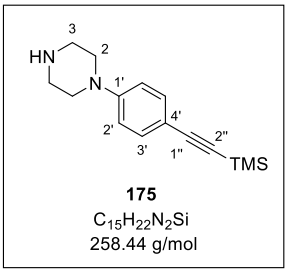

^{1}H-NMR (400 MHz, $CDCl_3$): δ [ppm] = 7.36 (d, $^3J_{H,H}$ = 9.0 Hz, 2H, H-3'), 6.80 (d, $^3J_{H,H}$ = 9.0 Hz, 2H, H-2'), 3.24-3.16 (m, 4H, H-2), 3.08-3.01 (m, 4H, H-3), 2.43 (s, 1H, N*H*), 0.23 (s, 9H, Si(C*H*$_3$)$_3$); **^{13}C-NMR** (101 MHz, $CDCl_3$): δ [ppm] = 151.4 (C-1'), 133.2 (C-3'), 115.2 (C-2'), 113.5 (C-4'), 105.9 (C-1''), 92.2 (C-2''), 49.3 (C-2), 45.8 (C-3), 0.26 (s, 9H, Si(C*H*$_3$)$_3$); **ATR-IR** (neat): $\tilde{\nu}$ [cm^{-1}] = 3404, 2955, 2898,

2823, 2146, 1603, 1509, 1246, 835, 811, 758; **MS** (EI): m/z calc.: 258.15 $[M]^+$, found: 258.10; $\mathbf{R_f}$: 0.40 (CH_2Cl_2/MeOH 19:1 v/v + 1% NEt_3).

1-(4-Ethynylphenyl)piperazine 182

According to general procedure III, the reaction was carried out by treating compound **175** (240 mg, 929 µmol) with potassium carbonate (642 mg, 4.64 mmol) in methanol (8 mL) for 4 h. Alkyne **182** (127 mg, 679 µmol, 73%) was obtained as a yellowish solid.

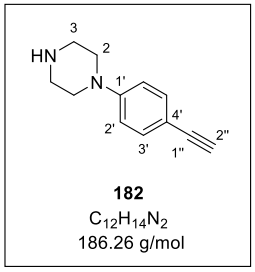

^{1}H-NMR (600 MHz, DMSO-d_6): δ [ppm] = 7.29 (d, $^3J_{H,H}$ = 8.8 Hz, 2H, H-3'), 6.88 (d $^3J_{H,H}$ = 8.8 Hz, 2H, H-2'), 3.91 (s, 1H, H-2''), 3.38 (s, 1H, N*H*), 3.14-3.09 (m, 4H, H-2), 2.86-2.81 (m, 4H, H-3); **^{13}C-NMR** (151 MHz, DMSO-d_6): δ [ppm] = 151.3 (C-1'), 132.6 (C-3'), 114.5 (C-2'), 110.6 (C-4'), 84.3 (C-1''), 78.5 (C-2''), 48.0 (C-2), 45.2 (C-3); **ATR-IR** (neat): $\tilde{\nu}$ [cm^{-1}] = 3394, 3193, 2917, 2815, 1603, 1509, 1433, 1280, 1255, 1233, 1121, 1092, 822, 547; **MS** (EI): m/z calc.: 186.12 $[M]^+$, found: 186.10; $\mathbf{R_f}$: 0.46 (CH_2Cl_2/MeOH 19:1 v/v + 1% NEt_3).

Methyl 5-((4-(piperazin-1-yl)phenyl)ethynyl)-2-propionamidobenzoate 230

The reaction was performed as described in general procedure IV with anthranilic acid **90** (158 mg, 474 µmol), copper iodide (4.5 mg, 24 µmol), $Pd(PPh_3)_4$ (27 mg, 24 µmol) and alkyne **182** (97.2 mg, 522 µmol) in triethylamine (4 mL) and THF (3 mL) at room temperature for 18 h. Purification by column chromatography (CH_2Cl_2/MeOH 19:1 v/v + 0.5% NEt_3) provided **230** (177 mg, 454 µmol, 96%) as a yellowish solid.

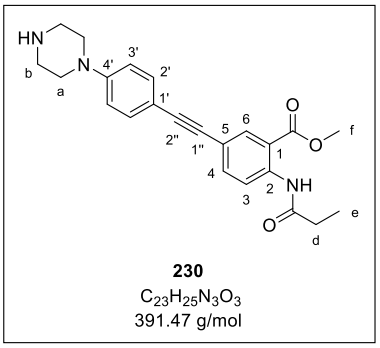

^{1}H-NMR (500 MHz, DMSO-d_6): δ [ppm] = 10.66 (s, 1H, CON*H*), 8.35 (d, $^3J_{H,H}$ = 8.7 Hz, 1H, H-3), 7.98 (d, $^4J_{H,H}$ = 2.1 Hz, 1H, H-6), 7.70 (dd, $^3J_{H,H}$ = 8.7 Hz, $^4J_{H,H}$ = 2.1 Hz, 1H, H-4), 7.41 (d, $^3J_{H,H}$ = 8.9 Hz, 2H, H-2'), 6.96 (d, $^3J_{H,H}$ = 8.9 Hz, 2H, H-3'), 3.87 (s, 3H, H-f), 3.32-3.23 (m, 4 H, H-a), 3.03-2.93 (m, 4H, H-b), 2.42 (q, $^3J_{H,H}$ = 7.5 Hz, 2H, H-d), 1.12 (t, $^3J_{H,H}$ = 7.5 Hz, 3H, H-e); **^{13}C-NMR** (126 MHz, DMSO-d_6): δ [ppm] = 172.1 (*C*ONH), 167.0 (*C*OOMe), 150.6 (C-4'), 139.3 (C-2), 136.0 (C-4), 133.0 (C-6), 132.4 (C-2'), 121.0 (C-3), 117.5 (C-1), 117.3 (C-5), 114.8 (C-3'), 111.4 (C-1'), 90.3 (C-2''), 86.4 (C-1''), 52.6 (C-f), 46.5 (C-a), 44.0 (C-b), 30.4 (C-d), 9.31 (C-e); **ATR-IR** (neat): $\tilde{\nu}$ [cm^{-1}] = 3301, 3261, 2922, 2832, 2160, 1686, 1587, 1516, 1230, 1187, 821, 786; **HRMS** (ESI^+): m/z calc.: 392.1969 $[M+H]^+$, found: 392.1989; $\mathbf{R_f}$: 0.40 (CH_2Cl_2/MeOH 19:1 v/v + 0.5% NEt_3).

5-((4-(Piperazin-1-yl)phenyl)ethynyl)-2-propionamidobenzoic acid 44

The saponification was carried out according to general procedure V with methyl ester **230** (158 mg, 404 µmol) and aqueous 1.0 M NaOH (2 mL) in THF (5 mL) for 20 h. After precipitation in acidic solution, target compound **44** (112 mg, 298 µmol, 74%) was isolated as a colorless solid.

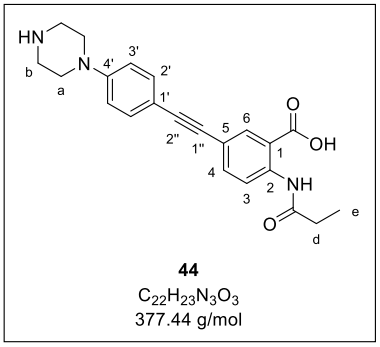

44
$C_{22}H_{23}N_3O_3$
377.44 g/mol

^{1}H-NMR (500 MHz, DMSO-d_6): δ [ppm] = 11.23 (s, 1H, CON*H*), 8.55 (d, $^3J_{H,H}$ = 8.7 Hz, 1H, H-3), 8.05 (d, $^4J_{H,H}$ = 2.2 Hz, 1H, H-6), 7.69 (dd, $^3J_{H,H}$ = 8.7 Hz, $^4J_{H,H}$ = 2.2 Hz, 1H, H-4), 7.44 (d, $^3J_{H,H}$ = 8.8 Hz, 2H, H-2'), 7.01 (d, $^3J_{H,H}$ = 8.8 Hz, 2H, H-3'), 3.50-3.44 (m, 4 H, H-a), 3.23-3.14 (m, 4H, H-b), 2.43 (q, $^3J_{H,H}$ = 7.5 Hz, 2H, H-d), 1.13 (t, $^3J_{H,H}$ = 7.5 Hz, 3H, H-e); **^{13}C-NMR** (126 MHz, DMSO-d_6): δ [ppm] = 172.1 (NH*C*O), 168.8 (*C*OOH), 149.7 (C-4'), 140.5 (C-2), 136.1 (C-4), 133.7 (C-6), 132.5 (C-2'), 120.0 (C-3), 116.7 (C-1), 116.6 (C-5), 115.3 (C-3'), 112.3 (C-1'), 89.7 (C-2''), 86.9 (C-1''), 44.5 (C-a), 42.2 (C-b), 30.7 (C-d), 9.27 (C-e); **ATR-IR** (neat): $\tilde{\nu}$ [cm^{-1}] = 3261, 2848, 2490, 1681, 1585, 1518, 1388, 1220, 1184, 1137, 926, 830; **HRMS** (ESI$^+$): m/z calc.: 378.1812 [M+H]$^+$, found: 378.1828; **R_f**: 0.04 (CH_2Cl_2/MeOH 19:1 v/v + 0.5% NEt_3).

1-(4-Iodophenyl)-4-methylpiperazine 114

The reaction was carried out as described in general procedure I with 1,4-diiodobenzene **120** (2.13 g, 6.44 mmol), copper iodide (246 mg, 1.29 mmol), L-proline (297 mg, 2.58 mmol), potassium carbonate (1.78 g, 12.9 mmol) and 1-methylpiperazine **122** (2.15 mL, 19.3 mmol) in DMSO (12 mL) at 50 °C for 24 h. The crude product was purified by column chromatography (CH_2Cl_2/MeOH 19:1 v/v + 1% NEt_3) to yield aryl halide **114** (1.10 g, 3.64 mmol, 56%) as a colorless solid.

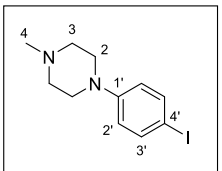

114
$C_{11}H_{15}IN_2$
302.16 g/mol

^{1}H-NMR (500 MHz, $CDCl_3$): δ [ppm] = 7.51 (d, $^3J_{H,H}$ = 9.0 Hz, 2H, H-3'), 6.68 (d $^3J_{H,H}$ = 9.0 Hz, 2H, H-2'), 3.21-3.15 (m, 4H, H-2), 2.59-2.53 (m, 4H, H-3), 2.34 (s, 3H, H-4); **^{13}C-NMR** (126 MHz, $CDCl_3$): δ [ppm] = 151.0 (C-1'), 137.9 (C-3'), 118.2 (C-2'), 81.5 (C-4'), 55.0 (C-3), 48.8 (C-2), 46.2 (C-4); **ATR-IR** (neat): $\tilde{\nu}$ [cm^{-1}] = 2931, 2831, 2790, 2743, 1584, 1489, 1444, 1291, 1234, 1142, 1008, 917, 810, 520; **HRMS** (ESI$^+$): m/z calc.: 303.0353 [M+H]$^+$, found: 303.0319; **R_f**: 0.33 (CH_2Cl_2/MeOH 19:1 v/v + 1% NEt_3).

1-Methyl-4-(4-((trimethylsilyl)ethynyl)phenyl)piperazine 176

According to general procedure II, the reaction was carried out with 1-(4-iodophenyl)-4-methylpiperazine **114** (980 mg, 3.24 mmol), copper iodide (30.9 mg, 162 µmol), $Pd(PPh_3)_4$ (187 mg, 162 µmol) and TMS acetylene (1.21 mL, 8.76 mmol) in triethylamine (13 mL) and THF (5 mL) at room temperature for 24 h. The crude product was purified by column chromatography and following preparative TLC (CH_2Cl_2/MeOH 19:1 v/v + 0.5% NEt_3) to afford **176** (234 mg, 860 µmol) as a colorless solid.

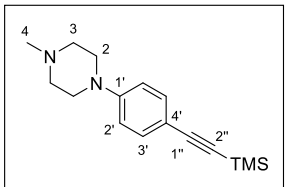

176
$C_{16}H_{24}N_2Si$
272.47 g/mol

^{1}H-NMR (400 MHz, $CDCl_3$): δ [ppm] = 7.35 (d, $^3J_{H,H}$ = 9.0 Hz, 2H, H-3'), 6.80 (d $^3J_{H,H}$ = 9.0 Hz, 2H, H-2'), 3.28-3.21 (m, 4H, H-2), 2.59-2.52 (m, 4H, H-3), 2.35 (s, 3H, H-4), 0.23 (s, 9H, Si(CH_3)$_3$); **^{13}C-NMR** (101 MHz, $CDCl_3$): δ [ppm] = 151.0 (C-1'), 133.2 (C-3'), 115.0 (C-2'), 113.3 (C-4'), 106.0 (C-1''), 92.1 (C-2''), 55.0 (C-3), 48.3 (C-2), 46.3 (C-4), 0.28 (Si(CH_3)$_3$); **ATR-IR** (neat): $\tilde{\nu}$ [cm^{-1}] = 2937, 2842, 2797, 2146, 1603, 1518, 1448, 1293, 1246, 1141, 1002, 919, 815, 756, 539; **HRMS** (ESI$^+$): m/z calc.: 273.1782 $[M+H]^+$, found: 273.1712; **R_f**: 0.53 (CH_2Cl_2/MeOH 19:1 v/v + 0.5% NEt_3).

1-(4-Ethynylphenyl)-4-methylpiperazine 183

The cleavage of the protecting group was performed as described in general procedure III by treating compound **176** (234 mg, 860 µmol) with potassium carbonate (594 mg, 4.30 mmol) in methanol (8 mL) for 4 h. Alkyne **183** (157 mg, 783 µmol, 91%) was obtained as a brownish solid.

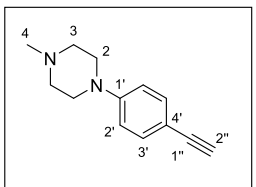

183
$C_{13}H_{16}N_2$
200.29 g/mol

^{1}H-NMR (400 MHz, $CDCl_3$): δ [ppm] = 7.38 (d, $^3J_{H,H}$ = 9.0 Hz, 2H, H-3'), 6.82 (d $^3J_{H,H}$ = 9.0 Hz, 2H, H-2'), 3.26-3.21 (m, 4H, H-2), 2.98 (s, 1H, H-2''), 2.58-2.52 (m, 4H, H-3), 2.34 (s, 3H, H-4); **^{13}C-NMR** (101 MHz, $CDCl_3$): δ [ppm] = 151.3 (C-1'), 133.3 (C-3'), 115.1 (C-2'), 112.1 (C-4'), 84.4 (C-1''), 75.5 (C-2''), 55.0 (C-3), 48.3 (C-2), 46.3 (C-4); **ATR-IR** (neat): $\tilde{\nu}$ [cm^{-1}] = 3199, 2944, 2832, 2811, 2093, 1605, 1513, 1445, 1293, 1247, 1137, 1001, 923, 812, 537; **MS** (EI): m/z calc.: 200.13 $[M]^+$, found: 200.10; **R_f**: 0.31 (CH_2Cl_2/MeOH 19:1 v/v + 0.5% NEt_3).

Methyl 5-((4-(4-methylpiperazin-1-yl)phenyl)ethynyl)-2-propionamidobenzoate 231

The reaction was carried out according to general procedure IV with anthranilic acid **90** (160 mg, 480 µmol), copper iodide (9.1 mg, 48 µmol), $Pd(PPh_3)_4$ (55 mg, 48 µmol) and alkyne **183** (144 mg, 720 µmol) in triethylamine (4 mL) and THF (3 mL) at room temperature

for 18 h. After purification by column chromatography (CH_2Cl_2/MeOH 19:1 v/v + 0.5% NEt_3), compound **231** (182 mg, 449 µmol, 93%) was obtained as an orange solid.

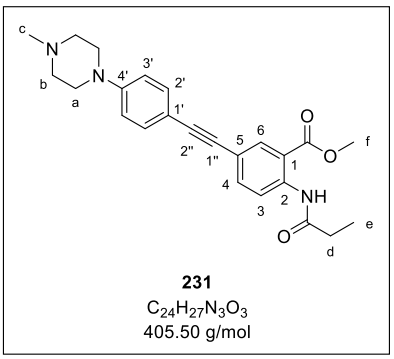

^{1}H-NMR (400 MHz, $CDCl_3$): δ [ppm] = 11.11 (s, 1H, CON*H*), 8.73 (d, $^3J_{H,H}$ = 8.8 Hz, 1H, H-3), 8.17 (d, $^4J_{H,H}$ = 2.0 Hz, 1H, H-6), 7.64 (dd, $^3J_{H,H}$ = 8.8 Hz, $^4J_{H,H}$ = 2.0 Hz, 1H, H-4), 7.41 (d, $^3J_{H,H}$ = 8.9 Hz, 2H, H-2'), 6.86 (d, $^3J_{H,H}$ = 8.9 Hz, 2H, H-3'), 3.94 (s, 3H, H-f), 3.31-3.24 (m, 4H, H-a), 2.61-2.54 (m, 4H, H-b), 2.49 (q, $^3J_{H,H}$ = 7.6 Hz, 2H, H-d), 2.36 (s, 3H, H-c), 1.28 (t, $^3J_{H,H}$ = 7.6 Hz, 3H, H-e); **^{13}C-NMR** (101 MHz, $CDCl_3$): δ [ppm] = 173.0 (*C*ONH), 168.4 (*C*OOMe), 151.0 (C-4'), 141.1 (C-2), 137.6 (C-4), 134.0 (C-6), 132.8 (C-2'), 120.4 (C-3), 118.1 (C-1), 115.2 (C-3'), 114.8 (C-5), 113.1 (C-1'), 90.1 (C-2''), 68.9 (C-1''), 55.0 (C-b), 52.6 (C-f), 48.3 (C-a), 46.3 (C-c), 31.9 (C-d), 9.68 (C-e); **ATR-IR** (neat): $\tilde{\nu}$ [cm^{-1}] = 3258, 2935, 2844, 2794, 2200, 1691, 1611,1519, 1439, 1289, 1232, 1184, 789; **HRMS** (ESI$^+$): m/z calc.: 406.2125 [M+H]$^+$, found: 406.2115; **R_f**: 0.47 (CH_2Cl_2/MeOH 19:1 v/v + 0.5% NEt_3).

5-((4-(4-Methylpiperazin-1-yl)phenyl)ethynyl)-2-propionamidobenzoic acid 45

According to general procedure V, the saponification was carried out by treating compound **231** (160 mg, 395 µmol) with aqueous 1.0 M NaOH (1.5 mL) in THF (5 mL). Precipitation in acidic solution provided target compound **45** (86.6 mg, 214 µmol, 54%) as a colorless solid.

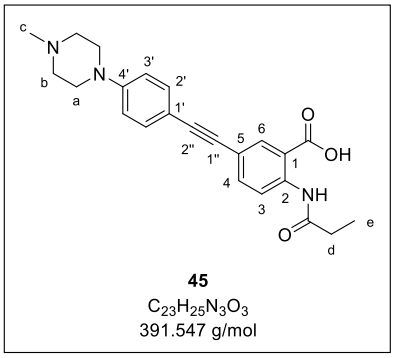

^{1}H-NMR (600 MHz, DMSO-d_6): δ [ppm] = 11.24 (s, 1H, CON*H*), 8.55 (d, $^3J_{H,H}$ = 8.7 Hz, 1H, H-3), 8.05 (d, $^4J_{H,H}$ = 2.2 Hz, 1H, H-6), 7.69 (dd, $^3J_{H,H}$ = 8.7 Hz, $^4J_{H,H}$ = 2.2 Hz, 1H, H-4), 7.45 (d, $^3J_{H,H}$ = 8.8 Hz, 2H, H-2'), 7.03 (d, $^3J_{H,H}$ = 8.9 Hz, 2H, H-3'), 2.81 (s, 3H, H-c), 2.43 (q, $^3J_{H,H}$ = 7.5 Hz, 2H, H-d), 1.13 (t, $^3J_{H,H}$ = 7.5 Hz, 3H, H-e); **^{13}C-NMR** (151 MHz, $CDCl_3$): δ [ppm] = 172.2 (*C*ONH), 168.9 (*C*OOH), 149.4 (C-4'), 140.6 (C-2), 136.2 (C-4), 133.7 (C-6), 132.5 (C-2'), 120.0 (C-3), 116.6 (C-1), 116.6 (C-5), 115.7 (C-1'), 115.4 (C-3'), 112.4 (C-1'), 89.7 (C-2''), 86.9 (C-1''), 42.0 (C-c), 30.7 (C-d), 9.29 (C-e); **ATR-IR** (neat): $\tilde{\nu}$ [cm^{-1}] = 2922, 2822, 2570, 1688, 1515, 1285, 1240, 1183, 982, 841, 827, 779, 734, 681, 574; **HRMS** (ESI$^+$): m/z calc.: 390.1823 [M-H]$^-$, found: 390.1805; **R_f**: 0.10 (CH_2Cl_2/MeOH 9:1).

4-(4-Bromophenyl)thiomorpholine 115

The reaction was carried out as described in general procedure I with 1-bromo-4-iodobenzene **119** (1.01 g, 3.56 mmol), copper iodide (135 mg, 711 µmol), L-proline (164 mg, 1.42 mmol), potassium carbonate (983 mg, 7.12 mmol) and thiomorpholine **123** (550 µL, 5.33 mmol) in DMSO (8 mL) at room temperature for 20 h. The crude product was purified by column chromatography (CH_2Cl_2/PE 1:1 v/v) to yield arylamine **115** (356 mg, 1.38 mmol, 39%) as a colorless solid.

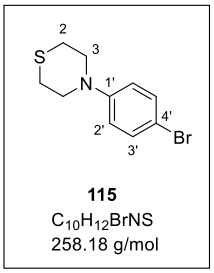

115
$C_{10}H_{12}BrNS$
258.18 g/mol

^{1}H-NMR (600 MHz, $CDCl_3$): δ [ppm] = 7.34 (d, $^3J_{H,H}$ = 8.9 Hz, 2H, H-3'), 6.76 (d, $^3J_{H,H}$ = 8.9 Hz, 2H, H-2'), 3.53-3.49 (m, 4H, H-3), 2.75-2.69 (m, 4H, H-2); **^{13}C-NMR** (151 MHz, $CDCl_3$): δ [ppm] = 150.4 (C-1'), 132.2 (C-3'), 118.8 (C-2'), 112.0 (C-4'), 52.1 (C-3), 26.8 (C-2); **ATR-IR** (neat): $\tilde{\nu}$ [cm^{-1}] = 2909, 2816, 1583, 1487, 1447, 1381, 1285, 1194, 1131, 965, 820, 525; **HRMS** (ESI$^+$): m/z calc.: 257.9947 [M+H]$^+$, found: 257.9943; **R_f**: 0.36 (CH_2Cl_2/PE 1:1 v/v).

4-(4-((Trimethylsilyl)ethynyl)phenyl)thiomorpholine 177

The reaction was carried out according to general procedure II with 4-(4-bromophenyl)-thiomorpholine **115** (330 mg, 1.28 mmol), copper iodide (24.3 mg, 128 µmol), $Pd(PPh_3)_4$ (148 mg, 128 µmol) and TMS acetylene (480 µL, 3.45 mmol) in triethylamine (6 mL) and THF (2 mL) at 70 °C for 20 h. Purification by column chromatography (CH_2Cl_2/PE 1:1 v/v) afforded **177** (274 mg, 995 µmol, 78%) as a yellow solid.

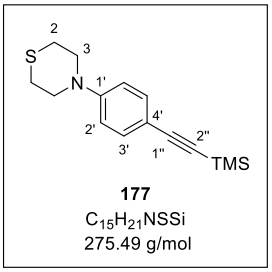

177
$C_{15}H_{21}NSSi$
275.49 g/mol

^{1}H-NMR (500 MHz, $CDCl_3$): δ [ppm] = 7.35 (d, $^3J_{H,H}$ = 8.8 Hz, 2H, H-3'), 6.76 (d, $^3J_{H,H}$ = 8.8 Hz, 2H, H-2'), 3.64-3.59 (m, 4H, H-3), 2.74-2.67 (m, 4H, H-2), 0.23 (s, 9H, Si(CH_3)$_3$); **^{13}C-NMR** (126 MHz, $CDCl_3$): δ [ppm] = 150.5 (C-1'), 133.4 (C-3'), 115.7 (C-2'), 113.2 (C-4'), 105.8 (C-1''), 92.3 (C-2''), 51.3 (C-3), 26.4 (C-2), 0.27 (Si(CH_3)$_3$); **ATR-IR** (neat): $\tilde{\nu}$ [cm^{-1}] = 2955, 2906, 2831, 2145, 1603, 1509, 1245, 1196, 838, 814, 761, 701; **HRMS** (ESI$^+$): m/z calc.: 276.1237 [M+H]$^+$, found: 276.1426; **R_f**: 0.51 (CH_2Cl_2/PE 1:1 v/v).

4-(4-Ethynylphenyl)thiomorpholine 184

The cleavage of the protecting group was performed according to general procedure III by treating compound **177** (250 mg, 907 µmol) with potassium carbonate (627 mg, 4.54 mmol) in methanol (8 mL) for 4 h. Alkyne **184** (138 mg, 680 µmol, 75%) was isolated as a colorless solid.

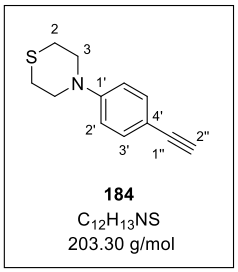

184
$C_{12}H_{13}NS$
203.30 g/mol

^{1}H-NMR (400 MHz, $CDCl_3$): δ [ppm] = 7.38 (d, $^3J_{H,H}$ = 8.9 Hz, 2H, H-3'), 6.78 (d, $^3J_{H,H}$ = 8.9 Hz, 2H, H-2'), 3.66-3.59 (m 4H, H-3), 2.98 (s, 1H, H-2''), 2.76-2.68 (m, 4H, H-2); **^{13}C-NMR** (101 MHz, $CDCl_3$): δ [ppm] = 150.7 (C-1'), 133.5 (C-3'), 115.8 (C-2'), 112.0 (C-1''), 75.61 (C-2''), 51. 3 (C-3), 26.4 (C-2); **ATR-IR** (neat): $\tilde{\nu}$ [cm^{-1}] = 3250, 2908, 2827, 2097, 1601, 1507, 1382, 1287, 1196, 1175, 1133, 968, 891, 833, 554; **HRMS** (ESI$^+$): m/z calc.: 204.0842 [M+H]$^+$, found: 204.0856; **R_f**: 0.38 (CH_2Cl_2/PE 1:1 v/v).

Methyl 2-propionamido-5-((4-thiomorpholinophenyl)ethynyl)benzoate 232

The reaction was carried out as described in general procedure IV with anthranilic acid **90** (150 mg, 450 µmol), copper iodide (8.6 mg, 45 µmol), $Pd(PPh_3)_4$ (52 mg, 45 µmol) and alkyne **184** (101 mg, 495 µmol) in triethylamine (4 mL) and THF (3 mL) at room temperature for 15 h. The crude product was purified by column chromatography (CH_2Cl_2/acetone 100:1 v/v) to yield **232** (158 mg, 387 µmol, 86%) as a yellow solid.

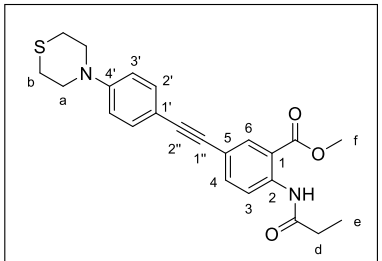

232
$C_{23}H_{24}N_2O_3S$
408.52 g/mol

^{1}H-NMR (500 MHz, $CDCl_3$): δ [ppm] = 11.11 (s, 1H, CON*H*), 8.74 (d, $^3J_{H,H}$ = 8.8 Hz, 1H, H-3), 8.18 (d, $^4J_{H,H}$ = 2.1 Hz, 1H, H-6), 7.65 (dd, $^3J_{H,H}$ = 8.8 Hz, $^4J_{H,H}$ = 2.1 Hz, 1H, H-4), 7.41 (d, $^3J_{H,H}$ = 8.9 Hz, 2H, H-2'), 6.82 (d, $^3J_{H,H}$ = 8.9 Hz, 2H, H-3'), 3.94 (s, 3H, H-f), 3.67-3.62 (m, 4H, H-a), 2.75-2.70 (m, 4H, H-b), 2.49 (q, $^3J_{H,H}$ = 7.5 Hz, 2H, H-d), 1.28 (t, $^3J_{H,H}$ = 7.5 Hz, 3H, H-e); **^{13}C-NMR** (126 MHz, $CDCl_3$): δ [ppm] = 173.0 (CON*H*), 168.2 (*C*OOMe), 150.4 (C-4'), 141.1 (C-2), 137.4 (C-4), 134.0 (C-6), 133.0 (C-2'), 120.4 (C-3), 117.8 (C-1), 115.9 (C-3'), 114.9 (C-5), 90.0 (C-2''), 87.0 (C-1''), 52.6 (C-f), 51.3 (C-a), 31.9 (C-d), 26.4 (C-b), 9.69 (C-e); **ATR-IR** (neat): $\tilde{\nu}$ [cm^{-1}] = 3250, 2951, 2905, 1697, 1682, 1590, 1517, 1288, 1252, 1217, 1191, 811, 787; **HRMS** (ESI$^+$): m/z calc.: 409.1581 [M+H]$^+$, found: 409.1570; **R_f**: 0.49 (CH_2Cl_2/acetone 100:1 v/v).

2-Propionamido-5-((4-thiomorpholinophenyl)ethynyl)benzoic acid 46

According to general procedure V, the saponification was performed with methyl ester **232** (140 mg, 343 µmol) and aqueous 1.0 M NaOH (1.5 mL) in THF (5 mL) for 16 h. Precipitation in acidic solution afforded target compound **46** (124 mg, 315 µmol, 92%) as a greyish solid.

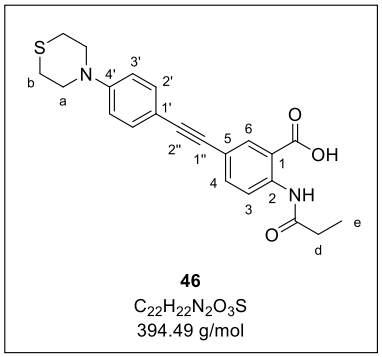

46
$C_{22}H_{22}N_2O_3S$
394.49 g/mol

^{1}H-NMR (500 MHz, DMSO-d_6): δ [ppm] = 11.19 (s, 1H, CON*H*), 8.55 (d, $^3J_{H,H}$ = 8.7 Hz, 1H, H-3), 8.04 (d, $^4J_{H,H}$ = 2.2 Hz, 1H, H-6), 7.68 (dd, $^3J_{H,H}$ = 8.7 Hz, $^4J_{H,H}$ = 2.2 Hz, 1H, H-4), 7.38 (d, $^3J_{H,H}$ = 8.9 Hz, 2H, H-2'), 6.93 (d, $^3J_{H,H}$ = 8.9 Hz, 2H, H-3'), 3.68-3.63 (m, 4H, H-a), 2.66-2.60 (m, 4H, H-b), 2.43 (q, $^3J_{H,H}$ = 7.5 Hz, 2H, H-d), 1.13 (t, $^3J_{H,H}$ = 7.5 Hz, 3H, H-e); **^{13}C-NMR** (126 MHz, DMSO-d_6): δ [ppm] = 172.1 (*C*ONH), 168.9 (*C*OOH), 149.7 (C-4'), 140.4 (C-2), 136.1 (C-4), 133.5 (C-6), 132.6 (C-2'), 120.0 (C-3), 116.9 (C-1), 116.5 (C-5), 115.0 (C-3'), 110.5 (C-1'), 90.1 (C-2''), 86.5 (C-1''), 50.0 (C-a), 30.7 (C-d), 24.9 (C-b), 9.25 (C-e); **ATR-IR** (neat): $\tilde{\nu}$ [cm^{-1}] = 2908, 2831, 1704, 1601, 1574, 1514, 1289, 1212, 1192, 830, 795, 674, 563; **HRMS** (ESI$^+$): m/z calc.: 393.1278 [M-H]$^-$, found: 393.1268; **R_f**: 0.38 (CH_2Cl_2/MeOH 9:1 v/v).

4-(4-Iodophenyl)thiomorpholine 1,1-dioxide 116

Ullmann-Goldberg reaction:

In a first attempt, the reaction was carried out according to general procedure I with 1,4-diiodobenzene **120** (2.00 g, 6.05 mmol), copper iodide (230 mg, 1.21 mmol), L-proline (279 mg, 2.42 mmol), potassium carbonate (1.67 g, 12.1 mmol) and thiomorpholine-1,1-dioxide **124** (1.23 g, 9.07 mmol) in DMSO (8 mL) at 70 °C for 24 h. Only little conversion was observed by TLC and the mixture was treated again with 1.5 eq. of thiomorpholine-1,1-dioxide. However, after stirring for another 24 h, conversion of the starting material was stagnating and the reaction was stopped. Purification by column chromatography (CH_2Cl_2 + 0.5% acetone v/v) provided **116** (196 mg, 580 µmol, 10%) as a yellowish solid.

Michael addition reaction:

In a second attempt, compound **116** was prepared in a Michael addition reaction in water. Therefore, a suspension of 4-iodoaniline **105** (660 mg, 3.01 mmol, 1.00 eq.) and divinylsulfone **126** (300 µL, 3.01, 1.00 eq.) in water (5 mL) was treated with glycerol (2-3 drops) and boric acid (55.9 mg, 904 µmol, 0.30 eq.). After stirring under reflux for 20 h, the supernatant was separated from the resulting solid by decantation. The solid was redissolved in CH_2Cl_2 and washed three times with water. The organic layer was dried over Na_2SO_4 and the solvent was removed under reduced pressure. The crude product was purified by column chromatography (CH_2Cl_2 + 0.5% acetone v/v) to yield **116** (582 mg, 1.72 mmol, 57%) as a brownish solid.

^{1}H-NMR (600 MHz, $CDCl_3$): δ [ppm] = 7.57 (d, $^{3}J_{H,H}$ = 9.0 Hz, 2H, H-3'), 6.68 (d, $^{3}J_{H,H}$ = 9.0 Hz, 2H, H-2'), 3.85-3.80 (m, 4H, H-3), 3.11-3.06 (m, 4H, H-2); **^{13}C-NMR** (151 MHz, $CDCl_3$): δ [ppm] = 147.4 (C-1'), 138.7 (C-3'), 118.5 (C-2'), 83.0 (C-4'), 50.6 (C-2), 47.6 (C-3); **ATR-IR** (neat): $\tilde{\nu}$ [cm^{-1}] = 2983, 2930, 2845, 1486, 1383, 1304, 1274, 1179, 1124, 820, 722, 674, 531, 432; **HRMS** (ESI^{+}): m/z calc.: 337.9706 $[M+H]^{+}$, found: 337.9720; **R_f**: 0.65 (CH_2Cl_2 + 0.5% acetone v/v).

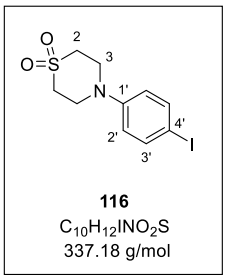

116
$C_{10}H_{12}INO_2S$
337.18 g/mol

4-(4-((Trimethylsilyl)ethynyl)phenyl)thiomorpholine 1,1-dioxide 178

According to general procedure II, the reaction was performed with 4-(4-iodophenyl)thiomorpholine 1,1-dioxide **116** (440 mg, 1.30 mmol), copper iodide (12.4 mg, 65.2 µmol), $Pd(PPh_3)_4$ (75.4 mg, 65.2 µmol) and TMS acetylene (490 µL, 3.52 mmol) in triethylamine (6 mL) and THF (2 mL) at room temperature for 19 h. After purification by column chromatography (PE/EA 3:1 v/v), **178** (305 mg, 993 µmol, 76%) was obtained as an orange solid.

^{1}H-NMR (600 MHz, $CDCl_3$): δ [ppm] = 7.40 (d, $^{3}J_{H,H}$ = 9.0 Hz, 2H, H-3'), 6.81 (d, $^{3}J_{H,H}$ = 9.0 Hz, 2H, H-2'), 3.91-3.86 (m, 4H, H-3), 3.10-3.06 (m, 4H, H-2), 3.08 (s, 9H, Si(CH_3)$_3$); **^{13}C-NMR** (151 MHz, $CDCl_3$): δ [ppm] = 147.2 (C-1'), 133.8 (C-3'), 115.4 (C-2'), 115.0 (C-4'), 105.0 (C-1''), 93.3 (C-2''), 50.8 (C-2), 47.1 (C-3), 0.19 (Si(CH_3)$_3$); **ATR-IR** (neat): $\tilde{\nu}$ [cm^{-1}] = 2956, 2844, 2157, 1602, 1508, 1385, 1316, 1279, 1250, 1179, 1112, 1044, 833, 758, 722; **MS** (EI): m/z calc.: 307.11 $[M]^{+}$, found: 307.10; **R_f**: 0.58 (PE/EA 2:1 v/v).

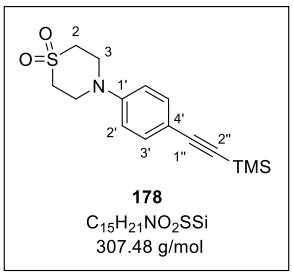

178
$C_{15}H_{21}NO_2SSi$
307.48 g/mol

4-(4-Ethynylphenyl)thiomorpholine 1,1-dioxide 185

The cleavage of the protecting group was carried out as described in general procedure III with compound **178** (285 mg, 928 µmol) and potassium carbonate (641 mg, 4.64 mmol) in methanol (8 mL) for 4 h. Alkyne **185** (169 mg, 716 µmol, 77%) was obtained as a yellow solid.

^{1}H-NMR (600 MHz, $CDCl_3$): δ [ppm] = 7.43 (d, $^{3}J_{H,H}$ = 8.8 Hz, 2H, H-3'), 6.83 (d, $^{3}J_{H,H}$ = 8.8 Hz, 2H, H-2'), 3.92-3.87 (m, 4H, H-3), 3.11-3.06 (m, 4H, H-2), 3.02 (s, 1H, H-2''); **^{13}C-NMR** (151 MHz, $CDCl_3$): δ [ppm] = 147.5 (C-1'), 133.9 (C-3'), 115.5 (C-2'), 113.8 (C-2''), 83.5 (C-1''), 76.4 (C-2''), 50.6 (C-2), 47.1 (C-3); **ATR-IR** (neat): $\tilde{\nu}$ [cm^{-1}] = 3277, 2928, 2837, 1602, 1509, 1386, 1307, 1273, 1117, 835, 818, 720, 667, 502,

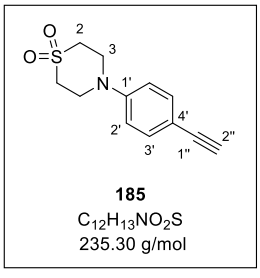

185
$C_{12}H_{13}NO_2S$
235.30 g/mol

433; **MS** (EI): m/z calc.: 235.07 $[M]^+$, found: 235.00; $\mathbf{R_f}$: 0.22 (CH_2Cl_2 + 0.5% acetone v/v).

Methyl 5-((4-(1,1-dioxidothiomorpholino)phenyl)ethynyl)-2-propionamidobenzoate 233

The reaction was carried out according to general procedure IV with anthranilic acid **90** (140 mg, 420 µmol), copper iodide (4.0 mg, 21 µmol), $Pd(PPh_3)_4$ (24 mg, 21 µmol) and alkyne **185** (148 mg, 630 µmol) in triethylamine (4 mL) and THF (3 mL) at room temperature for 16 h. The crude product was purified by column chromatography (CH_2Cl_2 + 0.5% acetone v/v) to yield **233** (121 mg, 274 µmol, 65%) as an ivory solid.

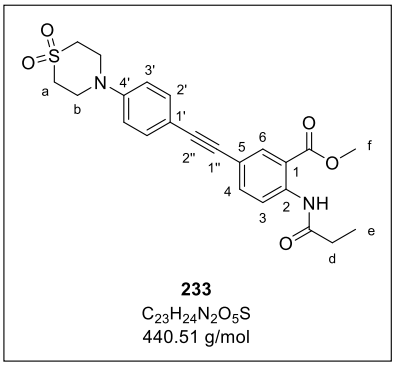

233
$C_{23}H_{24}N_2O_5S$
440.51 g/mol

^{1}H-NMR (600 MHz, $CDCl_3$): δ [ppm] = 11.12 (s, 1H, CON*H*), 8.75 (d, $^3J_{H,H}$ = 8.7 Hz, 1H, H-3), 8.19 (d, $^4J_{H,H}$ = 2.1 Hz, 1H, H-6), 7.65 (dd, $^3J_{H,H}$ = 8.7 Hz, $^4J_{H,H}$ = 2.1 Hz, 1H, H-4), 7.46 (d, $^3J_{H,H}$ = 8.9 Hz, 2H, H-2'), 6.87 (d, $^3J_{H,H}$ = 8.8 Hz, 2H, H-3'), 3.95 (s, 3H, H-f), 3.93-3.87 (m, 4H, H-b), 3.13-3.08 (m, 4H, H-a), 2.49 (q, $^3J_{H,H}$ = 7.6 Hz, 2H, H-d), 1.28 (t, $^3J_{H,H}$ = 7.6 Hz, 3H, H-e); **^{13}C-NMR** (151 MHz, $CDCl_3$): δ [ppm] = 173.1 (CON*H*), 168.4 (*C*OOMe), 147.1 (C-4'), 141.3 (C-2), 137.4 (C-4), 134.1 (C-6), 133.4 (C-2'), 120.5 (C-3), 117.7 (C-1), 115.6 (C-3'), 114.9 (C-5), 114.8 (C-1'), 89.2 (C-2''), 87.7 (C-1''), 52.6 (C-f), 51.0 (C-a), 47.2 (C-b), 31.7 (C-d), 9.68 (C-e); **ATR-IR** (neat): $\tilde{\nu}$ [cm^{-1}] = 3257, 2930, 1686, 1587, 1520, 1275, 1255, 1226, 1176, 1114, 837, 794; **HRMS** (ESI$^+$): m/z calc.: 441.1479 $[M+H]^+$, found: 441.1473; $\mathbf{R_f}$: 0.40 (CH_2Cl_2 + 0.5% acetone v/v).

5-((4-(1,1-Dioxidothiomorpholino)phenyl)ethynyl)-2-propionamidobenzoic acid 47

The reaction was performed according to general procedure V by treating methyl ester **233** (65.0 mg, 148 µmol) with aqueous 1.0 M NaOH (0.5 mL) in THF (2 mL) for 18 h. After precipitation in acidic solution, target compound **47** (50.3 mg, 118 µmol, 80%) was isolated as a colorless solid.

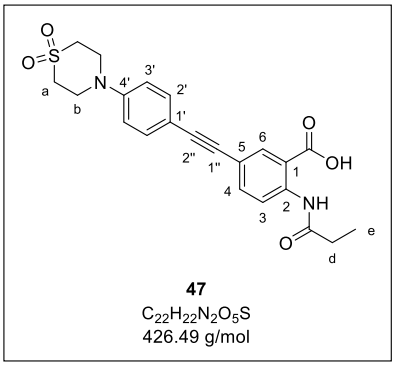

47
$C_{22}H_{22}N_2O_5S$
426.49 g/mol

^{1}H-NMR (300 MHz, DMSO-d_6): δ [ppm] = 11.27 (s, 1H, CON*H*), 8.56 (d, $^3J_{H,H}$ = 8.8 Hz, 1H, H-3), 8.05 (d, $^4J_{H,H}$ = 2.2 Hz, 1H, H-6), 7.68 (dd, $^3J_{H,H}$ = 8.8 Hz, $^4J_{H,H}$ = 2.2 Hz, 1H, H-4), 7.43 (d, $^3J_{H,H}$ = 8.8 Hz, 2H, H-2'), 7.05 (d, $^3J_{H,H}$ = 8.8 Hz, 2H, H-3'), 3.91-3.81 (m, 4H, H-b), 3.16-3.07 (m, 4H, H-a), 2.43 (q, $^3J_{H,H}$ = 7.6 Hz, 2H, H-d), 1.13 (t, $^3J_{H,H}$ = 7.6 Hz, 3H, H-e); **^{13}C-NMR** (75 MHz, DMSO-d_6): δ [ppm] = 172.1 (CON*H*), 168.9 (*C*OOH), 147.4 (C-4'), 140.5 (C-2), 136.1 (C-

4), 133.7 (C-6), 132.7 (C-2'), 120.0 (C-3), 116.8 (C-1), 116.7 (C-5), 115.1 (C-3'), 111.8 (C-1'), 89.8 (C-2''), 86.8 (C-1''), 49.9 (C-a), 46.0 (C-b), 30.7 (C-d), 9.29 (C-e); **ATR-IR** (neat): $\tilde{\nu}$ [cm^{-1}] = 3500, 2925, 1698, 1675, 1516, 1295, 1179, 1122, 1040, 825, 799, 433; **HRMS** (ESI$^+$): m/z calc.: 427.1322 $[M+H]^+$, found: 427.1328; $\mathbf{R_f}$: 0.40 (CH_2Cl_2/MeOH 9:1 v/v).

4-(4-Bromophenyl)tetrahydro-2*H*-pyran-4-ol 128

The reaction was carried out as described in the literature[171] with tetrahydro-4*H*-pyran-4-one **127** (382 mg, 3.81 mmol), 1-bromo-4-iodobenzene **119** (2.42 g, 8.55 mmol) and *n*-BuLi (2.5 M in THF, 1.60 mL, 3.82 mmol) in THF (45 mL). The crude product was purified by column chromatography to yield **128** (494 mg, 1.92 mmol, 50%) as a colorless solid.

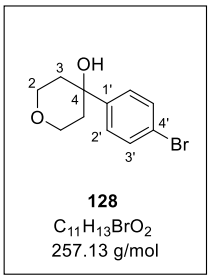

128
$C_{11}H_{13}BrO_2$
257.13 g/mol

^{1}H-NMR (400 MHz, $CDCl_3$): δ [ppm] = 7.49 (d, $^3J_{H,H}$ = 8.6 Hz, 2H, H-3'), 7.37 (d, $^3J_{H,H}$ = 8.6 Hz, 2H, H-2'), 3.98-3.80 (m, 4H, H-2), 2.20-2.06 (m, 2H, H-3), 1.71-1.61 (m, 2H, H-3); **^{13}C-NMR** (101 MHz, $CDCl_3$): δ [ppm] = 147.3 (C-1'), 131.7 (C-3'), 126.5 (C-2'), 121.4 (C-4'), 70.7 (C-4), 63.9 (C-2), 38.9 (C-3); **ATR-IR** (neat): $\tilde{\nu}$ [cm^{-1}] = 3578, 3389, 2952, 2871, 1585, 1397, 1382, 1231, 1234, 1119, 1102, 1030, 1005, 963, 822, 561, 535; **MS** (EI): m/z calc.: 256.01 $[M]^+$, found: 256.00; $\mathbf{R_f}$: 0.36 (CH_2Cl_2/acetone 9:1 v/v).

4-(4-Bromophenyl)tetrahydro-2*H*-pyran 118

The reaction was carried out as described in the literature[171] with **128** (470 mg, 1.83 mmol), triethylsilane (330 µL, 2.05 mmol), TFA (1.41 mL, 18.3 mmol) in CH_2Cl_2 (8 mL). Purification by column chromatography (CH_2Cl_2 + 0.5% acetone v/v) afforded **118** (321 mg, 1.33 mmol, 73%) as a colorless solid.

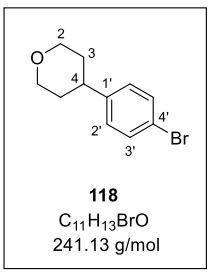

118
$C_{11}H_{13}BrO$
241.13 g/mol

The analytical data were in accordance to those described.[198]

Trimethyl((4-(tetrahydro-2*H*-pyran-4-yl)phenyl)ethynyl)silane 179

According to general procedure II, the reaction was performed with 4-(4-bromophenyl)-tetrahydro-2*H*-pyran **118** (290 mg, 1.20 mmol), copper iodide (22.9 mg, 120 µmol), $Pd(PPh_3)_4$ (139 mg, 120 µmol) and TMS acetylene (450 µL, 3.25 mmol) in triethylamine (5 mL) and THF (3 mL) at 70 °C for 20 h. After purification by column chromatography (CH_2Cl_2 + 0.5% acetone v/v), compound **179** (289 mg, 1.12 mmol, 93%) was obtained as a yellowish solid.

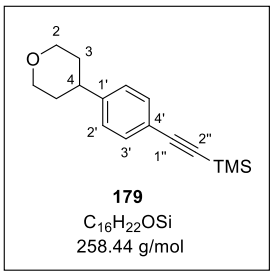

179
$C_{16}H_{22}OSi$
258.44 g/mol

^{1}H-NMR (500 MHz, $CDCl_3$): δ [ppm] = 7.41 (d, $^3J_{H,H}$ = 8.3 Hz, 2H, H-3'), 7.15 (d, $^3J_{H,H}$ = 8.3 Hz, 2H, H-2'), 4.11-4.04 (m, 2H, H-2), 3.51 (td, $^3J_{H,H}$ = 11.5 Hz, $^4J_{H,H}$ = 3.0 Hz, 2H, H-2), 2.74 (tt, $^3J_{H,H}$ = 11.5 Hz, $^4J_{H,H}$ = 4.4 Hz, 1H, H-4), 1.83-1.71 (m, 4H, H-3), 0.24 (s, 9H, Si(CH_3)$_3$); **^{13}C-NMR** (126 MHz, $CDCl_3$): δ [ppm] = 146.5 (C-1'), 132.3 (C-3'), 126.8 (C-2'), 121.2 (C-4'), 105.2 (C-1''), 93.8 (C-2''), 68.4 (C-2), 41.6 (C-4), 33.8 (C-3), 0.15 (Si(CH_3)$_3$); **ATR-IR** (neat): $\tilde{\nu}$ [cm^{-1}] = 2961, 2832, 2155, 1499, 1384, 1248, 1236, 1127, 1085, 979, 829, 760, 554; **MS** (EI): m/z calc.: 258.14 $[M]^+$, found: 258.20; **R_f**: 0.53 (CH_2Cl_2 + 0.5% acetone v/v).

4-(4-Ethynylphenyl)tetrahydro-2*H*-pyran 186

The cleavage of the protecting group was carried out as described in general procedure III by treating compound **179** (259 mg, 1.00 mmol) with potassium carbonate (693 mg, 5.01 mmol) in methanol (8 mL) for 4 h. Alkyne **186** (150 mg, 803 µmol, 80%) was obtained as a colorless solid.

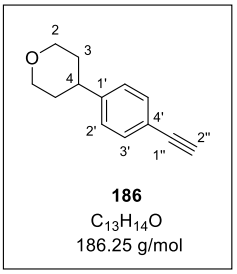

186
$C_{13}H_{14}O$
186.25 g/mol

^{1}H-NMR (500 MHz, $CDCl_3$): δ [ppm] = 7.44 (d, $^3J_{H,H}$ = 8.2 Hz, 2H, H-3'), 7.18 (d, $^3J_{H,H}$ = 8.2 Hz, 2H, H-2'), 4.12-4.04 (m, 2H, H-2), 3.52 (td, $^3J_{H,H}$ = 11.5 Hz, $^4J_{H,H}$ = 2.7 Hz, 2H, H-2), 3.05 (s, 1H, H-2''), 2.76 (tt, $^3J_{H,H}$ = 11.5 Hz, $^4J_{H,H}$ = 4.4 Hz, 1H, H-4), 1.86-1.71 (m, 4H, H-3); **^{13}C-NMR** (126 MHz, $CDCl_3$): δ [ppm] = 146.9 (C-1'), 132.5 (C-3'), 126.9 (C-2'), 120.18 (C-4'), 83.8 (C-1''), 77.6 (C-2''), 68.4 (C-2), 41.6 (C-4), 33.8 (C-3); **ATR-IR** (neat): $\tilde{\nu}$ [cm^{-1}] = 3210, 2941, 2917, 2840, 1385, 1237, 1121, 1095, 978, 894, 830, 810, 555; **MS** (EI): m/z calc.: 186.00 $[M]^+$, found: 186.10; **R_f**: 0.42 (CH_2Cl_2 + 0.5% acetone v/v).

Methyl 2-propionamido-5-((4-(tetrahydro-2*H*-pyran-4-yl)phenyl)ethynyl)benzoate 234

The reaction was performed according to general procedure IV with anthranilic acid **90** (198 mg, 594 µmol), copper iodide (11.3 mg, 59.4 µmol), $Pd(PPh_3)_4$ (68.7 mg, 59.4 µmol) and alkyne **186** (122 mg, 654 µmol) in triethylamine (4 mL) and THF (3 mL) at room temperature for 14 h. Purification by column chromatography (CH_2Cl_2/Acetone 100:1 v/v) provided **234** (191 mg, 488 µmol, 82%) as a brownish solid.

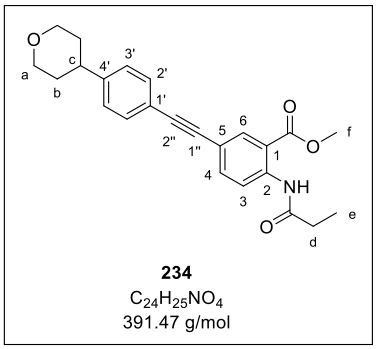

^{1}H-NMR (500 MHz, $CDCl_3$): δ [ppm] = 11.13 (s, 1H, CON*H*), 8.75 (d, $^3J_{H,H}$ = 8.8 Hz, 1H, H-3), 8.20 (d, $^4J_{H,H}$ = 2.1 Hz, 1H, H-6), 7.67 (dd, $^3J_{H,H}$ = 8.8 Hz, $^4J_{H,H}$ = 2.1 Hz, 1H, H-4), 7.47 (d, $^3J_{H,H}$ = 8.2 Hz, 2H, H-2'), 7.21 (d, $^3J_{H,H}$ = 8.2 Hz, 2H, H-3'), 4.12-4.05 (m, 2H, H-a), 3.95 (s, 3H, H-f), 3.53 (td, $^3J_{H,H}$ = 11.5 Hz, $^4J_{H,H}$ = 2.8 Hz, 2H, H-a), 2.77 (tt, $^3J_{H,H}$ = 11.5 Hz, $^4J_{H,H}$ = 4.4 Hz, 1H, H-c), 2.49 (q, $^3J_{H,H}$ = 7.6 Hz, 2H, H-d), 1.86-1.73 (m, 4H, H-b), 1.28 (t, $^3J_{H,H}$ = 7.6 Hz, 3H, H-e); **^{13}C-NMR** (126 MHz, $CDCl_3$): δ [ppm] = 173.1 (CON*H*), 168.4 (*C*OOMe), 146.4 (C-4'), 141.5 (C-2), 137.6 (C-4), 134.2 (C-6), 131.9 (C-2'), 127.0 (C-3'), 122.0 (C-1'), 120.5 (C-3), 117.6 (C-1), 114.9 (C-5), 89.4 (C-2''), 88.1 (C-1''), 68.4 (C-a), 52.6 (C-f), 41.7 (C-c), 33.9 (C-b), 31.9 (C-d), 9.67 (C-e); **ATR-IR** (neat): $\tilde{\nu}$ [cm^{-1}] = 3260, 2937, 2914, 2843, 1707, 1687, 1585, 1514, 1505, 1232, 1185, 1148, 1082, 858, 841, 832, 790; **HRMS** (ESI^+): m/z calc.: 392.1857 $[M+H]^+$, found: 392.1862; **R_f**: 0.24 (CH_2Cl_2/Acetone 100:1 v/v).

2-Propionamido-5-((4-(tetrahydro-2*H*-pyran-4-yl)phenyl)ethynyl)benzoic acid 48

The saponification was carried out according to general procedure V by treating methyl ester **234** (170 mg, 434 µmol) with aqueous 1.0 M NaOH (2 mL) in THF (5 mL) for 16 h. Precipitation in acidic solution afforded target compound **48** (119 mg, 316 µmol, 73%) as an ivory solid.

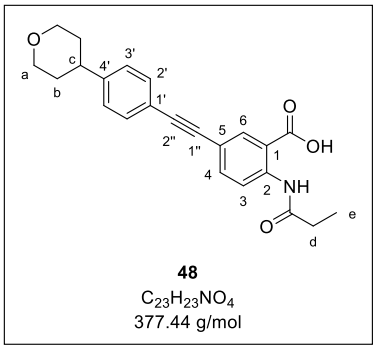

^{1}H-NMR (600 MHz, DMSO-d_6): δ [ppm] = 11.61 (s, 1H, CON*H*), 8.57 (d, $^3J_{H,H}$ = 8.7 Hz, 1H, H-3), 8.09 (d, $^4J_{H,H}$ = 2.1 Hz, 1H, H-6), 7.69 (dd, $^3J_{H,H}$ = 8.8 Hz, $^4J_{H,H}$ = 2.1 Hz, 1H, H-4), 7.49 (d, $^3J_{H,H}$ = 8.3 Hz, 2H, H-2'), 7.31 (d, $^3J_{H,H}$ = 8.3 Hz, 2H, H-3'), 3.97-3.91 (m, 2H, H-a), 3.43 (td, $^3J_{H,H}$ = 11.4 Hz, $^4J_{H,H}$ = 2.8 Hz, 2H, H-a), 2.80 (tt, $^3J_{H,H}$ = 11.4 Hz, $^4J_{H,H}$ = 4.4 Hz, 1H, H-c), 2.42 (q, $^3J_{H,H}$ = 7.6 Hz, 2H, H-d), 1.73-1.61 (m, 4H, H-b), 1.13 (t, $^3J_{H,H}$ = 7.6 Hz, 3H, H-e); **^{13}C-NMR** (151 MHz, DMSO-d_6): δ [ppm] = 172.1 (CON*H*), 168.8 (*C*OOH), 146.7 (C-4'), 140.9 (C-2), 136.0 (C-4), 134.0 (C-6), 131.4 (C-2'), 127.1 (C-3'), 120.0 (C-3), 119.8 (C-1'), 117.6 (C-1), 116.0 (C-5), 89.0 (C-2''), 88.0 (C-1''), 67.3 (C-a), 40.5 (C-c), 33.2 (C-b), 30.7 (C-d), 9.31 (C-e); **ATR-IR** (neat): $\tilde{\nu}$ [cm^{-1}] = 2937, 2839, 1708, 1647, 1577, 1516, 1498, 1290, 1213, 1127, 1084, 798, 548; **HRMS** (ESI^+): m/z calc.: 376.1554 $[M-H]^-$, found: 376.1547; **R_f**: 0.24 (CH_2Cl_2/MeOH 9:1 v/v).

6.3.5. Syntheses of hDHODH inhibitors 49-52 (cycle 1)

4-Iodo-*N*-(3,3,3-trifluoropropyl)aniline 104

The reductive amination was performed as described in general procedure VI with 4-iodoaniline **105** (1.00 g, 4.58 mmol), 3,3,3-trifluoropropanal **106** (420 µL, 5.04 mmol), glacial acetic acid (310 µL, 5.50 mmol) and STAB (1.46 mg, 6.88 mmol) in dichloromethane (10 mL). After purification by column chromatography (CH_2Cl_2/PE 1:5 v/v), **104** (573 mg, 1.82 mmol, 40%) was obtained as a yellowish oil.

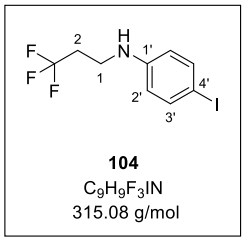

104
$C_9H_9F_3IN$
315.08 g/mol

^{1}H-NMR (500 MHz, $CDCl_3$): δ [ppm] = 7.45 (d, $^3J_{H\text{-}H}$ = 8.7 Hz, 2H, H-3'), 6.40 (d, $^3J_{H\text{-}H}$ = 8.7 Hz, 2H, H-2'), 3.42 (t, $^3J_{H\text{-}H}$ = 6.8 Hz, 2H, H-1), 2.40 (qt, $^3J_{H\text{-}F}$ = 10.7, $^3J_{H\text{-}H}$ = 6.8 Hz, 2H, H-2); **^{13}C-NMR** (126 MHz, $CDCl_3$): δ [ppm] = 146.7 (C-1'), 138.0 (C-3'), 127.6 (*C*F_3) 115.2 (C-2'), 79.0 (C-4'), 37.1 (C-1), 33.5 (C-2); **^{19}F-NMR** (565 MHz, $CDCl_3$): δ [ppm] = −65.0 (*C*F_3); **ATR-IR** (neat): $\tilde{\nu}$ [cm^{-1}] = 3378, 2866, 1877, 1589, 1478, 1439, 1406, 1313, 1241, 1136, 1080, 997, 865, 810, 665, 559, 504; **HRMS** (ESI^+): m/z calc.: 315.9805 $[M+H]^+$, found: 315.9803; $\mathbf{R_f}$: 0.29 (CH_2Cl_2/PE 1:5 v/v).

N-(3,3,3-Trifluoropropyl)-4-((trimethylsilyl)ethynyl)aniline 165

According to general procedure II, the reaction was carried out with 4-iodo-*N*-(3,3,3-trifluoropropyl)aniline **104** (542 mg, 1.72 mmol), copper iodide (32.8 mg, 172 µmol), $Pd(PPh_3)_4$ (199 mg, 172 µmol) and TMS acetylene (640 µL, 4.65 mmol) in triethylamine (8 mL) and THF (3 mL) at room temperature for 24 h. Purification by column chromatography (CH_2Cl_2/PE 1:3 v/v) afforded **165** (299 mg, 1.05 mmol, 61%) as a brown oil.

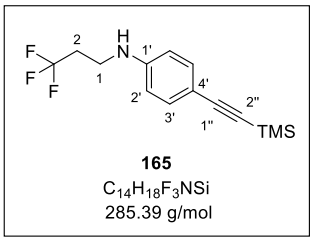

165
$C_{14}H_{18}F_3NSi$
285.39 g/mol

^{1}H-NMR (600 MHz, $CDCl_3$): δ [ppm] = 7.31 (d, $^3J_{H\text{-}H}$ = 8.5 Hz, 2H, H-3'), 6.5 ($^3J_{H\text{-}H}$ = 8.5 Hz, 2H, H-2'), 3.93 (s, 1H, N*H*), 3.45 (q, $^3J_{H\text{-}H}$ = 6.6 Hz, 2H, H-1), 2.40 (qt, $^3J_{H\text{-}F}$ = 10.7, $^3J_{H\text{-}H}$ = 6.9 Hz, 2H, H-2), 0.23 (s, 9H, Si(C*H*$_3$)$_3$); **^{13}C-NMR** (151 MHz, $CDCl_3$): δ [ppm] = 147.2 (C-1'), 133.7 (C-3'), 126.5 (*C*F_3), 112.4 (C-2'), 112.3 (C-4'), 106.0 (C-1''), 91.7 (C-2''), 36.9 (C-1), 33.4 (C-2), 0.28 (Si(*C*H$_3$)$_3$); **^{19}F-NMR** (565 MHz, $CDCl_3$): δ [ppm] = −65.0 (*C*F_3); **ATR-IR** (neat): $\tilde{\nu}$ [cm^{-1}] = 3430, 3029, 2958, 2147, 1608, 1517, 1475, 1387, 1326, 1246, 1144, 1088, 1022, 980, 822, 758, 700, 648, 547, 536, 466; **HRMS** (ESI^+): m/z calc.: 286.1234 $[M+H]^+$, found: 286.1299; $\mathbf{R_f}$: 0.44 (CH_2Cl_2/PE 1:5 v/v).

4-Ethynyl-*N*-(3,3,3-trifluoropropyl)aniline 171

The reaction was carried out as described in general procedure III with **165** (279 mg, 977 µmol) and potassium carbonate (675 mg, 4.89 mmol) in methanol (8 mL) for 4 h. Alkyne **171** (166 mg, 778 µmol, 80%) was isolated as a yellowish oil.

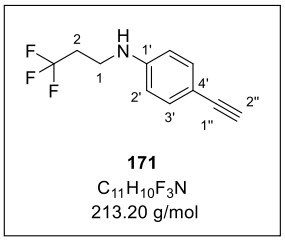

171
$C_{11}H_{10}F_3N$
213.20 g/mol

^{1}H-NMR (500 MHz, $CDCl_3$): δ [ppm] = 7.34 (d, $^3J_{H\text{-}H}$ = 8.6 Hz, 2H, H–3'), 6.53 (d, $^3J_{H\text{-}H}$ = 8.6 Hz, 2H, H–2'), 3.95 (s, 1H, N*H*), 3.46 (q, $^3J_{H\text{-}H}$ = 6.7 Hz, 2H, H–1), 2.97 (s, 1H, H–2''), 2.41 (qt, $^3J_{H\text{-}F}$ = 10.7 Hz, $^3J_{H\text{-}H}$ = 6.9 Hz, 2H, H–2); **^{13}C-NMR** (126 MHz, $CDCl_3$): δ [ppm] = 147.4 (C–1'), 133.8 (C–3'), 125.4 (*C*F_3), 112.6 (C–2'), 111.2 (C–4'), 84.5 (C-1''), 74.6 (C–2''), 36.8 (C–1), 33.7 (C–2); **^{19}F-NMR** (565 MHz, $CDCl_3$): δ [ppm] = −65.0 (*C*F_3); **ATR-IR** (neat): $\tilde{\nu}$ [cm^{-1}] = 3290, 3033, 2953, 2101, 1608, 1517, 1482, 1393, 1327, 1298, 1244, 1140, 1081, 998, 822, 659, 593, 532; **MS** (EI): m/z calc.: 213.08 $[M]^+$, found: 213.10; **R_f**: 0.40 (CH_2Cl_2/PE 1:5 v/v).

Methyl 2-propionamido-5-((4-((3,3,3-trifluoropropyl)amino)phenyl)ethynyl)benzoate 226

The reaction was carried out according to general procedure IV with anthranilic acid **90** (157 mg, 471 µmol), copper iodide (9.0 mg, 47 µmol), $Pd(PPh_3)_4$ (54.5mg, 47.1 µmol) and alkyne **171** (111 mg, 518 µmol) in triethylamine (4 mL) and THF (3 mL) at room temperature for 24 h. The crude product was purified by column chromatography (CH_2Cl_2/acetone 100:1 v/v) to yield **226** (183 mg, 438 µmol, 93%) as an orange solid.

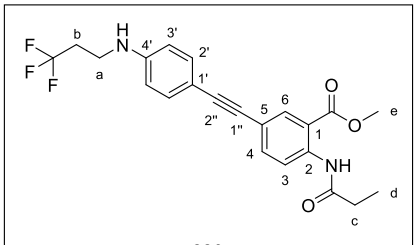

226
$C_{22}H_{21}F_3N_2O_3$
418.42 g/mol

^{1}H-NMR (500 MHz, $CDCl_3$): δ [ppm] = 11.11 (s, 1H, CON*H*), 8.73 (d, $^3J_{H\text{-}H}$ = 8.8 Hz, 1H, H-3), 8.17 (d, $^4J_{H\text{-}H}$ = 2.1 Hz, 1H, H-6), 7.64 (dd, $^3J_{H\text{-}H}$ = 8.8 Hz, $^4J_{H\text{-}H}$ = 2.1 Hz, 1H, H-4), 7.37 (d, $^3J_{H\text{-}H}$ = 8.6 Hz, 2H, H-2'), 6.56 (d, $^3J_{H\text{-}H}$ = 8.6 Hz, 2H, H-3'), 4.01 (s, 1H, N*H*), 3.94 (s, 3H, H-e), 3.47 (t, $^3J_{H\text{-}H}$ = 7.2 Hz, 2H, H-a), 2.49 (q, $^3J_{H\text{-}H}$ = 7.6 Hz, 2H, H-c), 2.42 (qt, $^3J_{H\text{-}F}$ = 10.7 Hz, $^3J_{H\text{-}H}$ = 6.9 Hz, 2H, H–b), 1.28 (t, $^3J_{H\text{-}H}$ = 7.6 Hz, 3H, H-d); **^{13}C-NMR** (126 MHz, $CDCl_3$): δ [ppm] = 173.0 (*C*ONH), 168.5 (*C*OOMe), 147.0 (C-4'), 141.0 (C-2), 137.3 (C-4), 133.9 (C-6), 133.2 (C-2'), 125.6 (*C*F_3), 120.4 (C-3), 118.1 (C-1), 114.9 (C-5), 112.6 (C-3'). 112.1 (C-1'), 89.9 (C-2''), 86.2 (C-1''), 52.6 (C-e), 36.9 (C-a), 33.4 (C-b), 31.9 (C-c), 9.68 (C-d); **^{19}F-NMR** (565 MHz, $CDCl_3$): δ [ppm] = −65.0 (*C*F_3); **ATR-IR** (neat): $\tilde{\nu}$ [cm^{-1}] = 3373, 3260, 2921, 2198, 1683, 1590, 1510, 1437, 1291, 1143, 1088, 839, 824, 790, 735, 693, 526, 481; **HRMS** (ESI^+): m/z calc.: 419.1577 $[M+H]^+$, found: 419.1634; **R_f**: 0.55 (CH_2Cl_2/acetone 100:1 v/v).

2-Propionamido-5-((4-((3,3,3-trifluoropropyl)amino)phenyl)ethynyl)benzoic acid 49

The saponification was performed as described in general procedure V by treating methyl ester **226** (155 mg, 370 µmol) with aqueous 1.0 M NaOH (1.5 mL) in THF (5 mL) for 24 h. Precipitation in acidic solution afforded target compound **49** (105 mg, 259 µmol, 70%) as a colorless solid.

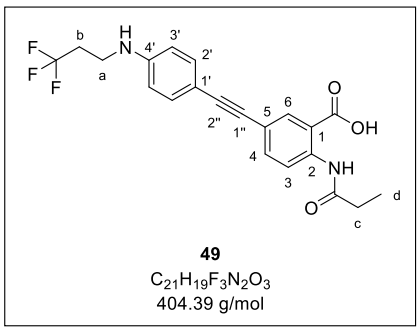

^{1}H-NMR (600 MHz, DMSO-*d*6): *δ* [ppm] = 11.20 (s, 1H, CON*H*), 8.54 (d, $^3J_{H\text{-}H}$ = 8.7 Hz, 1H, H–3), 8.01 (d, $^3J_{H\text{-}H}$ = 2.2 Hz, 1H, H–6), 7.65 (dd, $^3J_{H\text{-}H}$ = 8.7 Hz, $^4J_{H\text{-}H}$ = 2.2 Hz, 1H, H–4), 7.30 (d, $^3J_{H\text{-}H}$ = 8.7 Hz, 2H, H–2‘), 6.60 (d, $^3J_{H\text{-}H}$ = 8.7 Hz, 2H, H–3‘), 3.32 (t, $^3J_{H\text{-}H}$ = 7.0 Hz, 2H, H–a), 2.53 (qt, $^3J_{H\text{-}F}$ = 11.5 Hz, $^3J_{H\text{-}H}$ = 7.0 Hz, 2H, H–b), 2.42 (q, $^3J_{H\text{-}H}$ = 7.6 Hz, 1H, H–c), 1.13 (t, $^3J_{H\text{-}H}$ = 7.5 Hz, 2H, H–d); **^{13}C-NMR** (151 MHz, DMSO-*d*6): *δ* [ppm] = 172.1 (*C*ONH), 168.9 (*C*OOH), 148.5 (C–4‘), 140.3 (C–2), 136.0 (C–4), 133.4 (C–6), 132.7 (C–2‘), 127.9 (*C*F_3), 120.0 (C–3), 117.2 (C–1), 116.5 (C–5), 111.9 (C–3‘), 108.7 (C–1‘), 90.8 (C–2‘‘), 85.8 (C–1‘‘), 35.8 (C–a), 32.3 (C–b), 30.7 (C–c), 9.3 (C–d); **^{19}F-NMR** (565 MHz, DMSO-*d*6): *δ* [ppm] = −63.6 (*C*F_3); **ATR-IR** (neat): $\tilde{\nu}$ [cm^{-1}] = 3333, 2981, 2203, 1686, 1657, 1580, 1414, 1395, 1291, 1246, 1187, 1087, 1004, 896, 831, 794, 694, 677, 561, 487; **HRMS** (ESI$^+$): m/z calc.: 405.1421 [M+H]$^+$, found: 405.1529; **R_f**: 0.38 (CH_2Cl_2/MeOH 9:1).

1-(4-Bromophenyl)-4,4-difluoropiperidine 117

The reaction was carried out as described in general procedure I with 1-bromo-4-iodobenzene **119** (1.30 g, 4.60 mmol), copper iodide (175 mg, 920 µmol), L-proline (212 mg, 1.84 mmol), potassium carbonate (1.27 g, 9.20 mmol) and 4,4-difluoropiperidine **125** (836 mg, 6.90 mmol) in DMSO (10 mL) at room temperature for 24 h. The crude product was purified by column chromatography (CH_2Cl_2/PE 2:3 v/v) to yield arylamine **117** (442 mg, 1.60 mmol, 35%) as a colorless solid.

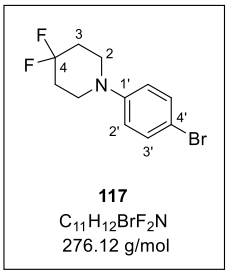

^{1}H-NMR (600 MHz, $CDCl_3$): δ [ppm] = 7.35 (d, $^3J_{H,H}$ = 9.0 Hz, 2H, H-3’), 6.81 (d, $^3J_{H,H}$ = 9.0 Hz, 2H, H-2’), 3.34-3.29 (m, 4H, H-2), 2.13-2.04 (m, 4H, H-3); **^{13}C-NMR** (151 MHz, $CDCl_3$): δ [ppm] = 149.3 (C-1’), 133.2 (C-3’), 121.9 (C-4), 118.6 (C-2’), 112.5 (C-4’), 46.8 (C-2), 33.6 (C-3); **^{19}F-NMR** (565 MHz, $CDCl_3$): δ [ppm] = −97.8 (C*F*$_2$); **ATR-IR** (neat): $\tilde{\nu}$ [cm^{-1}] = 2837, 1585, 1487, 1364, 1221, 1108, 981, 955, 906, 821, 664, 530; **HRMS** (ESI$^+$): m/z calc.: 276.0194 [M+H]$^+$, found: 276.0237; **R_f**: 0.67 (CH_2Cl_2/PE 2:3 v/v).

4,4-Difluoro-1-(4-((trimethylsilyl)ethynyl)phenyl)piperidine 180

According to general procedure II, the reaction was carried out with 1-(4-bromophenyl)-4,4-difluoropiperidine **117** (374 mg, 1.36 mmol), copper iodide (25.8 mg, 136 µmol), $Pd(PPh_3)_4$ (157 mg, 136 µmol) and TMS acetylene (510 µL, 3.66 mmol) in triethylamine (6 mL) and THF (3 mL) at 70 °C for 20 h. Purification by column chromatography (CH_2Cl_2/PE 1:1 v/v) provided **180** (307 mg, 1.05 mmol, 77%) as an ivory solid.

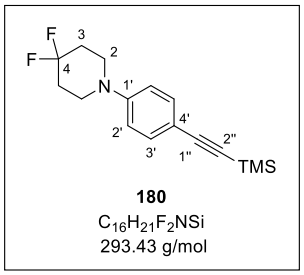

180
$C_{16}H_{21}F_2NSi$
293.43 g/mol

^{1}H-NMR (600 MHz, $CDCl_3$): δ [ppm] = 7.37 (d, $^3J_{H,H}$ = 8.8 Hz, 2H, H-3'), 6.82 (d, $^3J_{H,H}$ = 8.8 Hz, 2H, H-2'), 3.42-3.37 (m, 4H, H-2), 2.12-2.01 (m, 4H, H-3), 0.25 (s, 9H, Si(CH_3)$_3$); **^{13}C-NMR** (151 MHz, $CDCl_3$): δ [ppm] = 149.8 (C-1'), 133.4 (C-3'), 121.9 (C-4), 115.7 (C-2'), 113.8 (C-4'), 105.6 (C-1''), 92.5 (C-2''), 46.0 (C-2), 33.5 (C-3), 0.25 (Si(CH_3)$_3$); **^{19}F-NMR** (565 MHz, $CDCl_3$): δ [ppm] = −97.5 (CF_2); **ATR-IR** (neat): $\tilde{\nu}$ [cm^{-1}] = 2961, 2849, 2151, 1606, 1511, 1366, 1242, 1116, 965, 836, 815, 762, 702; **HRMS** (ESI$^+$): m/z calc.: 294.1484 $[M+H]^+$, found: 294.1557; **R_f**: 0.38 (CH_2Cl_2/PE 1:1 v/v).

1-(4-Ethynylphenyl)-4,4-difluoropiperidine 187

The reaction was performed as described in general procedure III by treating compound **180** (280 mg, 1.02 mmol) with potassium carbonate (703 mg, 5.08 mmol) in methanol (8 mL) for 4 h. Alkyne **187** (150 mg, 737 µmol, 73%) was isolated as an ivory solid.

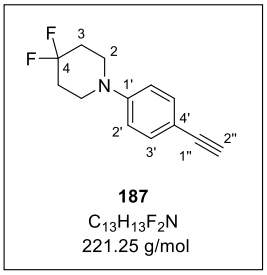

187
$C_{13}H_{13}F_2N$
221.25 g/mol

^{1}H-NMR (600 MHz, $CDCl_3$): δ [ppm] = 7.39 (d, $^3J_{H,H}$ = 8.8 Hz, 2H, H-3'), 6.85 (d, $^3J_{H,H}$ = 8.8 Hz, 2H, H-2'), 3.43-3.38 (m, 4H, H-2), 2.99 (s, 1H, H-2''), 2.12-2.03 (m, 4H, H-3); **^{13}C-NMR** (151 MHz, $CDCl_3$): δ [ppm] = 150.1 (C-1'), 133.5 (C-3'), 121.9 (C-4), 115.8 (C-2'), 112.7 (C-4'), 84.1 (C-1''), 75.8 (C-2''), 47.0 (C-2), 33.5 (C-3); **^{19}F-NMR** (565 MHz, $CDCl_3$): δ [ppm] = −97.5 (CF_2); **ATR-IR** (neat): $\tilde{\nu}$ [cm^{-1}] = 3290, 2838, 1603, 1510, 1366, 1237, 1106, 980, 955, 904, 820, 670; **HRMS** (ESI$^+$): m/z calc.: 222.1089 $[M+H]^+$, found: 222.1124; **R_f**: 0.34 (CH_2Cl_2/PE 1:1 v/v).

Methyl 5-((4-(4,4-difluoropiperidin-1-yl)phenyl)ethynyl)-2-propionamidobenzoate 235

The reaction was carried out as described in general procedure IV with anthranilic acid **90** (150 mg, 451 µmol), copper iodide (8.6 mg, 45 µmol), $Pd(PPh_3)_4$ (52.1 mg, 45.1 µmol) and alkyne **187** (110 mg, 496 µmol) in triethylamine (4 mL) and THF (3 mL) at room temperature for 6 h. After purification by column chromatography (CH_2Cl_2 + 0.5% acetone v/v), **235** (159 mg, 372 µmol, 82%) was obtained as a yellow solid.

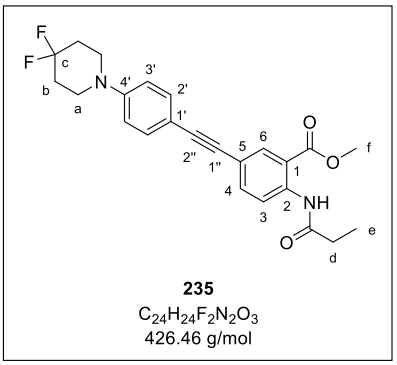

235
$C_{24}H_{24}F_2N_2O_3$
426.46 g/mol

^{1}H-NMR (600 MHz, $CDCl_3$): δ [ppm] = 11.11 (s, 1H, CON*H*), 8.74 (d, $^{3}J_{H,H}$ = 8.8 Hz, 1H, H-3), 8.18 (d, $^{4}J_{H,H}$ = 2.1 Hz, 1H, H-6), 7.65 (dd, $^{3}J_{H,H}$ = 8.8 Hz, $^{4}J_{H,H}$ = 2.1 Hz, 1H, H-4), 7.42 (d, $^{3}J_{H,H}$ = 8.9 Hz, 2H, H-2'), 6.88 (d, $^{3}J_{H,H}$ = 8.9 Hz, 2H, H-3'), 3.94 (s, 3H, H-f), 3.45-3.40 (m, 4H, H-a), 2.49 (q, $^{3}J_{H,H}$ = 7.6 Hz, 2H, H-d), 2.08 (m, 4H, H-b), 1.28 (t, $^{3}J_{H,H}$ = 7.6 Hz, 3H, H-e); **^{13}C-NMR** (151 MHz, $CDCl_3$): δ [ppm] = 173.0 (CON*H*), 168.4 (*C*OOMe), 149.8 (C-4'), 141.2 (C-2), 137.4 (C-4), 134.0 (C-6), 133.0 (C-2'), 121.9 (C-c), 120.4 (C-3), 117.9 (C-1), 115.9 (C-3'), 114.9 (C-5), 113.7 (C-1'), 89.8 (C-2''), 87.1 (C-1''), 52.6 (C-f), 46.0 (C-a), 33.5 (C-b), 31.9 (C-d), 9.68 (C-e); **^{19}F-NMR** (565 MHz, $CDCl_3$): δ [ppm] = −97.5 (CF_2); **ATR-IR** (neat): $\tilde{\nu}$ [cm^{-1}] = 3256, 2938, 2843, 2201, 1686, 1586, 1516, 1439, 1289, 1233, 1106, 1086, 956, 905, 792; **HRMS** (ESI$^+$): m/z calc.: 427.1828 [M+H]$^+$, found: 427.1903; **R_f**: 0.51 (CH_2Cl_2/Acetone 100:1 v/v).

5-((4-(4,4-Difluoropiperidin-1-yl)phenyl)ethynyl)-2-propionamidobenzoic acid 50

The saponification was carried out according to general procedure V with methyl ester **235** (140 mg, 328 µmol) and aqueous 1.0 M NaOH (1.5 mL) in THF (5 mL) for 18 h. Precipitation in acidic solution afforded target compound **50** (119 mg, 289 µmol, 88%) as an ivory solid.

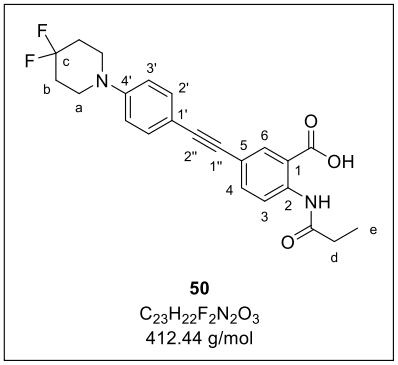

50
$C_{23}H_{22}F_2N_2O_3$
412.44 g/mol

^{1}H-NMR (600 MHz, DMSO-d_6): δ [ppm] = 11.20 (s, 1H, CON*H*), 8.55 (d, $^{3}J_{H,H}$ = 8.7 Hz, 1H, H-3), 8.04 (d, $^{4}J_{H,H}$ = 2.2 Hz, 1H, H-6), 7.68 (dd, $^{3}J_{H,H}$ = 8.7 Hz, $^{4}J_{H,H}$ = 2.2 Hz, 1H, H-4), 7.40 (d, $^{3}J_{H,H}$ = 8.8 Hz, 2H, H-2'), 7.02 (d, $^{3}J_{H,H}$ = 8.9 Hz, 2H, H-3'), 3.45-3.40 (m 4H, H-a), 2.43 (q, $^{3}J_{H,H}$ = 7.5 Hz, 2H, H-d), 2.07-1.98 (m, 4H, H-b), 1.13 (t, $^{3}J_{H,H}$ = 7.5 Hz, 3H, H-e); **^{13}C-NMR** (151 MHz, DMSO-d_6): δ [ppm] = 172.1 (CON*H*), 168.9 (*C*OOH), 149.4 (C-4'), 140.5 (C-2), 136.2 (C-4), 133.6 (C-6), 132.5 (C-2'), 122.8 (C-c), 120.0 (C-3), 116.8 (C-1), 116.6 (C-5), 115.3 (C-3'), 111.4 (C-1'), 90.0 (C-2''), 86.7 (C-1''), 44.7 (H-a), 32.7 (H-b), 30.7 (C-d), 9.29 (C-e); **^{19}F-NMR** (565 MHz, DMSO-d_6): δ [ppm] = −95.1 (CF_2); **ATR-IR** (neat): $\tilde{\nu}$ [cm^{-1}] = 3316, 2846, 1658, 1584, 1517, 1290, 1241, 1188, 1111, 902, 827; **HRMS** (ESI$^+$): m/z calc.: 411.1525 [M-H]$^-$, found: 411.1510; **R_f**: 0.32 (CH_2Cl_2/MeOH 9:1 v/v).

5-Bromo-1-propyl-1*H*-indole 107

To a solution of 5-bromo-1*H*-indole **109** (2.00 g, 10.2 mmol, 1.00 eq.) in DMF (30 mL), 1-bromopropane (930 µL, 10.2 mmol, 1.00 eq.) and caesium carbonate (6.65 g, 20.4 mmol, 2.00 eq.) were added and the resulting mixture was stirred for 2 h at 100 °C. The separated

solid was removed by filtration and ice-cold water was added to the filtrate. After extraction of the aqueous phase with petroleum ether (three times), the combined organic layers were dried over Na_2SO_4 and the solvent was removed under reduced pressure. The crude product was purified by column chromatography (PE/ CH_2Cl_2 19:1 v/v) to give **107** (1.63 g, 6.83 mmol, 67%) as a colorless oil.

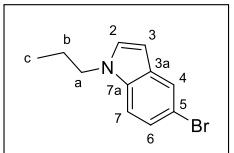

107
$C_{11}H_{12}BrN$
238.13 g/mol

^{1}H-NMR (600 MHz, $CDCl_3$): δ [ppm] = 7.75 (d, $^4J_{H\text{-}H}$ = 1.9 Hz, 1H, H-4), 7.27 (dd, $^3J_{H\text{-}H}$ = 8.7 Hz, $^4J_{H\text{-}H}$ = 1.9 Hz, 1H, H-6), 7.21 (d, $^3J_{H\text{-}H}$ = 8.7 Hz, 1H, H-7), 7.10 (d, $^3J_{H\text{-}H}$ = 3.1 Hz, 1H, H-2), 6.42 (d, $^3J_{H\text{-}H}$ = 3.1 Hz, 1H, H-3), 4.06 (t, $^3J_{H\text{-}H}$ = 7.3 Hz, 2H, H-a), 1.85 (sext, $^3J_{H\text{-}H}$ = 7.3 Hz, 2H, H-b), 0.92 (t, $^3J_{H\text{-}H}$ = 7.3 Hz, 3H, H-c); **^{13}C-NMR** (151 MHz, $CDCl_3$): δ [ppm] = 134.8 (C-7a), 130.4 (C-3a), 129.1 (C-2), 124.3 (C-6), 123.5 (C-4), 112.6 (C-5), 111.0 (C-7), 100.6 (C-3), 48.4 (C-a), 23.7 (C-b), 11.6 (C-c); **ATR-IR** (neat): $\tilde{\nu}$ [cm^{-1}] = 2963, 2931, 2874, 1466, 1446, 1396, 1327, 1274, 1206, 896, 866, 790, 751, 714, 582, 421; **R_f**: 0.53 (PE/CH_2Cl_2 19:1 v/v).

1-Propyl-5-((trimethylsilyl)ethynyl)-1*H*-indole 166

The reaction was carried out as described in general procedure II with 5-bromo-1-propyl-1*H*-indole **107** (600 mg, 2.52 mmol), copper iodide (48.0 mg, 252 µmol), $Pd(PPh_3)_4$ (291 mg, 252 µmol) and TMS acetylene (940 µL, 6.80 mmol) in triethylamine (10 mL) and THF (4 mL) at 70 °C for 24 h. After purification by column chromatography (PE/ CH_2Cl_2 19:1 v/v), **166** (390 mg, 1.53 mmol, 61%) was obtained as a yellow wax.

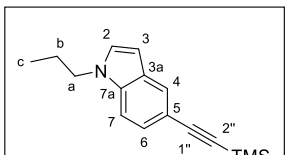

166
$C_{16}H_{21}NSi$
255.44 g/mol

^{1}H-NMR (400 MHz, $CDCl_3$): δ [ppm] = 7.82-7.77 (m, 1H, H-4), 7.31 (dd, $^3J_{H\text{-}H}$ = 8.7 Hz, $^4J_{H\text{-}H}$ = 1.6 Hz, 1H, H-6), 7.25 (d, $^3J_{H\text{-}H}$ = 8.7 Hz, 1H, H-7), 7.10 (d, $^3J_{H\text{-}H}$ = 3.1 Hz, 1H, H-2), 6.45 (d, $^3J_{H\text{-}H}$ = 3.1 Hz, 1H, H-3), 4.06 (t, $^3J_{H\text{-}H}$ = 7.3 Hz, 2H, H-a), 1.85 (sext, $^3J_{H\text{-}H}$ = 7.3 Hz, 2H, H-b), 0.92 (t, $^3J_{H\text{-}H}$ = 7.3 Hz, 3H, H-c), 0.27 (s, 9H, Si(CH_3)$_3$); **^{13}C-NMR** (101 MHz, $CDCl_3$): δ [ppm] = 135.9 (C-7a), 128.9 (C-2), 128.4 (C-3a), 125.5 (C-6), 125.4 (C-4), 113.6 (C-5), 109.4 (C-7), 107.3 (C-1''), 101.4 (C-3), 91.0 (C-2''), 48.3 (C-a), 23.7 (C-b), 11.6 (C-c), 0.34 (Si(CH_3)$_3$); **ATR-IR** (neat): $\tilde{\nu}$ [cm^{-1}] = 2959, 2148, 1479, 1392, 1330, 1248, 1204, 836, 805, 758, 735; **HRMS** (ESI$^+$): m/z calc.: 256.1516 $[M+H]^+$, found: 256.1519; **R_f**: 0.23 (PE/CH_2Cl_2 19:1 v/v).

5-Ethynyl-1-propyl-1*H*-indole 172

The cleavage of the protecting group was performed according to general procedure III by treating **166** (370 mg, 1.45 mmol) with potassium carbonate (1.00 g, 7.24 mmol) in methanol (12 mL) for 4 h. Alkyne **172** (201 mg, 1.10 mmol, 76%) was isolated as a yellow oil.

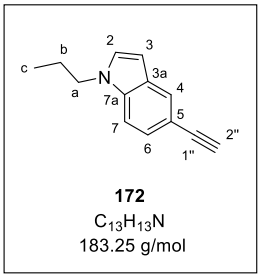

^{1}H-NMR (400 MHz, $CDCl_3$): δ [ppm] = 7.84-7.79 (m, 1H, H-4), 7.33 (dd, $^3J_{H\text{-}H}$ = 8.6 Hz, $^4J_{H\text{-}H}$ = 1.6 Hz, 1H, H-6), 7.28 (d, $^3J_{H\text{-}H}$ = 8.6 Hz, 1H, H-7), 7.12 (d, $^3J_{H\text{-}H}$ = 3.2 Hz, 1H, H-2), 6.47 (d, $^3J_{H\text{-}H}$ = 3.2 Hz, 1H, H-3), 4.07 (t, $^3J_{H\text{-}H}$ = 7.3 Hz, 2H, H-a), 3.00 (s, 1H, H-2''), 1.86 (sext, $^3J_{H\text{-}H}$ = 7.3 Hz, 2H, H-b), 0.92 (t, $^3J_{H\text{-}H}$ = 7.3 Hz, 3H, H-c); **^{13}C-NMR** (101 MHz, $CDCl_3$): δ [ppm] = 135.6 (C-7a), 129.1 (C-2), 128.4 (C-3a), 125.7 (C-6), 125.4 (C-4), 112.5 (C-5), 109.6 (C-7), 101.4 (C-3), 84.9 (C-1''), 74.6 (C-2''), 48.3 (C-a), 23.7 (C-b), 11.6 (C-c); **ATR-IR** (neat): $\tilde{\nu}$ [cm^{-1}] = 3285, 2964, 2932, 2875, 2101, 1479, 1330, 1205, 883, 800, 761, 719, 649, 586, 416; **HRMS** (ESI$^+$): m/z calc.: 184.1121 $[M+H]^+$, found: 184.1108; **R_f**: 0.19 (PE/CH_2Cl_2 19:1 v/v).

Methyl 2-propionamido-5-((1-propyl-1*H*-indol-5-yl)ethynyl)benzoate 227

The reaction was carried out as described in general procedure IV with anthranilic acid **90** (200 mg, 600 µmol), copper iodide (11.4 mg, 60.0 µmol), $Pd(PPh_3)_4$ (69.4mg, 60.0 µmol) and alkyne **172** (121 mg, 660 µmol) in triethylamine (4 mL) and THF (3 mL) at room temperature for 16 h. Purification by column chromatography (CH_2Cl_2/acetone 100:1 v/v) provided **227** (183 mg, 471 µmol, 79%) as a yellow solid.

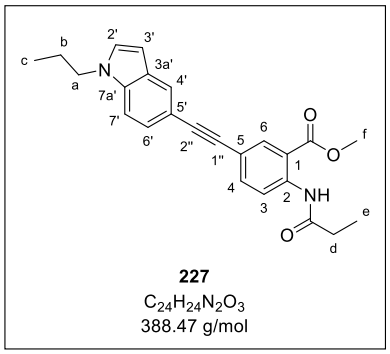

^{1}H-NMR (400 MHz, $CDCl_3$): δ [ppm] = 11.12 (s, 1H, CON*H*), 8.75 (d, $^3J_{H\text{-}H}$ = 8.8 Hz, 1H, H-3), 8.22 (d, $^4J_{H\text{-}H}$ = 2.1 Hz, 1H, H-6), 7.85-7.81 (m, 1H, H-4'), 7.69 (dd, $^3J_{H\text{-}H}$ = 8.8 Hz, $^4J_{H\text{-}H}$ = 2.1 Hz, 1H, H-4), 7.36 (dd, $^3J_{H\text{-}H}$ = 8.5 Hz, $^4J_{H\text{-}H}$ = 1.6 Hz, 1H, H-6'), 7.30 (d, $^3J_{H\text{-}H}$ = 8.5 Hz, 1H, H-7'), 7.13 (d, $^3J_{H\text{-}H}$ = 3.2 Hz, 1H, H-2'), 6.49 (d, $^3J_{H\text{-}H}$ = 3.2 Hz, 1H, H-3'), 4.08 (t, $^3J_{H\text{-}H}$ = 7.3 Hz, 2H, H-a), 3.95 (s, 3H, H-f), 2.50 (q, $^3J_{H\text{-}H}$ = 7.6 Hz, 2H, H-d), 1.88 (sext, $^3J_{H\text{-}H}$ = 7.3 Hz, 2H, H-b), 1.29 (t, $^3J_{H\text{-}H}$ = 7.6 Hz, 3H, H-e), 0.94 (t, $^3J_{H\text{-}H}$ = 7.3 Hz, 3H, H-c); **^{13}C-NMR** (101 MHz, $CDCl_3$): δ [ppm] = 173.0 (*C*ONH), 168.5 (*C*OOMe), 141.0 (C-2), 137.4 (C-4), 135.9 (C-7a'), 134.0 (C-6), 129.0 (C-2'), 128.6 (C-3a), 125.1 (C-6'), 125.0 (C-4'), 120.4 (C-3), 118.4 (C-1), 114.9 (C-5), 113.5 (C-5'), 109.7 (C-7'), 101.4 (C-3'), 91.4 (C-2''), 86.0 (C-1''), 52.6 (C-f), 48.3 (C-a), 31.9 (C-d), 23.7 (C-b), 11.6 (C-c), 9.70 (C-e); **ATR-IR** (neat): $\tilde{\nu}$ [cm^{-1}] = 3252, 2971, 2931, 1706, 1682, 1586, 1508, 1433, 1289, 1246, 1232, 1081, 787, 724; **HRMS** (ESI$^+$): m/z calc.: 389.1854 $[M+H]^+$, found: 389.1836; **R_f**: 0.28 (CH_2Cl_2/acetone 100:1 v/v).

2-Propionamido-5-((1-propyl-1*H*-indol-5-yl)ethynyl)benzoic acid 51

The saponification was carried out according to general procedure V with methyl ester **227** (155 mg, 370 µmol) and aqueous 1.0 M NaOH (1.5 mL) in THF (5 mL) for 16 h. Contrary to general procedure V, precipitation in acidic solution did not work and the crude product was isolated by extraction of the acidic phase with dichloromethane (three times). After dehydration of the combined organic layers over Na_2SO_4 and removal of the solvent under reduced pressure, the product was dissolved in CH_2Cl_2 and covered by a layer of petroleum ether for crystallization. **51** (86.8 mg, 232 µmol, 56%) was obtained as a an ivory solid.

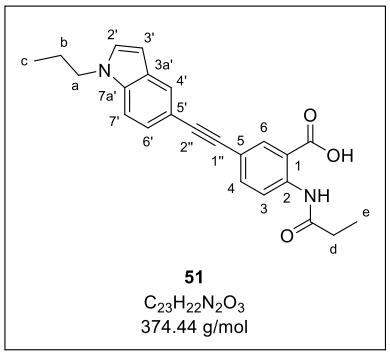

^{1}H-NMR (500 MHz, DMSO-*d*6): δ [ppm] = 13.90 (s, 1H, COO*H*), 11.22 (s, 1H, CON*H*), 8.58 (d, $^3J_{H\text{-}H}$ = 8.7 Hz, 1H, H-3), 8.09 (d, $^4J_{H\text{-}H}$ = 2.2 Hz, 1H, H-6), 7.79 (d, $^4J_{H\text{-}H}$ = 1.5 Hz, H-4'), 7.73 (dd, $^3J_{H\text{-}H}$ = 8.7 Hz, $^4J_{H\text{-}H}$ = 2.2 Hz, 1H, H-4), 7.53 (d, $^3J_{H\text{-}H}$ = 8.5 Hz, 1H, H-7'), 7.45 (d, $^3J_{H\text{-}H}$ = 3.1 Hz, 1H, H-2'), 7.30 (dd, $^3J_{H\text{-}H}$ = 8.5 Hz, $^4J_{H\text{-}H}$ = 1.5 Hz, 1H, H-6'), 6.47 (d, $^3J_{H\text{-}H}$ = 3.1 Hz, 1H, H-3'), 4.15 (t, $^3J_{H\text{-}H}$ = 7.3 Hz, 2H, H-a), 2.44 (q, $^3J_{H\text{-}H}$ = 7.5 Hz, 2H, H-d), 1.77 (sext, $^3J_{H\text{-}H}$ = 7.3 Hz, 2H, H-b), 1.13 (t, $^3J_{H\text{-}H}$ = 7.5 Hz, 3H, H-e), 0.83 (t, $^3J_{H\text{-}H}$ = 7.3 Hz, 3H, H-c); **^{13}C-NMR** (126 MHz, DMSO-*d*6): δ [ppm] = 172.1 (*C*ONH), 169.4 (*C*OOH), 140.5 (C-2), 136.3 (C-4), 135.5 (C-7a'), 133.7 (C-6), 130.1 (C-2'), 128.0 (C-3a'), 124.3 (C-6'), 124.2 (C-4'), 120.0 (C-3), 117.0 (C-1), 116.5 (C-5), 112.3 (C-5'), 110.4 (C-7'), 100.8 (C-3'), 91.2 (C-2''), 85.8 (C-1''), 47.2 (C-a), 30.9 (C-d), 23.2 (C-b), 11.1 (C-c), 9.28 (C-e); **ATR-IR** (neat): $\tilde{\nu}$ [cm^{-1}] = 2964, 2933, 2874, 1705, 1670, 1584, 1507, 1395, 1290, 1243, 1178, 836, 792, 718, 689; **HRMS** (ESI$^+$): m/z calc.: 373.1557 [M-H]$^-$, found: 373.1560; **R_f**: 0.25 (CH_2Cl_2/MeOH 19:1 v/v).

1-Propyl-5-((trimethylsilyl)ethynyl)-1*H*-benzo[*d*]imidazole 167

In a first reaction, 1-bromopropane (460 µL, 5.08 mmol, 1.00 eq.) and caesium carbonate (3.31 g, 10.2 mmol, 2.00 eq.) were added to a solution of 5-bromo-1*H*-benzo[*d*]imidazole **110** (1.00 g, 5.08 mmol, 1.00 eq.) in DMF (15 mL). After stirring for 2 h at 100 °C, the separated solid was removed by filtration and ice-cold water was added to the filtrate. The aqueous phase was extracted three times with petroleum ether, the combined organic layers were dried over Na_2SO_4 and the solvent was removed under reduced pressure. After purification by column chromatography, a compound mixture (1:1) of both regioisomers **108** and **111** (1.21 g, 5.07 mmol, 100%) was obtained.

The compound mixture (700 mg, 2.93 mmol) was used in the next reaction, that was carried out as described in general procedure II with copper iodide (55.8 mg, 293 µmol), $Pd(PPh_3)_4$ (338 mg, 293 µmol) and TMS acetylene (1.09 mL, 7.90 mmol) in triethylamine (12 mL) and

THF (5 mL) at 70 °C for 20 h. The regioisomers were separated by column chromatography (CH_2Cl_2/acetone/NEt_3 90:9:1) to obtain the desired product **167** (238 mg, 929 µmol, 32%) as a colorless solid.

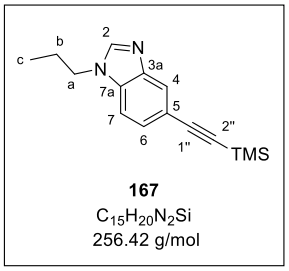

167
$C_{15}H_{20}N_2Si$
256.42 g/mol

^{1}H-NMR (400 MHz, $CDCl_3$): δ [ppm] = 8.35-8.30 (m, 1H, H-2), 8.00-7.96 (m, 1H, H-4), 7.45 (dd, $^3J_{H\text{-}H}$ = 8.4 Hz, $^4J_{H\text{-}H}$ = 1.1 Hz, 1H, H-6), 7.36 (d, $^3J_{H\text{-}H}$ = 8.4 Hz, 1H, H-7), 4.19 (t, $^3J_{H\text{-}H}$ = 7.3 Hz, 2H, H-a), 1.93 (sext, $^3J_{H\text{-}H}$ = 7.3 Hz, 2H, H-b), 0.97 (t, $^3J_{H\text{-}H}$ = 7.3 Hz, 3H, H-c), 0.27 (s, 9H, Si(CH_3)$_3$); **^{13}C-NMR** (101 MHz, $CDCl_3$): δ [ppm] = 143.6 (C-2), 134.8 (C-7a), 127.8 (C-6), 123.6 (C-4), 118.2 (C-5), 110.2 (C-7), 105.4 (C-1''), 93.5 (C-2''), 47.4 (C-a), 23.3 (C-b), 11.4 (C-c), 0.17 (Si(CH_3)$_3$); **ATR-IR** (neat): $\tilde{\nu}$ [cm^{-1}] = 2963, 2152, 1490, 1472, 1380, 1325, 1250, 1208, 946, 839, 815, 756, 651; **HRMS** (ESI$^+$): m/z calc.: 257.1469 $[M+H]^+$, found: 257.1473; **R_f**: 0.36 (CH_2Cl_2/acetone/NEt_3 90:9:1 v/v/v).

5-Ethynyl-1-propyl-1*H*-benzo[*d*]imidazole 173

The reaction was performed according to general procedure III by treating **167** (220 mg, 858 µmol) with potassium carbonate (593 mg, 4.29 mmol) in methanol (8 mL) for 4 h. Alkyne **173** (152 mg, 824 µmol, 96%) was obtained as a brownish oil.

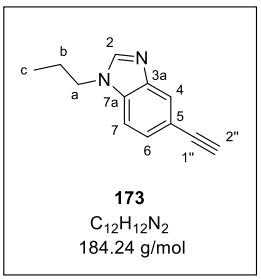

173
$C_{12}H_{12}N_2$
184.24 g/mol

^{1}H-NMR (600 MHz, $CDCl_3$): δ [ppm] = 7.97-7.95 (m, 1H, H-4), 7.92-7.90 (m, 1H, H-2), 7.43 (dd, $^3J_{H\text{-}H}$ = 8.4 Hz, $^4J_{H\text{-}H}$ = 1.4 Hz, 1H, H-6), 7.33 (d, $^3J_{H\text{-}H}$ = 8.4 Hz, 1H, H-7), 4.12 (t, $^3J_{H\text{-}H}$ = 7.3 Hz, 2H, H-a), 1.91 (sext, $^3J_{H\text{-}H}$ = 7.3 Hz, 2H, H-b), 0.96 (t, $^3J_{H\text{-}H}$ = 7.3 Hz, 3H, H-c); **^{13}C-NMR** (151 MHz, $CDCl_3$): δ [ppm] = 144.3 (C-2), 134.3 (C-7a), 127.1 (C-6), 124.8 (C-4), 115.8 (C-5), 110.1 (C-7), 84.0 (C-1''), 75.8 (C-2''), 47.0 (C-a), 23.3(C-b), 11.5 (C-c); **ATR-IR** (neat): $\tilde{\nu}$ [cm^{-1}] = 3297, 2957, 2930, 2872, 2104, 1494, 1469, 1382, 1324, 1262, 1208, 815, 803, 651, 609, 599, 522, 416; **HRMS** (ESI$^+$): m/z calc.: 185.1073 $[M+H]^+$, found: 195.1099; **R_f**: 0.30 (CH_2Cl_2/acetone/NEt_3 90:9:1 v/v/v).

Methyl 2-propionamido-5-((1-propyl-1*H*-benzo[*d*]imidazol-5-yl)ethynyl)benzoate 228

The reaction was carried out as described in general procedure IV with anthranilic acid **90** (150 mg, 450 µmol), copper iodide (8.6 mg, 45 µmol), $Pd(PPh_3)_4$ (52.0 mg, 45.0 µmol) and alkyne **173** (91.3 mg, 495 µmol) in triethylamine (4 mL) and THF (3 mL) at room temperature for 4 h. Purification by column chromatography (CH_2Cl_2/MeOH/NEt_3 95:5:1) provided **228** (175 mg, 450 µmol, 100%) as a yellowish solid.

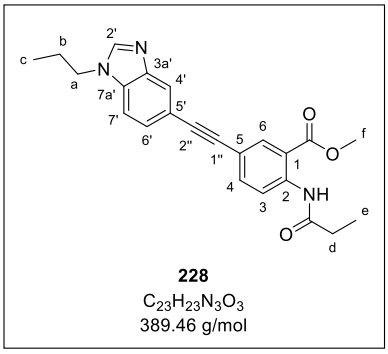

^{1}H-NMR (600 MHz, DMSO-*d*6): *δ* [ppm] = 10.69 (s, 1H, CON*H*), 8.39 (d, $^{3}J_{H\text{-}H}$ = 8.7 Hz, 1H, H-3), 8.35-8.32 (m, 1H, H-2'), 8.05 (d, $^{4}J_{H\text{-}H}$ = 2.1 Hz, 1H, H-6), 7.88-7.85 (m, 1H, H-4'), 7.77 (dd, $^{3}J_{H\text{-}H}$ = 8.7 Hz, $^{4}J_{H\text{-}H}$ = 2.1 Hz, 1H, H-4), 7.67 (d, $^{3}J_{H\text{-}H}$ = 8.5 Hz, 1H, H-7'), 7.45 (dd, $^{3}J_{H\text{-}H}$ = 8.4 Hz, $^{4}J_{H\text{-}H}$ = 1.6 Hz, 1H, H-6'), 4.23 (t, $^{3}J_{H\text{-}H}$ = 7.3 Hz, 2H, H-a), 3.89 (s, 1H, H-f), 2.43 (q, $^{3}J_{H\text{-}H}$ = 7.5 Hz, 2H, H-d), 1.81 (sext, $^{3}J_{H\text{-}H}$ = 7.3 Hz, 2H, H-b), 1.13 (t, $^{3}J_{H\text{-}H}$ = 7.5 Hz, 3H, H-e), 0.85 (t, $^{3}J_{H\text{-}H}$ = 7.3 Hz, 3H, H-c); **^{13}C-NMR** (151 MHz, DMSO-*d*6): *δ* [ppm] = 172.2 (*C*ONH), 167.0 (*C*OOMe), 145.6 (C-2'), 143.4 (C-3a'), 139.6 (C-2), 136.3 (C-4), 133.2 (C-6), 125.8 (C-6'), 122.7 (C-4'), 121.0 (C-3), 117.4 (C-5'), 117.1 (C-1), 115.0 (C-5), 111.1 (C-7'), 90.5 (C-2''), 86.4 (C-1''), 52.6 (C-f), 45.8 (C-a), 30.4 (C-d), 22.8 (C-b), 11.0 (C-c), 9.31 (C-e); **ATR-IR** (neat): $\tilde{\nu}$ [cm^{-1}] = 3309, 3265, 2964, 2934, 1687, 1583, 1507, 1436, 1289, 1254, 1179, 1083, 790, 648; **HRMS** (ESI^{+}): m/z calc.: 390.1812 [M+H]$^{+}$, found: 390.1867; **R$_f$**: 0.22 (CH_2Cl_2/acetone/NEt_3 95:5:1 v/v/v).

2-Propionamido-5-((1-propyl-1*H*-benzo[*d*]imidazol-5-yl)ethynyl)benzoic acid 52

The saponification was carried out according to general procedure V by treating methyl ester **228** (170 mg, 437 µmol) with aqueous 1.0 M NaOH (2.0 mL) in THF (5 mL) for 16 h. After precipitation in acidic solution, target compound **52** (48.3 mg, 129 µmol, 29%) was obtained as an ivory solid.

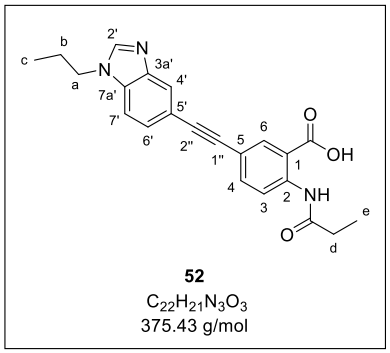

^{1}H-NMR (400 MHz, DMSO-*d*6): *δ* [ppm] = 14.37 (s, 1H, CON*H*), 8.51 (d, $^{3}J_{H\text{-}H}$ = 8.5 Hz, 1H, H-3), 8.33-8.29 (m, 1H, H-2'), 8.15 (d, $^{4}J_{H\text{-}H}$ = 2.1 Hz, 1H, H-6), 7.83-7.79 (m, 1H, H-4'), 7.65 (d, $^{3}J_{H\text{-}H}$ = 8.5 Hz, 1H, H-7'), 7.45-7.49 (m, 2H, H-4, H-6'), 4.22 (t, $^{3}J_{H\text{-}H}$ = 7.3 Hz, 2H, H-a), 2.33 (q, $^{3}J_{H\text{-}H}$ = 7.5 Hz, 2H, H-d), 1.82 (sext, $^{3}J_{H\text{-}H}$ = 7.3 Hz, 2H, H-b), 1.13 (t, $^{3}J_{H\text{-}H}$ = 7.5 Hz, 3H, H-e), 0.85 (t, $^{3}J_{H\text{-}H}$ = 7.3 Hz, 3H, H-c); **^{13}C-NMR** (101 MHz, DMSO-*d*6): *δ* [ppm] = 171.6 (*C*ONH), 168.9 (*C*OOH), 145.4 (C-2'), 143.4 (C-3a'), 141.0 (C-2), 134.4 (C-6), 132.5 (C-4). 125.7 (C-6'), 122.3 (C-4'), 118.2 (C-3), 115.8 (C-5'), 114.9 (C-1), 114.9 (C-5), 111.0 (C-7'), 88.8 (C-2''), 88.2 (C-1''), 45.7 (C-a), 31.0 (C-d), 22.8 (C-b), 11.0 (C-c), 9.71 (C-e); **ATR-IR** (neat): $\tilde{\nu}$ [cm^{-1}] = 3102, 2969, 2934, 1684, 1560, 1507, 1439, 1405, 1367, 1334, 1287, 1272, 1190, 818, 802, 647; **HRMS** (ESI^{+}): m/z calc.: 374.1510 [M-H]$^{-}$, found: 374.1515; **R$_f$**: 0.10 (CH_2Cl_2/MeOH 19:1 v/v).

6.3.6. Syntheses of hDHODH inhibitors 53-63 (cycle 2)

4-(5-Bromopyridin-2-yl)morpholine 129

The reaction was performed according to general procedure I with 5-bromo-2-iodopyridine **136** (1.00 g, 3.53 mmol), copper iodide (134 mg, 705 µmol), L-proline (162 mg, 1.41 mmol), potassium carbonate (974 mg, 7.05 mmol) and morpholine (460 µL, 5.29 mmol) in DMSO (8 mL) for 24 h. Purification by column chromatography (CH_2Cl_2/acetone 100:1 v/v) provided **129** (652 mg, 2.68 mmol, 76%) as a colorless solid.

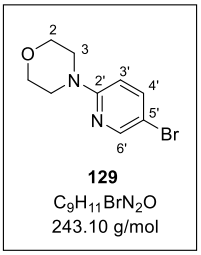

129
$C_9H_{11}BrN_2O$
243.10 g/mol

The analytical data was in accordance with those described.[199]

4-(5-((Trimethylsilyl)ethynyl)pyridin-2-yl)morpholine 188

According to general procedure II, the reaction was carried out with 4-(5-bromopyridin-2-yl)morpholine **129** (500 mg, 2.06 mmol), copper iodide (19.6 mg, 103 µmol), $Pd(PPh_3)_4$ (119 mg, 103 µmol) and TMS acetylene (770 µL, 5.55 mmol) in triethylamine (8 mL) and THF (3 mL) at 70 °C for 19 h. The crude product was purified by column chromatography (CH_2Cl_2/acetone 100:1 v/v) to yield **188** (506 mg, 1.94 mmol, 94%) as a brownish solid.

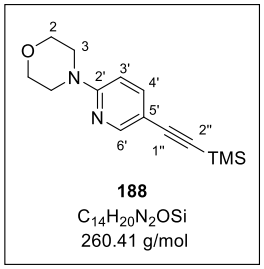

188
$C_{14}H_{20}N_2OSi$
260.41 g/mol

^{1}H-NMR (300 MHz, $CDCl_3$): δ [ppm] = 8.29 (d, $^3J_{H\text{-}H}$ = 2.3 Hz, 1H, H–6'), 7.54 (dd, $^3J_{H\text{-}H}$ = 8.8 Hz, $^4J_{H\text{-}H}$ = 2.3 Hz, 1H, H–4'), 6.52 (d, $^3J_{H\text{-}H}$ = 8.8 Hz, 1H, H–3'), 3.85-3.3.75 (m, 4H, H-2), 3.58-3.49 (m, 4H, H-3), 0.24 (s, 9H, Si(CH_3)$_3$); **^{13}C-NMR** (75 MHz, $CDCl_3$): δ [ppm] = 158.3 (C-2'), 151.8 (C-6'), 140.7 (C-4'), 109.2 (C-5'), 105.8 (C-3'), 103.1 (C-1''), 94.86 (C-2''), 66.8 (C-2), 45.4 (C-3), 0.20 (Si(CH_3)$_3$); **ATR-IR** (neat): $\tilde{\nu}$ [cm^{-1}] = 2973, 2858, 2145, 1601, 1490, 1254, 1239, 945, 836, 812, 761, 722, 700, 539, 530; **MS** (EI): m/z calc.: 260.13 $[M]^+$, found: 260.10; **R_f**: 0.32 (PE/EA 9:1 v/v).

4-(5-Ethynylpyridin-2-yl)morpholine 195

The cleavage of the protecting group was carried out as described in general procedure III by treating **188** (485 mg, 1.86 mmol) with potassium carbonate (1.29 g, 9.31 mmol) in methanol (16 mL) for 4 h. Alkyne **195** (221 mg, 1.18 mmol, 63%) was obtained as a yellow oil.

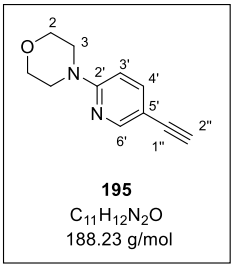

195
$C_{11}H_{12}N_2O$
188.23 g/mol

^{1}H-NMR (300 MHz, $CDCl_3$): δ [ppm] = 8.32 (d, $^3J_{H\text{-}H}$ = 2.4 Hz, 1H, H–6'), 7.56 (dd, $^3J_{H\text{-}H}$ = 8.8 Hz, $^4J_{H\text{-}H}$ = 2.4 Hz, 1H, H–4'), 6.55 (d, $^3J_{H\text{-}H}$ = 8.8 Hz, 1H, H–3'), 3.85-3.76 (m, 4H, H-2), 3.59-3.49 (m, 4H, H-3), 3.07 (s, 1H, H-2''); **^{13}C-NMR** (75 MHz, $CDCl_3$): δ [ppm] = 158.5 (C-2'), 151.9 (C-6'), 140.4 (C-4'), 108.0 (C-5'), 105.9 (C-3'), 80.9 (C-1''), 77.9 (C-2''), 66.8 (C-

2), 45.3 (C-3); **ATR-IR** (neat): $\tilde{\nu}$ [cm^{-1}] = 3211, 2853, 1593, 1542, 1491, 1449, 1397, 1314, 1242, 1113, 932, 814, 646, 525; **MS** (EI): m/z calc.: 188.10 $[M]^+$, found: 188.10; $\mathbf{R_f}$: 0.28 (PE/EA 9:1 v/v).

Methyl 5-((6-morpholinopyridin-3-yl)ethynyl)-2-propionamidobenzoate 236

The reaction was carried out according to general procedure IV with anthranilic acid **90** (206 mg, 618 µmol), copper iodide (5.9 mg, 31 µmol), $Pd(PPh_3)_4$ (35.7mg, 30.9 µmol) and alkyne **195** (175 mg, 928 µmol) in triethylamine (4 mL) and THF (3 mL) at room temperature for 18 h. Purification by column chromatography (CH_2Cl_2/acetone 39:1 v/v) afforded **236** (204 mg, 519 µmol, 84%) as a brownish solid.

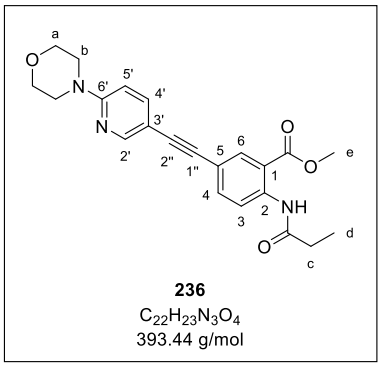

236
$C_{22}H_{23}N_3O_4$
393.44 g/mol

^{1}H-NMR (500 MHz, $CDCl_3$): δ [ppm] = 11.12 (s, 1H, CON*H*), 8.75 (d, $^3J_{H\text{-}H}$ = 8.8 Hz, 1H, H–3), 8.35 (d, $^4J_{H\text{-}H}$ = 2.3 Hz, 1H, H–2'), 8.19 (d, $^4J_{H\text{-}H}$ = 2.1 Hz, 1H, H–6), 7.65 (dd, $^3J_{H\text{-}H}$ = 8.8 Hz, $^4J_{H\text{-}H}$ = 2.1 Hz, 1H, H–4), 7.60 (dd, $^3J_{H\text{-}H}$ = 8.9 Hz, $^4J_{H\text{-}H}$ = 2.3 Hz, 1H, H–4'), 6.59 (d, $^3J_{H\text{-}H}$ = 8.9 Hz, 1H, H–5'), 3.95 (s, 3H, H-e), 3.85-3.79 (m, 4H, H-a), 3.60-3.54 (m, 4H, H-b), 2.49 (q, $^3J_{H\text{-}H}$ = 7.6 Hz, 2H, H–c), 1.28 (t, $^3J_{H\text{-}H}$ = 7.6 Hz, 3H, H–d); **^{13}C-NMR** (126 MHz, $CDCl_3$): δ [ppm] = 173.0 (*C*ONH), 168.3 (*C*OOMe), 159.0 (C-6'), 151.4 (C-2'), 141.3 (C-2), 140.2 (C-4'), 137.4 (C-4), 134.0 (C-6), 120.5 (C-3), 117.7 (C-1), 114.9 (C-5), 109.1 (C-3'), 106.1 (C-5'), 89.1 (C-1''), 87.4 (C-2''), 66.8 (C-a), 52.6 (C-e), 45.4 (C-b), 31.9 (C-c), 9.68 (C-d); **ATR-IR** (neat): $\tilde{\nu}$ [cm^{-1}] = 3260, 2960, 2866, 2201, 1685, 1591, 1511, 1248, 1183, 1118, 1085, 941, 839, 811, 789; **HRMS** (ESI$^+$): m/z calc.: 394.1762 $[M+H]^+$, found: 394.1761; $\mathbf{R_f}$: 0.40 (CH_2Cl_2/acetone 39:1 v/v).

5-((6-Morpholinopyridin-3-yl)ethynyl)-2-propionamidobenzoic acid 53

The saponification was performed as described in general procedure V with methyl ester **236** (182 mg, 463 µmol) and aqueous 1.0 M NaOH (1.5 mL) in THF (5 mL) for 18 h. After precipitation in acidic solution, the target compound **53** (138 mg, 364 µmol, 79%) was obtained as a colorless solid.

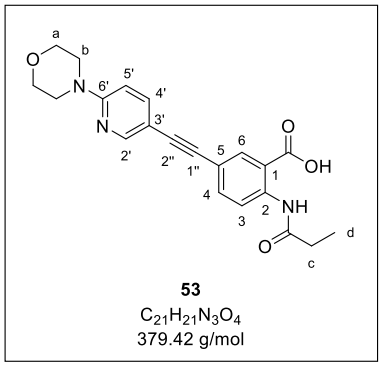

53
$C_{21}H_{21}N_3O_4$
379.42 g/mol

^{1}H-NMR (300 MHz, DMSO-*d*6): δ [ppm] = 11.19 (s, 1H, CON*H*), 8.56 (d, $^3J_{H\text{-}H}$ = 8.8 Hz, 1H, H–3), 8.32 (d, $^4J_{H\text{-}H}$ = 2.3 Hz, 1H, H–2'), 8.06 (d, $^4J_{H\text{-}H}$ = 2.1 Hz, 1H, H–6), 7.69 (dd, $^3J_{H\text{-}H}$ = 8.8 Hz, $^4J_{H\text{-}H}$ = 2.1 Hz, 2H, H–4, H-4'), 6.86 (d, $^3J_{H\text{-}H}$ = 8.9 Hz, 1H, H–5'), 3.73-3.64 (m, 4H, H-a), 3.56-3.46 (m, 4H, H-b), 2.43 (q, $^3J_{H\text{-}H}$ = 7.6 Hz, 2H, H–c), 1.13 (t, $^3J_{H\text{-}H}$ = 7.6 Hz,

3H, H–d); **^{13}C-NMR** (75 MHz, DMSO-*d*6): *δ* [ppm] = 172.2 (*C*ONH), 168.9 (*C*OOH), 157.8 (C-6'), 150.6 (C-2'), 140.7 (C-2), 139.9 (C-4'), 136.2 (C-4), 133.7 (C-6), 120.0 (C-3), 116.5 (C-1), 116.5 (C-5), 107.4 (C-3'), 106.5 (C-5'), 88.7 (C-1''), 87.4 (C-2''), 65.9 (C-a), 44.7 (C-b), 30.7 (C-c), 9.27 (C-d); **ATR-IR** (neat): $\tilde{\nu}$ [cm^{-1}] = 3034, 2970, 1685, 1509, 1289, 1118, 938, 832, 805, 565; **HRMS** (ESI$^+$): m/z calc.: 380.1605 [M+H]$^+$, found: 380.1596; **R_f**: 0.58 (CH_2Cl_2/MeOH 9:1).

4-(5-((Trimethylsilyl)ethynyl)pyrimidin-2-yl)morpholine 189

The reaction was carried out as described in general procedure II with 4-(5-bromopyrimidin-2-yl)morpholine **130** (1.00 g, 4.11 mmol), copper iodide (78.3 mg, 411 µmol), $Pd(PPh_3)_4$ (475 mg, 411 µmol) and TMS acetylene (1.54 mL, 11.1 mmol) in triethylamine (16 mL) and THF (6 mL) at 70 °C for 24 h. Purification by column chromatography (CH_2Cl_2/acetone 100:1 v/v) provided **189** (876 mg, 3.35 mmol, 82%) as a colorless solid.

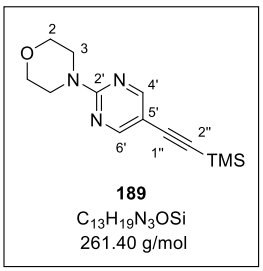

189
$C_{13}H_{19}N_3OSi$
261.40 g/mol

^{1}H-NMR (500 MHz, $CDCl_3$): *δ* [ppm] = 8.37 (s, 2H, H-4', H-6'), 3.84-3.80 (m, 4H, H-3), 3.76-3.72 (m, 4H, H-2), 0.24 (s, 9H, Si(C*H*$_3$)$_3$); **^{13}C-NMR** (126 MHz, $CDCl_3$): *δ* [ppm] = 160.5 (C-4', C-6'), 159.7 (C-2'), 107.3 (C-5'), 100.1 (C-1''), 97.7 (C-2''), 66.9 (C-2), 44.4 (C-3), 0.11 (Si(*C*H$_3$)$_3$); **ATR-IR** (neat): $\tilde{\nu}$ [cm^{-1}] = 2958, 2898, 2858, 2152, 1590, 1507, 1491, 1442, 1354, 1241, 1116, 955, 838, 790, 759, 539; **MS** (EI): m/z calc.: 261.13 [M]$^+$, found: 261.10; **R_f**: 0.50 (CH_2Cl_2/acetone 100:1 v/v).

4-(5-Ethynylpyrimidin-2-yl)morpholine 196

According to general procedure III, the cleavage of the protecting group was performed by treating **189** (850 mg, 3.25 mmol) with potassium carbonate (2.25 g, 16.3 mmol) in methanol (30 mL) for 4 h. Alkyne **196** (533 mg, 2.88 mmol, 88%) was isolated as a yellow oil.

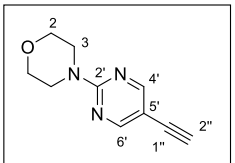

196
$C_{10}H_{11}N_3O$
189.22 g/mol

^{1}H-NMR (400 MHz, $CDCl_3$): *δ* [ppm] = 8.40 (s, 2H, H-4', H-6'), 3.86-3.79 (m, 4H, H-3), 3.77-3.72 (m, 4H, H-2), 3.18 (s, 1H, H-2''); **^{13}C-NMR** (101 MHz, $CDCl_3$): *δ* [ppm] = 160.7 (C-4', C-6'), 159.9 (C-2'), 106.1 (C-5'), 80.4 (C-2''), 78.9 (C-1''), 66.9 (C-2), 44.3 (C-3); **ATR-IR** (neat): $\tilde{\nu}$ [cm^{-1}] = 3315, 2965, 2858, 1596, 1507, 1304, 1103, 954, 939, 844, 788, 719, 666, 590, 533; **MS** (EI): m/z calc.: 189.09 [M]$^+$, found: 189.10; 0.47 (CH_2Cl_2/acetone 100:1 v/v).

Methyl 5-((2-morpholinopyrimidin-5-yl)ethynyl)-2-propionamidobenzoate 237

The reaction was carried out according to general procedure IV with anthranilic acid **90** (199 mg, 597 µmol), copper iodide (5.7 mg, 30 µmol), $Pd(PPh_3)_4$ (34.5 mg, 29.9 µmol) and alkyne **196** (170 mg, 896 µmol) in triethylamine (4 mL) and THF (3 mL) at room temperature for 4 h. After purification by column chromatography (CH_2Cl_2/acetone 19:1 v/v), **237** (231 mg, 585 µmol, 98%) was obtained as a colorless solid.

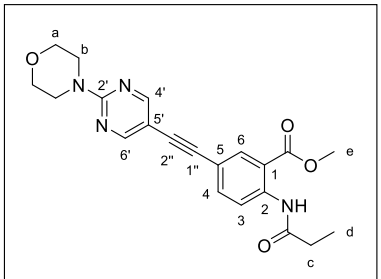

237
$C_{21}H_{22}N_4O_4$
394.43 g/mol

^{1}H-NMR (400 MHz, DMSO-*d*6): δ [ppm] = 11.13 (s, 1H, CON*H*), 8.76 (d, $^3J_{H\text{-}H}$ = 8.8 Hz, 1H, H-3), 8.44 (s, 2H, H-4', H-6'), 8.18 (d, $^4J_{H\text{-}H}$ = 2.1 Hz, 1H, H–6), 7.65 (dd, $^3J_{H\text{-}H}$ = 8.8 Hz, $^4J_{H\text{-}H}$ = 2.1 Hz, 1H, H-4), 3.95 (s, 3H, H-e), 3.89-3.81 (m, 4H, H-b), 3.81-3.73 (m, 4H, H-a), 2.49 (q, $^3J_{H\text{-}H}$ = 7.6 Hz, 2H, H-c), 1.28 (t, $^3J_{H\text{-}H}$ = 7.6 Hz, 3H, H-d); **^{13}C-NMR** (101 MHz, $CDCl_3$): δ [ppm] = 173.1 (*C*ONH), 168.3 (*C*OOMe), 160.0 (C-4',C-6'), 159.7 (C-2'), 141.5 (C-2), 137.3 (C-4), 134.0 (C-6), 120.5 (C-3), 117.2 (C-1), 114.9 (C-5), 107.1 (C-5'), 91.4 (C-1''), 84.3 (C-2''), 66.9 (C-a), 52.7 (C-e), 44.4 (C-b), 31.9 (C-c), 9.66 (C-d); **ATR-IR** (neat): $\tilde{\nu}$ [cm^{-1}] = 3304, 3270, 2975, 1685, 1592, 1514, 1293, 1250, 1236, 1187, 1112, 1086, 956, 842, 789; **HRMS** (ESI$^+$): m/z calc.: 395.1714 $[M+H]^+$, found: 395.1679; **R_f**: = 0.31 (CH_2Cl_2/acetone 19:1 v/v).

5-((2-Morpholinopyrimidin-5-yl)ethynyl)-2-propionamidobenzoic acid 54

The saponification was performed according to general procedure V by treating methyl ester **237** (116 mg, 370 µmol) with aqueous 1.0 M NaOH (1.5 mL) in THF (5 mL) for 24 h. Precipitation in acidic solution afforded target compound **54** (105 mg, 276 µmol, 94%) as a colorless solid.

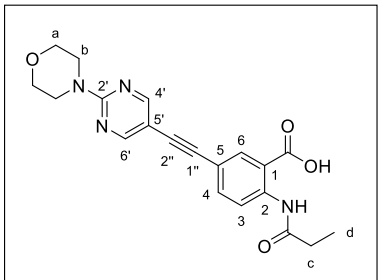

54
$C_{20}H_{20}N_4O_4$
380.40 g/mol

^{1}H-NMR (600 MHz, DMSO-*d*6): δ [ppm] = 11.21 (s, 1H, CON*H*), 8.57 (s, 2H, H-4', H-6'), 8.56 (d, $^3J_{H\text{-}H}$ = 8.7 Hz, 1H, H-3), 8.07 (d, $^4J_{H\text{-}H}$ = 2.1 Hz, 1H, H-6), 7.70 (dd, $^3J_{H\text{-}H}$ = 8.7 Hz, $^4J_{H\text{-}H}$ = 2.1 Hz, 1H, H-4), 3.77-3.73 (m, 4H, H-b), 3.68-3.63 (m, 4H, H-a), 2.43 (q, $^3J_{H\text{-}H}$ = 7.5 Hz, 2H, H-c), 1.12 (t, $^3J_{H\text{-}H}$ = 7.5 Hz, 3H, H-d); **^{13}C-NMR** (151 MHz, DMSO-*d*6): δ [ppm] = 172.3 (*C*ONH), 168.9 (*C*OOH), 160.1 (C-4', C-6'), 159.3 (C-2'), 140.9 (C-2), 136.3 (C-4), 133.9 (C-6), 120.1 (C-3), 116.7 (C-1), 116.2 (C-5), 106.0 (C-5'), 91.2 (C-1''), 84.6 (C-2''), 66.0 (C-a), 43.9 (C-b), 30.8 (C-c), 9.35 (C-d); **ATR-IR** (neat): $\tilde{\nu}$ [cm^{-1}] = 2968, 1868, 1681, 1592, 1506, 1449, 1403, 1359, 1296, 1225, 1116, 957, 843, 791, 743, 529; **HRMS** (ESI$^+$): m/z calc.: 379.1412 $[M-H]^-$, found: 379.1414; **R_f**: 0.53 (CH_2Cl_2/MeOH 9:1).

4-(4-Bromo-3-fluorophenyl)morpholine 131

The reaction was carried out as described in general procedure I with 1-bromo-2-fluoro-4-iodobenzene **137** (4.00 g, 13.3 mmol), copper iodide (506 mg, 2.66 mmol), L-proline (612 mg, 5.32 mmol), potassium carbonate (3.67 g, 26.6 mmol) and morpholine (1.74 mL, 19.9 mmol) in DMSO (20 mL) for 24 h. The crude product was purified by column chromatography (CH_2Cl_2/PE 2:1 v/v) to yield **131** (1.97 g, 7.58 mmol, 57%) as a colorless solid.

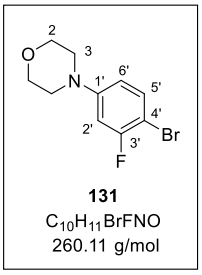

131
$C_{10}H_{11}BrFNO$
260.11 g/mol

^{1}H-NMR (400 MHz, $CDCl_3$): δ [ppm] = 7.36 (dd, $^3J_{H\text{-}H}$ = 8.9 Hz, $^4J_{H\text{-}F}$ = 8.1 Hz, 1H, H-5'), 6.64 (dd, $^3J_{H\text{-}F}$ = 11.8 Hz, $^4J_{H\text{-}H}$ = 2.8 Hz, 1H, H-2'), 6.56 (dd, $^3J_{H\text{-}H}$ = 8.9 Hz, $^4J_{H\text{-}H}$ = 2.8 Hz, 1H, H-6'), 3.88-3.81 (m, 4H, H-2), 3.17-3.10 (m, 4H, H-3); **^{13}C-NMR** (101 MHz, $CDCl_3$): δ [ppm] = 159.9 (C-3'), 152.3 (C-1'), 133.4 (C-5'), 112.3 (C-6'), 103.6 (C-2'), 97.8 (C-4'), 66.7 (C-2), 48.8 (C-3), **^{19}F-NMR** (565 MHz, $CDCl_3$): δ [ppm] = −106.6 (Ar-*F*); **ATR-IR** (neat): $\tilde{\nu}$ [cm^{-1}] = 2964, 2855, 2831, 1603, 1567, 1492, 1448, 1264, 1243, 1192, 1192, 1119, 1025, 972, 883, 829, 656; **MS** (EI): m/z calc.: 259.00 $[M]^+$, found: 259.00; **R_f**: 0.18 (CH_2Cl_2/PE 1:1 v/v).

4-(3-Fluoro-4-((trimethylsilyl)ethynyl)phenyl)morpholine 190

According to general procedure II, the reaction was carried out with 4-(4-bromo-3-fluorophenyl)morpholine **131** (470 mg, 1.81 mmol), copper iodide (17.2 mg, 90.3 µmol), $Pd(PPh_3)_4$ (104 mg, 90.3 µmol) and TMS acetylene (670 µL, 4.88 mmol) in triethylamine (8 mL) and THF (3 mL) at 70 °C for 24 h. Purification by column chromatography (PE/EA 9:1 v/v) provided **190** (326 mg, 1.18 mmol, 65%) as a yellow solid.

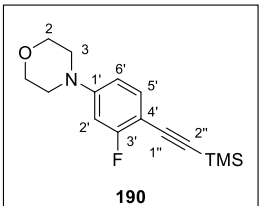

190
$C_{15}H_{20}FNOSi$
277.41 g/mol

^{1}H-NMR (600 MHz, $CDCl_3$): δ [ppm] = 7.33-7.29 (m, 1H, H-5'), 6.56 (dd, $^3J_{H\text{-}H}$ = 8.7 Hz, $^4J_{H\text{-}H}$ = 2.4 Hz, 1H, H-6'), 6.52 (dd, $^3J_{H\text{-}F}$ = 12.6 Hz, $^4J_{H\text{-}H}$ = 2.4 Hz, 1H, H-2'), 3.86-3.80 (m, 4H, H-2), 3.20-3.16 (m, 4H, H-3), 0.25 (s, 9H, Si(CH_3)$_3$); **^{13}C-NMR** (151 MHz, $CDCl_3$): δ [ppm] = 164.3 (C-3'), 152.8 (C-1'), 134.5 (C-5') 110.1 (C-6'), 101.8 (C-4'), 101.6 (C-2'), 98.8 (C-1''), 97.8 (C-2''), 66.7 (C-2), 48.1 (C-3), 0.18 (Si(CH_3)$_3$); **^{19}F-NMR** (565 MHz, $CDCl_3$): δ [ppm] = −108.3 (Ar-*F*); **ATR-IR** (neat): $\tilde{\nu}$ [cm^{-1}] = 2958, 2899, 2844, 2148, 1622, 1510, 1264, 1247, 1121, 1109, 886, 838, 799, 761, 700, 612; **MS** (EI): m/z calc.: 277.13 $[M]^+$, found: 277.20; **R_f**: 0.35 (PE/EA 9:1 v/v).

4-(4-Ethynyl-3-fluorophenyl)morpholine 197

The reaction was performed according to general procedure III by treating **190** (275 mg, 991 µmol) with potassium carbonate (685 mg, 4.96 mmol) in methanol (5 mL) for 4 h. Alkyne **197** (106 mg, 514 mmol, 52%) was obtained as a yellow solid.

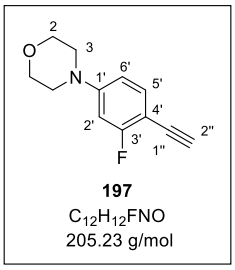

^{1}H-NMR (600 MHz, $CDCl_3$): δ [ppm] = 7.36-7.31 (m, 1H, H-5'), 6.59 (dd, $^3J_{H\text{-}H}$ = 8.7 Hz, $^4J_{H\text{-}H}$ = 2.5 Hz, 1H, H-6'), 6.55 (dd, $^3J_{H\text{-}F}$ = 12.6 Hz, $^4J_{H\text{-}H}$ = 2.5 Hz, 1H, H-2'), 3.86-3.81 (m, 4H, H-2), 3.21 (s, 1H, H-2''), 3.20-3.18 (m, 4H, H-3); **^{13}C-NMR** (151 MHz, $CDCl_3$): δ [ppm] = 164.5 (C-3'), 153.0 (C-1'), 134.5 (C-5'), 110.2 (C-6'), 101.6 (C-4'), 100.5 (C-1''), 80.5 (C-2''), 66.7 (C-2), 48.1 (C-3); **^{19}F-NMR** (565 MHz, $CDCl_3$): δ [ppm] = −108.9 (Ar-*F*); **ATR-IR** (neat): $\tilde{\nu}$ [cm^{-1}] = 3210, 2969, 2921, 2839, 1617, 1506, 1264, 1243, 1177, 1116, 1040, 971, 883, 836, 808, 638, 604; **MS** (EI): m/z calc.: 205.09 $[M]^+$, found: 205.10; **R_f**: 0.30 (PE/EA 9:1 v/v).

Methyl 5-((2-fluoro-4-morpholinophenyl)ethynyl)-2-propionamidobenzoate 238

The reaction was carried out as described in general procedure IV with anthranilic acid **90** (135 mg, 405 µmol), copper iodide (3.9 mg, 20 µmol), $Pd(PPh_3)_4$ (23.4 mg, 20.3 µmol) and alkyne **197** (91.5 mg, 446 µmol) in triethylamine (3 mL) and THF (2 mL) at room temperature for 5 h. The crude product was purified by column chromatography (CH_2Cl_2/acetone 100:1 v/v) to yield **238** (140 mg, 342 µmol, 84%) as a yellowish solid.

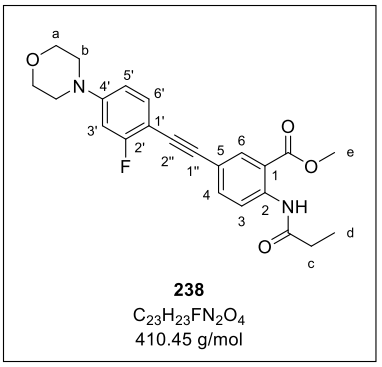

^{1}H-NMR (400 MHz, $CDCl_3$): δ [ppm] = 11.13 (s, 1H, CON*H*), 8.74 (d, $^3J_{H\text{-}H}$ = 8.8 Hz, 1H, H-3), 8.20 (d, $^4J_{H\text{-}H}$ = 2.1 Hz, 1H, H–6), 7.67 (dd, $^3J_{H\text{-}H}$ = 8.8 Hz, $^4J_{H\text{-}H}$ = 2.1 Hz, 1H, H-4), 7.40-7.32 (m, 1H, H-6'), 6.66-6.54 (m, 2H, H-5', H-3'), 3.94 (s, 3H, H-e), 3.88-3.80 (m, 4H, H-a), 3.24-3.17 (m, 4H, H-b), 2.49 (q, $^3J_{H\text{-}H}$ = 7.6 Hz, 2H, H-c), 1.28 (t, $^3J_{H\text{-}H}$ = 7.6 Hz, 3H, H-d); **^{13}C-NMR** (126 MHz, $CDCl_3$): δ [ppm] = 173.0 (*C*ONH), 168.4 (*C*OOMe), 163.9 (C-2'), 152.7 (C-4'), 141.4 (C-2), 137.4 (C-4), 134.1 (C-6), 133.9 (C-6'), 120.4 (C-3), 117.7 (C-1), 114.9 (C-5), 110.4 (C-5'), 101.8 (C-1'), 101.5 (C-3'), 91.6 (C-1''), 83.4 (C-2''), 66.7 (C-a), 52.6 (C-e), 48.2 (C-b), 31.9 (C-c), 9.67 (C-d); **^{19}F-NMR** (565 MHz, $CDCl_3$): δ [ppm] = −108.5 (Ar-*F*); **ATR-IR** (neat): $\tilde{\nu}$ [cm^{-1}] = 3262, 2952, 2851, 1686, 1622, 1584, 1519, 1505, 1243, 1234, 973, 789; **HRMS** (ESI$^+$): m/z calc.: 411.1715 $[M+H]^+$, found: 411.1848; **R_f**: 0.31 (CH_2Cl_2/acetone 100:1 v/v).

5-((2-Fluoro-4-morpholinophenyl)ethynyl)-2-propionamidobenzoic acid 55

The saponification was carried out according to general procedure V with methyl ester **238** (120 mg, 292 µmol) and aqueous 1.0 M NaOH (1.0 mL) in THF (3 mL) for 18 h. Precipitation in acidic solution provided target compound **55** (93.3 mg, 235 µmol, 81%) as a yellowish solid.

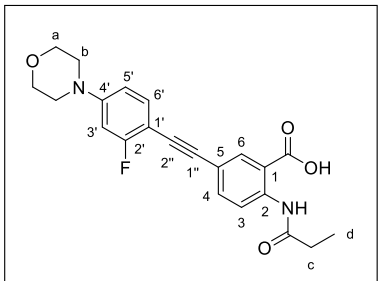

55
$C_{22}H_{21}FN_2O_4$
396.42 g/mol

^{1}H-NMR (600 MHz, DMSO-*d*6): δ [ppm] = 13.91 (s, 1H, COO*H*), 11.20 (s, 1H, CON*H*), 8.57 (d, $^3J_{H\text{-}H}$ = 8.7 Hz, 1H, H–3), 8.04 (d, $^4J_{H\text{-}H}$ = 2.2 Hz, 1H, H–6), 7.70 (dd, $^3J_{H\text{-}H}$ = 8.7 Hz, $^4J_{H\text{-}H}$ = 2.2 Hz, 1H, H–4), 7.44-7.39 (m, 1H, H-6'), 6.86 (dd, $^3J_{H\text{-}F}$ = 13.6 Hz, $^4J_{H\text{-}H}$ = 2.5 Hz, 1H, H-3'), 6.79 (dd, $^3J_{H\text{-}H}$ = 8.8 Hz, $^4J_{H\text{-}H}$ = 2.5 Hz, 1H, H-5'), 3.74-3.69 (m, 4H, H-a), 3.25-3.20 (m, 4H, H-b), 2.43 (q, $^3J_{H\text{-}H}$ = 7.6 Hz, 2H, H–c), 1.13 (t, $^3J_{H\text{-}H}$ = 7.6 Hz, 3H, H–d); **^{13}C-NMR** (151 MHz, DMSO-*d*6): δ [ppm] = 172.2 (*C*ONH), 168.8 (*C*OOH), 163.6 (C-2'), 152.7 (C-4'), 140.8 (C-2), 136.2 (C-4), 133.6 (C-6'), 133.6 (C-6'), 120.1 (C-3), 116.5 (C-1), 116.4 (C-5), 110.2 (C-5'), 101.0 (C-1'), 99.0 (C-3'), 91.1 (C-1''), 83.5 (C-2''), 65.8 (C-a), 47.0 (C-b), 30.7 (C-c), 9.27 (C-d); **^{19}F-NMR** (565 MHz, DMSO-*d*6): δ [ppm] = −109.4 (Ar-*F*); **ATR-IR** (neat): $\tilde{\nu}$ [cm^{-1}] = 2971, 2922, 1683, 1519, 1232, 1189, 1107, 1040, 972, 839, 793; **HRMS** (ESI$^+$): m/z calc.: 397.1558 $[M+H]^+$, found: 397.1549; **R_f**: 0.68 (CH_2Cl_2/MeOH 9:1 v/v).

4-(2-Fluoro-4-((trimethylsilyl)ethynyl)phenyl)morpholine 191

TMS-protected alkyne **191** was synthesized over two steps. The first reaction was performed according to general procedure I with 4-bromo-2-fluoro-1-iodobenzene **138** (2.00 g, 6.65 mmol), copper iodide (253 mg, 1.33 mmol), L-proline (306 mg, 2.66 mmol), potassium carbonate (1.84 g, 13.3 mmol) and morpholine (1.74 mL, 19.9 mmol) in DMSO (10 mL) for 30 h at 50 °C. The crude product was purified by column chromatography (CH_2Cl_2/PE 1:1 v/v) to yield **132** (221 mg, 851 µmol, 13%) as a colorless solid.

The second reaction was carried out as described in general procedure II with 4-(4-bromo-2-fluorophenyl)morpholine **132** (211 mg, 810 µmol), copper iodide (15.4 mg, 81.0 µmol), $Pd(PPh_3)_4$ (93.7 mg, 81.0 µmol) and TMS acetylene (300 µL, 6.36 mmol) in triethylamine (4 mL) and THF (1.5 mL) at 70 °C for 24 h. The crude product was purified by column chromatography (CH_2Cl_2/PE 1:1 v/v) to yield **191** (166 mg, 597 µmol, 74%) as a yellow solid.

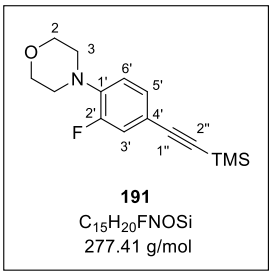

191
$C_{15}H_{20}FNOSi$
277.41 g/mol

^{1}H-NMR (600 MHz, $CDCl_3$): δ [ppm] = 7.20-7.17 (m, 1H, H-5'), 7.13 (dd, $^3J_{H\text{-}F}$ = 13.4 Hz, $^3J_{H\text{-}H}$ = 1.9 Hz, 1H, H-3'), 6.87-6.82 (m, 1H, H-6'), 3.88-3.85 (m, 4H, H-2), 3.13-3.09 (m, 4H, H-3), 0.023 (s, 9H, Si(CH_3)$_3$); **^{13}C-NMR** (151 MHz, $CDCl_3$): δ [ppm] = 154.7 (C-2'), 140.1 (C-1'), 128.8 (C-5'), 119.8 (C-3'), 118.4 (C-6'), 116.6 (C-4'), 104.1 (C-1''), 94.2 (C-2''), 67.0 (C-2), 50.8 (C-3), 0.10 (Si(CH_3)$_3$); **^{19}F-NMR** (565 MHz, $CDCl_3$): δ [ppm] = −122.5 (Ar-*F*); **ATR-IR** (neat): $\tilde{\nu}$ [cm^{-1}] = 2961, 2855, 2832, 2144, 1615, 1509, 1248, 1225, 1120, 920, 838, 760; **HRMS** (ESI$^+$): m/z calc.: 278.1371 $[M+H]^+$, found: 278.1396; **R_f**: 0.39 (CH_2Cl_2/PE 1:1 v/v).

4-(4-Ethynyl-2-fluorophenyl)morpholine 198

The reaction was performed according to general procedure III by treating **191** (166 mg, 597 µmol) with potassium carbonate (413 mg, 2.99 mmol) in methanol (5 mL) for 4 h. Alkyne **198** (98.9 mg, 482 mmol, 81%) was isolated as a yellowish solid.

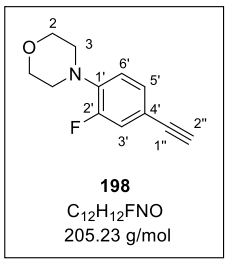

198
$C_{12}H_{12}FNO$
205.23 g/mol

^{1}H-NMR (600 MHz, $CDCl_3$): δ [ppm] = 7.22-7.20 (m, 1H, H-5'), 7.15 (dd, $^3J_{H\text{-}F}$ = 13.3 Hz, $^3J_{H\text{-}H}$ = 1.9 Hz, 1H, H-3'), 6.86-6.80 (m, 1H, H-6'), 3.88-3.85 (m, 4H, H-2) 3.13-3.09 (m, 4H, H-3), 3.03 (s, 1H, H-2''); **^{13}C-NMR** (151 MHz, $CDCl_3$): δ [ppm] = 154.7 (C-2'), 140.9 (C-1'), 129.0 (C-5'), 120.0 (C-3'), 118.4 (C-6'), 115.8 (C-4'), 82.7 (C-1''), 77.1 (C-2''), 67.0 (C-2), 50.7 (C-3); **^{19}F-NMR** (565 MHz, $CDCl_3$): δ [ppm] = −122.3 (Ar-*F*); **ATR-IR** (neat): $\tilde{\nu}$ [cm^{-1}] = 3215, 2956, 2859, 1613, 1506, 1448, 1244, 1110, 912, 869, 820, 693, 607; **HRMS** (ESI$^+$): m/z calc.: 206.0976 $[M+H]^+$, found: 206.1014; **R_f**: 0.35 (CH_2Cl_2/PE 1:1 v/v).

5-((3-Fluoro-4-morpholinophenyl)ethynyl)-2-propionamidobenzoic acid 56

The first reaction step was carried out according to general procedure IV with anthranilic acid **90** (100 mg, 300 µmol), copper iodide (5.7 mg, 30 µmol), $Pd(PPh_3)_4$ (34.7 mg, 30.0 µmol) and alkyne **198** (67.8 mg, 330 µmol) in triethylamine (3 mL) and THF (2 mL) at room temperature for 24 h. The crude product was purified by column chromatography (CH_2Cl_2/acetone 19:1 v/v) to give **239** (89.2 mg, 231 µmol, 77%) as a yellowish solid.

The second reaction step was performed according to general procedure V by treating methyl ester **239** (80.0 mg, 195 µmol) with aqueous 1.0 M NaOH (1 mL) in THF (4 mL) for 16 h. After precipitation in acidic solution, target compound **56** (65.8 mg, 166 µmol, 85%) was obtained as a colorless solid.

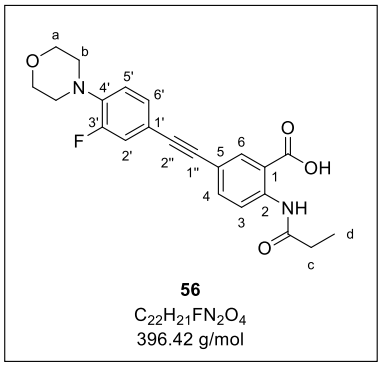

56
$C_{22}H_{21}FN_2O_4$
396.42 g/mol

^{1}H-NMR (600 MHz, DMSO-*d*6): δ [ppm] = 11.22 (s, 1H, CON*H*), 8.57 (d, $^{3}J_{H\text{-}H}$ = 8.7 Hz, 1H, H-3), 8.08 (d, $^{4}J_{H\text{-}H}$ = 2.1 Hz, 1H, H-6), 7.71 (dd, $^{3}J_{H\text{-}H}$ = 8.7 Hz, $^{4}J_{H\text{-}H}$ = 2.1 Hz, 1H, H-4), 7.36 (dd, $^{3}J_{H\text{-}F}$ = 13.6 Hz, $^{3}J_{H\text{-}H}$ = 2.0 Hz, 1H, H-2'), 7.32 (dd, $^{3}J_{H\text{-}H}$ = 8.5 Hz, $^{3}J_{H\text{-}H}$ = 2.0 Hz, H-6'), 7.06-7.00 (m, 1H, H-5'), 3.76-3.72 (m, 4H, H-a), 3.09-3.04 (m, 4H, H-b), 2.43 (q, $^{3}J_{H\text{-}H}$ = 7.5 Hz, 2H, H-c), 1.13 (t, $^{3}J_{H\text{-}H}$ = 7.6 Hz, 3H, H-d); **^{13}C-NMR** (151 MHz, DMSO-*d*6): δ [ppm] = 172.2 (*C*ONH), 168.8 (*C*OOH), 153.9 (C-3'), 140.9 (C-2), 140.3 (C-4'), 136.4 (C-4), 134.0 (C-6), 128.5 (C-6'), 120.0 (C-3), 119.0 (C-5'), 118.8 (C-2'), 116.6 (C-1), 116.1 (C-5), 115.3 (C-1'), 88.3 (C-2''), 88.0 (C-1''), 66.1 (C-a), 50.1 (C-b), 30.7 (C-c), 9.27 (C-d); **^{19}F-NMR** (565 MHz, DMSO-*d*6): δ [ppm] = −122.0 (Ar-*F*); **ATR-IR** (neat): $\tilde{\nu}$ [cm^{-1}] = 2971, 2925, 2854, 1688, 1586, 1517, 1291, 1264, 1217, 1200, 1184, 1107, 932, 796, 754; **HRMS** (ESI^{+}): m/z calc.: 395.1412 [M-H]$^{-}$, found: 395.1409; **R_f**: 0.64 (CH_2Cl_2/MeOH 9:1 v/v).

4-(2,3,5,6-Tetrafluoro-4-iodophenyl)morpholine 133

A mixture of morpholine (300 µL, 3.44 mmol, 1.00 eq.), 1,2,3,4,5-pentafluoro-6-iodobenzene **143** (920 µL, 6.89 mmol, 2.00 eq.) and triethylamine (480 µL, 3.44 mmol, 1.00 eq.) was stirred for 1 h at 150 °C. Subsequently, the solvent was removed under reduced pressure and the residue was purified by column chromatography (PE/EA 10:1 v/v) to yield **133** (851 mg, 2.36 mmol, 68%) as a colorless solid.

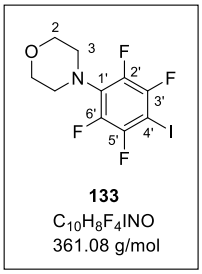

133
$C_{10}H_8F_4INO$
361.08 g/mol

^{1}H-NMR (400 MHz, $CDCl_3$): δ [ppm] = 3.84-3.77 (m, 4H, H-2), 3.32-3.23 (m, 4H, H-3); **^{13}C-NMR** (101 MHz, $CDCl_3$): δ [ppm] = 129.2 (C-1'), 67.4 (C-2), 62-9 (C-4'), 51.2 (C-3); **^{19}F-NMR** (565 MHz, $CDCl_3$): δ [ppm] = −122.2 (Ar-*F*), −148.5 (Ar-*F*); **ATR-IR** (neat): $\tilde{\nu}$ [cm^{-1}] = 2966, 2921, 2866, 1628, 1468, 1448, 1255, 1104, 1010, 967, 873, 548; **HRMS** (ESI^{+}): m/z calc.: 361.9660 [M+H]$^{+}$, found: 361.9654; **R_f**: 0.36 (PE/EA 10:1 v/v).

4-(2,3,5,6-Tetrafluoro-4-((trimethylsilyl)ethynyl)phenyl)morpholine 192

The reaction was carried out as described in general procedure II with 4-(2,3,5,6-tetrafluoro-4-iodophenyl)morpholine **133** (850 mg, 2.35 mmol), copper iodide (44.8 mg, 235 µmol), $Pd(PPh_3)_4$ (272 mg, 235 µmol) and TMS acetylene (880 µL, 6.36 mmol) in triethylamine (9 mL) and THF (8 mL) at 70 °C for 20 h. After purification by column chromatography (PE/EA 10:1 v/v), **192** (545 mg, 1.64 mmol, 70%) was obtained as a yellow solid.

^{1}H-NMR (400 MHz, $CDCl_3$): δ [ppm] = 3.83-3.77 (m, 4H, H-2), 3.33-3.26 (m, 4H, H-3), 0.27 (s, 9H, Si(CH_3)$_3$); **^{13}C-NMR** (101 MHz, $CDCl_3$): δ [ppm] = 107.10 (C-1''), 89.2 (C-2''), 67.4 (C-2), 51.3 (C-3), −0.17 (Si(CH_3)$_3$), **^{19}F-NMR** (565 MHz, $CDCl_3$): δ [ppm] = −138.1 (Ar-*F*), −151.8 (Ar-*F*); **ATR-IR** (neat): $\tilde{\nu}$ [cm^{-1}] = 2959, 2900, 2857, 2168, 2040, 1645, 1485, 1247, 1110, 983, 838, 759, 544; **HRMS** (ESI$^+$): m/z calc.: 332.1089 [M+H]$^+$, found: 332.1115; **R_f**: 0.45 (PE/EA 10:1 v/v).

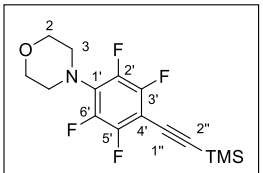

192
$C_{15}H_{17}F_4NOSi$
331.39 g/mol

4-(4-Ethynyl-2,3,5,6-tetrafluorophenyl)morpholine 199

The cleavage of the protecting group was performed according to general procedure III by treating **192** (545 mg, 1.65 mmol) with potassium carbonate (1.14 g, 8.23 mmol) in methanol (13 mL) for 4 h. Due to the alkyne's instability, the washing step after solvent removal was omitted, and the crude product was used for the next synthesis step.

Representative analytical data was obtained from a smaller batch purified by column chromatography (PE/EA 10:1 v/v).

^{1}H-NMR (400 MHz, $CDCl_3$): δ [ppm] = 3.84-3.77 (m, 4H, H-2), 3.53-3.52 (m, 1H, H-2''), 3.33-3.28 (m, 4H, H-3).

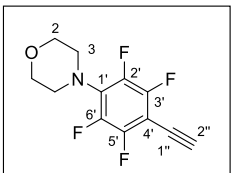

199
$C_{12}H_9F_4NO$
259.20 g/mol

Methyl 2-propionamido-5-((2,3,5,6-tetrafluoro-4-morpholinophenyl)ethynyl)benzoate 240

According to general procedure IV, the reaction was carried out with anthranilic acid **90** (200 mg, 600 µmol), copper iodide (11.4 mg, 60.0 µmol), $Pd(PPh_3)_4$ (69.4 mg, 60.0 µmol) and crude alkyne **199** (330 mg, 901 µmol) in triethylamine (4 mL) and THF (3 mL) at room temperature for 4 h. Purification by column chromatography (PE/EA 7:3 v/v) afforded **240** (33.0 mg, 71.1 µmol, 12%) as a colorless solid.

^{1}H-NMR (600 MHz, $CDCl_3$): δ [ppm] = 11.18 (s, 1H, CON*H*), 8.79 (d, $^{3}J_{H\text{-}H}$ = 8.8 Hz, 1H, H-3), 8.24 (d, $^{4}J_{H\text{-}H}$ = 2.1 Hz, 1H, H-6), 7.70 (dd, $^{3}J_{H\text{-}H}$ = 8.8 Hz, $^{4}J_{H\text{-}H}$ = 2.1 Hz, 1H, H-4), 3.96 (s, 3H, H-e), 3.84-3.80 (m, 4H, H-a), 3.35-3.30 (m, 4H, H-b), 2.50 (q, $^{3}J_{H\text{-}H}$ = 7.5 Hz, 2H, H-c), 1.29 (t, $^{3}J_{H\text{-}H}$ = 7.6 Hz, 3H, H–d); **^{13}C-NMR** (151 MHz, $CDCl_3$): δ [ppm] = 172.9 (*C*ONH), 168.1 (*C*OOMe), 137.7 (C-4), 134.5 (C-6), 120.5 (C-3), 115.3 (C-1), 115.3 (C-5), 98.4 (C-1''), 67.4 (C-a), 52.7 (C-f), 51.3 (C-c), 31.9 (C-d), 9.81 (C-e); **^{19}F-NMR** (565 MHz, $CDCl_3$): δ [ppm] = −138.3 (Ar-*F*), −151.6 (Ar-*F*); **ATR-IR** (neat): $\tilde{\nu}$ [cm^{-1}] = 3255, 2856, 1707, 1686, 1585, 1512, 1483, 1261, 1232,

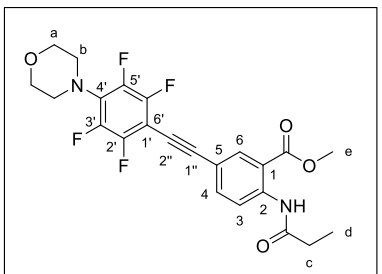

240
$C_{23}H_{20}F_4N_2O_4$
464.42 g/mol

1120, 1086, 978, 859, 792; **HRMS** (ESI$^+$): m/z calc.: 465.1432 [M+H]$^+$, found: 465.1449; **R_f**: 0.45 (PE/EA 7:3 v/v).

2-Propionamido-5-((2,3,5,6-tetrafluoro-4-morpholinophenyl)ethynyl)benzoic acid 57

The reaction was carried out as described in general procedure V with methyl ester **240** (50.3 mg, 108 µmol) and aqueous 1.0 M NaOH (0.5 mL) in THF (2 mL) for 18 h. Precipitation in acidic solution provided **57** (28.4 mg, 63.1 µmol, 58%) as a colorless solid.

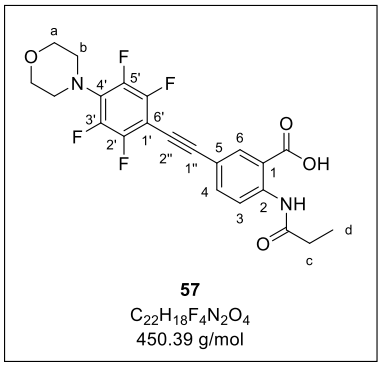

57
$C_{22}H_{18}F_4N_2O_4$
450.39 g/mol

ATR-IR (neat): $\tilde{\nu}$ [cm^{-1}] = 2911, 2218, 1706, 1688, 1586, 1511, 1482, 1444, 1289, 1211, 1182, 1104, 982, 840; **HRMS** (ESI$^+$): m/z calc.: 449.1130 [M-H]$^-$, found: 449.1106; **R_f**: 0.64 (CH_2Cl_2/MeOH 9:1 v/v).

4-(4-Bromo-3-(trifluoromethyl)phenyl)morpholine 134

The reaction was carried out according to general procedure I with 1-bromo-4-iodo- 2-(trifluoromethyl)benzene **139** (1.00 g, 2.85 mmol), copper iodide (109 mg, 570 µmol), L-proline (131 mg, 1.14 mmol), potassium carbonate (788 mg, 5.70 mmol) and morpholine (370 µL, 4.28 mmol) in DMSO (6 mL) for 24 h. The crude product was purified by column chromatography (CH_2Cl_2/PE 1:1 v/v) to give **134** (627 mg, 2.02 mmol, 71%) as a colorless solid.

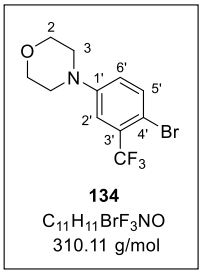

134
$C_{11}H_{11}BrF_3NO$
310.11 g/mol

^{1}H-NMR (500 MHz, $CDCl_3$): δ [ppm] = 7.53 (d, $^3J_{H\text{-}H}$ = 8.8 Hz, 1H, H-5'), 7.17 (d, $^4J_{H\text{-}H}$ = 3.0 Hz, H-2'), 6.87 (dd, $^3J_{H\text{-}H}$ = 8.8 Hz, $^4J_{H\text{-}H}$ = 3.0 Hz, H-6'), 3.89-3.83 (m, 4H, H-2), 3.20-3.14 (m, 4H, H-3); **^{13}C-NMR** (126 MHz, $CDCl_3$): δ [ppm] = 150.3 (C-1'), 135.5 (C-5'), 130.0 (C-3'), 123.2 (*C*F_3), 119.4 (C-6'), 114.7 (C-2'), 108.6 (C-4'), 66.7 (C-2), 48.7 (C-3); **^{19}F-NMR** (565 MHz, $CDCl_3$): δ [ppm] = −62.7 (C*F*$_3$); **ATR-IR** (neat): $\tilde{\nu}$ [cm^{-1}] = 2971, 2867, 2840, 1601, 1425, 1302, 1239, 1108, 949, 849, 809, 658; **MS** (EI): m/z calc.: 309.00 [M]$^+$, found: 309.00; **R_f**: 0.64 (CH_2Cl_2/PE 1:1 v/v).

4-(3-(Trifluoromethyl)-4-((trimethylsilyl)ethynyl)phenyl)morpholine 193

The reaction was performed according to general procedure II with 4-(4-bromo-3-(trifluoromethyl)phenyl)morpholine **134** (598 mg, 1.93 mmol), copper iodide (36.7 mg, 193 µmol), $Pd(PPh_3)_4$ (223 mg, 193 µmol) and TMS acetylene (720 µL, 5.21 mmol) in triethylamine (6 mL) and THF (3 mL) at 70 °C for 24 h. After pre-purification by column chro-

matography (PE/EA 9:1 v/v), the crude product was finally purified by preparative TLC (PE/EA 17:3 v/v) to yield **193** (162 mg, 493 µmol, 26%) as a yellow oil.

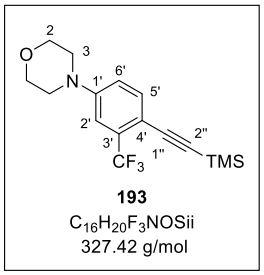

193
$C_{16}H_{20}F_3NOSii$
327.42 g/mol

^{1}H-NMR (400 MHz, $CDCl_3$): δ [ppm] = 7.47 (d, $^3J_{H\text{-}H}$ = 8.7 Hz, 1H, H-5'), 7.08 (d, $^4J_{H\text{-}H}$ = 2.6 Hz, H-2'), 6.90 (dd, $^3J_{H\text{-}H}$ = 8.7 Hz, $^4J_{H\text{-}H}$ = 2.6 Hz, H-6'), 3.88-3.82 (m, 4H, H-2), 3.25-3.20 (m, 4H, H-3), 0.24 (s, 9H, Si(CH_3)$_3$); **^{13}C-NMR** (101 MHz, $CDCl_3$): δ [ppm] = 150.5 (C-1'), 135.5 (C-5'), 133.3 (C-3'), 123.6 (CF_3), 116.8 (C-6'), 112.1 (C-2'), 111.3 (C-4'), 101.3 (C-1''), 98.3 (C-2''), 66.7 (C-2), 48.2 (C-3), −0.10 (Si(CH_3)$_3$); **^{19}F-NMR** (565 MHz, $CDCl_3$): δ [ppm] = −62.5 (CF_3); **ATR-IR** (neat): $\tilde{\nu}$ [cm^{-1}] = 2963, 2854, 2154, 1162, 1439, 1307, 1250, 1108, 950, 760; **MS** (EI): m/z calc.: 327.13 $[M]^+$, found: 327.10; **R_f**: 0.35 (PE/EA 9:1 v/v).

4-(4-Ethynyl-3-(trifluoromethyl)phenyl)morpholine 200

The cleavage of the protecting group was performed according to general procedure III by treating **193** (225 mg, 686 µmol) with potassium carbonate (474 mg, 3.43 mmol) in methanol (6 mL) for 4 h. Alkyne **200** (150 mg, 589 µmol, 86%) was obtained as a brown oil.

Due to the low stability of the alkyne, only one representative ^{1}H-NMR spectrum could be obtained.

^{1}H-NMR (300 MHz, $CDCl_3$): δ [ppm] = 7.52 (d, $^3J_{H\text{-}H}$ = 8.6 Hz, 1H, H-5'), 7.11 (d, $^4J_{H\text{-}H}$ = 2.7 Hz, H-2'), 6.93 (dd, $^3J_{H\text{-}H}$ = 8.6 Hz, $^4J_{H\text{-}H}$ = 2.7 Hz, H-6'), 3.92-3.81 (m, 4H, H-2), 3.28-3.20 (m, 5H, H-3, H-2'').

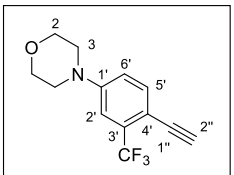

200
$C_{13}H_{12}F_3NO$
255.24 g/mol

Methyl 5-((4-morpholino-2-(trifluoromethyl)phenyl)ethynyl)-2-propionamidobenzoate 241

According to general procedure IV, the reaction was performed with anthranilic acid **90** (130 mg, 390 µmol), copper iodide (7.4 mg, 39 µmol), $Pd(PPh_3)_4$ (45.1 mg, 39.0 µmol) and alkyne **200** (149 mg, 585 µmol) in triethylamine (3 mL) and THF (2 mL) at room temperature for 4 h. Purification by column chromatography (CH_2Cl_2/acetone 50:1 v/v) afforded **241** (180 mg, 390 µmol, 100%) as an orange solid.

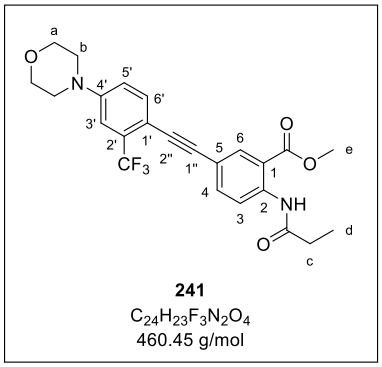

^{1}H-NMR (400 MHz, $CDCl_3$): δ [ppm] = 11.14 (s, 1H, CON*H*), 8.75 (d, $^3J_{H\text{-}H}$ = 8.8 Hz, 1H, H-3), 8.17 (d, $^4J_{H\text{-}H}$ = 2.1 Hz, 1H, H-6), 7.65 (dd, $^3J_{H\text{-}H}$ = 8.8 Hz, $^4J_{H\text{-}H}$ = 2.1 Hz, 1H, H-4), 7.53 (d, $^3J_{H\text{-}H}$ = 8.7 Hz, 1H, H-6'), 7.14 (d, $^4J_{H\text{-}H}$ = 2.6 Hz, H-3'), 6.97 (dd, $^3J_{H\text{-}H}$ = 8.7 Hz, $^4J_{H\text{-}H}$ = 2.6 Hz, H-5'), 3.95 (s, 3H, H-e), 3.91-3.82 (m, 4H, H-a), 3.30-3.22 (m, 4H, H-b), 2.49 (q, $^3J_{H\text{-}H}$ = 7.5 Hz, 2H, H-c), 1.28 (t, $^3J_{H\text{-}H}$ = 7.6 Hz, 3H, H-d); **^{13}C-NMR** (101 MHz, $CDCl_3$): δ [ppm] = 173.0 (*C*ONH), 168.4 (*C*OOMe), 150.4 (C-4'), 141.5 (C-2), 137.4 (C-4), 135.1 (C-6'), 134.0 (C-6), 132.6 (C-2'), 123.6 (*C*F_3), 120.4 (C-3), 117.5 (C-1), 117.1 (C-5'), 114.9 (C-5), 112.2 (C-3'), 111.1 (C-1'), 91.8 (C-1''), 86.0 (C-2''), 66.7 (C-a), 52.7 (C-e), 48.2 (C-b), 31.9 (C-c), 9.65 (C-d); **^{19}F-NMR** (565 MHz, $CDCl_3$): δ [ppm] = −62.4 (C*F*$_3$); **ATR-IR** (neat): $\tilde{\nu}$ [cm^{-1}] = 3262, 2957, 2920, 2855, 1682, 1588, 1509, 1439, 1304, 1253, 1234, 1106, 950, 812, 790; **HRMS** (ESI$^+$): m/z calc.: 461.1683 $[M+H]^+$, found: 461.1710; **R_f**: 0.44 (CH_2Cl_2/acetone 50:1 v/v).

5-((4-Morpholino-2-(trifluoromethyl)phenyl)ethynyl)-2-propionamidobenzoic acid 58

The saponification was carried out as described in general procedure V with methyl ester **241** (160 mg, 347 µmol) and aqueous 1.0 M NaOH (1.5 mL) in THF (4 mL) for 16 h. After precipitation in acidic solution, target compound **58** (147 mg, 330 µmol, 95%) was obtained as a yellowish solid.

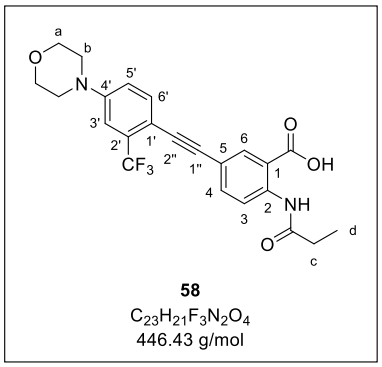

^{1}H-NMR (600 MHz, DMSO-*d*6): δ [ppm] = 11.31 (s, 1H, CON*H*), 8.58 (d, $^3J_{H\text{-}H}$ = 8.7 Hz, 1H, H-3), 8.03 (d, $^4J_{H\text{-}H}$ = 2.1 Hz, 1H, H-6), 7.66 (dd, $^3J_{H\text{-}H}$ = 8.7 Hz, $^4J_{H\text{-}H}$ = 2.1 Hz, 1H, H-4), 7.61 (d, $^3J_{H\text{-}H}$ = 8.7 Hz, 1H, H-6'), 7.23 (d, $^4J_{H\text{-}H}$ = 2.6 Hz, H-3'), 7.20 (dd, $^3J_{H\text{-}H}$ = 8.7 Hz, $^4J_{H\text{-}H}$ = 2.6 Hz, H-5'), 3.76-3.70 (m, 4H, H-a), 3.30-3.26 (m, 4H, H-b), 2.43 (q, $^3J_{H\text{-}H}$ = 7.6 Hz, 2H, H-c), 1.13 (t, $^3J_{H\text{-}H}$ = 7.6 Hz, 3H, H-d); **^{13}C-NMR** (151 MHz, DMSO-*d*6): δ [ppm] = 172.2 (*C*ONH), 168.8 (*C*OOH), 150.4 (C-4'), 140.9 (C-2), 136.0 (C-4), 135.0 (C-6'), 133.6 (C-6), 130.8 (C-2'), 123.8 (*C*F_3), 120.7 (C-3), 117.1 (C-5'), 116.9 (C-1), 116.2 (C-5), 111.1 (C-3'), 108.3 (C-1'), 91.2 (C-1''), 85.8 (C-2''), 65.8 (C-a), 47.0 (C-b), 30.7 (C-c), 9.25 (C-d); **^{19}F-NMR** (565 MHz, DMSO-*d*6): δ [ppm] = −60.9 (C*F*$_3$); **ATR-IR** (neat): $\tilde{\nu}$ [cm^{-1}] = 3327, 2967, 2850, 2824, 1672, 1581, 1520, 1306, 1293, 1253, 1236, 1123, 951, 834; **HRMS** (ESI$^+$): m/z calc.: 447.1526 $[M+H]^+$, found: 447.1541; **R_f**: 0.11 (CH_2Cl_2/MeOH 19:1 v/v).

1-(2-Bromo-5-iodophenyl)ethan-1-one 142

To a cooled solution of 1-(2-bromophenyl)ethan-1-one **141** (670 µL, 5.02 mmol, 1.00 eq.) in conc. sulfuric acid (10 mL), *N*-iodosuccinimide (1.13 g, 5.02 mmol, 1.00 eq.) was added in portions over a period of 10 min. After stirring for 16 h at room temperature, the reaction mixture was poured into ice-cooled water and extracted three times with ethyl acetate. The combined organic layers were washed two times with 10% aq. Na_2SO_3, water and sat. aq. NaCl and dried over Na_2SO_4 afterwards. All volatiles were removed in vacuo and the residue was purified by column chromatography (CH_2Cl_2/PE 1:1 v/v) to yield **142** (250 mg, 769 µmol, 15%) as a yellow oil.

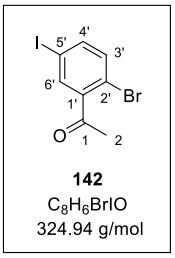

142
C_8H_6BrIO
324.94 g/mol

^{1}H-NMR (600 MHz, $CDCl_3$): δ [ppm] = 7.73 (d, $^4J_{H\text{-}H}$ = 2.1 Hz, 1H, H-6'), 7.59 (dd, $^3J_{H\text{-}H}$ = 8.3 Hz, $^4J_{H\text{-}H}$ = 2.1 Hz, 1H, H-4'), 7.33 (d, $^3J_{H\text{-}H}$ = 8.3 Hz, 1H, H-3'), 2.61 (s, 3H, H-2); **^{13}C-NMR** (151 MHz, $CDCl_3$): δ [ppm] = 199.8 (C-1), 143.3 (C-1'), 140.7 (C-4'), 137.6 (C-6'), 135.5 (C-3'), 118.8 (C-2'), 92.4 (C-5'), 30.4 (C-2); **ATR-IR** (neat): $\tilde{\nu}$ [cm^{-1}] = 3073, 3055, 2996, 1698, 1356, 1280, 1235, 1021, 968, 886, 807, 604, 550, 449; **HRMS** (ESI$^+$): m/z calc.: 324.8720 $[M+H]^+$, found: 324.8705; **R_f**: 0.31 (CH_2Cl_2/PE 1:1 v/v).

1-(2-Bromo-5-morpholinophenyl)ethan-1-one 135

The reaction was carried out according to general procedure I with 1-(2-bromo-5-iodophenyl)ethan-1-one **142** (480 mg, 1.48 mmol), copper iodide (56.3 mg, 296 µmol), L-proline (68.1 mg, 591 µmol), potassium carbonate (409 mg, 591 µmol) and morpholine (190 µL, 2.22 mmol) in DMSO (4 mL) for 24 h. Purification by column chromatography (CH_2Cl_2/acetone 100:1 v/v) provided **135** (140 mg, 493 mg, 33%) as a yellow oil.

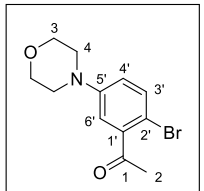

135
$C_{12}H_{14}BrNO_2$
284.15 g/mol

^{1}H-NMR (400 MHz, $CDCl_3$): δ [ppm] = 7.44 (d, $^3J_{H\text{-}H}$ = 8.8 Hz, 1H, H-3'), 6.93 (d, $^4J_{H\text{-}H}$ = 3.1 Hz, 1H, H-6'), 6.83 (dd, $^3J_{H\text{-}H}$ = 8.8 Hz, $^4J_{H\text{-}H}$ = 3.1 Hz, 1H, H-4'), 3.88-3.81 (m, 4H, H-3), 3.19-3.12 (m, 4H, H-4), 2.63 (s, 3H, H-2); **^{13}C-NMR** (101 MHz, $CDCl_3$): δ [ppm] = 202.2 (C-1), 150.5 (C-5'), 142.4 (C-1'), 134.3 (C-3'), 118.9 (C-4'), 115.7 (C-6'), 108.2 (C-2'), 66.7 (C-3), 48.9 (C-4), 30.6 (C-2); **ATR-IR** (neat): $\tilde{\nu}$ [cm^{-1}] = 2961, 2853, 1696, 1589, 1473, 1449, 1404, 1352, 1242, 1219, 1118, 936, 809; **MS** (EI): m/z calc.: 283.02 $[M]^+$, found: 283.00; **R_f**: 0.22 (CH_2Cl_2/acetone 100:1 v/v).

1-(5-Morpholino-2-((trimethylsilyl)ethynyl)phenyl)ethan-1-one 194

The reaction was performed according to general procedure II with 1-(2-bromo-5-morpholinophenyl)ethan-1-one **135** (239 mg, 842 µmol), copper iodide (16.0 mg, 84.2 µmol),

$Pd(PPh_3)_4$ (97.3 mg, 84.2 µmol) and TMS acetylene (310 µL, 2.27 mmol) in triethylamine (4 mL) and THF (1.5 mL) at 70 °C for 20 h. The crude product was purified by column chromatography (CH_2Cl_2/acetone 19:1 v/v) to give **194** (207 mg, 686 µmol, 81%) as a yellow oil.

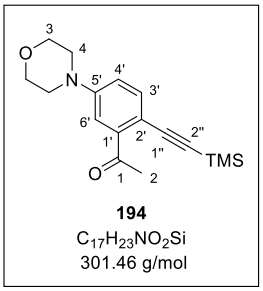

194
$C_{17}H_{23}NO_2Si$
301.46 g/mol

^{1}H-NMR (500 MHz, $CDCl_3$): δ [ppm] = 7.44 (d, $^3J_{H\text{-}H}$ = 8.6 Hz, 1H, H-3'), 7.16 (d, $^4J_{H\text{-}H}$ = 2.7 Hz, 1H, H-6'), 6.91 (dd, $^3J_{H\text{-}H}$ = 8.6 Hz, $^4J_{H\text{-}H}$ = 2.7 Hz, 1H, H-4'), 3.87-3.81 (m, 4H, H-3), 3.25-3.20 (m, 4H, H-4), 2.76 (s, 3H, H-2), 0.24 (s, 9H, Si(CH_3)$_3$); **^{13}C-NMR** (126 MHz, $CDCl_3$): δ [ppm] = 201.8 (C-1), 150.9 (C-5'), 142.6 (C-1'), 135.5 (C-3'), 117.4 (C-4'), 114.1 (C-6'), 111.1 (C-2'), 104.7 (C-1''), 99.1 (C-2''), 66.8 (C-3), 48.2 (C-4), 30.6 (C-2), −0.06 (Si(CH_3)$_3$); **ATR-IR** (neat): $\tilde{\nu}$ [cm^{-1}] = 2957, 2894, 2856, 2145, 1678, 1594, 1492, 1359, 1266, 1246, 1229, 1120, 935, 864, 836, 817; **HRMS** (ESI$^+$): m/z calc.: 302.1571 [M+H]$^+$, found: 302.1572; **R_f**: 0.51 (CH_2Cl_2/acetone 19:1 v/v).

Methyl 5-((2-acetyl-4-morpholinophenyl)ethynyl)-2-propionamidobenzoate 242

In a first step, the cleavage of the protecting group was performed according to general procedure III by treating **194** (393 mg, 1.31 mmol) with potassium carbonate (902 mg, 6.53 mmol) in methanol (12 mL) for 4 h. Due to the alkyne's instability, the washing step after solvent removal was omitted, and the crude product was used for the next synthesis step.

In a second step, the reaction was carried out as described in general procedure IV with anthranilic acid **90** (196 mg, 588 µmol), copper iodide (11.2 mg, 58.8 µmol), $Pd(PPh_3)_4$ (68.0 mg, 60.0 µmol) and crude alkyne **201** (216 mg, 647 µmol) in triethylamine (4 mL) and THF (3 mL) at room temperature for 4 h. Purification by column chromatography (CH_2Cl_2/acetone 9:1 v/v) provided **242** (50.1 mg, 115 µmol, 20%) as a yellow solid.

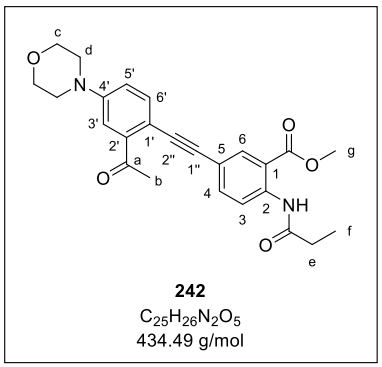

242
$C_{25}H_{26}N_2O_5$
434.49 g/mol

^{1}H-NMR (600 MHz, $CDCl_3$): δ [ppm] = 11.14 (s, 1H, CON*H*), 8.77 (d, $^3J_{H\text{-}H}$ = 8.8 Hz, 1H, H-3), 8.17 (d, $^4J_{H\text{-}H}$ = 2.1 Hz, 1H, H-6), 7.65 (dd, $^3J_{H\text{-}H}$ = 8.8 Hz, $^4J_{H\text{-}H}$ = 2.1 Hz, 1H, H-4), 7.51 (d, $^3J_{H\text{-}H}$ = 8.6 Hz, 1H, H-6'), 7.22 (d, $^4J_{H\text{-}H}$ = 2.7 Hz, 1H, H-3'), 6.98 (dd, $^3J_{H\text{-}H}$ = 8.6 Hz, $^4J_{H\text{-}H}$ = 2.7 Hz, 1H, H-5'), 3.95 (s, 3H, H-g), 3.89-3.84 (m, 4H, H-c), 3.28-3.24 (m, 4H, H-d), 2.80 (s, 3H, H-b), 2.50 (q, $^3J_{H\text{-}H}$ = 7.6 Hz, 2H, H-e), 1.29 (t, $^3J_{H\text{-}H}$ = 7.6 Hz, 3H, H-f); **^{13}C-NMR** (151 MHz, $CDCl_3$): δ [ppm] = 200.9 (C-a), 173.1 (*C*ONH), 168.2 (*C*OOMe), 150.6 (C-4'), 142.1 (C-2'), 141.6 (C-2), 137.2 (C-4), 135.2 (C-6'), 133.9 (C-6), 120.6 (C-3), 117.7 (C-5'), 117.5 (C-1), 114.4 (C-3'), 114.1 (C-5), 111.8 (C-1'), 92.4 (C-1''), 89.1 (C-2''), 66.8 (C-c), 52.7 (C-g), 48.3 (C-d), 31.9 (C-e), 30.4 (C-b), 9.66 (C-f); **ATR-IR** (neat): $\tilde{\nu}$ [cm^{-1}] = 3270, 2956, 2854, 2144, 1678, 1590, 1515, 1493,

1244, 1120, 935, 835; **HRMS** (ESI$^+$): m/z calc.: 435.1915 $[M+H]^+$, found: 435.1882; $\mathbf{R_f}$: 0.42 (CH_2Cl_2/acetone 9:1 v/v).

5-((2-Acetyl-4-morpholinophenyl)ethynyl)-2-propionamidobenzoic acid 59

According to general procedure V, the saponification was performed by treating methyl ester **242** (50.0 mg, 115 µmol) with aqueous 1.0 M NaOH (0.5 mL) in THF (3 mL) for 9 h. Precipitation in acidic solution afforded target compound **59** (13.8 mg, 32.8 µmol, 29%) as a yellowish solid.

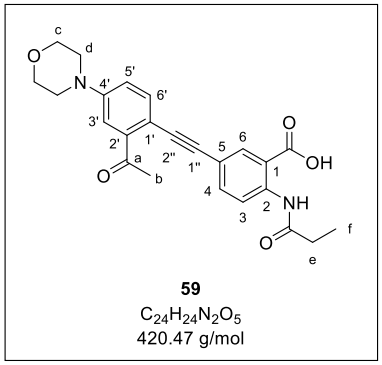

^{1}H-NMR (600 MHz, DMSO-*d*6): δ [ppm] = 13.91 (s, 1H, COO*H*), 11.27 (s, 1H, CON*H*), 8.56 (d, $^3J_{H\text{-}H}$ = 8.7 Hz, 1H, H-3), 8.05 (d, $^4J_{H\text{-}H}$ = 2.2 Hz, 1H, H-6), 7.68 (dd, $^3J_{H\text{-}H}$ = 8.7 Hz, $^4J_{H\text{-}H}$ = 2.2 Hz, 1H, H-4), 7.52 (d, $^3J_{H\text{-}H}$ = 8.6 Hz, 1H, H-6'), 7.26 (d, $^4J_{H\text{-}H}$ = 2.7 Hz, 1H, H-3'), 7.14 (dd, $^3J_{H\text{-}H}$ = 8.6 Hz, $^4J_{H\text{-}H}$ = 2.7 Hz, 1H, H-5'), 3.79-3.79 (m, 4H, H-c), 3.28-3.21 (m, 4H. H-d), 2.67 (s, 3H, H-b), 2.43 (q, $^3J_{H\text{-}H}$ = 7.5 Hz, 2H, H-e), 1.13 (t, $^3J_{H\text{-}H}$ = 7.5 Hz, 3H, H-f); **^{13}C-NMR** (151 MHz, DMSO-*d*6): δ [ppm] = 200.0 (C-a), 172.1 (*C*ONH), 168.8 (*C*OOH), 150.5 (C-4'), 141.6 (C-2'), 140.7 (C-2), 136.1 (C-4), 134.6 (C-6'), 133.6 (C-6), 120.0 (C-3), 117.0 (C-5'), 116.7 (C-1), 116.7 (C-5), 113.8 (C-3'), 109.1 (C-1'), 90.6 (C-1''), 89.1 (C-2''), 65.9 (C-c), 47.2 (C-d), 30.7 (C-e), 29.7 (C-b), 9.27 (C-f); **ATR-IR** (neat): $\tilde{\nu}$ [cm^{-1}] = 2966, 2829, 1680, 1591, 1513, 1291, 1206, 1118, 930, 851, 827, 794; **HRMS** (ESI$^+$): m/z calc.: 419.1612 $[M-H]^-$, found: 419.1602; $\mathbf{R_f}$: 0.38 (CH_2Cl_2/MeOH 19:1 v/v).

4-(4-Bromo-2-methoxyphenyl)morpholine 144

The reaction was carried out as described in general procedure VII with 4-bromo-1-iodo-2-methoxybenzene **149** (1.99 g, 6.36 mmol), morpholine (550 µL, 6.36 mmol), $Pd_2(dba)_3$ (175 mg, 191 µmol), xantphos (331 mg, 573 µmol) and NaOtBu (612 mg, 6.36 mmol) in toluene (40 mL) for 48 h. After purification by column chromatography (CH_2Cl_2), **144** (1.20 g, 4.41 mmol, 69%) was obtained as a yellowish solid.

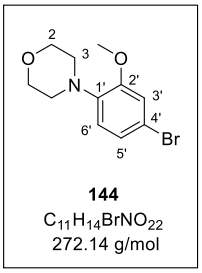

^{1}H-NMR (400 MHz, $CDCl_3$): δ [ppm] = 7.00 (dd, $^3J_{H\text{-}H}$ = 8.4 Hz, $^4J_{H\text{-}H}$ = 2.2 Hz, 1H, H-5'), 6.93 (d, $^4J_{H\text{-}H}$ = 2.2 Hz, 1H, H-3'), 6.72 (d, $^3J_{H\text{-}H}$ = 8.4 Hz, 1H, H-6'), 3.85-3.81 (m, 4H, H-2), 3.81 (s, 3H, OCH_3), 3.01-2.94 (m, 4H, H-3); **^{13}C-NMR** (101 MHz, $CDCl_3$): δ [ppm] = 152.9 (C-2'), 140.4 (C-1'), 123.8 (C-5'), 119.2 (C-6'), 115.4 (C-4'), 114.7 (C-3'), 67.0 (C-2), 55.7 (O*C*H$_3$), 51.0 (C-3); **ATR-IR** (neat): $\tilde{\nu}$ [cm^{-1}] = 2967, 2826, 1579, 1493, 1238, 1113,

1018, 849, 834, 808; **HRMS** (ESI$^+$): m/z calc.: 272.0281 $[M+H]^+$, found: 272.0256; $\mathbf{R_f}$: 0.38 (CH_2Cl_2).

4-(2-Methoxy-4-((trimethylsilyl)ethynyl)phenyl)morpholine 202

The reaction was performed according to general procedure II with 4-(4-bromo-2-methoxyphenyl)morpholine **144** (500 mg, 1.84 mmol), copper iodide (35.0 mg, 184 µmol), $Pd(PPh_3)_4$ (212 mg, 184 µmol) and TMS acetylene (690 µL, 4.96 mmol) in triethylamine (8 mL) and THF (3 mL) at 70 °C for 19 h. The crude product was purified by column chromatography (CH_2Cl_2/acetone 200:1 v/v) to yield **202** (435 mg, 1.50 mmol, 82%) as a colorless solid.

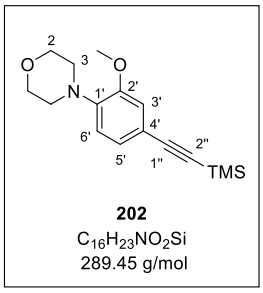

202
$C_{16}H_{23}NO_2Si$
289.45 g/mol

^{1}H-NMR (400 MHz, $CDCl_3$): δ [ppm] = 7.06 (dd, $^3J_{H-H}$ = 8.1 Hz, $^4J_{H-H}$ = 1.8 Hz, 1H, H-5'), 6.94 (d, $^4J_{H-H}$ = 1.8 Hz, 1H, H-3'), 6.80 (d, $^3J_{H-H}$ = 8.1 Hz, 1H, H-6'), 3.89-3.87 (m, 4H, H-2), 3.86 (s, 3H, OCH_3), 3.11-3.04 (m, 4H, H-3), 0.24 (s, 9 H, Si(CH_3)$_3$); **^{13}C-NMR** (101 MHz, $CDCl_3$): δ [ppm] = 151.7 (C-2'), 142.0 (C-1'), 125.6 (C-5'), 117.7 (C-6'), 117.3 (C-4'), 114.7 (C-3'), 105.5 (C-1''), 93.1 (C-2''), 67.2 (C-2), 55.6 (OCH_3), 51.0 (C-3), 0.24 (Si(CH_3)$_3$); **ATR-IR** (neat): $\tilde{\nu}$ [cm^{-1}] = 2960, 2157, 1505, 1446, 1248, 1229, 1167, 1114, 1031, 917, 840, 812, 758; **HRMS** (ESI$^+$): m/z calc.: 290.1571 $[M+H]^+$, found: 290.1569; $\mathbf{R_f}$: 0.26 (CH_2Cl_2/acetone 200:1 v/v).

4-(4-Ethynyl-2-methoxyphenyl)morpholine 206

The cleavage of the protecting group was carried out according to general procedure III by treating **202** (400 mg, 1.38 mmol) with potassium carbonate (955 mg, 6.91 mmol) in methanol (12 mL) for 4 h. Alkyne **206** (260 mg, 1.20 mmol, 87%) was isolated as a colorless solid.

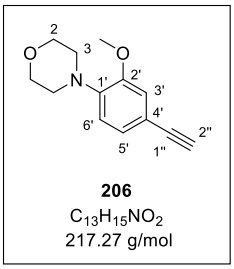

206
$C_{13}H_{15}NO_2$
217.27 g/mol

^{1}H-NMR (600 MHz, $CDCl_3$): δ [ppm] = 7.09 (dd, $^3J_{H-H}$ = 8.1 Hz, $^4J_{H-H}$ = 1.8 Hz, 1H, H-5'), 6.97 (d, $^4J_{H-H}$ = 1.8 Hz, 1H, H-3'), 6.82 (d, $^3J_{H-H}$ = 8.1 Hz, 1H, H-6'), 3.89-3.86 (m, 4H, H-2), 3.86 (s, 3H, OCH_3), 3.10-3.05 (m, 4H, H-3), 3.03 (s, 1H, H-2''); **^{13}C-NMR** (151 MHz, $CDCl_3$): δ [ppm] = 151.7 (C-2'), 142.2 (C-1'), 125.7 (C-5'), 117.8 (C-6'), 116.2 (C-4'), 114.9 (C-3'), 84.0 (C-1''), 76.3 (C-2''), 67.2 (C-2), 55.6 (OCH_3), 51.0 (C-3); **ATR-IR** (neat): $\tilde{\nu}$ [cm^{-1}] = 2962, 2857, 1505, 1252, 1225, 1109, 1028, 907, 846, 816, 734, 618; **HRMS** (ESI$^+$): m/z calc.: 218.1176 $[M+H]^+$, found: 218.1177; $\mathbf{R_f}$: 0.23 (CH_2Cl_2/acetone 200:1 v/v).

Methyl 5-((3-methoxy-4-morpholinophenyl)ethynyl)-2-propionamidobenzoate 243

According to general procedure IV, the reaction was carried out with anthranilic acid **90** (195 mg, 585 µmol), copper iodide (11.1 mg, 58.5 µmol), $Pd(PPh_3)_4$ (67.6 mg, 58.5 µmol) and alkyne **206** (140 mg, 585 µmol) in triethylamine (4 mL) and THF (3 mL) at room temperature for 19 h. Purification by column chromatography (CH_2Cl_2/acetone 200:1 v/v) provided **243** (230 mg, 545 µmol, 93%) as a yellowish solid.

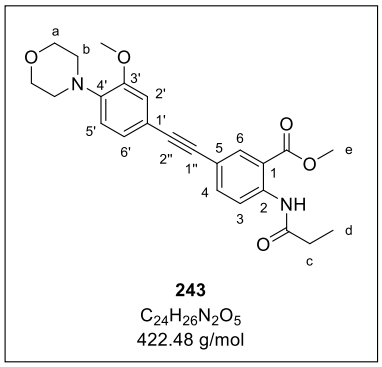

^{1}H-NMR (400 MHz, $CDCl_3$): δ [ppm] = 11.12 (s, 1H, CON*H*), 8.75 (d, $^3J_{H\text{-}H}$ = 8.8 Hz, 1H, H-3), 8.19 (d, $^4J_{H\text{-}H}$ = 2.1 Hz, 1H, H-6), 7.66 (dd, $^3J_{H\text{-}H}$ = 8.8 Hz, $^4J_{H\text{-}H}$ = 2.1 Hz, 1H, H-4), 7.12 (dd, $^3J_{H\text{-}H}$ = 8.1 Hz, $^4J_{H\text{-}H}$ = 1.8 Hz, 1H, H-6'), 7.01 (d, $^4J_{H\text{-}H}$ = 1.8 Hz, 1H, H-2'), 6.86 (d, $^3J_{H\text{-}H}$ = 8.1 Hz, 1H, H-5'), 3.94 (s, 3H, H-e), 3.91-3.95 (m, 7H, H-a, OCH_3), 3.13.3-07 (m, 4H, H-b), 2.49 (q, $^3J_{H\text{-}H}$ = 7.6 Hz, 2H, H-c), 1.28 (t, $^3J_{H\text{-}H}$ = 7.6 Hz, 3H, H-d); **^{13}C-NMR** (101 MHz, $CDCl_3$): δ [ppm] = 173.0 (*C*ONH), 168.4 (*C*OOMe), 151.9 (C-3'), 141.8 (C-4'), 141.3 (C-2), 137.4 (C-4), 134.1 (C-6), 125.1 (C-6'), 120.5 (C-3), 117.9 (C-5'), 117.7 (C-1), 117.2 (C-1'), 114.9 (C-5), 114.4 (C-2'), 89.7 (C-2''), 87.5 (C-1''), 67.2 (C-a), 55.7 (O*C*H_3), 52.6 (C-e), 51.0 (C-b), 31.9 (C-c), 9.67 (C-d); **ATR-IR** (neat): $\tilde{\nu}$ [cm^{-1}] = 2948, 2835, 1684, 1586, 1510, 1430, 1217, 1188, 1113, 1082, 1033, 845, 815, 789; **HRMS** (ESI$^+$): m/z calc.: 423.1915 $[M+H]^+$, found: 423.1978; **R_f**: 0.14 (CH_2Cl_2/acetone 200:1 v/v).

5-((3-Methoxy-4-morpholinophenyl)ethynyl)-2-propionamidobenzoic acid 60

The saponification was performed according to general procedure V by treating methyl ester **243** (200 mg, 473 µmol) with aqueous 1.0 M NaOH (2 mL) in THF (5 mL) for 16 h. After precipitation in acidic solution, target compound **60** (138 mg, 338 µmol, 71%) was obtained as a colorless solid.

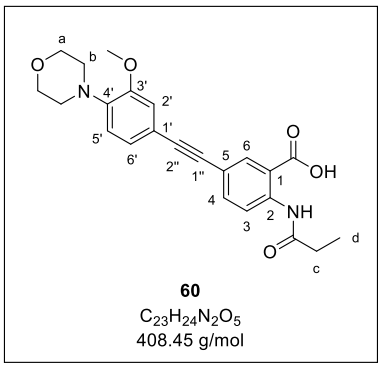

^{1}H-NMR (600 MHz, DMSO-*d*6): δ [ppm] = 13.89 (s, 1H, COO*H*), 11.19 (s,1H, CON*H*), 8.57 (d, $^3J_{H\text{-}H}$ = 8.7 Hz, 1H, H-3), 8.08 (d, $^4J_{H\text{-}H}$ = 2.2 Hz, 1H, H-6), 7.71 (dd, $^3J_{H\text{-}H}$ = 8.7 Hz, $^4J_{H\text{-}H}$ = 2.2 Hz, 1H, H-4), 7.13-7.08 (m, 2H, H-6', H-2'), 6.89 (d, $^3J_{H\text{-}H}$ = 8.6 Hz, 1H, H-5'), 3.83 (s, 3H, OCH_3), 3.74-3.70 (m, 4H, H-a), 3.04-2.98 (m, 4H, H-b), 2.43 (q, $^3J_{H\text{-}H}$ = 7.5 Hz, 2H, H-c), 1.13 (t, $^3J_{H\text{-}H}$ = 7.5 Hz, 3H, H-d); **^{13}C-NMR** (151 MHz, DMSO-*d*6): δ [ppm] = 172.2 (*C*ONH), 168.9 (*C*OOH), 151.5 (C-3'), 141.7 (C-4'), 140.7 (C-2), 136.3 (C-4), 133.8 (C-6), 124.6 (C-6'), 120.0 (C-3), 117.8 (C-5'), 116.5 (C-1), 116.5 (C-5), 115.6 (C-1'), 114.4 (C-2'), 89.8 (C-2''), 87.2 (C-1''),

66.2 (C-a), 55.6 (O*C*H$_3$), 50.3 (C-b), 30.7 (C-c), 9.27 (C-d); **ATR-IR** (neat): $\tilde{\nu}$ [cm^{-1}] = 2945, 2833, 1703, 1672, 1588, 1511, 1289, 1182, 1116, 926, 886, 840; **HRMS** (ESI$^+$): m/z calc.: 407.1612 [M-H]$^-$, found: 407.1614; **R$_f$**: 0.19 (CH_2Cl_2/MeOH 19:1 v/v).

4-Bromo-2-ethoxy-1-iodobenzene 150

To a solution of 5-bromo-2-iodophenol **148** (1.00 g, 3.35 mmol, 1.0 eq) in acetone (13 mL), ethyl iodide (540 µL, 6.69 mmol, 2.0 eq.) and K_2CO_3 (925 mg, 6.69 mmol, 2.0 eq.) were added and the resulting mixture was stirred at room temperature for 16 h. K_2CO_3 was removed by filtration and after evaporation of the solvent, the residue was purified by column chromatography (PE) to give **150** (964 mg, 2.95 mmol, 88%) as a colorless oil.

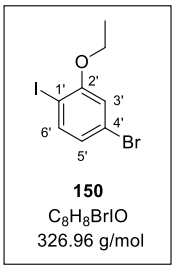

150
C_8H_8BrIO
326.96 g/mol

^{1}H-NMR (400 MHz, $CDCl_3$): δ [ppm] = 7.60 (d, $^3J_{H\text{-}H}$ = 8.3 Hz, 1H, H-6'), 6.91 (d, $^4J_{H\text{-}H}$ = 2.1 Hz, 1H, H-3'), 6.84 (dd, $^3J_{H\text{-}H}$ = 8.3 Hz, $^4J_{H\text{-}H}$ = 2.1 Hz, 1H, H-5'), 4.07 (q, $^3J_{H\text{-}H}$ = 7.0 Hz, 2H, OC*H*$_2$), 1.38 (t, $^3J_{H\text{-}H}$ = 7.0 Hz, 3H, C*H*$_3$); **^{13}C-NMR** (101 MHz, $CDCl_3$): δ [ppm] = 158.5 (C-2'), 140.3 (C-6'), 125.5 (C-5'), 123.0 (C-4'), 115.7 (C-3'), 85.0 (C-1'), 65.4 (O*C*H$_2$), 14.7 (*C*H$_3$); **ATR-IR** (neat): $\tilde{\nu}$ [cm^{-1}] = 2980, 2930, 2882, 1568, 1462, 1384, 1245, 1039, 1013, 933, 840, 793; **HRMS** (ESI$^+$): m/z calc.: 281.8536 [M−OEt+H]$^+$, found: 282.2827; **R$_f$**: 0.63 (PE).

4-(4-Bromo-2-ethoxyphenyl)morpholine 145

The reaction was carried out according to general procedure VII with 4-bromo-2-ethoxy-1-iodobenzene **150** (940 mg, 2.88 mmol), morpholine (250 µL, 2.88 mmol), $Pd_2(dba)_3$ (79.0 mg, 86.2 µmol), xantphos (150 mg, 259 µmol) and NaOtBu (276 mg, 2.88 mmol) in toluene (18 mL) for 48 h. After purification by column chromatography (CH_2Cl_2/acetone 100:1 v/v), **145** (327 mg, 1.14 mmol, 40%) was isolated as a yellow wax.

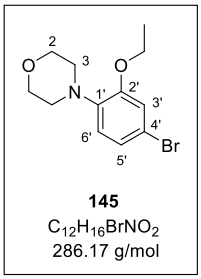

145
$C_{12}H_{16}BrNO_2$
286.17 g/mol

^{1}H-NMR (400 MHz, $CDCl_3$): δ [ppm] = 7.03 (dd, $^3J_{H\text{-}H}$ = 8.4 Hz, $^4J_{H\text{-}H}$ = 2.2 Hz, 1H, H-5'), 6.96 (d, $^4J_{H\text{-}H}$ = 2.2 Hz, 1H, H-3'), 6.75 (d, $^3J_{H\text{-}H}$ = 8.4 Hz, 1H, H-6'), 4.05 (q, $^3J_{H\text{-}H}$ = 7.0 Hz, 2H, OC*H*$_2$), 3.90-3.83 (m, 4H, H-2), 3.08-3.01 (m, 4H, H-3), 1.45 (t, $^3J_{H\text{-}H}$ = 7.0 Hz, 3H, C*H*$_3$); **^{13}C-NMR** (101 MHz, $CDCl_3$): δ [ppm] = 152.4 (C-2'), 140.5 (C-1'), 123.9 (C-5'), 119.3 (C-6'), 116.0 (C-4'), 115.4 (C-3'), 67.2 (C-2), 64.2 (O*C*H$_2$), 51.1 (C-3), 14.9 (*C*H$_3$); **ATR-IR** (neat): $\tilde{\nu}$ [cm^{-1}] = 2970, 2858, 2817, 1580, 1495, 1397, 1242, 1220, 1113, 1040, 917, 852, 838, 800; **HRMS** (ESI$^+$): m/z calc.: 286.0437 [M+H]$^+$, found: 286.0560; **R$_f$**: 0.17 (CH_2Cl_2/acetone 100:1 v/v).

4-(2-Ethoxy-4-((trimethylsilyl)ethynyl)phenyl)morpholine 203

The reaction was performed according to general procedure II with 4-(4-bromo-2-ethoxyphenyl)morpholine **145** (400 mg, 1.40 mmol), copper iodide (26.6 mg, 140 µmol), $Pd(PPh_3)_4$ (162 mg, 140 µmol) and TMS acetylene (520 µL, 3.77 mmol) in triethylamine (6 mL) and THF (2 mL) at 70 °C for 20 h. Purification by column chromatography (CH_2Cl_2/acetone 100:1 v/v) provided **203** (288 mg, 949 µmol, 68%) as a colorless solid.

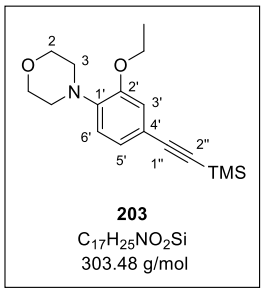

203
$C_{17}H_{25}NO_2Si$
303.48 g/mol

^{1}H-NMR (600 MHz, $CDCl_3$): δ [ppm] = 7.05 (dd, $^3J_{H\text{-}H}$ = 8.1 Hz, $^4J_{H\text{-}H}$ = 1.8 Hz, 1H, H-5'), 6.93 (d, $^4J_{H\text{-}H}$ = 1.8 Hz, 1H, H-3'), 6.78 (d, $^3J_{H\text{-}H}$ = 8.1 Hz, 1H, H-6'), 4.06 (q, $^3J_{H\text{-}H}$ = 7.0 Hz, 2H, OCH_2), 3.89-3.85 (m, 4H, H-2), 3.12-3.07 (m, 4H, H-3), 1.45 (t, $^3J_{H\text{-}H}$ = 7.0 Hz, 3H, CH_3), 0.24 (s, 9 H, Si(CH_3)$_3$); **^{13}C-NMR** (151 MHz, $CDCl_3$): δ [ppm] = 151.0 (C-2'), 142.0 (C-1'), 125.5 (C-5'), 117.7 (C-6'), 117.1 (C-4'), 115.8 (C-3'), 105.6 (C-1''), 92.9 (C-2''), 67.2 (C-2), 63.9 (OCH_2), 51.0 (C-3), 15.0 (CH_3), 0.21 (Si(CH_3)$_3$); **ATR-IR** (neat): $\tilde{\nu}$ [cm^{-1}] = 1972, 2856, 2818, 2144, 1507, 1260, 1249, 1226, 1178, 1132, 1045, 920, 840, 761, 621; **HRMS** (ESI$^+$): m/z calc.: 304.1728 $[M+H]^+$, found: 304.1728; **R_f**: 0.31 (CH_2Cl_2/acetone 100:1 v/v).

4-(2-Ethoxy-4-ethynylphenyl)morpholine 207

The cleavage of the protecting group was performed according to general procedure III by treating **203** (260 mg, 857 µmol) with potassium carbonate (592 mg, 4.28 mmol) in methanol (8 mL) for 4 h. Alkyne **207** (173 mg, 748 µmol, 87%) was obtained as a colorless solid.

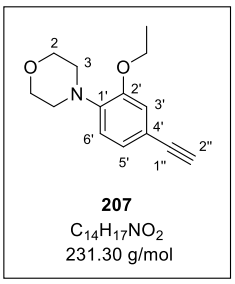

207
$C_{14}H_{17}NO_2$
231.30 g/mol

^{1}H-NMR (600 MHz, $CDCl_3$): δ [ppm] = 7.08 (dd, $^3J_{H\text{-}H}$ = 8.1 Hz, $^4J_{H\text{-}H}$ = 1.8 Hz, 1H, H-5'), 6.96 (d, $^4J_{H\text{-}H}$ = 1.8 Hz, 1H, H-3'), 6.81 (d, $^3J_{H\text{-}H}$ = 8.1 Hz, 1H, H-6'), 4.06 (q, $^3J_{H\text{-}H}$ = 7.0 Hz, 2H, OCH_2), 3.90-3.84 (m, 4H, H-2), 3.11 (s, 1H, H-2''), 3.13-3.08 (m, 4H, H-3), 1.45 (t, $^3J_{H\text{-}H}$ = 7.0 Hz, 3H, CH_3); **^{13}C-NMR** (151 MHz, $CDCl_3$): δ [ppm] = 151.1 (C-2'), 142.2 (C-1'), 125.6 (C-5'), 117.8 (C-6'), 116.0 (C-4'), 116.0 (C-3'), 84.1 (C-1''), 76.2 (C-2''), 67.2 (C-2), 64.0 (OCH_2), 51.0 (C-3), 15.0 (CH_3); **ATR-IR** (neat): $\tilde{\nu}$ [cm^{-1}] = 3220, 2959, 2852, 1506, 1252, 1206, 1161, 1131, 1111, 1040, 920,848, 829, 617; **HRMS** (ESI$^+$): m/z calc.: 232.1332 $[M+H]^+$, found: 232.1336; **R_f**: 0.41 (CH_2Cl_2/acetone 100:1 v/v).

Methyl 5-((3-ethoxy-4-morpholinophenyl)ethynyl)-2-propionamidobenzoate 244

The reaction was carried out as described in general procedure IV with anthranilic acid **90** (200 mg, 600 µmol), copper iodide (11.4 mg, 60.0 µmol), $Pd(PPh_3)_4$ (69.4 mg, 60.0 µmol) and alkyne **207** (153 mg, 660 µmol) in triethylamine (4 mL) and THF (3 mL) at room temperature

for 19 h. Purification by column chromatography (CH_2Cl_2/acetone 200:1 v/v) afforded **244** (233 mg, 534 µmol, 89%) as a colorless solid.

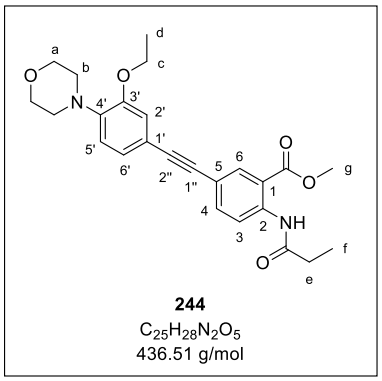

^{1}H-NMR (600 MHz, $CDCl_3$): δ [ppm] = 11.14 (s, 1H, CON*H*), 8.76 (d, $^3J_{H\text{-}H}$ = 8.8 Hz, 1H, H-3), 8.21 (d, $^4J_{H\text{-}H}$ = 2.1 Hz, 1H, H-6), 7.68 (dd, $^3J_{H\text{-}H}$ = 8.8 Hz, $^4J_{H\text{-}H}$ = 2.1 Hz, 1H, H-4), 7.12 (dd, $^3J_{H\text{-}H}$ = 8.1 Hz, $^4J_{H\text{-}H}$ = 1.8 Hz, 1H, H-6'), 7.02 (d, $^4J_{H\text{-}H}$ = 1.8 Hz, 1H, H-2'), 6.86 (d, $^3J_{H\text{-}H}$ = 8.1 Hz, 1H, H-5'), 4.11 (q, $^3J_{H\text{-}H}$ = 7.0 Hz, 2H, H-c), 3.96 (s, 3H, H-g), 3.93-3.87 (m, 4H, H-a), 3.17-3.12 (m, 4H, H-b), 2.51 (q, $^3J_{H\text{-}H}$ = 7.6 Hz, 2H, H-e), 1.49 (t, $^3J_{H\text{-}H}$ = 7.0 Hz, 3H, H-d), 1.30 (t, $^3J_{H\text{-}H}$ = 7.6 Hz, 3H, H-f); **^{13}C-NMR** (151 MHz, $CDCl_3$): δ [ppm] = 173.0 (*C*ONH), 168.4 (*C*OOMe), 151.2 (C-3'), 141.9 (C-4'), 141.3 (C-2), 137.4 (C-4), 134.1 (C-6), 125.0 (C-6'), 120.5 (C-3), 117.9 (C-5'), 117.7 (C-1), 117.0 (C-1'), 115.5 (C-2'), 115.0 (C-5), 89.8 (C-2''), 87.4 (C-1''), 67.2 (C-a), 64.0 (C-c), 52.6 (C-b), 51.0 (C-g), 31.9 (C-e), 15.0 (C-d), 9.68 (C-g); **ATR-IR** (neat): $\tilde{\nu}$ [cm^{-1}] = 3266, 2958, 1685, 1589, 1515, 1229, 1218, 1191, 1169, 1120, 920, 842, 788; **HRMS** (ESI$^+$): m/z calc.: 437.2071 $[M+H]^+$, found: 437.2143; **R_f**: 0.20 (CH_2Cl_2/acetone 100:1 v/v).

5-((3-Ethoxy-4-morpholinophenyl)ethynyl)-2-propionamidobenzoic acid 61

The saponification was carried out according to general procedure V by treating methyl ester **244** (210 mg, 481 µmol) with aqueous 1.0 M NaOH (2 mL) in THF (5 mL) for 16 h. Precipitation in acidic solution afforded target compound **61** (162 mg, 383 µmol, 80%) as a colorless solid.

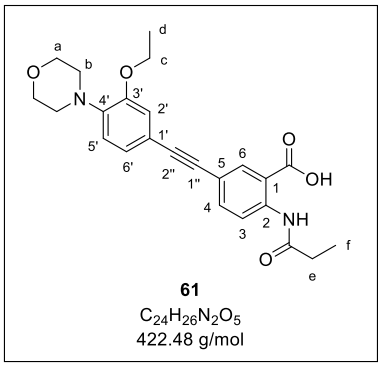

^{1}H-NMR (600 MHz, DMSO-*d*6): δ [ppm] = 13.90 (s, 1H, COO*H*), 11.20 (s, 1H, CON*H*), 8.57 (d, $^3J_{H\text{-}H}$ = 8.7 Hz, 1H, H-3), 8.07 (d, $^4J_{H\text{-}H}$ = 2.2 Hz, 1H, H-6), 7.70 (dd, $^3J_{H\text{-}H}$ = 8.7 Hz, $^4J_{H\text{-}H}$ = 2.2 Hz, 1H, H-4), 7.13-7.06 (m, 2H, H-6', H-2'), 6.86 (d, $^3J_{H\text{-}H}$ = 8.2 Hz, 1H, H-5'), 4.06 (q, $^3J_{H\text{-}H}$ = 6.9 Hz, 2H, H-c), 3.74-3.69 (m, 4H, H-a), 3.06-3.01 (m, 4H, H-b), 2.43 (q, $^3J_{H\text{-}H}$ = 7.5 Hz, 2H, H-e), 1.35 (t, $^3J_{H\text{-}H}$ = 6.9 Hz, 3H, H-d), 1.13 (t, $^3J_{H\text{-}H}$ = 7.5 Hz, 3H, H-f); **^{13}C-NMR** (151 MHz, DMSO-*d*6): δ [ppm] = 172.2 (*C*ONH), 168.9 (*C*OOH), 150.6 (C-3'), 141.6 (C-4'), 140.7 (C-2), 136.3 (C-4), 133.8 (C-6), 124.6 (C-6'), 120.0 (C-3), 117.8 (C-5'), 116.5 (C-1), 116.5 (C-5), 115.4 (C-2'), 115.3 (C-1'), 89.8 (C-2''), 87.1 (C-1''), 66.2 (C-a), 63.5 (C-c), 50.2 (C-b), 30.7 (C-e), 14.7 (C-d), 9.27 (C-g); **ATR-IR** (neat): $\tilde{\nu}$ [cm^{-1}] = 2972, 1682, 1591, 1518, 1290, 1208, 1191, 1110, 1046, 914, 846; **HRMS** (ESI$^+$): m/z calc.: 421.1769 $[M-H]^-$, found: 421.1776; **R_f**: 0.20 (CH_2Cl_2/MeOH 19:1 v/v).

4-Bromo-1-iodo-2-isopropoxybenzene 151

To a solution of 5-bromo-2-iodophenol **148** (1.00 g, 3.35 mmol, 1.0 eq) in DMF (8 mL), 2-bromopropane (380 µL, 4.02 mmol, 1.2 eq.) and Cs_2CO_3 (2.73 g, 8.36 mmol, 2.5 eq.) were added and the resulting mixture was stirred at room temperature for 20 h. Cs_2CO_3 was removed by filtration and after evaporation of the solvent, the crude product was purified by column chromatography (CH_2Cl_2/PE 1:8 v/v) to yield **151** (964 mg, 2.83 mmol, 84%) as a colorless solid.

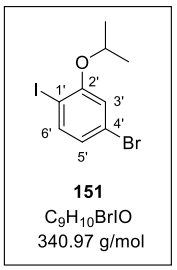

151
$C_9H_{10}BrIO$
340.97 g/mol

^{1}H-NMR (400 MHz, $CDCl_3$): δ [ppm] = 7.60 (d, $^3J_{H\text{-}H}$ = 8.3 Hz, 1H, H-6'), 6.93 (d, $^4J_{H\text{-}H}$ = 2.1 Hz, 1H, H-3'), 6.83 (dd, $^3J_{H\text{-}H}$ = 8.3 Hz, $^4J_{H\text{-}H}$ = 2.1 Hz, 1H, H-5'), 4.54 (sept, $^3J_{H\text{-}H}$ = 6.1 Hz, 1H, OC*H*), 1.39 (d, $^3J_{H\text{-}H}$ = 6.1 Hz, 6H, CH(CH_3)$_2$); **^{13}C-NMR** (101 MHz, $CDCl_3$): δ [ppm] = 157.7 (C-2'), 140.4 (C-6'), 125.6 (C-5'), 122.8 (C-4'), 117.5 (C-3'), 86.7 (C-1'), 72.7 (O*C*H), 22.1 (CH(*C*H_3)$_2$); **ATR-IR** (neat): $\tilde{\nu}$ [cm^{-1}] = 2976, 2931, 1567, 1461, 1386, 1243, 1104, 1015, 955, 876, 793; **HRMS** (ESI$^+$): m/z calc.: 281.8536 [M−iPr+H]$^+$, found: 282.2734; **R_f**: 0.45 (CH_2Cl_2/PE 1:8 v/v).

4-(2-Isopropoxy-4-((trimethylsilyl)ethynyl)phenyl)morpholine 204

The first reaction step was carried out as described in general procedure VII with 4-bromo-1-iodo-2-isopropoxybenzene **151** (930 mg, 2.73 mmol), morpholine (470 µL, 5.56 mmol), $Pd_2(dba)_3$ (125 mg, 136 µmol), xantphos (237 mg, 409 µmol) and NaOtBu (262 mg, 2.73 mmol) in toluene (18 mL) for 48 h. Purification by column chromatography (CH_2Cl_2/acetone 100:1 v/v) provided **146** (202 mg, 674 µmol, 25%) as a violet solid.

The second reaction step was carried out according to general procedure II with 4-(4-bromo-2-isopropoxyphenyl)morpholine **146** (293 mg, 976 µmol), copper iodide (18.6 mg, 97.6 µmol), $Pd(PPh_3)_4$ (113 mg, 97.6 µmol) and TMS acetylene (360 µL, 2.64 mmol) in triethylamine (4 mL) and THF (2 mL) at 70 °C for 20 h. After purification by column chromatography (CH_2Cl_2/acetone 100:1 v/v), **204** (253 mg, 798 µmol, 82%) was obtained as a yellowish solid.

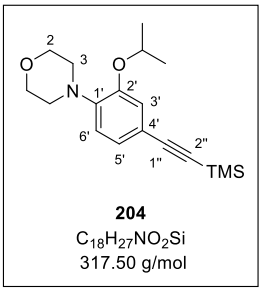

204
$C_{18}H_{27}NO_2Si$
317.50 g/mol

^{1}H-NMR (600 MHz, $CDCl_3$): δ [ppm] = 7.04 (dd, $^3J_{H\text{-}H}$ = 8.2 Hz, $^4J_{H\text{-}H}$ = 1.8 Hz, 1H, H-5'), 6.94 (d, $^4J_{H\text{-}H}$ = 1.8 Hz, 1H, H-3'), 6.77 (d, $^3J_{H\text{-}H}$ = 8.2 Hz, 1H, H-6'), 4.59 (sept, $^3J_{H\text{-}H}$ = 6.1 Hz, 1H, OC*H*), 3.87-3.83 (m, 4H, H-2), 3.12-3.07 (m, 4H, H-3), 1.35 (d, $^3J_{H\text{-}H}$ = 6.1 Hz, 6H, CH(CH_3)$_2$), 0.24 (s, 9 H, Si(CH_3)$_3$); **^{13}C-NMR** (151 MHz, $CDCl_3$): δ [ppm] = 149.7 (C-2'), 143.3 (C-1'), 125.8 (C-5'), 118.7 (C-3'), 117.9 (C-6'), 116.9 (C-4'), 105.7 (C-1''), 92.8 (C-2''), 70.7 (O*C*H), 67.3 (C-2), 50.9 (C-3), 22.4 (CH(*C*H_3)$_2$), 0.22 (Si(*C*H_3)$_3$); **ATR-IR** (neat): $\tilde{\nu}$ [cm^{-1}] = 2960, 2852, 2144, 1504, 1256, 1226,

1117, 1107, 995, 913, 839, 760; **HRMS** (ESI$^+$): m/z calc.: 318.1884 [M+H]$^+$, found: 318.1877; **R_f**: 0.23 (CH_2Cl_2/acetone 100:1 v/v).

4-(4-Ethynyl-2-isopropoxyphenyl)morpholine 208

The cleavage of the protecting group was performed according to general procedure III by treating **204** (230 mg, 724 µmol) with potassium carbonate (501 mg, 3.62 mmol) in methanol (8 mL) for 4 h. Alkyne **208** (160 mg, 651 µmol, 90%) was isolated as a colorless solid.

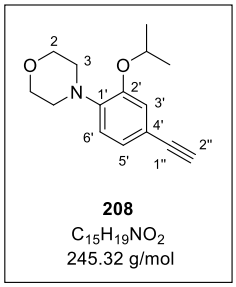

^{1}H-NMR (400 MHz, $CDCl_3$): δ [ppm] = 7.07 (dd, $^3J_{H-H}$ = 8.1 Hz, $^4J_{H-H}$ = 1.8 Hz, 1H, H-5'), 6.98 (d, $^4J_{H-H}$ = 1.8 Hz, 1H, H-3'), 6.79 (d, $^3J_{H-H}$ = 8.1 Hz, 1H, H-6'), 4.58 (sept, $^3J_{H-H}$ = 6.0 Hz, 1H, OC*H*), 3.89-3.82 (m, 4H, H-2), 3.14-3.07 (m, 4H, H-3), 3.01 (s, 1H, H-2''), 1.35 (d, $^3J_{H-H}$ = 6.0 Hz, 6H, CH(C*H*$_3$)$_2$); **^{13}C-NMR** (101 MHz, $CDCl_3$): δ [ppm] = 149.9 (C-2'), 143.5 (C-1'), 125.9 (C-5'), 119.0 (C-3'), 118.0 (C-6'), 115.8 (C-4'), 84.2 (C-1''), 76.0 (C-2''), 70.8 (O*C*H), 67.3 (C-2), 50.9 (C-3), 22.3 (CH(*C*H$_3$)$_2$); **ATR-IR** (neat): $\tilde{\nu}$ [cm^{-1}] = 3207, 2961, 2860, 1506, 1451, 1372, 1253, 1111, 991, 905, 857, 818, 621; **HRMS** (ESI$^+$): m/z calc.: 246.1489 [M+H]$^+$, found: 246.1530; **R_f**: 0.25 (CH_2Cl_2/acetone 100:1 v/v).

Methyl 5-((3-isopropoxy-4-morpholinophenyl)ethynyl)-2-propionamidobenzoate 245

The reaction was carried out as described in general procedure IV with anthranilic acid **90** (150 mg, 450 µmol), copper iodide (8.6 mg, 45 µmol), $Pd(PPh_3)_4$ (52.0 mg, 45.0 µmol) and alkyne **208** (122 mg, 495 µmol) in triethylamine (4 mL) and THF (3 mL) at room temperature for 18 h. The crude product was purified by column chromatography (CH_2Cl_2/acetone 100:1 v/v) to give **245** (157 mg, 348 µmol, 77%) as an orange solid.

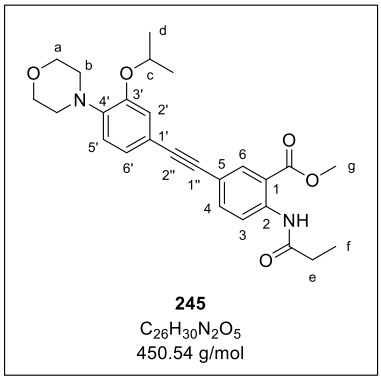

^{1}H-NMR (500 MHz, $CDCl_3$): δ [ppm] = 11.12 (s, 1H, N*H*CO), 8.75 (d, $^3J_{H-H}$ = 8.8 Hz, 1H, H-3), 8.19 (d, $^4J_{H-H}$ = 2.0 Hz, 1H, H-6), 7.66 (dd, $^3J_{H-H}$ = 8.8 Hz, $^4J_{H-H}$ = 2.0 Hz, 1H, H-4), 7.10 (dd, $^3J_{H-H}$ = 8.2 Hz, $^4J_{H-H}$ = 1.8 Hz, 1H, H-6'), 7.01 (d, $^4J_{H-H}$ = 1.8 Hz, 1H, H-2'), 6.83 (d, $^3J_{H-H}$ = 8.2 Hz, 1H, H-5'), 4.62 (sept, $^3J_{H-H}$ = 6.1 Hz, 1H, H-c), 3.94 (s, 3H, H-g), 3.89-3.84 (m, 4H, H-a), 3.15-3.10 (m, 4H, H-b), 2.49 (q, $^3J_{H-H}$ = 7.6 Hz, 2H, H-e), 1.38 (d, $^3J_{H-H}$ = 6.1 Hz, 6H, H-d), 1.28 (t, $^3J_{H-H}$ = 7.6 Hz, 3H, H-f); **^{13}C-NMR** (126 MHz, $CDCl_3$): δ [ppm] = 173.0 (*C*ONH), 168.4 (*C*OOMe), 150.0 (C-3'), 143.0 (C-4'), 141.3 (C-2), 137.5 (C-4), 134.1 (C-6), 125.3 (C-6'), 120.5 (C-3), 118.4 (C-2'), 118.1 (C-5'), 117.8 (C-1), 117.1 (C-1'), 114.9 (C-5), 89.9 (C-2''), 87.3 (C-1''), 70.8 (C-c), 67.3 (C-a), 52.6 (C-b), 50.9 (C-g), 31.9 (C-e), 22.4 (C-d), 9.67 (C-f); **ATR-IR**

(neat): $\tilde{\nu}$ [cm^{-1}] = 3312, 2965, 2844, 1682, 1583, 1511, 1434, 1328, 1290, 1231, 1184, 1112, 1085, 970; **HRMS** (ESI^+): m/z calc.: 451.2228 $[M+H]^+$, found: 451.2263; $\mathbf{R_f}$: 0.18 (CH_2Cl_2/acetone 100:1 v/v).

5-((3-Isopropoxy-4-morpholinophenyl)ethynyl)-2-propionamidobenzoic acid 62

According to general procedure V, the reaction was performed by treating methyl ester **245** (145 mg, 322 µmol) with aqueous 1.0 M NaOH (1.5 mL) in THF (4 mL) for 18 h. Precipitation in acidic solution afforded target compound **62** (134 mg, 307 µmol, 95%) as an ivory solid.

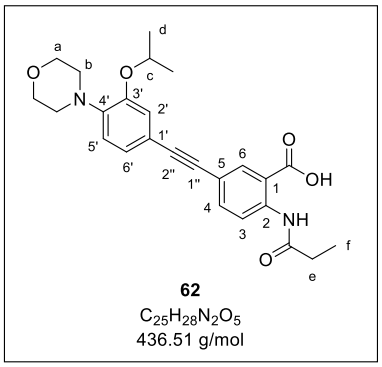

62
$C_{25}H_{28}N_2O_5$
436.51 g/mol

^{1}H-NMR (600 MHz, DMSO-*d*6): δ [ppm] = 13.89 (s, 1H, COO*H*), 11.19 (s, 1H, CON*H*), 8.57 (d, $^3J_{H\text{-}H}$ = 8.7 Hz, 1H, H-3), 8.07 (d, $^4J_{H\text{-}H}$ = 2.2 Hz, 1H, H-6), 7.71 (dd, $^3J_{H\text{-}H}$ = 8.7 Hz, $^4J_{H\text{-}H}$ = 2.2 Hz, 1H, H-4), 7.12-7.07 (m, 2H, H-6', H-2'), 6.88 (d, $^3J_{H\text{-}H}$ = 8.1 Hz, 1H, H-5'), 4.67 (sept, $^3J_{H\text{-}H}$ = 6.0 Hz, 1H, H-c), 3.75-3.69 (m, 4H, H-a), 3.06-3.00 (m, 4H, H-b), 2.43 (q, $^3J_{H\text{-}H}$ = 7.5 Hz, 2H, H-e), 1.28 (d, $^3J_{H\text{-}H}$ = 6.0 Hz, 6H, H-d), 1.13 (t, $^3J_{H\text{-}H}$ = 7.5 Hz, 3H, H-f); **^{13}C-NMR** (151 MHz, DMSO-*d*6): δ [ppm] = 172.2 (*C*ONH), 168.9 (*C*OOH), 149.3 (C-3'), 143.1 (C-4'), 140.7 (C-2), 136.3 (C-4), 133.8 (C-6), 124.9 (C-6'), 120.0 (C-3), 118.2 (C-5'), 117.9 (C-2'), 116.5 (C-1), 116.5 (C-5), 89.8 (C-2''), 87.1 (C-1''), 69.8 (C-c), 66.2 (C-a), 50.2 (C-b), 30.7 (C-e), 21.9 (C-d), 9.27 (C-f); **ATR-IR** (neat): $\tilde{\nu}$ [cm^{-1}] = 2970, 1682, 1585, 1509, 1289, 1232, 1214, 1186, 1107, 916, 846, 833, 809; **HRMS** (ESI^+): m/z calc.: 435.1925 $[M-H]^-$, found: 435.1934; $\mathbf{R_f}$: 0.22 (CH_2Cl_2/MeOH 19:1 v/v).

4-Bromo-1-iodo-2-(2,2,2-trifluoroethoxy)benzene 152

An ice-cold mixture of 4-bromo-2-fluoro-1-iodobenzene **138** (1.19 g, 3.95 mmol, 1.0 eq.) and KOH (444 mg, 7.91 mmol, 2.0 eq.) in DMF (3 mL) was treated dropwise with 2,2,2-trifluoroethanol (600 µL, 7.91 mmol, 2.0 eq.). After stirring for 5 h at 60 °C, the reaction mixture was diluted with water and extracted three times with petroleum ether. The combined organic layers were dried over Na_2SO_4 and the solvent was removed under reduced pressure. The crude product was purified by column chromatography (PE/CH_2Cl_2 9:1 v/v) to yield **152** (861 mg, 2.63 mmol, 67%) as a colorless solid.

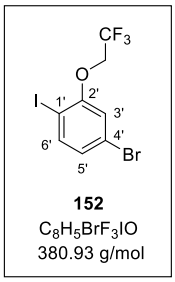

152
$C_8H_5BrF_3IO$
380.93 g/mol

^{1}H-NMR (400 MHz, $CDCl_3$): δ [ppm] = 7.66 (d, $^3J_{H\text{-}H}$ = 8.8 Hz, 1H, H-6'), 7.01-6.94 (m, 2H, H-5', H-3'), 4.38 (q, $^3J_{H\text{-}H}$ = 7.9 Hz, 2H, OCH_2); **^{13}C-NMR** (101 MHz, $CDCl_3$): δ [ppm] = 157.1 (C-2'), 140.9 (C-6'), 127.8 (C-5'), 122.9 (CF_3), 122.4 (C-4'), 116.9 (C-3'), 85.0 (C-1'), 67.2 (OCH_2); **^{19}F-NMR** (565 MHz, $CDCl_3$): δ [ppm] = −73.7 (CF_3); **ATR-IR** (neat): $\tilde{\nu}$ [cm^{-1}] = 2951, 1563, 1469, 1455, 1391, 1277, 1241, 1176, 1153, 1068, 1016, 972, 883, 835, 800, 659; **HRMS** (ESI$^+$): m/z calc.: 281.8536 $[M+H\text{-}OCH_2CF_3]^+$, found: 282.2679; **R_f**: 0.49 (PE/CH_2Cl_2 9:1 v/v).

4-(4-Bromo-2-(2,2,2-trifluoroethoxy)phenyl)morpholine 147

The reaction was carried out according to general procedure VII with 4-bromo-1-iodo-2-(2,2,2-trifluoroethoxy)benzene **152** (820 mg, 2.15 mmol), morpholine (370 µL, 3.75 mmol), $Pd_2(dba)_3$ (98.6 mg, 108 µmol), xantphos (187 mg, 323 µmol) and NaOtBu (207 mg, 2.15 mmol) in toluene (12 mL) for 48 h. After purification by column chromatography (PE/CH_2Cl_2 1:4 v/v), **147** (269 mg, 791 µmol, 37%) was obtained as a colorless solid.

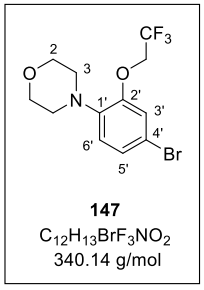

147
$C_{12}H_{13}BrF_3NO_2$
340.14 g/mol

^{1}H-NMR (600 MHz, $CDCl_3$): δ [ppm] = 7.18 (dd, $^3J_{H\text{-}H}$ = 8.5 Hz, $^4J_{H\text{-}H}$ = 2.2 Hz, 1H, H-5'), 7.03 (d, $^4J_{H\text{-}H}$ = 2.2 Hz, 1H, H-3'), 6.93-6.85 (m, 1H, H-6'), 4.39 (q, $^3J_{H\text{-}F}$ = 8.1 Hz, 2H, OCH_2), 3.91-3.84 (m, 4H, H-a), 3.10-3.04 (m, 4H, H-b); **^{13}C-NMR** (151 MHz, $CDCl_3$): δ [ppm] = 150.7 (C-2'), 140.9 (C-1'), 126.9 (C-5'), 123.4 (CF_3), 120.6 (C-6'), 119.3 (C-3'), 115.2 (C-4'), 67.0 (C-a), 66.8 (OCH_2), 51.2 (C-b); **^{19}F-NMR** (565 MHz, $CDCl_3$): δ [ppm] = −73.9 (CF_3); **ATR-IR** (neat): $\tilde{\nu}$ [cm^{-1}] = 2947, 2858, 1721, 1496, 1450, 1284, 1238, 1219, 1155, 1112, 1064, 970, 880, 853, 809, 651; **HRMS** (ESI$^+$): m/z calc.: 340.0155 $[M+H]^+$, found: 340.0174; **R_f**: 0.16 (PE/CH_2Cl_2 1:4 v/v).

4-(4-Ethynyl-2-(2,2,2-trifluoroethoxy)phenyl)morpholine 209

The first reaction was performed according to general procedure II with 4-(4-bromo-2-(2,2,2-trifluoroethoxy)phenyl)morpholine **147** (245 mg, 720 µmol), copper iodide (13.7 mg, 72.0 µmol), $Pd(PPh_3)_4$ (83.2 mg, 72.0 µmol) and TMS acetylene (270 µL, 1.95 mmol) in triethylamine (4 mL) and THF (2 mL) at 70 °C for 24 h. Purification by column chromatography (CH_2Cl_2) provided **205** (236 mg, 66.1 µmol, 92%) as a colorless resin.

The second reaction was performed according to general procedure III with **205** (225 mg, 629 µmol) and potassium carbonate (435 mg, 3.15 mmol) in methanol (6 mL) for 4 h. Alkyne **209** (153 mg, 535 µmol, 85%) was isolated as a pale orange solid.

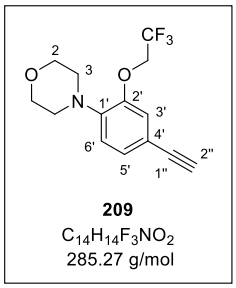

209
$C_{14}H_{14}F_3NO_2$
285.27 g/mol

^{1}H-NMR (600 MHz, $CDCl_3$): δ [ppm] = 7.19 (dd, $^3J_{H\text{-}H}$ = 8.2 Hz, $^4J_{H\text{-}H}$ = 1.8 Hz, 1H, H-5'), 6.99 (d, $^4J_{H\text{-}H}$ = 1.8 Hz, 1H, H-3'), 6.86 (d, $^3J_{H\text{-}H}$ = 8.2 Hz, 1H, H-6'), 4.37 (q, $^3J_{H\text{-}F}$ = 8.1 Hz, 2H, OCH_2), 3.88-3.83 (m, 4H, H-2), 3.12-3.07 (m, 4H, H-3); **^{13}C-NMR** (151 MHz, $CDCl_3$): δ [ppm] = 149.5 (C-2'), 143.3 (C-1'), 128.2 (C-5'), 123.4 (CF_3), 119.1 (C-3'), 118.6 (C-6'), 116.2 (C-4'), 83.2 (C-1''), 76.9 (C-2''), 67.2 (C-2), 66.6 (OCH_2), 51.0 (C-3); **^{19}F-NMR** (565 MHz, $CDCl_3$): δ [ppm] = −74.0 (CF_3); **ATR-IR** (neat): $\tilde{\nu}$ [cm^{-1}] = 3304, 2966, 2827, 1604, 1511, 1451, 1290, 1249, 1229, 1156, 1115, 1065, 970, 914, 818, 671, 652, 590; **HRMS** (ESI$^+$): m/z calc.: 286.1050 [M+H]$^+$, found: 286.1095; **R_f**: 0.19 (CH_2Cl_2).

Methyl 5-((4-morpholino-3-(2,2,2-trifluoroethoxy)phenyl)ethynyl)-2-propionamidobenzoate 246

According to general procedure IV, the reaction was carried out with anthranilic acid **90** (200 mg, 600 µmol), copper iodide (11.4 mg, 60.0 µmol), $Pd(PPh_3)_4$ (69.4 mg, 60.0 µmol) and alkyne **209** (144 mg, 660 µmol) in triethylamine (4 mL) and THF (3 mL) at room temperature for 16 h. The crude product was purified by column chromatography (CH_2Cl_2/acetone 100:1 v/v) to give **246** (157 mg, 372 µmol, 62%) as a yellowish solid.

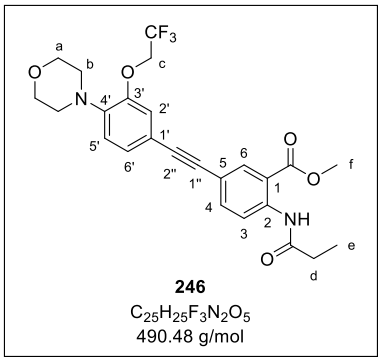

246
$C_{25}H_{25}F_3N_2O_5$
490.48 g/mol

^{1}H-NMR (600 MHz, $CDCl_3$): δ [ppm] = 11.14 (s, 1H, CONH), 8.77 (d, $^3J_{H\text{-}H}$ = 8.8 Hz, 1H, H-3), 8.20 (d, $^4J_{H\text{-}H}$ = 2.1 Hz, 1H, H-6), 7.66 (dd, $^3J_{H\text{-}H}$ = 8.8 Hz, $^4J_{H\text{-}H}$ = 2.1 Hz, 1H, H-4), 7.24 (dd, $^3J_{H\text{-}H}$ = 8.2 Hz, $^4J_{H\text{-}H}$ = 1.8 Hz, 1H, H-6'), 7.05 (d, $^4J_{H\text{-}H}$ = 1.8 Hz, 1H, H-2'), 4.44 (q, $^3J_{H\text{-}F}$ = 8.1 Hz, 2H, H-c), 3.95 (s, 3H, H-f), 3.97-3.92 (m, 4H, H-a), 3.25-3.18 (m, 4H, H-b), 2.50 (q, $^3J_{H\text{-}H}$ = 7.6 Hz, 2H, H-d), 1.29 (t, $^3J_{H\text{-}H}$ = 7.6 Hz, 3H, H-e); **^{13}C-NMR** (151 MHz, $CDCl_3$): δ [ppm] = 173.1 (CONH), 168.3 (COOMe), 149.7 (C-3'), 141.6 (C-4'), 141.2 (C-2), 137.5 (C-4), 134.2 (C-6), 127.5 (C-6'), 120.5 (C-3), 118.3 (C-2'), 117.2 (C-1), 114.9 (C-5), 86.7 (C-2''), 84.0 (C-1''), 66.8 (C-c), 66.6 (C-a), 52.7 (C-f), 52.3 (C-b), 31.9 (C-d), 9.67 (C-e); **^{19}F-NMR** (565 MHz, $CDCl_3$): δ [ppm] = −78.6 (CF_3); **ATR-IR** (neat): $\tilde{\nu}$ [cm^{-1}] = 3307, 3277, 2973, 2854, 1687, 1585, 1515, 1230, 1216, 1175, 1155, 1119, 1085, 1064, 977, 920, 839, 786; **HRMS** (ESI$^+$): m/z calc.: 491.1789 [M+H]$^+$, found: 491.1782; **R_f**: 0.23 (CH_2Cl_2/acetone 100:1 v/v).

5-((4-Morpholino-3-(2,2,2-trifluoroethoxy)phenyl)ethynyl)-2-propionamidobenzoic acid 63

The saponification was carried out as described in general procedure V by treating methyl ester **246** (120 mg, 224 µmol) with aqueous 1.0 M NaOH (1.0 mL) in THF (3 mL) for 16 h.

After precipitation in acidic solution, target compound **63** (105 mg, 222 µmol, 98%) was obtained as an ivory solid.

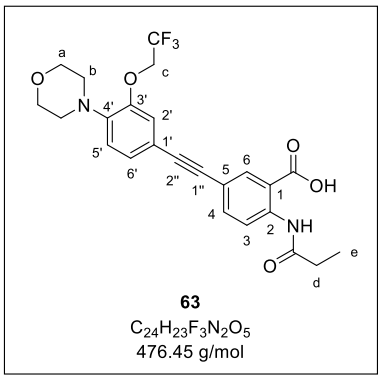

63
$C_{24}H_{23}F_3N_2O_5$
476.45 g/mol

^{1}H-NMR (600 MHz, DMSO-*d*6): δ [ppm] = 13.91 (s, 1H, COO*H*), 11.20 (s, 1H, CON*H*), 8.58 (d, $^3J_{H\text{-}H}$ = 8.7 Hz, 1H, H-3), 8.08 (d, $^4J_{H\text{-}H}$ = 2.2 Hz, 1H, H-6), 7.71 (dd, $^3J_{H\text{-}H}$ = 8.7 Hz, $^4J_{H\text{-}H}$ = 2.2 Hz, 1H, H-4), 7.24 (d, $^4J_{H\text{-}H}$ = 1.8 Hz, 1H, H-2'), 7.21 (dd, $^3J_{H\text{-}H}$ = 8.2 Hz, $^4J_{H\text{-}H}$ = 1.8 Hz, 1H, H-6'), 6.95 (d, $^3J_{H\text{-}H}$ = 8.2 Hz, 1H, H-5'), 4.80 (q, $^3J_{H\text{-}F}$ = 8.8 Hz, 2H, H-c), 3.75-3.69 (m, 4H, H-a), 3.06-2.99 (m, 4H, H-b), 2.44 (q, $^3J_{H\text{-}H}$ = 7.5 Hz, 2H, H-d), 1.13 (t, $^3J_{H\text{-}H}$ = 7.5 Hz, 3H, H-e); **^{13}C-NMR** (151 MHz, DMSO-*d*6): δ [ppm] = 172.2 (*C*ONH), 168.8 (*C*OOH), 148.9 (C-3'), 142.1 (C-4'), 140.8 (C-2), 136.3 (C-4), 133.9 (C-6), 126.3 (C-6'), 124.0 (*C*F3), 120.1 (C-3), 118.5 (C-5'), 116.9 (C-2'), 116.5 (C-1), 116.3 (C-5), 115.5 (C-1'), 89.3 (C-2''), 87.5 (C-1''), 66.2 (C-a), 65.0 (C-c), 50.3 (C-b), 30.7 (C-d), 9.27 (C-e); **^{19}F-NMR** (565 MHz, DMSO-*d*6): δ [ppm] = −72.6 (C*F*$_3$); **ATR-IR** (neat): $\tilde{\nu}$ [cm^{-1}] = 2974, 2829, 1684, 1590, 1517, 1230, 1206, 1192, 1155, 1110, 978, 918, 843, 819; **HRMS** (ESI$^+$): m/z calc.: 475.1486 [M-H]$^-$, found: 475.1490; **R_f**: 0.30 (CH_2Cl_2/MeOH 19:1 v/v).

6.3.7. Syntheses of hDHODH inhibitors 65-73 (cycle 3)

((4-Cyclohexylphenyl)ethynyl)trimethylsilane 211

The reaction was carried out as described in the literature with 1-bromo-4-cyclohexylbenzene **210** (390 µL, 2.09 mmol), copper iodide (19.9 mg, 104 µmol), $Pd(PPh_3)_4$ (121 mg, 104 µmol) and TMS acetylene (780 µL, 5.65 mmol) in triethylamine (9 mL) and THF (3 mL) to afford TMS-protected alkyne **211** (448 mg, 1.75 mmol, 84%) as a yellowish oil.

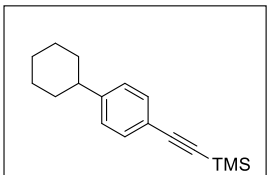

211
$C_{17}H_{24}Si$
256.46 g/mol

The analytical data were in accordance to those described.[160]

1-Cyclohexyl-4-ethynylbenzene 212

The reaction was carried out as described in the literature with TMS-protected alkyne **211** (377 mg, 1.47 mmol) and potassium carbonate (1.02 g, 7.35 mmol) in methanol (12 mL) to afford alkyne **212** (239 mg, 1.30 mmol, 88%) as a colorless oil.

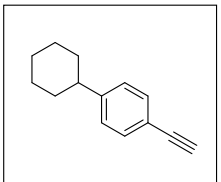

212
$C_{14}H_{16}$
184.28 g/mol

The analytical data were in accordance to those described.[160]

Methyl 5-((4-cyclohexylphenyl)ethynyl)-2-pivalamidobenzoate 247

The reaction was carried out as described in general procedure IV with anthranilic acid **91** (200 mg, 637 µmol), copper iodide (12.1 mg, 63.7 µmol), $Pd(PPh_3)_4$ (73.6 mg, 63.7 µmol) and alkyne **212** (129 mg, 700 µmol) in triethylamine (4 mL) and THF (3 mL) at room temperature for 18 h. Purification by column chromatography (CH_2Cl_2) provided **247** (167 mg, 400 µmol, 63%) as a yellow solid.

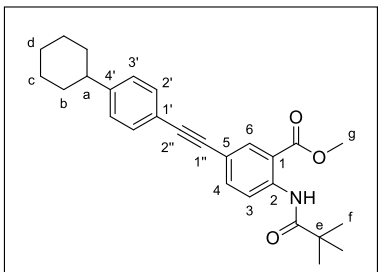

^{1}H-NMR (400 MHz, $CDCl_3$) : δ [ppm] = 11.37 (s, 1H, CON*H*), 8.79 (d, $^3J_{H\text{-}H}$ = 8.8 Hz, 1H, H-3), 8.21 (d, $^4J_{H\text{-}H}$ = 2.1 Hz, 1H, H-6), 7.66 (dd, $^3J_{H\text{-}H}$ = 8.8 Hz, $^4J_{H\text{-}H}$ = 2.1 Hz, 1H, H-4), 7.44 (d, $^3J_{H\text{-}H}$ = 8.3 Hz, 2H, H-2'), 7.19 (d, $^3J_{H\text{-}H}$ = 8.3 Hz, 2H, H-3'), 3.95 (s, 3H, H-g), 2.55-2.46 (m, 1H, H-a), 1.90-1.80 (m 4H, H-$b_{(eq.)}$, H-$c_{(eq.)}$), 1.80-1.72 (m, 1H, H-$d_{(eq.)}$), 1.45-1.37 (m, 4H, H-$b_{(ax.)}$, H-$c_{(ax.)}$), 1.36 (s, 9H, H-f), 1.31-1.23 (m, 1H, H-$d_{(ax.)}$); **^{13}C-NMR** (101 MHz, $CDCl_3$): δ [ppm] = 178.1 (*C*ONH), 168.5 (*C*OOMe), 148.8 (C-4'), 141.7 (C-2), 137.5 (C-4), 134.2 (C-6), 131.7 (C-2'), 127.1 (C-3'), 120.5 (C-1'), 120.4 (C-3), 117.6 (C-1), 115.1 (C-5), 89.7 (C-2''), 87.8 (C-1''), 52.7 (C-g), 44.7 (C-a), 40.6 (C-e), 34.4 (C-b), 27.7 (C-f), 27.0 (C-c), 26.3 (C-d); **ATR-IR** (neat): $\tilde{\nu}$ [cm^{-1}] = 3266, 2926, 2849, 1703, 1676, 1585, 1512, 1478, 1436, 1290, 1250, 1227, 1163, 1147, 1081, 828, 788; **HRMS** (ESI^+): m/z calc.: 418.2377 $[M+H]^+$, found: 418.2396; $\mathbf{R_f}$: 0.37 (CH_2Cl_2).

5-((4-Cyclohexylphenyl)ethynyl)-2-pivalamidobenzoic acid 65

According to general procedure V, the saponification was carried out with methyl ester **247** (140 mg, 335 µmol) and aqueous 1.0 M NaOH (1.5 mL) in THF (4 mL) for 17 h. After precipitation in acidic solution, target compound **65** (102 mg, 253 µmol, 75%) was obtained as an ivory solid.

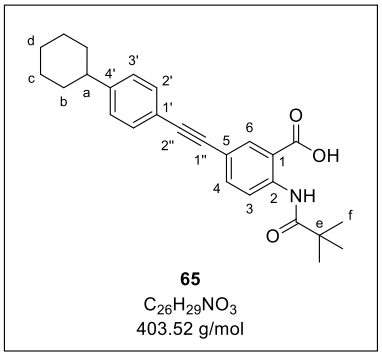

^{1}H-NMR (400 MHz, DMSO-*d*6): δ [ppm] = 11.64 (s, 1H, CON*H*), 8.67 (d, $^3J_{H\text{-}H}$ = 8.7 Hz, 1H, H-3), 8.11 (d, $^4J_{H\text{-}H}$ = 2.2 Hz, 1H, H-6), 7.72 (dd, $^3J_{H\text{-}H}$ = 8.7 Hz, $^4J_{H\text{-}H}$ = 2.2 Hz, 1H, H-4), 7.46 (d, $^3J_{H\text{-}H}$ = 7.8 Hz, 2H, H-2'), 7.26 (d, $^3J_{H\text{-}H}$ = 7.8 Hz, 2H, H-3'), 2.56-2.50 (m, 1H, H-a), 1.82-1.73 (m, 4H, H-$b_{(eq.)}$, H-$c_{(eq.)}$), 1.73-1.65 (m, 1H, H-$d_{(eq.)}$), 1.43-1.32 (m, 4H, H-$b_{(ax.)}$, H-$c_{(ax.)}$), 1.29-1.20 (m, 10H, H-$d_{(ax.)}$, H-f); **^{13}C-NMR** (101 MHz, DMSO-*d*6): δ [ppm] = 176.8 (*C*ONH), 169.2 (*C*OOH), 148.5 (C-4'), 141.3 (C-2), 136.5 (C-4),

134.0 (C-6), 131.3 (C-2'), 127.1 (C-3'), 119.7 (C-3), 119.5 (C-1'), 116.3 (C-1), 116.1 (C-5), 89.3 (C-2''), 87.7 (C-1''), 43.6 (C-a), 40.1 (C-e), 33.6 (C-b), 27.1 (C-f), 26.2 (C-c), 25.5 (C-d); **ATR-IR** (neat): $\tilde{\nu}$ [cm^{-1}] = 2921, 2849, 1702, 1656, 1581, 1515, 1480, 1291, 1206, 1178, 847, 824, 797, 689, 547; **HRMS** (ESI^+): m/z calc.: 402.2074 $[M-H]^-$, found: 402.2131; $\mathbf{R_f}$: 0.24 (CH_2Cl_2/MeOH 19:1 v/v).

Methyl 5-((4-cyclohexylphenyl)ethynyl)-2-((methoxycarbonyl)amino)benzoate 248

The reaction was carried out as described in general procedure IV with anthranilic acid **92** (200 mg, 597 µmol), copper iodide (11.4 mg, 59.7 µmol), $Pd(PPh_3)_4$ (69.4 mg, 59.7 µmol) and alkyne **212** (121 mg, 657 µmol) in triethylamine (4 mL) and THF (3 mL) at room temperature for 18 h. Purification by column chromatography (CH_2Cl_2) afforded **248** (209 mg, 533 µmol, 89%) as an orange solid.

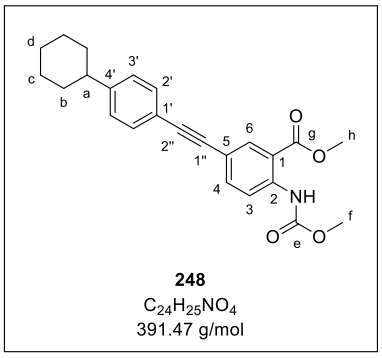

248
$C_{24}H_{25}NO_4$
391.47 g/mol

^{1}H-NMR (400 MHz, $CDCl_3$) : δ [ppm] = 10.56 (s, 1H, CON*H*), 8.44 (d, $^3J_{H-H}$ = 8.8 Hz, 1H, H-3), 8.18 (d, $^4J_{H-H}$ = 2.0 Hz, 1H, H-6), 7.66 (dd, $^3J_{H-H}$ = 8.8 Hz, $^4J_{H-H}$ = 2.0 Hz, 1H, H-4), 7.44 (d, $^3J_{H-H}$ = 8.3 Hz, 2H, H-2'), 7.19 (d, $^3J_{H-H}$ = 8.3 Hz, 2H, H-3'), 3.94 (s, 3H, H-h), 3.80 (s, 3H, H-f), 2.55-2.45 (m, 1H, H-a), 1.90-1.81 (m, 4H, H-$b_{(eq.)}$, H-$c_{(eq.)}$), 1.80-1.71 (m, 1H, H-$d_{(eq.)}$), 1.48-1.34 (m, 4H, H-$b_{(ax.)}$, H-$c_{(ax.)}$), 1.31-1.20 (m, 1H, H-$d_{(ax.)}$); **^{13}C-NMR** (101 MHz, $CDCl_3$): δ [ppm] = 168.1 (C-g), 154.1 (C-e), 148.8 (C-4'), 141.5 (C-2), 137.5 (C-4), 134.3 (C-6), 131.7 (C-2'), 127.1 (C-3'), 120.5 (C-1'), 118.9 (C-3) 117.0 (C-1), 114.7 (C-5), 89.5 (C-2''), 87.7 (C-1''), 52.6 (C-f), 52.6 (C-h), 44.7 (C-a), 34.4 (C-b), 27.0 (C-c), 26.3 (C-d); **ATR-IR** (neat): $\tilde{\nu}$ [cm^{-1}] = 3257, 2921, 2849, 1734, 1693, 1587, 1518, 1436, 1236, 1217, 1057, 838, 824, 791, 766; **HRMS** (ESI^+): m/z calc.: 392.1857 $[M+H]^+$, found: 392.1854; $\mathbf{R_f}$: 0.50 (CH_2Cl_2).

5-((4-Cyclohexylphenyl)ethynyl)-2-((methoxycarbonyl)amino)benzoic acid 66

The saponification was performed according to general procedure V by treating methyl ester **248** (190 mg, 485 µmol) with aqueous 1.0 M NaOH (2.0 mL) in THF (5 mL) for 16 h. Precipitation in acidic solution provided target compound **66** (179 mg, 474 µmol, 98%) as a greyish solid.

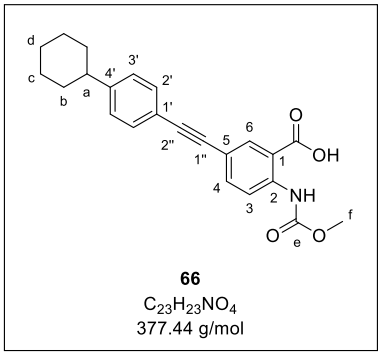

66
$C_{23}H_{23}NO_4$
377.44 g/mol

^{1}H-NMR (600 MHz, DMSO-*d*6): δ [ppm] = 14.02 (s, 1H, COO*H*), 10.87 (s, 1H, CON*H*), 8.32 (d, $^3J_{H\text{-}H}$ = 8.8 Hz, 1H, H-3), 8.08 (d, $^4J_{H\text{-}H}$ = 2.2 Hz, 1H, H-6), 7.74 (dd, $^3J_{H\text{-}H}$ = 8.8 Hz, $^4J_{H\text{-}H}$ = 2.2 Hz, 1H, H-4), 7.46 (d, $^3J_{H\text{-}H}$ = 8.3 Hz, 2H, H-2'), 7.26 (d, $^3J_{H\text{-}H}$ = 8.3 Hz, 2H, H-3'), 3.72 (s, 3H, H-f), 2.55-2.50 (m, 1H, H-a), 1.82-1.74 (m, 4H, H-$b_{(eq.)}$, H-$c_{(eq.)}$), 1.72-1.66 (m, 1H, H-$d_{(eq.)}$), 1.44-1.31 (m, 4H, H-$b_{(ax.)}$, H-$c_{(ax.)}$), 1.27-1.19 (m, 1H, H-$d_{(ax.)}$); **^{13}C-NMR** (151 MHz, DMSO-*d*6): δ [ppm] = 169.0 (C-g), 153.1 (C-e), 148.5 (C-4'), 141.1 (C-2), 136.7 (C-4), 134.1 (C-6), 131.4 (C-2'), 127.1 (C-3'), 119.6 (C-1'), 118.4 (C-3), 115.9 (C-1), 115.7 (C-5), 89.2 (C-2''), 87.6 (C-1''), 52.4 (C-f), 43.6 (C-a), 33.7 (C-b), 26.3 (C-c), 25.5 (C-d); **ATR-IR** (neat): $\tilde{\nu}$ [cm^{-1}] = 3311, 2918, 2845, 1750, 1739, 1668, 1583, 1524, 1247, 1222, 1061, 848, 826, 764, 691; **HRMS** (ESI^+): m/z calc.: 376.1554 $[M\text{-}H]^+$, found: 376.1545; **R_f**: 0.25 (CH_2Cl_2/MeOH 19:1 v/v).

5-((4-Cyclohexylphenyl)ethynyl)-2-(3,3-dimethylureido)benzoic acid 67

The compound was synthesized in a previous study and was provided for use in this work.[160]

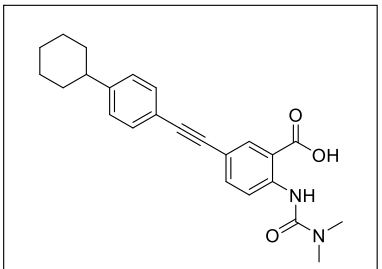

67
$C_{24}H_{26}N_2O_3$
390.48 g/mol

5-((4-Cyclohexylphenyl)ethynyl)-2-ethyl-1H-benzo[d]imidazole-7-carboxylic acid 68

The compound was synthesized in a previous study and was provided for use in this work.[160]

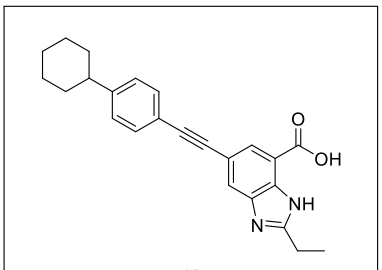

68
$C_{24}H_{24}N_2O_2$
372.47 g/mol

Methyl 5-bromo-1*H*-benzo[*d*]imidazole-7-carboxylate 98

To a solution of diamine **97** (1.20 g, 4.90 mmol, 1.00 eq.) in trimethyl orthoformate (5.36 mL, 49.0 mmol, 10.0 eq.), one drop of H_2SO_4 was added and the reaction mixture was stirred for 30 min at room temperature. The separated solid was collected by filtration, washed with water and dried under vacuum. The crude product was purified by column chromatography (CH_2Cl_2/MeOH 39:1 v/v) to yield **98** (766 mg, 3.00 mmol, 61%) as a brownish solid.

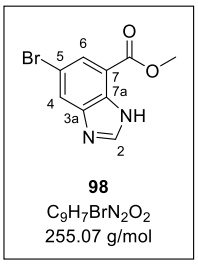

^{1}H-NMR (400 MHz, DMSO-*d*6): δ [ppm] = 8.39 (s, 1H, H-2), 8.17 (d, $^4J_{H\text{-}H}$ = 1.9 Hz, 1H, H-4), 7.89 (d, $^4J_{H\text{-}H}$ = 1.9 Hz, 1H, H-6), 3.95 (s, 3H, OCH_3); **^{13}C-NMR** (101 MHz, DMSO-*d*6): δ [ppm] = 164.4 (*C*OOMe), 145.5 (C-3a), 145.3 (C-2), 132.3 (C-7a), 126.6 (C-6), 126.4 (C-4), 112.9 (C-5), 112.9 (C-7) , 52.4 (O*C*H$_3$); **ATR-IR** (neat): $\tilde{\nu}$ [cm^{-1}] = 3000, 2947, 2810, 1712, 1458, 1430, 1304, 1267, 1241, 1191, 1166, 1034, 915, 861, 781; **HRMS** (ESI$^+$): m/z calc.: 254.9764 [M+H]$^+$, found: 254.9764; **R$_f$**: 0.31 (CH_2Cl_2/MeOH 39:1 v/v).

Methyl 5-bromo-1-ethyl-1*H*-benzo[*d*]imidazole-7-carboxylate 93

Benzimidazole **98** (500 mg, 1.96 mmol, 1.00 eq.) was dissolved in DMF (5 mL) and K_2CO_3 (271 mg, 1.96 mmol, 1.00 eq.) and ethyl iodide (320 µL, 3.92 mmol, 2.00 eq.) were added. After stirring for 6 h at room temperature, the reaction mixture was quenched with water. The separated solid was collected by filtration and dried under vacuum. The regioisomers were separated by column chromatography (CH_2Cl_2/MeOH 39:1 v/v) to obtain the desired product **93** (157 mg, 554 µmol, 28%) as a brownish solid.

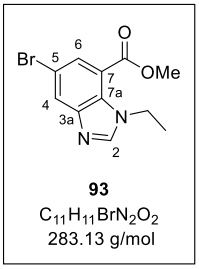

^{1}H-NMR (400 MHz, $CDCl_3$) : δ [ppm] = 8.11 (d, $^4J_{H\text{-}H}$ = 2.0 Hz, 1H, H-6), 7.97 (d, $^4J_{H\text{-}H}$ = 2.0 Hz, 1H, H-4), 7.95 (s, 1H, H-2), 4.56 (q, $^3J_{H\text{-}H}$ = 7.2 Hz, 2H, CH_2CH$_3$), 3.98 (s, 3H, OCH_3), 1.38 (t, $^3J_{H\text{-}H}$ = 7.2 Hz, 3H, CH$_2$CH_3); **^{13}C-NMR** (101 MHz, $CDCl_3$): δ [ppm] = 165.6 (*C*OOMe), 147.5 (C-3a), 146.6 (C-2), 130.4 (C-7a), 129.1 (C-4), 127.8 (C-6), 117.8 (C-5), 114.2 (C-7), 52.8 (O*C*H$_3$), 43.5 (*C*H$_2$CH$_3$), 16.5 (CH$_2$*C*H$_3$); **ATR-IR** (neat): $\tilde{\nu}$ [cm^{-1}] = 2964, 2947, 2929, 1728, 1498, 1259, 1234, 1196, 1177, 1107, 1028, 929, 863, 777, 746, 638; **HRMS** (ESI$^+$): m/z calc.: 283.0077 [M+H]$^+$, found: 283.0261; **R$_f$**: 0.53 (CH_2Cl_2/MeOH 39:1 v/v).

5-((4-Cyclohexylphenyl)ethynyl)-1-ethyl-1*H*-benzo[*d*]imidazole-7-carboxylic acid 69

The first reaction was performed according to general procedure IV with benzimidazole **93** (150 mg, 530 µmol), copper iodide (10.1 mg, 53.0 µmol), Pd(PPh$_3$)$_4$ (61.2 mg, 53.0 µmol) and alkyne **212** (293 mg, 1.59 mmol) in triethylamine (4 mL) and THF (3 mL) at 70 °C for 24 h.

The crude product was purified by column chromatography (CH_2Cl_2/acetone 10:1 v/v) to yield **249** (69.9 mg, 181 µmol, 34%) as a yellow solid.

The second reaction was carried out as described in general procedure V by treating methyl ester **249** (60.0 mg, 155 µmol) with aqueous 1.0 M NaOH (0.5 mL) in THF (2 mL) for 16 h. After precipitation in acidic solution, target compound **69** (50.4 mg, 135 µmol, 87%) was obtained as a colorless solid.

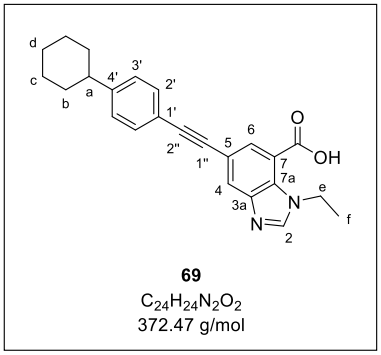

69
$C_{24}H_{24}N_2O_2$
372.47 g/mol

^{1}H-NMR (400 MHz, DMSO-*d*6): *δ* [ppm] = 13.59 (s, 1H, COO*H*), 8.50-8.39 (m, 1H, H-6), 8.06-7.98 (m, 1H, H-4), 7.83 (s, 1H, H-2), 7.49 (d, $^3J_{H\text{-}H}$ = 8.2 Hz, 2H, H-2'), 7.27 (d, $^3J_{H\text{-}H}$ = 8.2 Hz, 2H, H-3'), 4.55 (q, $^3J_{H\text{-}H}$ = 7.1 Hz, 2H, H-e), 2.56-2.50 (m, 1H, H-a), 1.82-1.75 (m, 4H, H-$b_{(eq.)}$, H-$c_{(eq.)}$), 1.74-1.66 (m, 1H, H-$d_{(eq.)}$), 1.47-1.32 (m, 4H, H-$b_{(ax.)}$, H-$c_{(ax.)}$), 1.28 (t, $^3J_{H\text{-}H}$ = 7.1 Hz, 3H, H-f), 1.25-1.20 (m, 1H, H-$d_{(ax.)}$); **^{13}C-NMR** (101 MHz, DMSO-*d*6): *δ* [ppm] = 167.0 (*C*OOH), 148.5 (C-3a), 148.3 (C-4'), 131.4 (C-2'), 131.1 (C-7a), 128.0 (C-2), 127.1 (C-3'), 126.1 (C-4), 119.8 (C-1'), 118.6 (C-5), 115.1 (C-7), 88.5 (C-2''), 88.4 (C-1''), 43.6 (C-a), 42.2 (C-e), 33.7 (C-b), 26.3 (C-c), 25.5 (C-d), 16.1 (C-f); **ATR-IR** (neat): $\tilde{\nu}$ [cm^{-1}] = 2922, 2850, 1705, 1511, 1270, 1240, 1207, 1123, 824, 784, 729, 676; **HRMS** (ESI^+): m/z calc.: 371.1765 $[M\text{-}H]^-$, found: 371.1764; **R_f**: 0.10 (CH_2Cl_2/MeOH 19:1 v/v).

Methyl 5-bromo-2-ethyl-2H-indazole-7-carboxylate 95 and methyl 5-bromo-1-ethyl-1H-indazole-7-carboxylate 94

To a suspension of indazole **100** (493 mg, 1.96 mmol, 1.00 eq.) and K2CO3 (271 mg, 1.96 mmol, .00 eq.) in DMF (4 mL), ethyl iodide (320 µL, 3.92 mmol, 2.00 eq.) was added. After stirring for 6 h at room temperature, the reaction mixture was quenched with water. The separated solid was collected by filtration and dried under vacuum. The regioisomers were separated by column chromatography (CH2Cl2/MeOH 39:1 v/v) to obtain **94** (174 mg, 731 mmol, 28%) and **95** (128 mg, 533 mmol, 38%) both as yellowish solids.

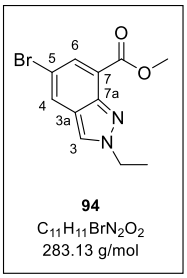

94
$C_{11}H_{11}BrN_2O_2$
283.13 g/mol

^{1}H-NMR (400 MHz, $CDCl_3$) δ [ppm] = 8.13 (d, *J* = 1.8 Hz, 1H, H-3), 8.03 (d, *J* = 1.9 Hz, 1H, H-4), 8.01 (s, 1H, H-6), 4.58 (q, *J* = 7.4 Hz, 2H, CH_2CH$_3$), 4.01 (s, 3H, OCH_3), 1.67 (t, 3H, CH$_2$CH_3); **^{13}C-NMR** (101 MHz, $CDCl_3$) δ [ppm] = 165.50 (*C*OOMe), 144.65 (C-7a), 133.63 (C-3), 127.94 (C-4), 124.97 (C-7), 122.14 (C-6), 120.75 (C-5), 113.69 (C-3a), 52.57 (OCH$_3$), 49.22 (CH_2CH$_3$), 15.81 (CH$_2$CH_3); **ATR-IR** (neat): ν̃ [cm^{-1}] = 3750, 3734, 3675, 3648, 3131, 2982, 2942, 1701, 1541, 1508, 1433, 1408, 1344, 1258, 1225, 1196, 1175, 1155, 1039, 963,

870, 806, 780, 663, 628, 493, 386; **HRMS** (ESI$^+$): calc.: 283.0077 [M+H]$^+$, found.: 283.0083; **R_f**: 0.20 (PE/EtOAc 1:3 v/v).

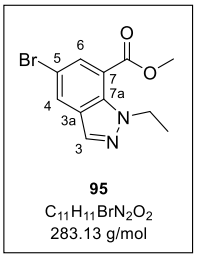

95
$C_{11}H_{11}BrN_2O_2$
283.13 g/mol

^{1}H-NMR (400 MHz, $CDCl_3$) δ [ppm] = 8.05 – 7.98 (m, 3H, H-3, H-4, H-6), 4.71 (q, *J* = 7.2 Hz, 2H, C*H*$_2$CH$_3$), 4.00 (s, 3H, OC*H*$_3$), 1.40 (t, *J* = 7.2 Hz, 3H, CH$_2$C*H*$_3$); **^{13}C-NMR** (101 MHz, $CDCl_3$) δ [ppm] = 165.83 (*C*OOMe), 135.0 (C-7a), 133.2 (C-3), 132.8 (C-4), 128.4 (C-3a), 128.2 (C-6), 116.7 (C-7), 112.2 (C-5), 52.8 (O*C*H$_3$), 47.9 (*C*H$_2$CH$_3$), 15.6 (CH$_2$*C*H$_3$); **ATR-IR** (neat): ṽ [cm^{-1}] =3097, 2989, 2976, 2951, 2933, 1717, 1558, 1491, 1455, 1432, 1417, 1310, 1258, 1190, 1165, 1114, 1091, 1078, 1043, 936, 881, 771, 749, 646, 617, 501, 419, 397; **HRMS** (ESI$^+$): calc.: 283.0077 [M+H]$^+$, found: 282.0072; **R_f**: 0.85 (PE/EtOAc 1:3 v/v).

Methyl 5-((4-cyclohexylphenyl)ethynyl)-2-ethyl-2*H*-indazole-7-carboxylate 250

According to general procedure IV, the reaction was carried out with indazole **94** (98.4 mg, 348 µmol), copper iodide (7.7 mg, 35 µmol), Pd(PPh$_3$)$_4$ (40 mg, 35 µmol) and alkyne **212** (74 mg, 39 mmol) in triethylamine (4 mL) and THF (3 mL) at 70 °C for 21 h. Purification by column chromatography (CH_2Cl_2/acetone 17:1 v/v) afforded **250** (92.2 mg, 239 µmol, 68%) as a yellowish solid.

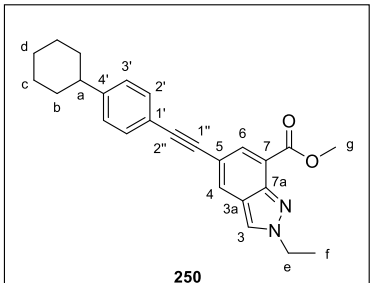

250
$C_{25}H_{26}N_2O_2$
386.50 g/mol

^{1}H-NMR (400 MHz, $CDCl_3$) δ [ppm] = 8.20 (d, *J* = 1.5 Hz, 1H, H-3), 8.07 – 8.04 (m, 2H, H-6, H-4), 7.50 – 7.43 (m, 2H, H-2‘), 7.23 – 7.17 (m, 2H, H-3‘), 4.59 (q, *J* = 7.4 Hz, 2H, H-e), 4.02 (s, 3H, H-g), 2.59 – 2.45 (m, 1H, H-a), 1.91 – 1.80 (m, 4H, H-b$_{(eq.)}$, H-c$_{(eq.)}$), 1.80 – 1.71 (m, 1H, H-d$_{(eq.)}$), 1.68 (t, *J* = 7.4 Hz, 3H, H-f), 1.49 – 1.32 (m, 4H, H-b$_{(ax.)}$, H-c$_{(ax.)}$), 1.31 – 1.19 (m, 1H, H-d$_{(ax.)}$); **^{13}C-NMR** (101 MHz, $CDCl_3$) δ [ppm] = 166.1 (*C*OOMe), 148.7 (C-4‘), 145.3 (C-7a), 133.9 (C-6), 131.7 (*C*-2‘), 129.0 (C-3), 127.1 (C-3‘), 123.7 (C-4), 123.1 (C-3a), 120.6 (C-1‘), 119.5 (C-5 or C-7), 116.1 (C-5 or C-7), 89.2 (C-2‘‘), 88.6 (C-1‘‘), 52.4 (C-g), 49.1 (C-e), 44.7 (C-a), 34.4 (C-b), 27.0 (C-c), 26.3 (C-d), 15.8 (C-f); **ATR-IR** (neat): ṽ [cm^{-1}] = 3648, 3628, 2987, 2922, 2851, 1716, 1558, 1541, 1521, 1339, 1256, 1199, 1046, 890, 827, 785, 418, 396; **HRMS** (ESI$^+$): calc.: 387.2067 [M+H]$^+$, found.: 387.2083; **R_f**: 0.50 (CH_2Cl_2/acetone 17:1 v/v).

5-((4-Cyclohexylphenyl)ethynyl)-2-ethyl-2*H*-indazole-7-carboxylic acid 70

The saponification was performed according to general procedure V by treating methyl ester **250** (62.0 mg, 160 µmol) with aqueous 1.0 M NaOH (1 mL) in THF (5 mL) for 20 h. Precipitation in acidic solution provided target compound **70** (51.9 mg, 139 µmol, 87%) as a yellowish solid.

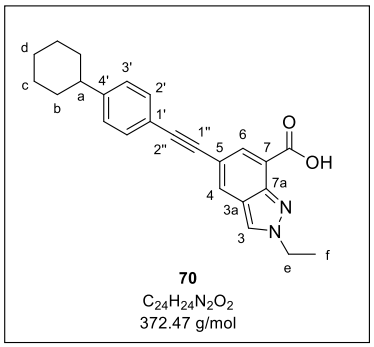

70
$C_{24}H_{24}N_2O_2$
372.47 g/mol

^{1}H-NMR (500 MHz, DMSO) δ [ppm] = 8.61 (s, 1H, H-3), 8.22 (d, *J* = 1.6 Hz, 1H, H-4), 7.93 (d, *J* = 1.6 Hz, 1H, H-6), 7.52 – 7.46 (m, 2H, H-2‘), 7.31 – 7.25 (m, 2H, *H*-3‘), 4.53 (q, *J* = 7.3 Hz, 2H, H-e), 1.85 – 1.76 (m, 4H, H-$b_{(eq.)}$, H-$c_{(eq.)}$), 1.74 – 1.66 (m, 1H, H-$d_{(eq.)}$), 1.53 (t, *J* = 7.3 Hz, 3H, H-f), 1.47 – 1.30 (m, 4H, H-$b_{(ax.)}$, H-$c_{(ax.)}$), 1.29 – 1.18 (m, 1H, H-$d_{(ax.)}$); **^{13}C-NMR** (126 MHz, DMSO) δ [ppm] = 166.1 (*C*OOMe), 148.3 (C-4‘), 144.3 (C-7a), 131.9 (C-4), 131.3 (C-6), 129.2 (C-2‘), 127.1 (C-3), 125.0 (C-3‘), 123.1 (C-3a), 120.2 (C-1‘), 119.8 (C-7 or C-5), 113.9 (C-7 o. C-5), 88.8 (C-2‘‘), 88.5 (C-1‘‘), 48.18 (C-e), 43.6 (C-a), 33.7 (C-b), 26.2 (C-c), 25.5 (C-d), 15.7 (C-f); **ATR-IR** (neat): ṽ [cm^{-1}] = 3118, 2986, 2922, 2849, 1734, 1709, 1507, 1446, 1393, 1386, 1229, 1191, 1149, 1080, 1056, 888, 827, 801, 726, 680, 556, 418; **HRMS** (ESI^+): calc.: 373.1911 $[M+H]^+$, found.: 373.1888; **R_f**: 0.15 (CH_2Cl_2/MeOH 9:1 v/v).

Methyl 5-((4-cyclohexylphenyl)ethynyl)-1-ethyl-1H-indazole-7-carboxylate 251

According to general procedure IV, the reaction was carried out with indazole **95** (100 mg, 353 µmol), copper iodide (7.9 mg, 35 µmol), $Pd(PPh_3)_4$ (41 mg, 35 µmol) and alkyne **212** (73 mg, 39 mmol) in triethylamine (4 mL) and THF (3 mL) at 70 °C for 21 h. Purification by column chromatography (PE/EtOAc 6:1 v/v) afforded **251** (91.1 mg, 236 µmol, 67%) as a yellowish solid.

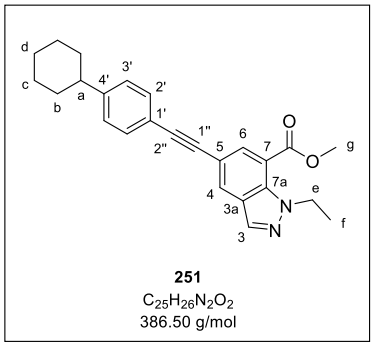

251
$C_{25}H_{26}N_2O_2$
386.50 g/mol

^{1}H-NMR (400 MHz, $CDCl_3$) δ [ppm] = 8.11 – 8.03 (m, 3H, H-3, H-4, H-6), 7.50 – 7.43 (m, 2H, H-2‘), 7.24 – 7.16 (m, 2H, H-3‘), 4.73 (q, *J* = 7.2 Hz, 2H, H-e), 4.01 (s, 3H, H-g), 2.56 – 2.47 (m, 1H, H-a), 1.92 – 1.81 (m, 4H, H-$b_{(eq.)}$, *H*-$c_{(eq.)}$), 1.81 – 1.72 (m, 1H, H-$d_{(eq.)}$), 1.48 – 1.33 (m, 7H, H-f, H-$b_{(ax.)}$, H-$c_{(ax.)}$), 1.30 – 1.21 (m, 1H, H-$d_{(ax.)}$); **^{13}C-NMR** (101 MHz, $CDCl_3$) δ [ppm] = 166.4 (*C*OOMe), 148.7 (C-4’), 135.4 (*C*-7a), 134.2 (C-4), 133.5 (C-6), 131.7 (C-2’), 129.0 (C-3), 127.1 (C-3’), 127.0 (C-3a), 120.5 (C-1’), 115.6 (C-5 o. C-7), 115.3 (C-5 o. C-7), 89.0 (C-2‘‘), 88.0 (C-1‘‘), 52.7 (C-g), 47.8 (C-e), 44.68 (C-a), 34.4 (C-b), 27.0 (C-c), 26.3 (C-d), 15.6 (C-f); **ATR-IR** (neat): ṽ [cm^{-1}] = 2974, 2924, 2851, 1723,

1516, 1448, 1436, 1342, 1256, 1233, 1193, 1168, 1079, 1041, 893, 843, 827, 780, 553; **HRMS** (ESI$^+$): calc.: 387.2067 [M+H]$^+$, found.: 387.2059; $\mathbf{R_f}$: 0.35 (PE/EtOAc 9:1 v/v).

5-((4-Cyclohexylphenyl)ethynyl)-1-ethyl-1*H*-indazole-7-carboxylic acid 71

The saponification was carried out as described in general procedure V by treating methyl ester **251** (75.0 mg, 194 µmol) with aqueous 1.0 M NaOH (1 mL) in THF (5 mL) for 20 h. Precipitation in acidic solution provided target compound **71** (62.5 mg, 168 µmol, 86%) as a yellowish solid.

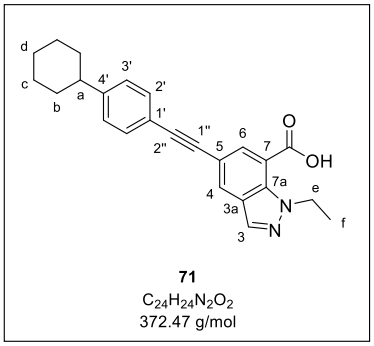

71
$C_{24}H_{24}N_2O_2$
372.47 g/mol

^{1}H-NMR (600 MHz, DMSO) δ [ppm] = 8.26 (s, 1H, H-3), 8.21 (d, *J* = 1.6 Hz, 1H, H-4), 7.94 (d, *J* = 1.6 Hz, 1H, H-6), 7.52 – 7.47 (m, 2H, H-2‘), 7.30 – 7.25 (m, 2H, H-3‘), 4.67 (q, *J* = 7.2 Hz, 2H, H-e), 2.56-2.50 (m, 1H, H-a), 1.82 – 1.75 (m, 4H, H-$b_{(eq.)}$, H-$c_{(eq.)}$), 1.73 – 1.67 (m, 1H, H-$d_{(eq.)}$), 1.45 – 1.34 (m, 4H, H-$b_{(ax.)}$, H-$c_{(ax.)}$), 1.31 (t, *J* = 7.2 Hz, 3H, H-f), 1.29 – 1.19 (m, 1H, H-$d_{(ax.)}$); **^{13}C-NMR** (151 MHz, DMSO) δ [ppm] = 167.0 (*C*OOMe) 148.4 (C-4‘), 134.6 (C-7a), 134.3 (C-4), 131.8 (C-6), 131.4 (*C*-2‘), 128.4 (C-3), 127.1 (C-3‘), 126.5 (C-3a), 119.7 (C-1‘), 117.2 (C-7 o. C-5), 113.9 (C-7 o. C-5), 88.6 (C-2‘‘), 88.1 (C-1‘‘), 46.8 (C-e), 43.6 (C-a), 33.7 (C-b), 26.3 (C-c), 25.5 (C-d), 15.3 (C-f); **ATR-IR** (neat): ṽ [cm^{-1}] = 3343, 2918, 2848, 2650, 1742, 1716, 1672, 1556, 1515, 1256, 1443, 1337, 1240, 1187, 1131, 1098, 1081, 1017, 957, 890, 846, 821, 783, 736, 720, 671, 643, 548; **HRMS** (ESI$^+$): calc.: 373.1911 [M+H]$^+$, found.: 373.1791; $\mathbf{R_f}$: 0.15 (CH_2Cl_2/MeOH 9:1 v/v).

6-((4-Cyclohexylphenyl)ethynyl)-2-ethyl-2H-benzo[d][1,2,3]triazole-4-carboxylic acid 72

The compound was synthesized in a previous study and was provided for use in this work.[160]

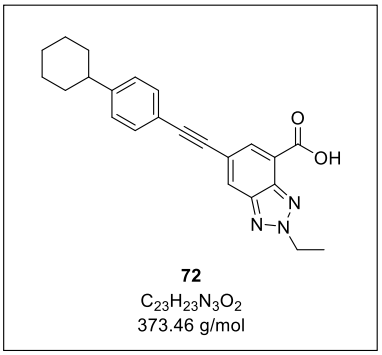

72
$C_{23}H_{23}N_3O_2$
373.46 g/mol

Methyl 5-((4-cyclohexylphenyl)ethynyl)-1-ethyl-1*H*-benzo[*d*][1,2,3]triazole-7-carboxylate 252

According to general procedure IV, the reaction was carried out with benzotriazole **96** (200 mg, 704 µmol), copper iodide (13.4 mg, 70.4 µmol), $Pd(PPh_3)_4$ (81.3 mg, 70.4 µmol) and alkyne **212** (195 mg, 1.06 mmol) in triethylamine (4 mL) and THF (3 mL) at 70 °C for 30 h. Purification by column chromatography (CH_2Cl_2/acetone 40:1 v/v) afforded **252** (245 mg, 631 µmol, 90%) as a greyish solid.

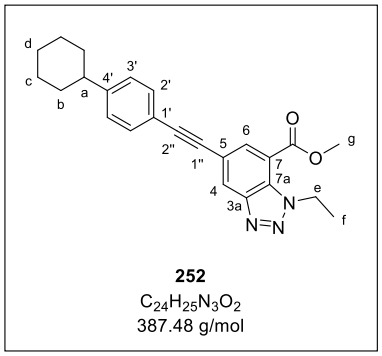

252
$C_{24}H_{25}N_3O_2$
387.48 g/mol

^{1}H-NMR (600 MHz, $CDCl_3$) : δ [ppm] = 8.38 (d, $^4J_{H\text{-}H}$ = 1.5 Hz, 1H, H-4), 8.27 (d, $^4J_{H\text{-}H}$ = 1.5 Hz, 1H, H-6), 7.49 (d, $^3J_{H\text{-}H}$ = 8.2 Hz, 2H, H-2'), 7.22 (d, $^3J_{H\text{-}H}$ = 8.2 Hz, 2H, H-3'), 5.12 (q, $^3J_{H\text{-}H}$ = 7.2 Hz, 2H, H-e), 4.02 (s, 3H, H-g), 2.56-2.49 (m, 1H, H-a), 1.92-1.82 (m, 4H, H-$b_{(eq.)}$, H-$c_{(eq.)}$), 1.79-1.73 (m, 1H, H-$d_{(eq.)}$), 1.53 (t, $^3J_{H\text{-}H}$ = 7.2 Hz, 3H, H-f), 1.47-1.35 (m, 4H, H-$b_{(ax.)}$, H-$c_{(ax.)}$), 1.30-1.22 (m, 1H, H-$d_{(ax.)}$); **^{13}C-NMR** (151 MHz, $CDCl_3$): δ [ppm] = 165.0 (*C*OOMe), 149.2 (C-4'), 148.1 (C-3a), 134.6 (C-6), 131.8 (C-2'), 130.0 (C-7a), 127.8 (C-4), 127.2 (C-3'), 120.0 (C-1'), 119.1 (C-5), 115.9 (C-7), 90.6 (C-2''), 87.1 (C-1''), 52.9 (C-g), 47.2 (C-e), 44.7 (C-a), 34.4 (C-b), 26.9 (C-c), 26.2 (C-d), 16.4 (C-f); **ATR-IR** (neat): $\tilde{\nu}$ [cm^{-1}] = 2924, 2850, 1728, 1435, 1255, 1211, 1163, 1048, 906, 826, 783; **HRMS** (ESI$^+$): m/z calc.: 388.2020 $[M+H]^+$, found: 388.2017; **R_f**: 0.56 (CH_2Cl_2/acetone 40:1 v/v).

5-((4-Cyclohexylphenyl)ethynyl)-1-ethyl-1H-benzo[*d*][1,2,3]triazole-7-carboxylic acid 73

The saponification was carried out as described in general procedure V by treating methyl ester **252** (210 mg, 542 µmol) with aqueous 1.0 M NaOH (2 mL) in THF (5 mL) for 8 h. Precipitation in acidic solution provided target compound **72** (175 mg, 468 µmol, 86%) as a colorless solid.

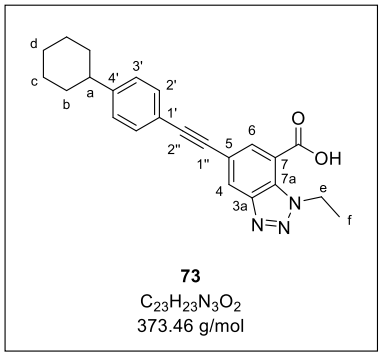

73
$C_{23}H_{23}N_3O_2$
373.46 g/mol

^{1}H-NMR (300 MHz, DMSO-*d*6): δ [ppm] = 8.50 (d, $^4J_{H\text{-}H}$ = 1.5 Hz, 1H, H-4), 8.15 (d, $^4J_{H\text{-}H}$ = 1.5 Hz, 1H, H-6), 7.53 (d, $^3J_{H\text{-}H}$ = 8.2 Hz, 2H, H-2'), 7.29 (d, $^3J_{H\text{-}H}$ = 8.2 Hz, 2H, H-3'), 5.03 (q, $^3J_{H\text{-}H}$ = 7.2 Hz, 2H, C-e), 2.59-2.49 (m, 1H, H-a), 1.82-1.74 (m, 4H, H-$b_{(eq.)}$, H-$c_{(eq.)}$), 1.43 (t, $^3J_{H\text{-}H}$ = 7.2 Hz, 3H, H-f), 1.44-1.32 (m, 4H, H-$b_{(ax.)}$, H-$c_{(ax.)}$), 1.31-1.18 (m, 1H, H-$d_{(ax.)}$); **^{13}C-NMR** (75 MHz, DMSO-*d*6): δ [ppm] = 165.6 (*C*OOH), 148.8 (C-4'), 147.3 (C-3a), 133.3 (C-6), 131.6 (C-2'), 129.5 (C-7a), 127.2 (C-3'), 126.4 (C-4), 119.3 (C-1'), 117.8 (C-5), 117.8 (C-7), 90.0 (C-2''), 87.2 (C-1''), 46.4 (C-e), 43.7 (C-a), 33.7 (C-b), 26.3 (C-c), 25.5 (C-d), 15.9 (C-f); **ATR-IR** (neat): $\tilde{\nu}$ [cm^{-1}] = 1709, 1253,

1175, 1162, 1056, 824, 785, 720, 673, 548; **HRMS** (ESI$^+$): m/z calc.: 374.1863 $[M+H]^+$, found: 374.1860; **R_f**: 0.40 (CH_2Cl_2/MeOH 9:1 v/v).

6.3.8. Syntheses of final hDHODH inhibitors 77-82

Methyl 2-(3,3-dimethylureido)-5-iodobenzoate 259

The compound was synthesized in a previous study and was provided for use in this work.[160]

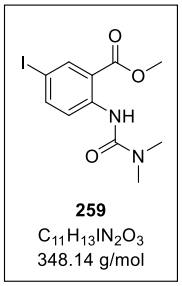

259
$C_{11}H_{13}IN_2O_3$
348.14 g/mol

3-Fluoro-4-iodo-*N*-propylaniline 153

The reductive amination was carried out as described in general procedure VI with 3-fluoro-4-iodoaniline **158** (2.00 g, 8.44 mmol), propionaldehyde (670 µL, 9.28 mmol), glacial acetic acid (580 µL, 10.1 mmol) and STAB (2.68 g, 12.7 mmol) in dichloromethane (20 mL). After purification by column chromatography (PE/CH_2Cl_2 5:1 v/v), **153** (1.49 g, 5.32 mmol, 63%) was obtained as a brownish oil.

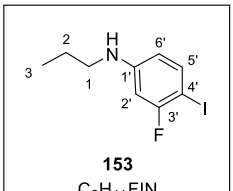

153
$C_9H_{11}FIN$
279.10 g/mol

^{1}H-NMR (500 MHz, $CDCl_3$): *δ* [ppm] = 7.38 (dd, $^3J_{H-H}$ = 8.6 Hz, $^4J_{H-F}$ = 7.3 Hz, 1H, H-5'), 6.33 (dd, $^3J_{H-F}$ = 10.7 Hz, $^4J_{H-H}$ = 2.6 Hz, 1H, H-2'), 6.19 (dd, $^3J_{H-H}$ = 8.6 Hz, $^4J_{H-H}$ = 2.6 Hz, 1H, H-6'), 3.82 (s, 1H, N*H*), 3.04 (t, $^3J_{H-H}$ = 7.3 Hz, 2H, H-1), 1.63 (h, $^3J_{H-H}$ = 7.3 Hz, 2H, H-2), 0.99 (t, $^3J_{H-H}$ = 7.3 Hz, 3H, H-3); **^{13}C-NMR** (126 MHz, $CDCl_3$): *δ* [ppm] = 162.7 (C-3'), 150.7 (C-1'), 138.9 (C-5'), 111.1 (C-6'), 99.8 (C-2'), 63.4 (C-4'), 45.7 (C-1), 22.6 (C-2), 11.7 (C-3); **^{19}F-NMR** (565 MHz, $CDCl_3$): δ [ppm] = −94.5 (Ar-*F*); **ATR-IR** (neat): $\tilde{\nu}$ [cm^{-1}] = 3418, 2960, 2931, 2873, 1604, 1576, 1500, 1416, 1331, 1241, 1182, 1148, 1122, 824, 795; **HRMS** (ESI$^+$): m/z calc.: 279.9993 $[M+H]^+$, found: 279.9998; **R_f**: 0.29 (PE/CH_2Cl_2 5:1 v/v).

3-Fluoro-*N*-propyl-4-((trimethylsilyl)ethynyl)aniline 213

According to general procedure II, the reaction was performed with 3-fluoro-4-iodo-*N*-propylanilin **153** (1.09 g, 3.90 mmol), copper iodide (74.3 mg, 390 µmol), $Pd(PPh_3)_4$ (451 mg, 390 µmol) and TMS acetylene (1.46 mL, 10.5 mmol) in triethylamine (16 mL) and THF (9 mL) at room temperature for 24 h. Purification by column chromatography (PE/CH_2Cl_2 6:1 v/v) provided **213** (741 mg, 2.97 mmol, 76%) as a brownish oil.

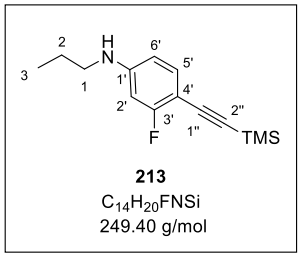

213
$C_{14}H_{20}FNSi$
249.40 g/mol

^{1}H-NMR (500 MHz, $CDCl_3$): *δ* [ppm] = 7.22-7.18 (m, 1H, H-5'), 6.25 (dd, $^{3}J_{H\text{-}H}$ = 8.3 Hz, $^{4}J_{H\text{-}H}$ = 2.4 Hz, 1H, H-6'), 6.23 (dd, $^{3}J_{H\text{-}F}$ = 11.9 Hz, $^{4}J_{H\text{-}H}$ = 2.4 Hz, 1H, H-2'), 3.93 (s, 1H, N*H*), 3.05 (t, $^{3}J_{H\text{-}H}$ = 7.3 Hz, 2H, H-1), 1.63 (h, $^{3}J_{H\text{-}H}$ = 7.3 Hz, 2H, H-2), 0.99 (t, $^{3}J_{H\text{-}H}$ = 7.3 Hz, 3H, H-3), 0.24 (s, 9H, Si(C*H*$_3$)$_3$); **^{13}C-NMR** (126 MHz, $CDCl_3$): *δ* [ppm] = 164.7 (C-3'), 150.6 (C-1'), 134.6 (C-5'), 108.5 (C-6'), 99.6 (C-4'), 99.1 (C-1''), 98.7 (C-2'), 96.6 (C-2''), 45.5 (C-1), 22.6 (C-2), 11.7 (C-3), 0.26 (Si(*C*H$_3$)$_3$); **^{19}F-NMR** (565 MHz, $CDCl_3$): δ [ppm] = −109.0 (Ar-*F*); **ATR-IR** (neat): $\tilde{\nu}$ [cm^{-1}] = 3418, 2961, 2876, 2151, 1622, 1517, 1337, 1248, 1222, 1181, 1111, 857, 836, 804, 757, 698, 632; **HRMS** (ESI$^+$): m/z calc.: 250.1422 $[M+H]^+$, found: 250.1532; **R_f**: 0.24 (PE/CH_2Cl_2 6:1 v/v).

4-Ethynyl-3-fluoro-*N*-propylaniline 218

The cleavage of the protecting group was carried out as described in general procedure III by treating **213** (971 mg, 3.89 mmol) with potassium carbonate (2.69 g, 19.5 mmol) in methanol (30 mL) for 4 h. Alkyne **218** (199 mg, 1.12 mmol, 29%) was obtained as a yellowish oil.

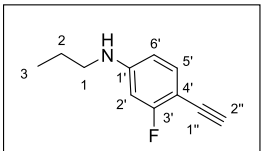

218
$C_{11}H_{12}FN$
177.22 g/mol

^{1}H-NMR (600 MHz, $CDCl_3$): *δ* [ppm] = 7.24-7.20 (m, 1H, H-5'), 6.28 (dd, $^{3}J_{H\text{-}H}$ = 8.3 Hz, $^{4}J_{H\text{-}H}$ = 2.4 Hz, 1H, H-6'), 6.25 (dd, $^{3}J_{H\text{-}F}$ = 12.0 Hz, $^{4}J_{H\text{-}H}$ = 2.4 Hz, 1H, H-2'), 3.96 (s, 1H, N*H*), 3.17 (s, 1H, H-2''), 3.09-3.03 (m, 2H, H-1), 1.63 (sext, $^{3}J_{H\text{-}H}$ = 7.3 Hz, 2H, H-2), 0.99 (t, $^{3}J_{H\text{-}H}$ = 7.3 Hz, 3H, H-3); **^{13}C-NMR** (151 MHz, $CDCl_3$): *δ* [ppm] = 165.0 (C-3'), 150.8 (C-1'), 134.6 (C-5'), 108.6 (C-6'), 98.7 (C-2'), 97.8 (C-4'), 79.6 (C-2''), 78.4 (C-1''), 45.5 (C-1), 22.6 (C-2), 11.7 (C-3); **^{19}F-NMR** (565 MHz, $CDCl_3$): δ [ppm] = −109.7 (Ar-*F*); **ATR-IR** (neat): $\tilde{\nu}$ [cm^{-1}] = 3417, 3293, 2963, 2933, 2875, 2104, 1622, 1568, 1516, 1475, 1460, 1335, 1245, 1181, 1108, 826, 805, 631; **MS** (EI): m/z calc.: 177.10 $[M]^+$, found: 177.10; **R_f**: 0.29 (PE/CH_2Cl_2 5:1 v/v).

Methyl 2-(3,3-dimethylureido)-5-((2-fluoro-4-(propylamino)phenyl)ethynyl)benzoate 253

The reaction was performed according to general procedure IV with urea derivative **259** (145 mg, 415 µmol), copper iodide (7.9 mg, 42 µmol), $Pd(PPh_3)_4$ (48.0 mg, 41.5 µmol) and alkyne **218** (81.0 mg, 457 µmol) in triethylamine (4 mL) and THF (3 mL) at room temperature for 20 h. The crude product was purified by column chromatography (CH_2Cl_2/acetone 19:1 v/v) to yield **253** (138 mg, 346 µmol, 83%) as an orange solid.

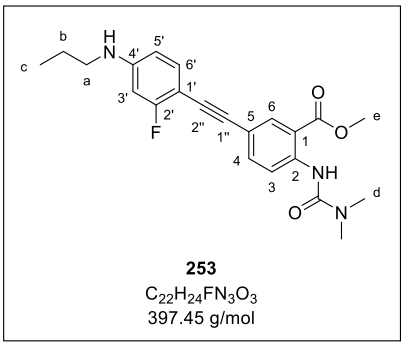

^{1}H-NMR (600 MHz, $CDCl_3$): *δ* [ppm] = 10.71 (s, 1H, CON*H*), 8.60 (d, $^{3}J_{H-H}$ = 8.9 Hz, 1H, H-3), 8.16 (d, $^{4}J_{H-H}$ = 2.1 Hz, 1H, H-6), 7.62 (dd, $^{3}J_{H-H}$ = 8.9 Hz, $^{4}J_{H-H}$ = 2.1 Hz, 1H, H-4), 7.23-7.26 (m, 1H, H-6'), 6.31 (dd, $^{3}J_{H-H}$ = 8.3 Hz, $^{4}J_{H-H}$ = 2.3 Hz, 1H, H-5'), 6.29 (dd, $^{3}J_{H-F}$ = 12.0 Hz, $^{4}J_{H-H}$ = 2.3 Hz, 1H, H-3'), 3.92 (s, 3H, H-e), 3.09 (s, 6H, H-d), 3.09-3.05 (m, 2H, H-a), 1.64 (sext, $^{3}J_{H-H}$ = 7.3 Hz, 2H, H-b), 1.00 (t, $^{3}J_{H-H}$ = 7.3 Hz, 3H, H-c); **^{13}C-NMR** (151 MHz, $CDCl_3$): *δ* [ppm] = 169.1 (*C*OOMe), 164.3 (C-2'), 155.5 (*C*ONH), 150.4 (C-4'), 143.2 (C-2), 137.3 (C-4), 134.0 (C-6'), 133.9 (C-6), 119.4 (C-3), 116.1 (C-5), 113.8 (C-1), 108.7 (C-5'), 99.1 (C-4'), 98.8 (C-3'), 91.1 (C-1''), 83.3 (C-2''), 52.5 (C-e), 45.6 (C-a), 36.5 (C-d), 22.6 (C-b), 11.7 (C-c); **^{19}F-NMR** (565 MHz, $CDCl_3$): δ [ppm] = −109.4 (Ar-*F*); **ATR-IR** (neat): $\tilde{\nu}$ [cm^{-1}] = 3360, 3251, 2928, 2875, 1669, 1627, 1590, 1524, 1481, 1359, 1292, 1248, 1231, 830, 790; **HRMS** (ESI^+): m/z calc.: 398.1875 $[M+H]^+$, found: 398.1883; **R_f**: 0.61 (CH_2Cl_2/acetone 19:1 v/v).

2-(3,3-Dimethylureido)-5-((2-fluoro-4-(propylamino)phenyl)ethynyl)benzoic acid 77

The saponification was carried out according to general procedure V with methyl ester **253** (117 mg, 294 µmol) and aqueous 1.0 M NaOH (1.5 mL) in THF (4 mL) for 24 h. After precipitation in acidic solution, target compound **77** (107 mg, 280 µmol, 95%) was isolated as an ivory solid.

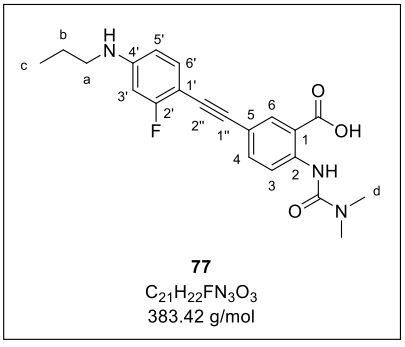

^{1}H-NMR (600 MHz, DMSO-*d*6): *δ* [ppm] = 13.80 (s, 1H, COO*H*), 10.92 (s, 1H, CON*H*), 8.52 (d, $^{3}J_{H-H}$ = 8.9 Hz, 1H, H-3), 7.99 (d, $^{4}J_{H-H}$ = 2.2 Hz, 1H, H-6), 7.60 (dd, $^{3}J_{H-H}$ = 8.9 Hz, $^{4}J_{H-H}$ = 2.2 Hz, 1H, H-4), 7.26-7.21 (m, 1H, H-6'), 6.42-6.36 (m, 2H, H-5', H-3'), 3.02-2.96 (m, 2H, H-a), 2.98 (s, 6H, H-d), 1.55 (sext, $^{3}J_{H-H}$ = 7.3 Hz, 2H, H-b), 0.93 (t, $^{3}J_{H-H}$ = 7.3 Hz, 3H, H-c); **^{13}C-NMR** (151 MHz, DMSO-*d*6): *δ* [ppm] = 169.7 (*C*OOH), 163.4 (C-2'), 154.4 (*C*ONH), 151.4 (C-4'), 142.9 (C-2), 136.1 (C-4), 133.6 (C-6'), 133.4 (C-6), 118.7 (C-3), 114.8 (C-5), 114.5 (C-1), 108.5 (C-5'), 97.5 (C-3'), 95.6 (C-4'), 90.4 (C-1''), 83.7 (C-2''), 44.3 (C-a), 35.8 (C-d), 21.7 (C-b), 11.6 (C-c); **^{19}F-NMR** (565 MHz, DMSO-*d*6): δ [ppm] = −110.2 (Ar-*F*); **ATR-IR** (neat): $\tilde{\nu}$ [cm^{-1}] = 2958, 2923, 2851, 2203, 1681, 1626, 1602, 1575, 1525, 1389, 1344, 1291, 1209, 1191, 1103, 836, 796; **HRMS** (ESI^+): m/z calc.: 384.1718 $[M+H]^+$, found: 384.1731; **R_f**: 0.34 (CH_2Cl_2/MeOH 9:1 v/v).

4-Iodo-*N*-propyl-3-(trifluoromethyl)aniline 157

According to general procedure VI, the reductive amination was carried out with 4-iodo-3-(trifluoromethyl)aniline **159** (1.00 g, 3.48 mmol), propionaldehyde (270 µL, 3.83 mmol), glacial acetic acid (240 µL, 4.18 mmol) and STAB (1.11 g, 5.23 mmol) in dichloromethane (10 mL). The crude product was purified by column chromatography (PE/CH_2Cl_2 4:1 v/v) to give **157** (1.02 g, 3.10 mmol, 89%) as a colorless oil.

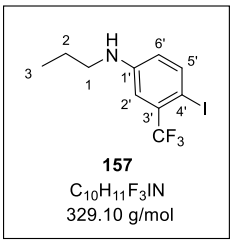

157
$C_{10}H_{11}F_3IN$
329.10 g/mol

^{1}H-NMR (600 MHz, $CDCl_3$): *δ* [ppm] = 7.68 (d, $^3J_{H\text{-}H}$ = 8.6 Hz, 1H, H-5'), 6.88 (d, $^4J_{H\text{-}H}$ = 2.9 Hz, 1H, H-2'), 6.42 (dd, $^3J_{H\text{-}H}$ = 8.6 Hz, $^4J_{H\text{-}H}$ = 2.9 Hz, 1H, H-6'), 3.94 (s, 1H, N*H*), 3.08 (t, $^3J_{H\text{-}H}$ = 7.3 Hz, 2H, H-1), 1.64 (sext, $^3J_{H\text{-}H}$ = 7.3 Hz, 2H, H-2), 1.00 (t, $^3J_{H\text{-}H}$ = 7.3 Hz, 1H, H-3); **^{13}C-NMR** (151 MHz, $CDCl_3$): *δ* [ppm] = 148.1 (C-1'), 142.3 (C-5'), 133.9 (C-3'), 123.0 (*C*F_3), 116.7 (C-6'), 112.3 (C-2'), 72.5 (C-4'), 45.6 (C-1), 22.5 (C-2), 11.5 (C-3); **^{19}F-NMR** (565 MHz, $CDCl_3$): δ [ppm] = −62.9 (C*F*$_3$); **ATR-IR** (neat): $\tilde{\nu}$ [cm^{-1}] = 3424, 2963, 2934, 2876, 1603, 1498, 1471, 1417, 1333, 1263, 1244, 1168, 1120, 1092, 1003, 811; **HRMS** (ESI$^+$): m/z calc.: 330.9961 $[M+H]^+$, found: ; **R_f**: 0.43 (PE/CH_2Cl_2 4:1 v/v).

N-Propyl-3-(trifluoromethyl)-4-((trimethylsilyl)ethynyl)aniline 214

The reaction was carried out as described in general procedure II with 4-iodo-*N*-propyl-3-(trifluoromethyl)aniline **157** (990 mg, 3.01 mmol), copper iodide (57.3 mg, 301 µmol), $Pd(PPh_3)_4$ (348 mg, 301 µmol) and TMS acetylene (1.12 mL, 8.12 mmol) in triethylamine (12 mL) and THF (6 mL) at room temperature for 24 h. Purification by column chromatography (PE/CH_2Cl_2 6:1 v/v) provided **214** (767 mg, 2.56 mmol, 85%) as a yellowish oil.

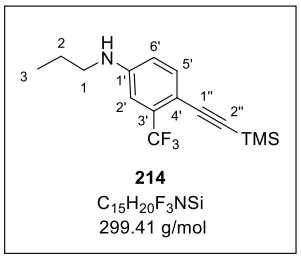

214
$C_{15}H_{20}F_3NSi$
299.41 g/mol

^{1}H-NMR (600 MHz, $CDCl_3$): *δ* [ppm] = 7.37 (d, $^3J_{H\text{-}H}$ = 8.4 Hz, 1H, H-5'), 6.80 (d, $^4J_{H\text{-}H}$ = 2.5 Hz, 1H, H-2'), 6.62 (dd, $^3J_{H\text{-}H}$ = 8.4 Hz, $^4J_{H\text{-}H}$ = 2.5 Hz, 1H, H-6'), 3.10 (t, $^3J_{H\text{-}H}$ = 7.3 Hz, 2H, H-1), 1.65 (sext, $^3J_{H\text{-}H}$ = 7.3 Hz, 2H, H-2), 1.00 (t, $^3J_{H\text{-}H}$ = 7.3 Hz, 1H, H-3), 0.23 (s, 9H, Si(*C*H_3)$_3$); **^{13}C-NMR** (151 MHz, $CDCl_3$): *δ* [ppm] = 147.6 (C-1'), 135.7 (C-5'), 132.3 (C-3'), 123.9 (*C*F_3), 114.5 (C-6'), 110.0 (C-2'), 108.4 (C-4'), 102.0 (C-1''), 97.1 (C-2''), 45.6 (C-1), 22.5 (C-2), 11.7 (C-3), −0.02 (Si(*C*H_3)$_3$); **^{19}F-NMR** (565 MHz, $CDCl_3$): δ [ppm] = −62.6 (C*F*$_3$); **ATR-IR** (neat): $\tilde{\nu}$ [cm^{-1}] = 3430, 2962, 2878, 2154, 1615, 1514, 1341, 1248, 1164, 1126, 1043, 855, 838, 758; **HRMS** (ESI$^+$): m/z calc.: 329.9961 $[M+H]^+$, found: 329.9982; **R_f**: 0.38 (PE/CH_2Cl_2 4:1 v/v).

4-Ethynyl-*N*-propyl-3-(trifluoromethyl)aniline 219

The cleavage of the protecting group was performed according to general procedure III by treating **214** (350 mg, 1.17 mmol) with potassium carbonate (807 mg, 5.85 mmol) in methanol (10 mL) for 4 h. Alkyne **219** (257 mg, 1.13 mmol, 97%) was isolated as an orange oil.

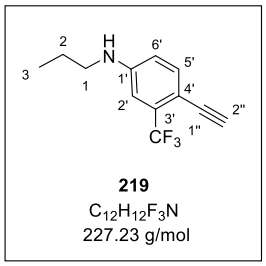

^{1}H-NMR (600 MHz, $CDCl_3$): *δ* [ppm] = 7.41 (d, $^3J_{H-H}$ = 8.4 Hz, 1H, H-5'), 6.79 (d, $^4J_{H-H}$ = 2.5 Hz, 1H, H-2'), 6.61 (dd, $^3J_{H-H}$ = 8.4 Hz, $^4J_{H-H}$ = 2.5 Hz, 1H, H-6'), 4.03 (s, 1H, N*H*), 3.18 (s, 1H, H-2''), 3.14-3.09 (m, 2H, H-1), 1.65 (sext, $^3J_{H-H}$ = 7.3 Hz, 2H, H-2), 1.01 (t, $^3J_{H-H}$ = 7.3 Hz, 1H, H-3); **^{13}C-NMR** (151 MHz, $CDCl_3$): *δ* [ppm] = 148.4 (C-1'), 136.2 (C-5'), 133.4 (C-3), 123.7 (*C*F_3), 114.3 (C-6'), 109.7 (C-2'), 107.1 (C-4'), 80.7 (C-1''), 79.6 (C-2''), 45.4 (C-1), 22.6 (C-2), 11.7 (C-3); **^{19}F-NMR** (565 MHz, $CDCl_3$): δ [ppm] = −62.5 (C*F*$_3$); **ATR-IR** (neat): $\tilde{\nu}$ [cm^{-1}] = 3424, 3301, 2965, 2936, 2878, 1616, 1513, 1339, 1266, 1249, 1161, 1120, 1081, 1041, 821, 647, 595, 545; **HRMS** (ESI$^+$): m/z calc.: 228.0995 $[M+H]^+$, found: 228.1004; **R$_f$**: 0.34 (PE/CH_2Cl_2 4:1 v/v).

Methyl 2-(3,3-dimethylureido)-5-((4-(propylamino)-2-(trifluoromethyl)phenyl)ethynyl)-benzoate 254

The reaction was carried out as described in general procedure IV with urea derivative **259** (150 mg, 431 µmol), copper iodide (8.2 mg, 43 µmol), $Pd(PPh_3)_4$ (49.8 mg, 43.1 µmol) and alkyne **219** (108 mg, 474 µmol) in triethylamine (4 mL) and THF (3 mL) at room temperature for 4 h. After purification by column chromatography (CH_2Cl_2/acetone 50:1 v/v), **254** (117 mg, 261 µmol, 61%) was obtained as a yellowish solid.

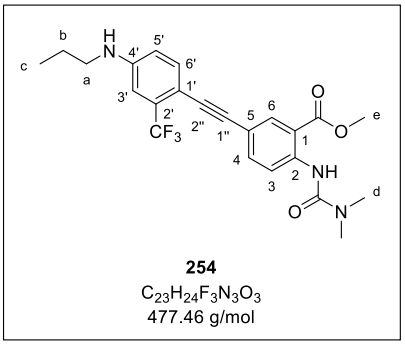

^{1}H-NMR (600 MHz, $CDCl_3$): *δ* [ppm] = 10.73 (s, 1H, CON*H*), 8.61 (d, $^3J_{H-H}$ = 8.9 Hz, 1H, H-3), 8.13 (d, $^4J_{H-H}$ = 2.1 Hz, 1H, H-6), 7.61 (dd, $^3J_{H-H}$ = 8.9 Hz, $^4J_{H-H}$ = 2.1 Hz, 1H, H-4), 7.42 (d, $^3J_{H-H}$ = 8.4 Hz, 1H, H-6'), 6.83 (d, $^4J_{H-H}$ = 2.5 Hz, 1H, H-3'), 6.65 (dd, $^3J_{H-H}$ = 8.4 Hz, $^4J_{H-H}$ = 2.5 Hz, 1H, H-5'), 4.02 (t, $^3J_{H-H}$ = 5.5 Hz, 1H, N*H*), 3.93 (s, 3H, H-e), 3.13 (td, $^3J_{H-H}$ = 7.3 Hz, $^3J_{H-H}$ = 5.5 Hz, 2H, H-a), 3.09 (s, 6H, H-d), 1.66 (sext, $^3J_{H-H}$ = 7.3 Hz, 2H, H-b), 1.02 (t, $^3J_{H-H}$ = 7.3 Hz, 3H, H-c); **^{13}C-NMR** (151 MHz, $CDCl_3$): *δ* [ppm] = 169.1 (*C*OOMe), 155.5 (NH*C*O), 148.0 (C-4'), 143.4 (C-2), 137.3 (C-4), 135.2 (C-6'), 133.9 (C-6), 123.4 (*C*F_3), 119.4 (C-3), 116.0 (C-5), 114.5 (C-5'), 113.8 (C-1), 109.8 (C-3'), 108.5 (C-1'), 91.1 (C-1''), 85.9 (C-2''), 52.5 (C-e), 45.5 (C-a), 36.5 (C-d), 22.6 (C-b), 11.7 (C-c); **^{19}F-NMR** (565 MHz, $CDCl_3$): δ [ppm] = −62.5 (C*F*$_3$); **ATR-IR** (neat): $\tilde{\nu}$ [cm^{-1}] = 3307, 2929, 2871, 1660, 1617, 1588, 1517, 1489, 1435, 1334, 1296, 1248, 1233, 1171, 1124, 1085,

1040; **HRMS** (ESI$^+$): m/z calc.: 448.1843 $[M+H]^+$, found: 448.1901; $\mathbf{R_f}$: 0.33 (CH_2Cl_2/acetone 50:1 v/v).

2-(3,3-Dimethylureido)-5-((4-(propylamino)-2-(trifluoromethyl)phenyl)ethynyl)benzoic acid 78

The saponification was performed according to general procedure V by treating methyl ester **254** (100 mg, 223 µmol) with aqueous 1.0 M NaOH (1 mL) in THF (3 mL) for 16 h. Precipitation in acidic solution afforded target compound **78** (76.5 mg, 177 µmol, 79%) as an ivory solid.

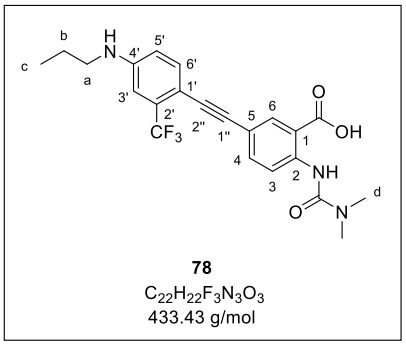

^{1}H-NMR (400 MHz, DMSO-*d*6): δ [ppm] = 13.82 (s, 1H, COO*H*), 10.94 (s, 1H, CON*H*), 8.53 (d, $^3J_{H\text{-}H}$ = 8.9 Hz, 1H, H-3), 7.99 (d, $^4J_{H\text{-}H}$ = 2.2 Hz, 1H, H-6), 7.57 (dd, $^3J_{H\text{-}H}$ = 8.9 Hz, $^4J_{H\text{-}H}$ = 2.2 Hz, 1H, H-4), 7.44 (d, $^3J_{H\text{-}H}$ = 8.5 Hz, 1H, H-6'), 6.92 (d, $^4J_{H\text{-}H}$ = 2.4 Hz, 1H, H-3'), 6.76 (dd, $^3J_{H\text{-}H}$ = 8.5 Hz, $^4J_{H\text{-}H}$ = 2.4 Hz, 1H, H-5'), 6.62-6.52 (s, 1H, N*H*), 3.04 (t, $^3J_{H\text{-}H}$ = 7.3 Hz, 2H, H-a), 2.98 (s, 6H, H-d), 1.57 (sext, $^3J_{H\text{-}H}$ = 7.3 Hz, 2H, H-b), 0.94 (t, $^3J_{H\text{-}H}$ = 7.3 Hz, 3H, H-c); **^{13}C-NMR** (101 MHz, DMSO-*d*6): δ [ppm] = 169.6 (COO*H*), 154.4 (*C*ONH), 149.0 (C-4'), 143.1 (C-2), 135.9 (C-4), 135.0 (C-6'), 133.4 (C-6), 130.8 (C-2'), 123.9 (*C*F_3), 118.8 (C-3), 114.6 (C-5), 114.6 (C-1), 113.8 (C-5'), 109.1 (C-3'), 104.8 (C-1'), 90.3 (C-1''), 86.0 (C-2''), 44.1 (C-a), 35.8 (C-d), 21.6 (C-b), 11.5 (C-c); **ATR-IR** (neat): $\tilde{\nu}$ [cm^{-1}] = 2929, 2879, 1648, 1617, 1601, 1580, 1523, 1352, 1296, 1281, 1264, 1211, 1193, 1168, 1146, 1123, 1041, 846; **HRMS** (ESI$^+$): m/z calc.: 432.1540 $[M-H]^-$, found: 432.1546; $\mathbf{R_f}$: 0.22 (CH_2Cl_2/MeOH 9:1 v/v).

1-(4-Bromo-3-fluorophenyl)piperidine 154

The reaction was performed according to general procedure I with 1-bromo-2-fluoro-4-iodobenzene **137** (1.00 g, 3.32 mmol), copper iodide (127 mg, 665 µmol), L-proline (153 mg, 1.33 mmol), potassium carbonate (919 mg, 6.65 mmol) and piperidine (490 µL, 4.99 mmol) in DMSO (6 mL) for 24 h. Purification by column chromatography (PE/CH_2Cl_2 4:1 v/v) afforded **154** (335 mg, 1.30 mmol, 39%) as a colorless solid.

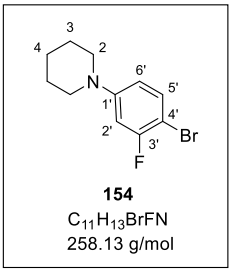

^{1}H-NMR (600 MHz, $CDCl_3$): δ [ppm] = 7.33-7.29 (m, 1H, H-5'), 6.65 (dd, $^3J_{H\text{-}F}$ = 12.2 Hz, $^4J_{H\text{-}H}$ = 2.8 Hz, 1H, H-2'), 6.57 (dd, $^3J_{H\text{-}H}$ = 8.7 Hz, $^4J_{H\text{-}H}$ = 2.8 Hz, H-6'), 3.18-3.15 (m, 4H, H-2), 1.71-1.65 (m, 4H, H-3), 1.62-1.56 (m, 2H, H-4); **^{13}C-NMR** (151 MHz, $CDCl_3$): δ [ppm] = 159.8 (C-3'), 152.9 (C-1'), 133.2 (C-5'), 112.9 (C-6'), 103.9 (C-2'), 96.1 (C-4'), 50.0 (C-2),

25.5 (C-3), 24.3 (C-4); **^{19}F-NMR** (565 MHz, $CDCl_3$): δ [ppm] = −107.3 (Ar-*F*); **ATR-IR** (neat): $\tilde{\nu}$ [cm^{-1}] = 2940, 2849, 1601, 1561, 1492, 1446, 1355, 1247, 1223, 1198, 1122, 965, 812, 783; **HRMS** (ESI^+): m/z calc.: 258.0288 $[M+H]^+$, found: 258.0292; **R_f**: 0.26 (PE/CH_2Cl_2 9:1 v/v).

1-(3-Fluoro-4-((trimethylsilyl)ethynyl)phenyl)piperidine 215

According to general procedure II, the reaction was carried out with 1-(4-bromo-3-fluorophenyl)piperidine **154** (319 mg, 1.24 mmol), copper iodide (23.5 mg, 123 µmol), $Pd(PPh_3)_4$ (143 mg, 123 µmol) and TMS acetylene (460 µL, 3.33 mmol) in triethylamine (5 mL) and THF (2 mL) at 70 °C for 24 h. Purification by column chromatography (PE/CH_2Cl_2 4:1 v/v) provided **215** (288mg, 1.04 mmol, 85%) as a yellow solid.

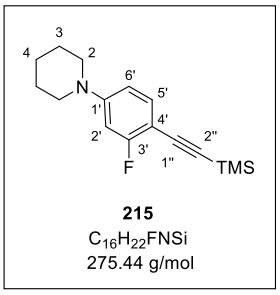

215
$C_{16}H_{22}FNSi$
275.44 g/mol

^{1}H-NMR (600 MHz, $CDCl_3$): *δ* [ppm] = 7.30-7.24 (m, 4H, H-5'), 6.57 (dd, $^3J_{H-H}$ = 8.7 Hz, $^4J_{H-H}$ = 2.5 Hz, H-6'), 6.53 (dd, $^3J_{H-F}$ = 13.2 Hz, $^4J_{H-H}$ = 2.5 Hz, 1H, H-2'), 3.25-3.21 (m, 4H, H-2), 1.71-1.64 (m, 4H, H-3), 1.64-1.59 (m, 2H, H-4), 0.26 (s, 9H, $Si(CH_3)_3$); **^{13}C-NMR** (151 MHz, $CDCl_3$): *δ* [ppm] = 164.3 (C-3'), 155.3 (C-1'), 134.3 (C-5'), 110.5 (C-6'), 101.6 (C-2'), 99.8 (C-4'), 99.3 (C-1''), 97.1 (C-2''), 49.2 (C-2), 25.5 (C-3), 24.4 (C-4), 0.24 ($Si(CH_3)_3$); **^{19}F-NMR** (565 MHz, $CDCl_3$): δ [ppm] = −108.8 (Ar-*F*); **ATR-IR** (neat): $\tilde{\nu}$ [cm^{-1}] = 2930, 2856, 2150, 1619, 1543, 1509, 1445, 1245, 1222, 1113, 832, 792, 758, 698, 613, 598; **HRMS** (ESI^+): m/z calc.: 276.1579 $[M+H]^+$, found: 276.1588, **R_f**: 0.14 (PE/CH_2Cl_2 4:1 v/v).

1-(4-Ethynyl-3-fluorophenyl)piperidine 220

The reaction was carried out as described in general procedure III by treating **215** (288 mg, 1.04 mmol) with potassium carbonate (722 mg, 5.22 mmol) in methanol (8 mL) for 4 h. Alkyne **220** (168 mg, 825 µmol, 79%) was obtained as a yellowish solid.

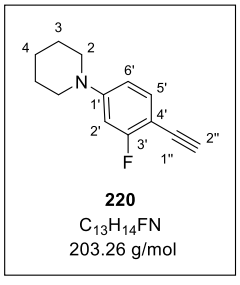

220
$C_{13}H_{14}FN$
203.26 g/mol

^{1}H-NMR (600 MHz, $CDCl_3$): *δ* [ppm] = 7.32-7.27 (m, 1H, H-5'), 6.58 (dd, $^3J_{H-H}$ = 8.7 Hz, $^4J_{H-H}$ = 2.5 Hz, H-6'), 6.54 (dd, $^3J_{H-F}$ = 13.2 Hz, $^4J_{H-H}$ = 2.5 Hz, 1H, H-2'), 3.26-3.21 (m, 4H, H-2), 3.18 (s, 1H, H-2''), 1.70-1.64 (m, 4H, H-3), 1.64-1.59 (m, 2H, H-4); **^{13}C-NMR** (151 MHz, $CDCl_3$): *δ* [ppm] = 164.8 (C-3'), 153.4 (C-1'), 134.4 (C-5'), 110.6 (C-6'), 101.7 (C-2'), 99.8 (C-4'), 80.0 (C-2''), 78.3 (C-1''), 49.2 (C-2), 25.4 (C-3), 24.4 (C-4); **^{19}F-NMR** (565 MHz, $CDCl_3$): δ [ppm] = −109.4 (Ar-*F*); **ATR-IR** (neat): $\tilde{\nu}$ [cm^{-1}] = 3295, 2940, 2840, 2017, 1616, 1544, 1507, 1442, 1351, 1248, 1228, 1183, 1104, 827, 800, 671, 606; **MS** (EI): m/z calc.: 203.11 $[M]^+$, found: 203.10; **R_f**: 0.49 (PE/CH_2Cl_2 2:1 v/v).

Methyl 2-(3,3-dimethylureido)-5-((2-fluoro-4-(piperidin-1-yl)phenyl)ethynyl)benzoate 255

The reaction was carried out according to general procedure IV with urea derivative **259** (200 mg, 574 µmol), copper iodide (10.9 mg, 57.4 µmol), $Pd(PPh_3)_4$ (66.4 mg, 57.4 µmol) and alkyne **220** (128 mg, 632 µmol) in triethylamine (4 mL) and THF (3 mL) at room temperature for 20 h. The crude product was purified by column chromatography (CH_2Cl_2/acetone 100:1 v/v) to give **255** (243 mg, 575 µmol, 100%) as a brownish solid.

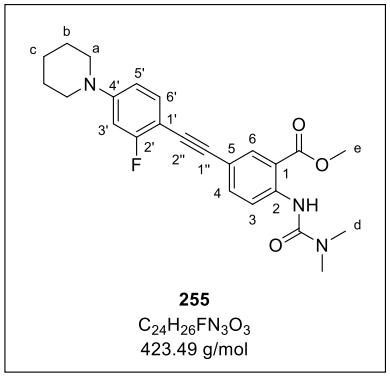

^{1}H-NMR (600 MHz, $CDCl_3$): *δ* [ppm] = 10.72 (s, 1H, CON*H*), 8.61 (d, $^3J_{H-H}$ = 8.9 Hz, 1H, H-3), 8.18 (d, $^4J_{H-H}$ = 2.1 Hz, 1H, H-6), 7.63 (dd, $^3J_{H-H}$ = 8.9 Hz, $^4J_{H-H}$ = 2.1 Hz, 1H, H-4), 7.33-7.29 (m, 1H, H-6'), 6.62 (dd, $^3J_{H-H}$ = 8.7 Hz, $^4J_{H-H}$ = 2.5 Hz, H-5'), 6.58 (dd, $^3J_{H-F}$ = 13.2 Hz, $^4J_{H-H}$ = 2.5 Hz, 1H, H-3'), 3.92 (s, 3H, H-e), 3.26-3.22 (m, 4H, H-a), 3.09 (s, 6H, H-d), 1.70-1.65 (m, 4H, H-b), 1.64-1.59 (m, 2H, H-c); **^{13}C-NMR** (151 MHz, $CDCl_3$): *δ* [ppm] = 169.0 (*C*OOMe), 164.0 (C-2'), 155.5 (*C*ONH), 153.0 (C-4'), 143.3 (C-2), 137.4 (C-4), 134.0 (C-6), 133.7 (C-6'), 119.4 (C-3), 116.0 (C-5), 113.8 (C-1), 110.7 (C-5'), 101.8 (C-3'), 100.2 (C-1'), 91.5 (C-1''), 83.1 (C-2''), 52.5 (C-e), 49.3 (C-a), 36.5 (C-d), 25.5 (C-b), 24.4 (C-c); **^{19}F-NMR** (565 MHz, $CDCl_3$): δ [ppm] = −109.2 (Ar-*F*); **ATR-IR** (neat): $\tilde{\nu}$ [cm^{-1}] = 3296, 3260, 2923, 2847, 1667, 1586, 1516, 1490, 1435, 1298, 1232, 1176, 1081, 849, 787; **HRMS** (ESI^+): m/z calc.: 424.2031 $[M+H]^+$, found: 424.2034, **R_f**: 0.23 (CH_2Cl_2/acetone 200:1 v/v).

2-(3,3-Dimethylureido)-5-((2-fluoro-4-(piperidin-1-yl)phenyl)ethynyl)benzoic acid 79

The saponification was performed according to general procedure V by treating methyl ester **255** (219 mg, 516 µmol) with aqueous 1.0 M NaOH (2 mL) in THF (6 mL) for 20 h. Precipitation in acidic solution afforded target compound **79** (196 mg, 479 µmol, 93%) as a greyish solid.

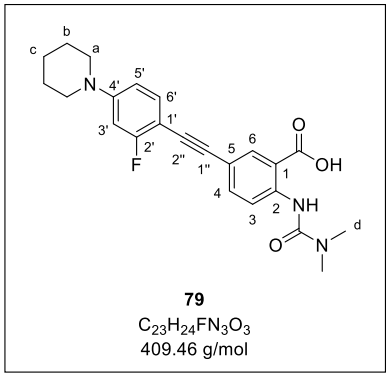

^{1}H-NMR (600 MHz, DMSO-*d*6): *δ* [ppm] = 13.84 (s, 1H, COO*H*), 10.96 (s, 1H, CON*H*), 8.53 (d, $^3J_{H-H}$ = 8.8 Hz, 1H, H-3), 8.02 (d, $^4J_{H-H}$ = 2.2 Hz, 1H, H-6), 7.62 (dd, $^3J_{H-H}$ = 8.8 Hz, $^4J_{H-H}$ = 2.2 Hz, 1H, H-4), 7.37-7.32 (m, 1H, H-6'), 6.80 (dd, $^3J_{H-F}$ = 13.9 Hz, $^4J_{H-H}$ = 2.5 Hz, 1H, H-3'), 6.74 (dd, $^3J_{H-H}$ = 8.8 Hz, $^4J_{H-H}$ = 2.5 Hz, H-5'), 3.30-3.26 m, 4H, H-a), 2.98 (s, 6H, H-c), 1.59-1.54 (m, 6H, H-b, H-c); **^{13}C-NMR** (151 MHz, DMSO-*d*6): *δ* [ppm] = 169.0 (*C*OOH), 163.1 (C-2'), 154.4

(*C*ONH), 152.5 (C-4'), 143.2 (C-2), 136.2 (C-4), 133.6 (C-6), 133.5 (C-6'), 118.7 (C-3), 114.6 (C-5), 114.4 (C-1), 110.4 (C-5'), 100.8 (C-3'), 97.8 (C-1'), 91.1 (C-1''), 83.1 (C-2''), 48.0 (C-a), 35.8 (C-d), 24.8 (C-b), 23.9 (C-c); **^{19}F-NMR** (565 MHz, DMSO-*d*6): δ [ppm] = −109.6 (Ar-*F*); **ATR-IR** (neat): $\tilde{\nu}$ [cm^{-1}] = 2939, 2819, 1643, 1602, 1579, 1529, 1373, 1301, 1247, 1211, 1191, 1104, 845, 803, 710; **HRMS** (ESI$^+$): m/z calc.: 410.1875 [M+H]$^+$, found: 410.1895; **R_f**: 0.45 (CH_2Cl_2/MeOH 9:1 v/v).

Methyl 2-(3,3-dimethylureido)-5-((2-fluoro-4-morpholinophenyl)ethynyl)benzoate 256

The reaction was carried out according to general procedure IV with urea derivative **259** (200 mg, 574 µmol), copper iodide (10.9 mg, 57.4 µmol), $Pd(PPh_3)_4$ (66.4 mg, 57.4 µmol) and alkyne **197** (144 mg, 660 µmol) in triethylamine (4 mL) and THF (3 mL) at room temperature for 20 h. The crude product was purified by column chromatography (CH_2Cl_2/acetone 19:1 v/v) to yield **256** (236 mg, 555 µmol, 97%) as an ivory solid.

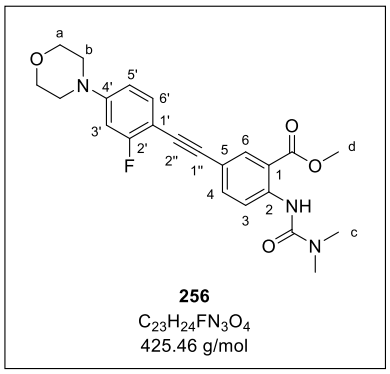

256
$C_{23}H_{24}FN_3O_4$
425.46 g/mol

^{1}H-NMR (600 MHz, $CDCl_3$): *δ* [ppm] = 10.73 (s, 1H, CON*H*), 8.62 (d, $^3J_{H\text{-}H}$ = 8.9 Hz, 1H, H-3), 8.18 (d, $^4J_{H\text{-}H}$ = 2.1 Hz, 1H, H-6), 7.63 (dd, $^3J_{H\text{-}H}$ = 8.9 Hz, $^4J_{H\text{-}H}$ = 2.1 Hz, 1H, H-4), 7.38-7.34 (m, 1H, H-6'), 6.62 (dd, $^3J_{H\text{-}H}$ = 8.7 Hz, $^4J_{H\text{-}H}$ = 2.5 Hz, H-5'), 6.58 (dd, $^3J_{H\text{-}F}$ = 12.7 Hz, $^4J_{H\text{-}H}$ = 2.5 Hz, 1H, H-3'), 3.92 (s, 3H, H-d), 3.87-3.82 (m, 4H, H-a), 3.23-3.18 (m, 4H, H-b), 3.09 (s, 6H, H-c); **^{13}C-NMR** (151 MHz, $CDCl_3$): *δ* [ppm] = 169.0 (COOMe), 163.9 (C-2'), 155.4 (*C*ONH), 152.6 (C-4'), 143.5 (C-2), 137.4 (C-4), 134.1 (C-6), 133.9 (C-6'), 119.4 (C-3), 115.7 (C-5), 113.8 (C-1), 110.4 (C-5'), 101.7 (C-1'), 101.7 (C-3'), 92.0 (C-1''), 82.7 (C-2''), 66.7 (C-a), 52.5 (C-d), 48.2 (C-b), 36.5 (C-c); **^{19}F-NMR** (565 MHz, $CDCl_3$): δ [ppm] = −108.7 (Ar-*F*); **ATR-IR** (neat): $\tilde{\nu}$ [cm^{-1}] = 3246, 2958, 2852, 1671, 1589, 1519, 1440, 1233, 1183, 1121, 1084, 971, 836, 789; **HRMS** (ESI$^+$): m/z calc.: 426.1824 [M+H]$^+$, found: 426.1827; **R_f**: 0.27 (CH_2Cl_2/acetone 99:1 v/v).

2-(3,3-Dimethylureido)-5-((2-fluoro-4-morpholinophenyl)ethynyl)benzoic acid 80

The saponification was performed according to general procedure V by treating methyl ester **256** (230 mg, 541 µmol) with aqueous 1.0 M NaOH (2 mL) in THF (6 mL) for 19 h. After precipitation in acidic solution, target compound **80** (172 mg, 418 µmol, 77%) was isolated as a colorless solid.

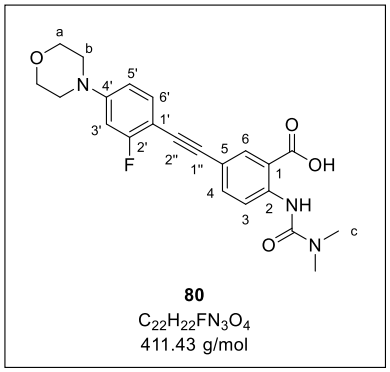

80
$C_{22}H_{22}FN_3O_4$
411.43 g/mol

^{1}H-NMR (600 MHz, DMSO-*d*6): *δ* [ppm] = 13.85 (s, 1H, COO*H*), 10.97 (s, 1H, CON*H*), 8.53 (d, $^3J_{H\text{-}H}$ = 8.8 Hz, 1H, H-3), 8.03 (d, $^4J_{H\text{-}H}$ = 2.2 Hz, 1H, H-6), 7.63 (dd, $^3J_{H\text{-}H}$ = 8.8 Hz, $^4J_{H\text{-}H}$ = 2.2 Hz, 1H, H-4), 7.43-7.38 (m, 1H, H-6'), 6.86 (dd, $^3J_{H\text{-}F}$ = 13.5 Hz, $^4J_{H\text{-}H}$ = 2.5 Hz, 1H, H-3'), 6.78 (dd, $^3J_{H\text{-}H}$ = 8.8 Hz, $^4J_{H\text{-}H}$ = 2.5 Hz, H-5'), 3.74-3.69 (m, 4H, H-a), 3.24-3.20 (m, 4H, H-b), 2.98 (s, 6H, H-c); **^{13}C-NMR** (151 MHz, DMSO-*d*6): *δ* [ppm] = 169.6 (*C*OOH), 163.0 (C-2'), 154.4 (*C*ONH), 152.6 (C-4'), 143.2 (C-2), 136.2 (C-4), 133.7 (C-6), 133.6 (C-6'), 118.7 (C-3), 114.6 (C-1), 114.2 (C-5), 110.2 (C-5'), 101.0 (C-3'), 99.2 (C-1'), 91.4 (C-1''), 82.8 (C-2''), 65.8 (C-a), 47.1 (C-b), 35.8 (C-c); **^{19}F-NMR** (565 MHz, DMSO-*d*6): δ [ppm] = −109.5 (Ar-*F*); **ATR-IR** (neat): *ṽ* [cm^{-1}] = 2959, 2843, 1624, 1579, 1521, 1374, 1296, 1244, 1189, 884, 842, 795; **HRMS** (ESI$^+$): m/z calc.: 412.1667 [M+H]$^+$, found: 412.1675; **R_f**: 0.43 (CH_2Cl_2/MeOH 9:1 v/v).

3-Fluoro-4-iodo-*N*-(3,3,3-trifluoropropyl)aniline 155

The reductive amination was performed according to general procedure VI with 3-fluoro-4-iodoaniline **158** (500 mg, 2.11 mmol), 3,3,3-trifluoropropanal **106** (190 µL, 2.32 mmol), glacial acetic acid (150 µL, 2.53 mmol) and STAB (671 mg, 3.16 mmol) in dichloromethane (7 mL). The crude product was purified by column chromatography (PE/CH_2Cl_2 3:1 v/v) to yield **155** (487 mg, 1.46 mmol, 69%) as a yellow liquid.

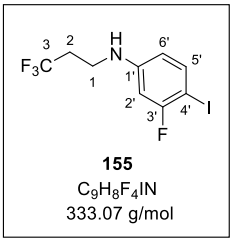

155
$C_9H_8F_4IN$
333.07 g/mol

^{1}H-NMR (600 MHz, $CDCl_3$): *δ* [ppm] = 7.44 (dd, $^3J_{H\text{-}H}$ = 8.6 Hz, $^4J_{H\text{-}F}$ = 7.2 Hz, 1H, H-5'), 6.34 (dd, $^3J_{H\text{-}F}$ = 10.4 Hz, $^4J_{H\text{-}H}$ = 2.7 Hz, 1H, H-2'), 6.21 (dd, $^3J_{H\text{-}H}$ = 8.6 Hz, $^4J_{H\text{-}H}$ = 2.7 Hz, 1H, H-6'), 4.02-3.92 (m, 1H, NH), 3.42 (q, $^3J_{H\text{-}H}$ = 6.7 Hz, 2H, H-1), 2.40 (qt, $^3J_{H\text{-}F}$ = 10.7 Hz, $^3J_{H\text{-}H}$ = 6.7 Hz, 2H, H-2); **^{13}C-NMR** (151 MHz, $CDCl_3$): *δ* [ppm] = 162.8 (C-3'), 149.1 (C-1'), 139.3 (C-5'), 126.4 (C-3), 111.1 (C-6'), 100.2 (C-2'), 65.1 (C-4'), 37.1 (C-1), 33.3 (C-2); **^{19}F-NMR** (565 MHz, $CDCl_3$): δ [ppm] = −65.0 (C*F*$_3$), −94.7 (Ar-*F*); **ATR-IR** (neat): *ṽ* [cm^{-1}] = 3430, 1605, 1580, 1505, 1487, 1390, 1335, 1240, 1185, 1139, 1086, 1001, 950, 938, 826, 795, 545; **HRMS** (ESI$^+$): m/z calc.: 333.9710 [M+H]$^+$, found: 333.9720; **R_f**: 0.30 (PE/CH_2Cl_2 5:1 v/v).

3-Fluoro-*N*-(3,3,3-trifluoropropyl)-4-((trimethylsilyl)ethynyl)aniline 216

The reaction was carried out as described in general procedure II with 3-Fluoro-4-iodo-*N*-(3,3,3-trifluoropropyl)aniline **155** (745 mg, 2.24 mmol), copper iodide (42.6 mg, 224 µmol), $Pd(PPh_3)_4$ (259 mg, 224 µmol) and TMS acetylene (840 µL, 6.04 mmol) in triethylamine

(8 mL) and THF (4 mL) at room temperature for 20 h. The crude product was purified by column chromatography (PE/CH_2Cl_2 5:1 v/v) to give **216** (382 mg, 1.26 mmol, 56%) as a yellow solid.

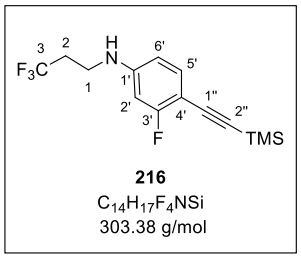

216
$C_{14}H_{17}F_4NSi$
303.38 g/mol

^{1}H-NMR (600 MHz, $CDCl_3$): *δ* [ppm] = 7.26-7.23 (m, 1H, H-5'), 6.29 (dd, $^3J_{H-H}$ = 8.4 Hz, $^4J_{H-H}$ = 2.4 Hz, 1H, H-6'), 6.26 (dd, $^3J_{H-F}$ = 11.6 Hz, $^4J_{H-H}$ = 2.4 Hz, 1H, H-2'), 4.09-4.04 (m, 1H, N*H*), 3.43 (q, $^3J_{H-H}$ = 6.7 Hz, 2H, H-1), 2.40 (qt, $^3J_{H-F}$ = 10.7 Hz, $^3J_{H-H}$ = 6.7 Hz, 2H, H-2), 0.24 (s, 9H, Si(C*H*$_3$)$_3$); **^{13}C-NMR** (151 MHz, $CDCl_3$): *δ* [ppm] = 164.6 (C-3'), 149.0 (C-1'), 134.9 (C-5'), 126.5 (C-3), 108.6 (C-6'), 100.6 (C-4'), 99.2 (C-2'), 99.0 (C-1''), 97.3 (C-2''), 37.0 (C-1), 33.4 (C-2), 0.20 (Si(*C*H$_3$)$_3$); **^{19}F-NMR** (565 MHz, $CDCl_3$): δ [ppm] = −65.0 (C*F*$_3$), −108.4 (Ar-*F*); **ATR-IR** (neat): $\tilde{\nu}$ [cm^{-1}] = 3427, 2960, 2153, 1624, 1519, 1341, 1246, 1225, 1185, 1145, 837, 807, 758; **HRMS** (ESI$^+$): m/z calc.: 304.1139 [M+H]$^+$, found: 304.1155; **R$_f$**: 0.14 (PE/CH_2Cl_2 5:1 v/v).

4-Ethynyl-3-fluoro-*N*-(3,3,3-trifluoropropyl)aniline 221

According to general procedure III, the cleavage of the protecting group was performed by treating **216** (295 mg, 972 µmol) with potassium carbonate (672 mg, 486 mmol) in methanol (8 mL) for 4 h. Alkyne **221** (199 mg, 862 µmol, 89%) was obtained as a yellow oil.

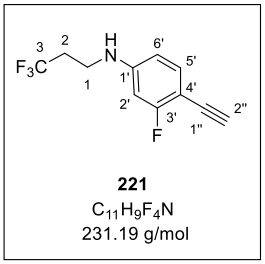

221
$C_{11}H_9F_4N$
231.19 g/mol

^{1}H-NMR (600 MHz, $CDCl_3$): *δ* [ppm] = 7.30-7.25 (m, 1H, H-5'), 6.31 (dd, $^3J_{H-H}$ = 8.4 Hz, $^4J_{H-H}$ = 2.4 Hz, 1H, H-6'), 6.28 (dd, $^3J_{H-F}$ = 11.6 Hz, $^4J_{H-H}$ = 2.4 Hz, 1H, H-2'), 4.13-4.08 (s, 1H, N*H*), 3.44 (q, $^3J_{H-H}$ = 6.7 Hz, 2H, H-1), 3.19 (s, 1H, H-2''), 2.41 (qt, $^3J_{H-F}$ = 10.7 Hz, $^3J_{H-H}$ = 6.7 Hz, 2H, H-2); **^{13}C-NMR** (151 MHz, $CDCl_3$): *δ* [ppm] = 164.9 (C-3'), 149.3 (C-1'), 135.0 (C-5'), 126.4 (C-3), 108.7 (C-6'), 99.2 (C-2'), 99.2 (C-4'), 80.2 (C-2''), 77.9 (C-1''), 36.8 (C-1), 33.4 (C-2); **^{19}F-NMR** (565 MHz, $CDCl_3$): δ [ppm] = −65.0 (C*F*$_3$), −108.4 (Ar-*F*); **ATR-IR** (neat): $\tilde{\nu}$ [cm^{-1}] = 3427, 3298, 2107, 1624, 1519, 1340, 1243, 1185, 1141, 1111, 1079, 1003, 830, 807, 603; **HRMS** (ESI$^+$): m/z calc.: 232.0744 [M+H]$^+$, found: 232.0731; **R$_f$**: 0.46 (PE/CH_2Cl_2 4:1 v/v).

Methyl 2-(3,3-dimethylureido)-5-((2-fluoro-4-((3,3,3-trifluoropropyl)amino)phenyl)ethynyl)benzoate 257

The reaction was carried out according to general procedure IV with urea derivative **259** (150 mg, 431 µmol), copper iodide (8.2 mg, 43 µmol), $Pd(PPh_3)_4$ (49.8 mg, 43.1 µmol) and alkyne **221** (149 mg, 646 µmol) in triethylamine (4 mL) and THF (3 mL) at room temperature

for 18 h. After purification by column chromatography (CH_2Cl_2/MeOH 19:1 v/v), **257** (135 mg, 299 µmol, 69%) was obtained as a yellowish solid.

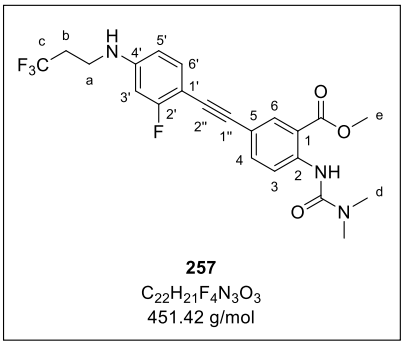

^{1}H-NMR (600 MHz, $CDCl_3$): δ [ppm] = 10.72 (s, 1H, CON*H*), 8.61 (d, $^3J_{H\text{-}H}$ = 8.9 Hz, 1H, H-3), 8.17 (d, $^4J_{H\text{-}H}$ = 2.1 Hz, 1H, H-6), 7.62 (dd, $^3J_{H\text{-}H}$ = 8.9 Hz, $^4J_{H\text{-}H}$ = 2.1 Hz, 1H, H-4), 7.31-7.28 (m, 1H, H-6'), 6.34 (dd, $^3J_{H\text{-}H}$ = 8.4 Hz, $^4J_{H\text{-}H}$ = 2.4 Hz, 1H, H-5'), 6.32 (dd, $^3J_{H\text{-}F}$ = 11.6 Hz, $^4J_{H\text{-}H}$ = 2.4 Hz, 1H, H-3'), 4.13-4.09 (s, 1H, N*H*), 3.92 (s, 3H, H-e), 3.45 (s, 6H, H-d), 3.45 (q, $^3J_{H\text{-}H}$ = 6.7 Hz, 2H, H-a), 3.09 (s, 6H, H-d), 2.43 (qt, $^3J_{H\text{-}F}$ = 10.7 Hz, $^3J_{H\text{-}H}$ = 6.7 Hz, 2H, H-b); **^{13}C-NMR** (151 MHz, $CDCl_3$): δ [ppm] = 169.0 (*C*OOMe), 164.1 (C-2'), 155.5 (*C*ONH), 148.8 (C-4'), 143.4 (C-2), 137.4 (C-4), 134.3 (C-6'), 134.0 (C-6), 126.5 (C-c), 119.4 (C-3), 115.8 (C-5), 113.8 (C-1), 108.9 (C-5'), 100.6 (C-1'), 99.4 (C-3'), 91.5 (C-1''), 82.8 (C-2''), 52.5 (C-e), 37.0 (C-a), 36.5 (C-d), 33.5 (C-b); **^{19}F-NMR** (565 MHz, $CDCl_3$): δ [ppm] = −65.0 (C*F*$_3$), −108.7 (Ar-*F*); **ATR-IR** (neat): $\tilde{\nu}$ [cm^{-1}] = 3329, 3243, 2923, 1656, 1624, 1591, 1537, 1513, 1485, 1435, 1360, 1295, 1246, 1232, 1182, 1137, 1082, 1007, 832, 819, **HRMS** (ESI$^+$): m/z calc.: 452.1592 [M+H]$^+$, found: 452.1561; **R$_f$**: 0.35 (CH_2Cl_2/acetone 100:1).

2-(3,3-dimethylureido)-5-((2-fluoro-4-((3,3,3-trifluoropropyl)amino)phenyl)ethynyl)-benzoic acid 81

The saponification was carried out according to general procedure V with methyl ester **257** (149 mg, 330 µmol) and aqueous 1.0 M NaOH (1.5 mL) in THF (4 mL) for 16 h. Precipitation in acidic solution afforded **81** (79.1 mg, 181 µmol, 55%) as an ivory solid.

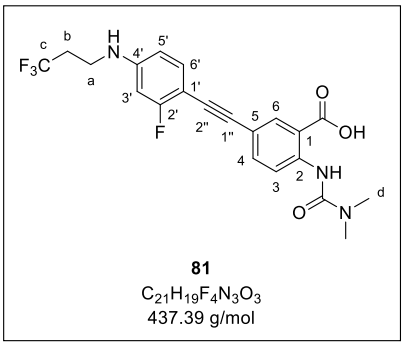

^{1}H-NMR (600 MHz, DMSO-*d*6): δ [ppm] = 13.86 (s, 1H, COO*H*), 11.00 (s, 1H, CON*H*), 8.52 (d, $^3J_{H\text{-}H}$ = 8.8 Hz, 1H, H-3), 8.01 (d, $^4J_{H\text{-}H}$ = 2.2 Hz, 1H, H-6), 7.60 (dd, $^3J_{H\text{-}H}$ = 8.9 Hz, $^4J_{H\text{-}H}$ = 2.2 Hz, 1H, H-4), 7.31-7.27 (m, 1H, H-6'), 6.60-6.56 (m, 1H, N*H*), 6.49-6.43 (m, 2H, H-3', H-5'), 3.36-3.30 (m, 2H, H-a), 2.98 (s, 6H, H-d), 2.58-2.51 (m, 2H, H-b); **^{13}C-NMR** (151 MHz, DMSO-*d*6): δ [ppm] = 169.6 (*C*OOH), 163.4 (C-2'), 154.4 (*C*ONH), 150.5 (C-4'), 143.0 (C-2), 136.0 (C-4), 133.7 (C-6'), 135.5 (C-6), 127.0 (C-c), 118.8 (C-3), 114.7 (C-5), 114.5 (C-1), 108.8 (C-5'), 98.0 (C-3'), 96.7 (C-1'), 90.7 (C-1''), 83.3 (C-2''), 35.8 (C-d), 35.8 (C-a), 32.2 (C-b); **^{19}F-NMR** (565 MHz, DMSO-*d*6): δ [ppm] = −63.6 (C*F*$_3$), −109.9 (Ar-*F*); **ATR-IR** (neat): $\tilde{\nu}$ [cm^{-1}] = 3387, 2874, 1627, 1574, 1524, 1484, 1392, 1294, 1248, 1215, 1147, 1108, 1107, 834; **HRMS** (ESI$^+$): m/z calc.: 438.1436 [M+H]$^+$, found: 438.1454; **R$_f$**: 0.22 (CH_2Cl_2/MeOH 9:1 v/v).

1-(4-Bromo-3-fluorophenyl)-4,4-difluoropiperidine 156

The reaction was carried out according to general procedure I with 1-bromo-2-fluoro-4-iodobenzene **137** (2.00 g, 6.65 mmol), copper iodide (253 mg, 1.33 mmol), L-proline (306 mg, 2.66 mmol), potassium carbonate (1.84 g, 13.3 mmol) and 4,4-difluoropiperidine (1.21 g, 9.97 mmol) in DMSO (12 mL) for 24 h. The crude product was purified by column chromatography (PE/CH_2Cl_2 3:2 v/v) to yield **156** (1.12 g, 3.82 mmol, 57%) as a colorless oil.

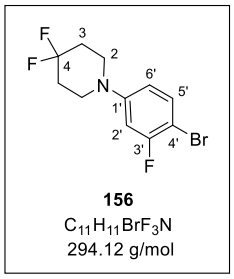

156
$C_{11}H_{11}BrF_3N$
294.12 g/mol

^{1}H-NMR (600 MHz, $CDCl_3$): *δ* [ppm] = 7.36 (dd, $^3J_{H\text{-}H}$ = 8.9 Hz, $^4J_{H\text{-}F}$ = 8.1 Hz, 1H, H-5'), 6.67 (dd, $^3J_{H\text{-}F}$ = 11.7 Hz, $^4J_{H\text{-}H}$ = 2.8 Hz, 1H, H-2'), 6.59 (dd, $^3J_{H\text{-}H}$ = 8.9 Hz, $^4J_{H\text{-}H}$ = 2.8 Hz, 1H, H-6'), 3.37-3.32 (m, 4H, H-2), 2.12-2.03 (m, 4H, H-3); **^{13}C-NMR** (151 MHz, $CDCl_3$): *δ* [ppm] = 159.7 (C-3'), 152.9 (C-1'), 133.6 (C-5'), 121.7 (C-4), 123.3 (C-6'), 104.6 (C-2'), 97.9 (C-4'), 46.3 (C-2), 33.4 (C-3); **^{19}F-NMR** (565 MHz, $CDCl_3$): δ [ppm] = −97.8 (C*F*$_2$), −106.3 (Ar-*F*); **ATR-IR** (neat): *ṽ* [cm^{-1}] = 2986, 2949, 2852, 1604, 1568, 1494, 1468, 1425, 1361, 1237, 1198, 1103, 1046, 1027, 984, 970, 940, 849, 816, 796, 652, 616, 551, 501, 482, 447; **HRMS** (ESI^+): m/z calc.: 294.0100 $[M+H]^+$, found: 294.0095; **R_f**: 0.41 (PE/CH_2Cl_2 3:2 v/v).

4,4-Difluoro-1-(3-fluoro-4-((trimethylsilyl)ethynyl)phenyl)piperidine 217

According to general procedure II, the reaction was carried out with 1-(4-bromo-3-fluorophenyl)-4,4-difluoropiperidine **156** (1.10 g, 3.74 mmol), copper iodide (71.3 mg, 374 µmol), $Pd(PPh_3)_4$ (433 mg, 374 µmol) and TMS acetylene (1.40 mL, 10.1 mmol) in triethylamine (12 mL) and THF (6 mL) at room temperature for 24 h. Purification by column chromatography (PE/CH_2Cl_2 5:1 v/v) afforded **217** (983 mg, 3.16 mmol, 84%) as a colorless crystalline solid.

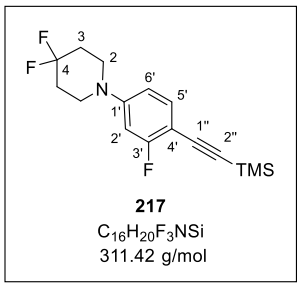

217
$C_{16}H_{20}F_3NSi$
311.42 g/mol

^{1}H-NMR (500 MHz, $CDCl_3$): *δ* [ppm] = 7.33-7.28 (m, 1H, H-5'), 6.59 (dd, $^3J_{H\text{-}H}$ = 8.6 Hz, $^4J_{H\text{-}H}$ = 2.6 Hz, 1H, H-6'), 6.55 (dd, $^3J_{H\text{-}F}$ = 12.5 Hz, $^4J_{H\text{-}H}$ = 2.6 Hz, 1H, H-2'), 3.44-3.38 (m, 4H, H-2), 2.11-2.00 (m, 4H, H-3), 0.25 (s, 9H, Si(C*H*$_3$)$_3$); **^{13}C-NMR** (126 MHz, $CDCl_3$): *δ* [ppm] = 164.5 (C-3'), 151.1 (C-1'), 134.7 (C-5'), 121.5 (C-4), 110.9 (C-6'), 102.4 (C-2'), 98.3 (C-4'), 45.6 (C-2), 33.4 (C-3), 0.17 (Si(*C*H$_3$)$_3$); **^{19}F-NMR** (565 MHz, $CDCl_3$): δ [ppm] = −97.6 (C*F*$_2$), −108.0 (Ar-*F*); **ATR-IR** (neat): *ṽ* [cm^{-1}] = 2961, 2852, 2153, 1623, 1547, 1509, 1466, 1436, 1251, 1187, 1133, 1101, 987, 951, 836, 800, 762, 703, 623, 485, 439; **HRMS** (ESI^+): m/z calc.: 312.1390 $[M+H]^+$, found: 312.1614; **R_f**: 0.25 (PE/CH_2Cl_2 5:1 v/v).

1-(4-Ethynyl-3-fluorophenyl)-4,4-difluoropiperidine 222

The cleavage of the protecting group was carried out as described in general procedure III by treating **217** (439 mg, 1.41 mmol) with potassium carbonate (974 mg, 7.05 mmol) in methanol (12 mL) for 4 h. Alkyne **222** (276 mg, 1.15 mmol, 82%) was obtained as a colorless solid.

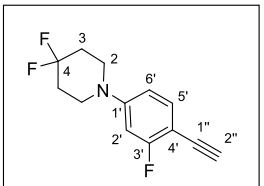

222
$C_{13}H_{12}F_3N$
239.24 g/mol

^{1}H-NMR (600 MHz, $CDCl_3$): *δ* [ppm] = 7.36-7.31 (m, 1H, H-5'), 6.61 (dd, $^3J_{H-H}$ = 8.6 Hz, $^4J_{H-H}$ = 2.6 Hz, 1H, H-6'), 6.58 (dd, $^3J_{H-F}$ = 12.5 Hz, $^4J_{H-H}$ = 2.6 Hz, 1H, H-2'), 3.45-3.40 (m, 4H, H-2), 3.21 (s, 1H, H-2''), 2.11-2.01 (m, 4H, H-3); **^{13}C-NMR** (151 MHz, $CDCl_3$): *δ* [ppm] = 164.6 (C-3'), 151.6 (C-1'), 134.7 (C-5'), 121.7 (C-4), 111.0 (C-6'), 102.4 (C-2'), 100.5 (C-4'), 80.6 (C-2''), 77.6 (C-1''), 45.6 (C-2), 33.4 (C-3); **^{19}F-NMR** (565 MHz, $CDCl_3$): δ [ppm] = −97.6 (C*F*$_2$), −108.6 (Ar-*F*); **ATR-IR** (neat): $\tilde{\nu}$ [cm^{-1}] = 3301, 2884, 2105, 1625, 1348, 1264, 1249, 1186, 1093, 974, 934, 823, 799, 658, 618, 602; **HRMS** (ESI$^+$): m/z calc.: 240.0995 [M+H]$^+$, found: 240.0999; **R$_f$**: 0.21 (PE/CH_2Cl_2 5:1 v/v).

Methyl 5-((4-(4,4-difluoropiperidin-1-yl)-2-fluorophenyl)ethynyl)-2-(3,3-dimethylureido)-benzoate 258

The reaction was carried out according to general procedure IV with urea derivative **259** (202 mg, 580 µmol), copper iodide (11.1 mg, 58.0 µmol), $Pd(PPh_3)_4$ (67.1 mg, 58.0 µmol) and alkyne **222** (208 mg, 474 µmol) in triethylamine (4 mL) and THF (3 mL) at 70 °C for 3 h. Purification by column chromatography (CH_2Cl_2/MeOH 19:1 v/v) provided **258** (164 mg, 358 µmol, 62%) as a yellowish solid.

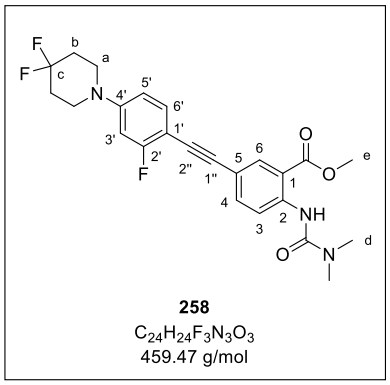

258
$C_{24}H_{24}F_3N_3O_3$
459.47 g/mol

^{1}H-NMR (600 MHz, $CDCl_3$): *δ* [ppm] = 10.73 (s, 1H, CON*H*), 8.62 (d, $^3J_{H-H}$ = 8.9 Hz, 1H, H-3), 8.18 (d, $^4J_{H-H}$ = 2.1 Hz, 1H, H-6), 7.63 (dd, $^3J_{H-H}$ = 8.9 Hz, $^4J_{H-H}$ = 2.1 Hz, 1H, H-4), 7.38-7.33 (m, 1H, H-6'), 6.64 (dd, $^3J_{H-H}$ = 8.6 Hz, $^4J_{H-H}$ = 2.5 Hz, H-5'), 6.61 (dd, $^3J_{H-F}$ = 12.5 Hz, $^4J_{H-H}$ = 2.5 Hz, 1H, H-3'), 3.93 (s, 3H, H-e), 3.45-3.40 (m, 4H, H-a), 3.09 (s, 6H, H-d), 2.12-2.03 (m, 4H, H-b); **^{13}C-NMR** (151 MHz, $CDCl_3$): *δ* [ppm] = 169.0 (*C*OOMe), 163.9 (C-2'), 155.4 (*C*ONH), 151.1 (C-4'), 143.5 (C-2), 137.4 (C-4), 134.1 (C-6), 134.1 (C-6'), 121.8 (C-c), 119.4 (C-3), 115.6 (C-5), 113.8 (C-1), 111.2 (C-5'), 102.6 (C-3'), 101.9 (C-1'), 92.0 (C-1''), 82.5 (C-2''), 52.5 (C-e), 45.7 (C-a), 36.5 (C-d), 33.4 (C-b); **^{19}F-NMR** (565 MHz, $CDCl_3$): δ [ppm] = −97.6 (C*F*$_2$), −108.4 (Ar-*F*); **ATR-IR** (neat): $\tilde{\nu}$ [cm^{-1}] = 3240, 2944, 2849, 1667, 1518, 1437, 1364, 1296, 1235, 1172, 1132, 989, 915, 814; **HRMS** (ESI$^+$): m/z calc.: 460.1843 [M+H]$^+$, found: 460.1691; **R$_f$**: 0.35 (CH_2Cl_2/acetone 100:1 v/v).

5-((4-(4,4-Difluoropiperidin-1-yl)-2-fluorophenyl)ethynyl)-2-(3,3-dimethylureido)benzoic acid 82

The saponification was performed according to general procedure V by treating methyl ester **258** (142 mg, 308 µmol) with aqueous 1.0 M NaOH (1.5 mL) in THF (4 mL) for 16 h. After precipitation in acidic solution, target compound **82** (85.8 mg, 193 µmol, 62%) was obtained as a yellowish solid.

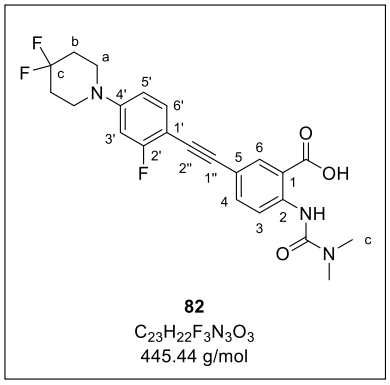

82
$C_{23}H_{22}F_3N_3O_3$
445.44 g/mol

^{1}H-NMR (600 MHz, DMSO-*d*6): *δ* [ppm] = 13.85 (s, 1H, COO*H*), 10.96 (s, 1H, CON*H*), 8.53 (d, $^3J_{H\text{-}H}$ = 8.9 Hz, 1H, H-3), 8.03 (d, $^4J_{H\text{-}H}$ = 2.1 Hz, 1H, H-6), 7.63 (dd, $^3J_{H\text{-}H}$ = 8.9 Hz, $^4J_{H\text{-}H}$ = 2.1 Hz, 1H, H-4), 7.43-7.38 (m, 1H, H-6'), 6.95 (dd, $^3J_{H\text{-}F}$ = 13.6 Hz, $^4J_{H\text{-}H}$ = 2.5 Hz, 1H, H-3'), 6.85 (dd, $^3J_{H\text{-}H}$ = 8.8 Hz, $^4J_{H\text{-}H}$ = 2.5 Hz, H-5'), 3.50-3.45 (m, 4H, H-a), 2.98 (s, 6H, H-d), 2.06-1.96 (m, 4H, H-b); **^{13}C-NMR** (151 MHz, DMSO-*d*6): *δ* [ppm] = 169.6 (*C*OOH), 163.2 (C-2'), 154.4 (*C*ONH), 151.0 (C-4'), 143.3 (C-2), 136.2 (C-4), 133.7 (C-6), 133.7 (C-6'), 122.7 (C-c), 118.7 (C-3), 114.6 (C-5), 114.2 (C-1), 110.9 (C-5'), 101.7 (C-3'), 99.2 (C-1'), 91.4 (C-1''), 82.7 (C-2''), 44.4 (C-a), 35.8 (C-d), 32.6 (C-b); **^{19}F-NMR** (565 MHz, DMSO-*d*6): δ [ppm] = −95.1 (C*F*$_2$), −109.3 (Ar-*F*); **ATR-IR** (neat): $\tilde{\nu}$ [cm^{-1}] = 2851, 1622, 1574, 1520, 1487, 1466, 1384, 1364, 1293, 1235, 1187, 1091, 839, 797, 676; **HRMS** (ESI$^+$): m/z calc.: 446.1687 [M+H]$^+$, found: 446.1651; **R$_f$**: 0.76 (CH_2Cl_2/MeOH 9:1 v/v).

7. References

[1] E. Bekerman, S. Einav, Combating emerging viral threats, *Science*, **2015**, *348*, 282–283.

[2] J.-D. Zhu, W. Meng, X.-J. Wang, H.-C. R. Wang, Broad-spectrum antiviral agents, *Frontiers in microbiology*, **2015**, *6*, 517.

[3] G. R. Painter, M. G. Natchus, O. Cohen, W. Holman, W. P. Painter, Developing a direct acting, orally available antiviral agent in a pandemic: the evolution of molnupiravir as a potential treatment for COVID-19, *Current opinion in virology*, **2021**, *50*, 17–22.

[4] A. Ianevski, S. Ahmad, K. Anunnitipat, V. Oksenych, E. Zusinaite, T. Tenson, M. Bjørås, D. E. Kainov, Seven classes of antiviral agents, *Cellular and molecular life sciences : CMLS*, **2022**, *79*, 605.

[5] D. E. Kainov, E. Ravlo, A. Ianevski, Seeking innovative concepts in development of antiviral drug combinations, *Antiviral research*, **2025**, *234*, 106079.

[6] World Health Organization, Prioritizing diseases for research and development in emergency contexts, https://www.who.int/activities/prioritizing-diseases-for-research-and-development-in-emergency-contexts (Retrieved: 14.08.2025).

[7] C. F. Basler, Molecular pathogenesis of viral hemorrhagic fever, *Seminars in immunopathology*, **2017**, *39*, 551–561.

[8] M. Bray, Pathogenesis of viral hemorrhagic fever, *Current opinion in immunology*, **2005**, *17*, 399–403.

[9] M. Eslava, S. Carlos, G. Reina, Crimean-Congo Hemorrhagic Fever Virus: An Emerging Threat in Europe with a Focus on Epidemiology in Spain, *Pathogens*, **2024**, *13*, 770.

[10] J. Brem, B. Elankeswaran, D. Erne, N. Hedrich, T. Lovey, V. Marzetta, L. T. Salvado, C. Züger, P. Schlagenhauf, Dengue "homegrown" in Europe (2022 to 2023), *New microbes and new infections*, **2024**, *56*, 101205.

[11] J. P. Martinez, F. Sasse, M. Brönstrup, J. Diez, A. Meyerhans, Antiviral drug discovery: broad-spectrum drugs from nature, *Natural product reports*, **2015**, *32*, 29–48.

[12] V. C. Chitalia, A. H. Munawar, A painful lesson from the COVID-19 pandemic: the need for broad-spectrum, host-directed antivirals, *Journal of translational medicine*, **2020**, *18*, 390.

[13] X. Ji, Z. Li, Medicinal chemistry strategies toward host targeting antiviral agents, *Medicinal research reviews*, **2020**, *40*, 1519–1557.

[14] P. Das, X. Deng, L. Zhang, M. G. Roth, B. M. A. Fontoura, M. A. Phillips, J. K. de Brabander, SAR Based Optimization of a 4-Quinoline Carboxylic Acid Analog with Potent Anti-Viral Activity, *ACS medicinal chemistry letters*, **2013**, *4*, 517–521.

[15] C. Li, Y. Zhou, J. Xu, X. Zhou, Z. Huang, T. Zeng, X. Yang, L. Tao, K. Gou, X. Zhong et al., A novel series of teriflunomide derivatives as orally active inhibitors of human dihydroorotate dehydrogenase for the treatment of colorectal carcinoma, *European journal of medicinal chemistry*, **2022**, *238*, 114489.

[16] D. D. Richman, R. J. Whitley, F. G. Hayden, *Clinical virology,* fourth edition, ASM Press, Washington DC, **2017**.

[17] D. Belhadi, M. El Baied, G. Mulier, D. Malvy, F. Mentré, C. Laouénan, The number of cases, mortality and treatments of viral hemorrhagic fevers: A systematic review, *PLoS neglected tropical diseases*, **2022**, *16*, e0010889.

[18] V. Mariappan, P. Pratheesh, L. Shanmugam, S. R. Rao, A. B. Pillai, Viral hemorrhagic fever: Molecular pathogenesis and current trends of disease management-an update, *Current Research in Virological Science*, **2021**, *2*, 100009.

[19] L. Flórez-Álvarez, E. E. de Souza, V. F. Botosso, D. B. L. de Oliveira, P. L. Ho, C. P. Taborda, G. Palmisano, M. L. Capurro, J. R. R. Pinho, H. L. Ferreira et al., Hemorrhagic fever viruses: Pathogenesis, therapeutics, and emerging and re-emerging potential, *Frontiers in microbiology*, **2022**, *13*, 1040093.

[20] R. Gurgel-Gonçalves, W. K. de Oliveira, J. Croda, The greatest Dengue epidemic in Brazil: Surveillance, Prevention, and Control, *Revista da Sociedade Brasileira de Medicina Tropical*, **2024**, *57*, e002032024.

[21] S. K. Singh, J. H. Kuhn, *Defense Against Biological Attacks,* second edition, Springer, Cham, **2019**.

[22] D. E. Bloom, S. Black, R. Rappuoli, Emerging infectious diseases: A proactive approach, *Proceedings of the National Academy of Sciences of the United States of America*, **2017**, *114*, 4055–4059.

[23] F. Amraoui, A. Pain, G. Piorkowski, M. Vazeille, D. Couto-Lima, X. de Lamballerie, R. Lourenço-de-Oliveira, A.-B. Failloux, Experimental Adaptation of the Yellow Fever Virus to the Mosquito Aedes albopictus and Potential risk of urban epidemics in Brazil, South America, *Scientific reports*, **2018**, *8*, 14337.

[24] S. K. Wikel, Ticks and Tick-Borne Infections: Complex Ecology, Agents, and Host Interactions, *Veterinary sciences*, **2018**, *5*, 60.

[25] K. O. Douglas, K. Payne, G. Sabino-Santos, J. Agard, Influence of Climatic Factors on Human Hantavirus Infections in Latin America and the Caribbean: A Systematic Review, *Pathogens*, **2021**, *11*, 15.

[26] S. Beermann, G. Dobler, M. Faber, C. Frank, B. Habedank, P. Hagedorn, H. Kampen, C. Kuhn, T. Nygren, J. Schmidt-Chanasit et al., Impact of climate change on vector- and rodent-borne infectious diseases, *Journal of health monitoring*, **2023**, *8*, 33–61.

[27] S. Jain, E. Martynova, A. Rizvanov, S. Khaiboullina, M. Baranwal, Structural and Functional Aspects of Ebola Virus Proteins, *Pathogens*, **2021**, *10*, 1330.

[28] S. Modrow, U. Truyen, H. Schätzl, *Molekulare Virologie,* fourth edition, Springer, Berlin, Heidelberg, **2021**.

[29] F. Hansen, H. Feldmann, M. A. Jarvis, Targeting Ebola virus replication through pharmaceutical intervention, *Expert opinion on investigational drugs*, **2021**, *30*, 201–226.

[30] M. Mehedi, D. Falzarano, J. Seebach, X. Hu, M. S. Carpenter, H.-J. Schnittler, H. Feldmann, A new Ebola virus nonstructural glycoprotein expressed through RNA editing, *Journal of virology*, **2011**, *85*, 5406–5414.

[31] D. R. Beniac, T. F. Booth, Structure of the Ebola virus glycoprotein spike within the virion envelope at 11 Å resolution, *Scientific reports*, **2017**, *7*, 46374.

[32] T. Hoenen, A. Groseth, F. de Kok-Mercado, J. H. Kuhn, V. Wahl-Jensen, Minigenomes, transcription and replication competent virus-like particles and beyond: reverse genetics systems for filoviruses and other negative stranded hemorrhagic fever viruses, *Antiviral research*, **2011**, *91*, 195–208.

[33] T. Hoenen, A. Groseth, H. Feldmann, Therapeutic strategies to target the Ebola virus life cycle, *Nature reviews. Microbiology*, **2019**, *17*, 593–606.

[34] D.-S. Yu, T.-H. Weng, X.-X. Wu, F. X. C. Wang, X.-Y. Lu, H.-B. Wu, N.-P. Wu, L.-J. Li, H.-P. Yao, The lifecycle of the Ebola virus in host cells, *Oncotarget*, **2017**, *8*, 55750–55759.

[35] L. D. Presser, J. Coffin, L. Koivogui, A. Campbell, J. Campbell, F. Barrie, J. Ngobeh, Z. Souma, S. Sorie, D. Harding et al., The deployment of mobile diagnostic laboratories for Ebola virus disease diagnostics in Sierra Leone and Guinea, *African journal of laboratory medicine*, **2021**, *10*, 1414.

[36] T. Racine, G. P. Kobinger, Challenges and perspectives on the use of mobile laboratories during outbreaks and their use for vaccine evaluation, *Human vaccines & immunotherapeutics*, **2019**, *15*, 2264–2268.

[37] E. Gianchecchi, V. Cianchi, A. Torelli, E. Montomoli, Yellow Fever: Origin, Epidemiology, Preventive Strategies and Future Prospects, *Vaccines*, **2022**, *10*, 372.

[38] N. P. Lindsey, J. Horton, A. D. T. Barrett, M. Demanou, T. P. Monath, O. Tomori, M. van Herp, H. Zeller, I. S. Fall, L. Cibrelus et al., Yellow fever resurgence: An avoidable crisis?, *NPJ vaccines*, **2022**, *7*, 137.

[39] A. Rojas, W. Hachey, G. Kaur, J. Korejwo, R. Muhammad, Enhanced safety surveillance of STAMARIL® yellow fever vaccine provided under the expanded access investigational new drug program in the USA, *Journal of travel medicine*, **2023**, *30*.

[40] M. F. Lee, C. M. Long, C. L. Poh, Current status of the development of dengue vaccines, *Vaccine: X*, **2025**, *22*, 100604.

[41] A. Wilder-Smith, Entwicklung von Impfstoffen gegen Dengue: aktueller Stand und Zukunft, *Bundesgesundheitsblatt, Gesundheitsforschung, Gesundheitsschutz*, **2020**, *63*, 40–44.

[42] Paul-Ehrlich-Institut, Denguefieber-Impfstoffe, https://www.pei.de/DE/arzneimittel/impfstoffe/denguefieber/dengue-node.html (Retrieved: 09.09.2025).

[43] M. Angelin, J. Sjölin, F. Kahn, A. Ljunghill Hedberg, A. Rosdahl, P. Skorup, S. Werner, S. Woxenius, H. H. Askling, Qdenga® - A promising dengue fever vaccine; can it be recommended to non-immune travelers?, *Travel medicine and infectious disease*, **2023**, *54*, 102598.

[44] Robert Koch Institut, Antworten auf häufig gestellte Fragen zu Dengue und zur Impfung, https://www.rki.de/SharedDocs/FAQs/DE/Dengue/FAQ-Liste.html#entry_16870128 (Retrieved: 09.09.2025).

[45] T. Saito, R. A. Reyna, S. Taniguchi, K. Littlefield, S. Paessler, J. Maruyama, Vaccine Candidates against Arenavirus Infections, *Vaccines*, **2023**, *11*, 635.

[46] M. Mousavi-Jazi, H. Karlberg, A. Papa, I. Christova, A. Mirazimi, Healthy individuals' immune response to the Bulgarian Crimean-Congo hemorrhagic fever virus vaccine, *Vaccine*, **2012**, *30*, 6225–6229.

[47] A. Khan, O. S. Shin, J. Na, J. K. Kim, R.-K. Seong, M.-S. Park, J. Y. Noh, J. Y. Song, H. J. Cheong, Y. H. Park et al., A Systems Vaccinology Approach Reveals the Mechanisms of Immunogenic Responses to Hantavax Vaccination in Humans, *Scientific reports*, **2019**, *9*, 4760.

[48] E. M. Anderson, B.-A. G. Coller, Translational success of fundamental virology: a VSV-vectored Ebola vaccine, *Journal of virology*, **2024**, *98*, e0162723.

[49] J. Wolf, R. Jannat, S. Dubey, S. Troth, M. T. Onorato, B.-A. Coller, M. E. Hanson, J. K. Simon, Development of Pandemic Vaccines: ERVEBO Case Study, *Vaccines*, **2021**, *9*, 190.

[50] O. Tomori, M. O. Kolawole, Ebola virus disease: current vaccine solutions, *Current opinion in immunology*, **2021**, *71*, 27–33.

[51] Paul-Ehrlich-Institut, Ebola-Impfstoffe, https://www.pei.de/DE/arzneimittel/impfstoffe/ebola/ebola-node.html?cms_gts=174436_list%253Dtitle_text_sort%252Bdesc (Retrieved: 09.09.2025).

[52] C. Woolsey, T. W. Geisbert, Current state of Ebola virus vaccines: A snapshot, *PLoS pathogens*, **2021**, *17*, e1010078.

[53] European Medicines Agency, New vaccine for prevention of Ebola virus disease recommended for approval in the European Union, https://www.ema.europa.eu/en/news/new-vaccine-prevention-ebola-virus-disease-recommended-approval-european-union (Retrieved: 09.09.2025).

[54] D. Falzarano, H. Feldmann, Vaccines for viral hemorrhagic fevers--progress and shortcomings, *Current opinion in virology*, **2013**, *3*, 343–351.

[55] E. Taki, R. Ghanavati, T. Navidifar, S. Dashtbin, M. Heidary, M. Moghadamnia, Ebanga™: The most recent FDA-approved drug for treating Ebola, *Frontiers in pharmacology*, **2023**, *14*, 1083429.

[56] N. J. Snell, Ribavirin--current status of a broad spectrum antiviral agent, *Expert opinion on pharmacotherapy*, **2001**, *2*, 1317–1324.

[57] S. Brillanti, G. Mazzella, E. Roda, Ribavirin for chronic hepatitis C: and the mystery goes on, *Digestive and liver disease*, **2011**, *43*, 425–430.

[58] D. Safronetz, K. Rosenke, J. B. Westover, C. Martellaro, A. Okumura, Y. Furuta, J. Geisbert, G. Saturday, T. Komeno, T. W. Geisbert et al., The broad-spectrum antiviral favipiravir protects guinea pigs from lethal Lassa virus infection post-disease onset, *Scientific reports*, **2015**, *5*, 14775.

[59] J. W. Huggins, Prospects for Treatment of Viral Hemorrhagic Fevers with Ribavirin, a Broad-Spectrum Antiviral Drug, *Reviews of Infectious Diseases*, **1989**, *11*, 750-761.

[60] J. J. Bugert, F. Hucke, P. Zanetta, M. Bassetto, A. Brancale, Antivirals in medical biodefense, *Virus genes*, **2020**, *56*, 150–167.

[61] R. J. Geraghty, M. T. Aliota, L. F. Bonnac, Broad-Spectrum Antiviral Strategies and Nucleoside Analogues, *Viruses*, **2021**, *13*, 667.

[62] J. Paeshuyse, K. Dallmeier, J. Neyts, Ribavirin for the treatment of chronic hepatitis C virus infection: a review of the proposed mechanisms of action, *Current opinion in virology*, **2011**, *1*, 590–598.

[63] R. Swanstrom, R. F. Schinazi, Lethal mutagenesis as an antiviral strategy, *Science*, **2022**, *375*, 497–498.

[64] K. Shiraki, T. Daikoku, Favipiravir, an anti-influenza drug against life-threatening RNA virus infections, *Pharmacology & therapeutics*, **2020**, *209*, 107512.

[65] Y. Furuta, T. Komeno, T. Nakamura, Favipiravir (T-705), a broad spectrum inhibitor of viral RNA polymerase, *Proceedings of the Japan Academy, Series B*, **2017**, *93*, 449–463.

[66] D. Sissoko, C. Laouenan, E. Folkesson, A.-B. M'Lebing, A.-H. Beavogui, S. Baize, A.-M. Camara, P. Maes, S. Shepherd, C. Danel et al., Experimental Treatment with Favipiravir for Ebola Virus Disease (the JIKI Trial): A Historically Controlled, Single-Arm Proof-of-Concept Trial in Guinea, *PLoS medicine*, **2016**, *13*, e1001967.

[67] A. Rezagholizadeh, S. Khiali, P. Sarbakhsh, T. Entezari-Maleki, Remdesivir for treatment of COVID-19; an updated systematic review and meta-analysis, *European journal of pharmacology*, **2021**, *897*, 173926.

[68] J. Pardo, A. M. Shukla, G. Chamarthi, A. Gupte, The journey of remdesivir: from Ebola to COVID-19, *Drugs in context*, **2020**, *9*.

[69] M. R. Hickman, D. L. Saunders, C. A. Bigger, C. D. Kane, P. L. Iversen, The development of broad-spectrum antiviral medical countermeasures to treat viral hemorrhagic fevers caused by natural or weaponized virus infections, *PLoS neglected tropical diseases*, **2022**, *16*, e0010220.

[70] M. G. Santoro, E. Carafoli, Remdesivir: From Ebola to COVID-19, *Biochemical and biophysical research communications*, **2021**, *538*, 145–150.

[71] R. T. Eastman, J. S. Roth, K. R. Brimacombe, A. Simeonov, M. Shen, S. Patnaik, M. D. Hall, Remdesivir: A Review of Its Discovery and Development Leading to Emergency Use Authorization for Treatment of COVID-19, *ACS central science*, **2020**, *6*, 672–683.

[72] A. Nili, A. Farbod, A. Neishabouri, M. Mozafarihashjin, S. Tavakolpour, H. Mahmoudi, Remdesivir: A beacon of hope from Ebola virus disease to COVID-19, *Reviews in medical virology*, **2020**, *30*, 1–13.

[73] J. Malin, I. Suárez, V. Priesner, G. Fätkenheuer, J. Rybniker, Remdesivir against COVID-19 and Other Viral Diseases, *Clinical microbiology reviews*, **2021**, *34*, e00162-20.

[74] G. Li, R. Hilgenfeld, R. Whitley, E. de Clercq, Therapeutic strategies for COVID-19: progress and lessons learned, *Nature reviews. Drug discovery*, **2023**, *22*, 449–475.

[75] K. Pfaff, *Synthese von Inhibitoren der zellulären Enzyme DHS und DHODH als potentielle Wirkstoffe gegen virale Infektionen*, Dissertation, Universität Hamburg, **2018**.

[76] D. R. Tompa, A. Immanuel, S. Srikanth, S. Kadhirvel, Trends and strategies to combat viral infections: A review on FDA approved antiviral drugs, *International journal of biological macromolecules*, **2021**, *172*, 524–541.

[77] X. Ji, Z. Li, Medicinal chemistry strategies toward host targeting antiviral agents, *Medicinal research reviews*, **2020**, *40*, 1519–1557.

[78] J. P. Martinez, F. Sasse, M. Brönstrup, J. Diez, A. Meyerhans, Antiviral drug discovery: broad-spectrum drugs from nature, *Natural product reports*, **2015**, *32*, 29–48.

[79] N. Kumar, S. Sharma, R. Kumar, B. N. Tripathi, S. Barua, H. Ly, B. T. Rouse, Host-Directed Antiviral Therapy, *Clinical microbiology reviews*, **2020**, *33*, e00168-19.

[80] V. C. Chitalia, A. H. Munawar, A painful lesson from the COVID-19 pandemic: the need for broad-spectrum, host-directed antivirals, *Journal of translational medicine*, **2020**, *18*, 390.

[81] C. S. Sepúlveda, C. C. García, E. B. Damonte, Inhibitors of Nucleotide Biosynthesis as Candidates for a Wide Spectrum of Antiviral Chemotherapy, *Microorganisms*, **2022**, *10*, 1631.

[82] H.-L. Wu, Y. Gong, P. Ji, Y.-F. Xie, Y.-Z. Jiang, G.-Y. Liu, Targeting nucleotide metabolism: a promising approach to enhance cancer immunotherapy, *Journal of hematology & oncology*, **2022**, *15*, 45.

[83] A. Okesli, C. Khosla, M. C. Bassik, Human pyrimidine nucleotide biosynthesis as a target for antiviral chemotherapy, *Current opinion in biotechnology*, **2017**, *48*, 127–134.

[84] M. Löffler, L. D. Fairbanks, E. Zameitat, A. M. Marinaki, H. A. Simmonds, Pyrimidine pathways in health and disease, *Trends in molecular medicine*, **2005**, *11*, 430–437.

[85] I. Fritzson, B. Svensson, S. Al-Karadaghi, B. Walse, U. Wellmar, U. J. Nilsson, D. Da Graça Thrige, S. Jönsson, Inhibition of human DHODH by 4-hydroxycoumarins, fenamic acids, and N-(alkylcarbonyl)anthranilic acids identified by structure-guided fragment selection, *ChemMedChem*, **2010**, *5*, 608–617.

[86] Y. Zhou, L. Tao, X. Zhou, Z. Zuo, J. Gong, X. Liu, Y. Zhou, C. Liu, N. Sang, H. Liu et al., DHODH and cancer: promising prospects to be explored, *Cancer & metabolism*, **2021**, *9*, 22.

[87] Y. Zheng, S. Li, K. Song, J. Ye, W. Li, Y. Zhong, Z. Feng, S. Liang, Z. Cai, K. Xu, A Broad Antiviral Strategy: Inhibitors of Human DHODH Pave the Way for Host-Targeting Antivirals against Emerging and Re-Emerging Viruses, *Viruses*, **2022**, *14*, 928.

[88] J. T. Madak, A. Bankhead, C. R. Cuthbertson, H. D. Showalter, N. Neamati, Revisiting the role of dihydroorotate dehydrogenase as a therapeutic target for cancer, *Pharmacology & therapeutics*, **2019**, *195*, 111–131.

[89] W. L. Nyhan, Nucleotide Synthesis via Salvage Pathway. In: *Encyclopedia of Life Sciences*, Wiley, Chichester, **2005**.

[90] P. Das, X. Deng, L. Zhang, M. G. Roth, B. M. A. Fontoura, M. A. Phillips, J. K. de Brabander, SAR Based Optimization of a 4-Quinoline Carboxylic Acid Analog with Potent Anti-Viral Activity, *ACS medicinal chemistry letters*, **2013**, *4*, 517–521.

[91] J. M. Orozco Rodriguez, H. P. Wacklin-Knecht, L. A. Clifton, O. Bogojevic, A. Leung, G. Fragneto, W. Knecht, New Insights into the Interaction of Class II Dihydroorotate Dehydrogenases with Ubiquinone in Lipid Bilayers as a Function of Lipid Composition, *International journal of molecular sciences*, **2022**, *23*, 2437.

[92] T. Zeng, Z. Zuo, Y. Luo, Y. Zhao, Y. Yu, Q. Chen, A novel series of human dihydroorotate dehydrogenase inhibitors discovered by in vitro screening: inhibition activity and crystallographic binding mode, *FEBS open bio*, **2019**, *9*, 1348–1354.

[93] M. Hansen, J. Le Nours, E. Johansson, T. Antal, A. Ullrich, M. Löffler, S. Larsen, Inhibitor binding in a class 2 dihydroorotate dehydrogenase causes variations in the membrane-associated N-terminal domain, *Protein science*, **2004**, *13*, 1031–1042.

[94] S. Liu, E. A. Neidhardt, T. H. Grossman, T. Ocain, J. Clardy, Structures of human dihydroorotate dehydrogenase in complex with antiproliferative agents, *Structure*, **2000**, *8*, 25–33.

[95] Y. Zhou, L. Tao, X. Zhou, Z. Zuo, J. Gong, X. Liu, Y. Zhou, C. Liu, N. Sang, H. Liu et al., DHODH and cancer: promising prospects to be explored, *Cancer & metabolism*, **2021**, *9*, 22.

[96] C. Li, Y. Zhou, J. Xu, X. Zhou, S. Liu, Z. Huang, Z. Qiu, T. Zeng, K. Gou, L. Tao et al., Discovery of potent human dihydroorotate dehydrogenase inhibitors based on a benzophenone scaffold, *European journal of medicinal chemistry*, **2022**, *243*, 114737.

[97] S. Galati, S. Sainas, M. Giorgis, D. Boschi, M. L. Lolli, G. Ortore, G. Poli, T. Tuccinardi, Identification of Human Dihydroorotate Dehydrogenase Inhibitor by a Pharmacophore-Based Virtual Screening Study, *Molecules*, **2022**, *27*, 3660.

[98] M. L. Lolli, S. Sainas, A. C. Pippione, M. Giorgis, D. Boschi, F. Dosio, Use of human Dihydroorotate Dehydrogenase (hDHODH) Inhibitors in Autoimmune Diseases and New Perspectives in Cancer Therapy, *Recent patents on anti-cancer drug discovery*, **2018**, *13*, 86–105.

[99] A. Muehler, H. Kohlhof, M. Groeppel, D. Vitt, The Selective Oral Immunomodulator Vidofludimus in Patients with Active Rheumatoid Arthritis: Safety Results from the COMPONENT Study, *Drugs in R&D*, **2019**, *19*, 351–366.

[100] Fox, R. I., et al., Mechanism of Action for Leflunomide in Rheumatoid Arthritis, *Clinical Immunology*, **1999**, *93*, 198–208.

[101] A. Luganini, D. Boschi, M. L. Lolli, G. Gribaudo, DHODH inhibitors: What will it take to get them into the clinic as antivirals?, *Antiviral research*, **2025**, *236*, 106099.

[102] J. Luban, R. A. Sattler, E. Mühlberger, J. D. Graci, L. Cao, M. Weetall, C. Trotta, J. M. Colacino, S. Bavari, C. Strambio-De-Castillia et al., The DHODH inhibitor PTC299 arrests SARS-CoV-2 replication and suppresses induction of inflammatory cytokines, *Virus research*, **2021**, *292*, 198246.

[103] L. Cao, M. Weetall, C. Trotta, K. Cintron, J. Ma, M. J. Kim, B. Furia, C. Romfo, J. D. Graci, W. Li et al., Targeting of Hematologic Malignancies with PTC299, A Novel Potent Inhibitor of Dihydroorotate Dehydrogenase with Favorable Pharmaceutical Properties, *Molecular cancer therapeutics*, **2019**, *18*, 3–16.

[104] R. A. Bender Ignacio, J. Y. Lee, M. A. Rudek, D. P. Dittmer, R. F. Ambinder, S. E. Krown, Brief Report: A Phase 1b/Pharmacokinetic Trial of PTC299, a Novel PostTranscriptional VEGF Inhibitor, for AIDS-Related Kaposi's Sarcoma: AIDS Malignancy Consortium Trial 059, *Journal of acquired immune deficiency syndromes*, **2016**, *72*, 52–57.

[105] J. Leban, M. Kralik, J. Mies, M. Gassen, K. Tentschert, R. Baumgartner, SAR, species specificity, and cellular activity of cyclopentene dicarboxylic acid amides as DHODH inhibitors, *Bioorganic & medicinal chemistry letters*, **2005**, *15*, 4854–4857.

[106] A. Nair, P. J. Barde, K. V. Routhu, S. Viswanadha, S. Veeraraghavan, S. Pak, J. A. Peterson, S. Vakkalanka, A first in man study to evaluate the safety, pharmacokinetics and pharmacodynamics of RP7214, a dihydroorotate dehydrogenase inhibitor in healthy subjects, *British journal of clinical pharmacology*, **2023**, *89*, 1127–1138.

[107] A. Muehler, E. Peelen, H. Kohlhof, M. Gröppel, D. Vitt, Vidofludimus calcium, a next generation DHODH inhibitor for the Treatment of relapsing-remitting multiple sclerosis, *Multiple sclerosis and related disorders*, **2020**, *43*, 102129.

[108] M. J. G. T. Vehreschild, P. Atanasov, K. Yurko, C. Oancea, G. Popov, V. Smesnoi, G. Placinta, H. Kohlhof, D. Vitt, E. Peelen et al., Safety and Efficacy of Vidofludimus Calcium in Patients Hospitalized with COVID-19: A Double-Blind, Randomized, Placebo-Controlled, Phase 2 Trial, *Infectious diseases and therapy*, **2022**, *11*, 2159–2176.

[109] A. Nair, P. Barde, K. V. Routhu, S. Vakkalanka, A Phase 2, Randomized, Double-blind, Placebo-controlled Study of oral RP7214, a DHODH inhibitor, in Patients with Symptomatic Mild SARS-CoV-2 Infection (preprint), **2023**.

[110] N. C. Laubach, *Development of Novel Inhibitors of Human Dihydroorotate Dehydrogenase as Antiviral Drug Candidates - Design, Synthesis and Pharmacological Evaluation*, Dissertation, Universität Hamburg, **2022**.

[111] M. Winkler, *unpublished results*, Universität Hamburg.

[112] S. Joensson, G. Andersson, U. Wellmar, I. Fritzon, Preparation of substituted anthranilic acids as potent dihydroorotate dehydrogenase inhibitors. Publication date: 18.08.2005. WO 2005/075410 Al.

[113] B. J. Bennion, N. A. Be, M. W. McNerney, V. Lao, E. M. Carlson, C. A. Valdez, M. A. Malfatti, H. A. Enright, T. H. Nguyen, F. C. Lightstone et al., Predicting a Drug's Membrane Permeability: A Computational Model Validated With in Vitro Permeability Assay Data, *The journal of physical chemistry. B*, **2017**, *121*, 5228–5237.

[114] Y. S. Kiani, I. Jabeen, Lipophilic Metabolic Efficiency (LipMetE) and Drug Efficiency Indices to Explore the Metabolic Properties of the Substrates of Selected Cytochrome P450 Isoforms, *ACS omega*, **2020**, *5*, 179–188.

[115] P. Shah, A. D. Westwell, The role of fluorine in medicinal chemistry, *Journal of enzyme inhibition and medicinal chemistry*, **2007**, *22*, 527–540.

[116] J. Vrbanac, R. Slauter, ADME in Drug Discovery. In: *A Comprehensive Guide to Toxicology*, Academic Press, **2017**, 39–67.

[117] Thomas D.Y. Chung, David B. Terry, and Layton H. Smith., In Vitro and In Vivo Assessment of ADME and PK Properties During Lead Selection and Lead Optimization –

Guidelines, Benchmarks and Rules of Thumb. In: *Assay Guidance Manual*, Bethesda (MD), **2004**.

[118] K. T. Savjani, A. K. Gajjar, J. K. Savjani, Drug solubility: importance and enhancement techniques, *ISRN pharmaceutics*, **2012**, *2012*, 195727.

[119] M. Ishikawa, Y. Hashimoto, Improvement in aqueous solubility in small molecule drug discovery programs by disruption of molecular planarity and symmetry, *Journal of medicinal chemistry*, **2011**, *54*, 1539–1554.

[120] C. Saal, A. C. Petereit, Optimizing solubility: kinetic versus thermodynamic solubility temptations and risks, *European journal of pharmaceutical sciences*, **2012**, *47*, 589–595.

[121] K. Valko, D. P. Reynolds, High-Throughput Physicochemical and In Vitro ADMET Screening, *American Journal of Drug Delivery*, **2005**, *3*, 83–100.

[122] P. Lassalas, B. Gay, C. Lasfargeas, M. J. James, van Tran, K. G. Vijayendran, K. R. Brunden, M. C. Kozlowski, C. J. Thomas, A. B. Smith et al., Structure Property Relationships of Carboxylic Acid Isosteres, *Journal of medicinal chemistry*, **2016**, *59*, 3183–3203.

[123] R. Guha, T. S. Dexheimer, A. N. Kestranek, A. Jadhav, A. M. Chervenak, M. G. Ford, A. Simeonov, G. P. Roth, C. J. Thomas, Exploratory analysis of kinetic solubility measurements of a small molecule library, *Bioorganic & medicinal chemistry*, **2011**, *19*, 4127–4134.

[124] D. Klimoszek, M. Jeleń, B. Morak-Młodawska, M. Dołowy, Evaluation of the Lipophilicity of Angularly Condensed Diquino- and Quinonaphthothiazines as Potential Candidates for New Drugs, *Molecules*, **2024**, *29*, 1683.

[125] T. W. Johnson, R. A. Gallego, M. P. Edwards, Lipophilic Efficiency as an Important Metric in Drug Design, *Journal of medicinal chemistry*, **2018**, *61*, 6401–6420.

[126] J. D. Hughes, J. Blagg, D. A. Price, S. Bailey, G. A. Decrescenzo, R. V. Devraj, E. Ellsworth, Y. M. Fobian, M. E. Gibbs, R. W. Gilles et al., Physiochemical drug properties associated with in vivo toxicological outcomes, *Bioorganic & medicinal chemistry letters*, **2008**, *18*, 4872–4875.

[127] A. Andrés, M. Rosés, C. Ràfols, E. Bosch, S. Espinosa, V. Segarra, J. M. Huerta, Setup and validation of shake-flask procedures for the determination of partition coefficients (logD) from low drug amounts, *European journal of pharmaceutical sciences*, **2015**, *76*, 181–191.

[128] F. Lombardo, M. Y. Shalaeva, K. A. Tupper, F. Gao, ElogD(oct): a tool for lipophilicity determination in drug discovery. 2. Basic and neutral compounds, *Journal of medicinal chemistry*, **2001**, *44*, 2490–2497.

[129] M. Lapins, S. Arvidsson, S. Lampa, A. Berg, W. Schaal, J. Alvarsson, O. Spjuth, A confidence predictor for logD using conformal regression and a support-vector machine, *Journal of cheminformatics*, **2018**, *10*, 17.

[130] S. Sainas, M. Giorgis, P. Circosta, G. Poli, M. Alberti, A. Passoni, V. Gaidano, A. C. Pippione, N. Vitale, D. Bonanni et al., Targeting Acute Myelogenous Leukemia Using Potent Human Dihydroorotate Dehydrogenase Inhibitors Based on the 2-Hydroxypyrazolo1,5-apyridine Scaffold: SAR of the Aryloxyaryl Moiety, *Journal of medicinal chemistry*, **2022**, *65*, 12701–12724.

[131] W. Yang, M. Lipert, R. Nofsinger, Current screening, design, and delivery approaches to address low permeability of chemically synthesized modalities in drug discovery and early clinical development, *Drug discovery today*, **2023**, *28*, 103685.

[132] J. Wang, S. Skolnik, Permeability diagnosis model in drug discovery: a diagnostic tool to identify the most influencing properties for gastrointestinal permeability, *Current topics in medicinal chemistry*, **2013**, *13*, 1308–1316.

[133] J. L. Daniel Schmidt, Evaluation of the reproducibility of Parallel Artificial Membrane Permeation Assays (PAMPA), https://www.sigmaaldrich.com/DE/de/technical-documents/technical-article/research-and-disease-areas/pharmacology-and-drug-discovery-research/evaluation-of-the-reproducibility-of-pampa (Retrieved: 09.09.2025).

[134] J. Goscianska, A. Ejsmont, A. Olejnik, D. Ludowicz, A. Stasiłowicz, J. Cielecka-Piontek, Design of Paracetamol Delivery Systems Based on Functionalized Ordered Mesoporous Carbons, *Materials*, **2020**, *13*, 4151.

[135] X. Chen, A. Murawski, K. Patel, C. L. Crespi, P. V. Balimane, A novel design of artificial membrane for improving the PAMPA model, *Pharmaceutical research*, **2008**, *25*, 1511–1520.

[136] J. J. Milligan, S. Saha, A Nanoparticle's Journey to the Tumor: Strategies to Overcome First-Pass Metabolism and Their Limitations, *Cancers*, **2022**, *14*, 1741.

[137] R. Pignatello, M. Rudrapal, *Drug Metabolism and Pharmacokinetics*, IntechOpen, London, **2024**.

[138] G. L. Patrick, *An introduction to medicinal chemistry,* sixth edition, Oxford University Press, Oxford, **2017**.

[139] A. Talevi, P. A. Quiroga, *ADME Processes in Pharmaceutical Sciences*. *Dosage, Design, and Pharmacotherapy,* second edition, Springer, Cham, **2024**.

[140] F. P. Guengerich, Mechanisms of Cytochrome P450-Catalyzed Oxidations, *ACS catalysis*, **2018**, *8*, 10964–10976.

[141] S. J. Richardson, A. Bai, A. A. Kulkarni, M. F. Moghaddam, Efficiency in Drug Discovery: Liver S9 Fraction Assay As a Screen for Metabolic Stability, *Drug metabolism letters*, **2016**, *10*, 83–90.

[142] M. Ooka, C. Lynch, M. Xia, Application of In Vitro Metabolism Activation in High-Throughput Screening, *International journal of molecular sciences*, **2020**, *21*, 8182.

[143] Y. Shao, A. Schiwy, L. Glauch, L. Henneberger, M. König, M. Mühlenbrink, H. Xiao, B. Thalmann, R. Schlichting, H. Hollert et al., Optimization of a pre-metabolization procedure using rat liver S9 and cell-extracted S9 in the Ames fluctuation test, *The Science of the total environment*, **2020**, *749*, 141468.

[144] J. D. Manna, S. J. Richardson, M. F. Moghaddam, Implementation of A Novel Ultra Fast Metabolic Stability Analysis Method Using Exact Mass TOF-MS, *Bioanalysis*, **2017**, *9*, 359–368.

[145] G. C. Forti, M. Paolini, P. Hrelia, C. Corsi, G. L. Biagi, G. Bronzetti, NADPH-generating system: Influence on microsomal mono-oxygenase stability during incubation for the liver-microsomal assay with rat and mouse S9 fractions, *Mutation Research/Fundamental and Molecular Mechanisms of Mutagenesis*, **1984**, *129*, 291–297.

[146] J. Brendt, S. E. Crawford, M. Velki, H. Xiao, B. Thalmann, H. Hollert, A. Schiwy, Is a liver comparable to a liver? A comparison of different rat-derived S9-fractions with a biotechnological animal-free alternative in the Ames fluctuation assay, *The Science of the total environment*, **2021**, *759*, 143522.

[147] M. V. Krishna, K. Padmalatha, G. Madhavi, *In vitro* Metabolic Stability of Drugs and Applications of LC-MS in Metabolite Profiling. In: *Drug Metabolism*, IntechOpen, **2021**.

[148] M. B. Reddy, M. B. Bolger, G. Fraczkiewicz, L. Del Frari, L. Luo, V. Lukacova, A. Mitra, J. S. Macwan, J. M. Mullin, N. Parrott et al., PBPK Modeling as a Tool for Predicting and Understanding Intestinal Metabolism of Uridine 5'-Diphosphoglucuronosyltransferase Substrates, *Pharmaceutics*, **2021**, *13*, 1325.

[149] H. Munier-Lehmann, M. Lucas-Hourani, S. Guillou, O. Helynck, G. Zanghi, A. Noel, F. Tangy, P.-O. Vidalain, Y. L. Janin, Original 2-(3-alkoxy-1H-pyrazol-1-yl)pyrimidine derivatives as inhibitors of human dihydroorotate dehydrogenase (DHODH), *Journal of medicinal chemistry*, **2015**, *58*, 860–877.

[150] M. Nakahara, S. Watanabe, M. Sato, H. Okumura, M. Kawatani, H. Osada, K. Hara, H. Hashimoto, K. Watanabe, Structural and Functional Analyses of Inhibition of Human Dihydroorotate Dehydrogenase by Antiviral Furocoumavirin, *Biochemistry*, **2024**, *63*, 1241–1245.

[151] S. Yin, T. Kabashima, Q. Zhu, T. Shibata, M. Kai, Fluorescence assay of dihydroorotate dehydrogenase that may become a cancer biomarker, *Scientific reports*, **2017**, *7*, 40670.

[152] F. P. Guengerich, Mechanisms of Cytochrome P450-Catalyzed Oxidations, *ACS catalysis*, **2018**, *8*, 10964–10976.

[153] E. Henary, S. Casa, T. L. Dost, J. C. Sloop, M. Henary, The Role of Small Molecules Containing Fluorine Atoms in Medicine and Imaging Applications, *Pharmaceuticals (Basel, Switzerland)*, **2024**, *17*, 281.

[154] S. Sundriyal, Basic nitrogen (BaN): a 'privileged element' in medicinal chemistry, *Future medicinal chemistry*, **2024**, *16*, 2069–2071.

[155] A. S. Nair, A. K. Singh, A. Kumar, S. Kumar, S. Sukumaran, V. P. Koyiparambath, L. K. Pappachen, T. M. Rangarajan, H. Kim, B. Mathew, FDA-Approved Trifluoromethyl Group-Containing Drugs: A Review of 20 Years, *Processes*, **2022**, *10*, 2054.

[156] S. Christian, C. Merz, L. Evans, S. Gradl, H. Seidel, A. Friberg, A. Eheim, P. Lejeune, K. Brzezinka, K. Zimmermann et al., The novel dihydroorotate dehydrogenase (DHODH) inhibitor BAY 2402234 triggers differentiation and is effective in the treatment of myeloid malignancies, *Leukemia*, **2019**, *33*, 2403–2415.

[157] S. Kumari, A. V. Carmona, A. K. Tiwari, P. C. Trippier, Amide Bond Bioisosteres: Strategies, Synthesis, and Successes, *Journal of medicinal chemistry*, **2020**, *63*, 12290–12358.

[158] S. S. R. Thunuguntla, H. Subramanya, S. R. Kunnam, C. Bingi, R. Kusanur, M. Schwarz, M. Arlt, Dihydroorotate Dehydrogenase Inhibitors. Publication date: 14.04.2025. US 9,006,454 B2.

[159] Z.-S. Li, W.-X. Wang, J.-D. Yang, Y.-W. Wu, W. Zhang, Photoinduced and N-bromosuccinimide-mediated cyclization of 2-azido-N-phenylacetamides, *Organic letters*, **2013**, *15*, 3820–3823.

[160] D. Rijono, *Synthese und Optimierung von DHODH-Inhibitoren als potenzielle Wirkstoffe gegen Bunyaviren*, master thesis, Universität Hamburg, **2020**.

[161] M. Ebisawa, T. Suzuki, N. Haginoya, T. Hamada, T. Murata, K. Uoto, R. Murakami, T. Takata, Aminopyrazolone Derivative. Publication date: 20.04.2017. US 2017/0107207 A1.

[162] A. F. Abdel-Magid, K. G. Carson, B. D. Harris, C. A. Maryanoff, R. D. Shah, Reductive Amination of Aldehydes and Ketones with Sodium Triacetoxyborohydride. Studies on Direct and Indirect Reductive Amination Procedures, *Journal of Organic Chemistry*, **1996**, *61*, 3849–3862.

[163] J. Clayden, N. Greeves, S. Warren, *Organic Chemistry,* second edition, Oxford University Press, New York, **2012**.

[164] J. Chen, Y. Zhou, S. Wang, M. Guo, D. Yang, L. Jiao, Y. Jing, X. Qian, L. Liu, L. Bai et al., Indoloquinolone Compounds as Anaplastic Lymphoma Kinase (ALK) Inhibitors. Publication date: 03.09.2015. WO 2015/127629 Al.

[165] E. Sperotto, G. P. M. van Klink, G. van Koten, J. G. de Vries, The mechanism of the modified Ullmann reaction, *Dalton transactions (Cambridge, England : 2003)*, **2010**, *39*, 10338–10351.

[166] G. Evano, N. Blanchard, *Copper-Mediated Cross-Coupling Reactions,* first edition, John Wiley & Sons, Hoboken (New Jersey), **2013**.

[167] X. Ribas, I. Güell, Cu(I)/Cu(III) catalytic cycle involved in Ullmann-type cross-coupling reactions, *Pure and Applied Chemistry*, **2014**, *86*, 345–360.

[168] C. Sambiagio, S. P. Marsden, A. J. Blacker, P. C. McGowan, Copper catalysed Ullmann type chemistry: from mechanistic aspects to modern development, *Chemical Society Reviews*, **2014**, *43*, 3525.

[169] C. Deldaele, G. Evano, Room-Temperature Practical Copper-Catalyzed Amination of Aryl Iodides, *ChemCatChem*, **2016**, *8*, 1319–1328.

[170] A. Z. Halimehjnai, S. Hosseyni, H. Gholami, M. M. Hashemi, Boric Acid / Glycerol as an Efficient Catalyst for Synthesis of Thiomorpholine 1,1-Dioxide by Double Michael Addition Reaction in Water, *Synthetic Communications*, **2013**, *43*, 191–197.

[171] B. Wang, D. Chu, A. J. Bridges, Glucosylceramide Synthase Inhibitors for the Treatment of Diseases. Publication date: 26.03.2015. WO 2015/042397 A1.

[172] M. Bergström, G. Suresh, V. R. Naidu, C. R. Unelius, N -Iodosuccinimide (NIS) in Direct Aromatic Iodination, *Eur J Org Chem*, **2017**, *2017*, 3234–3239.

[173] J. J. Dressler, S. A. Miller, B. T. Meeuwsen, A. M. S. Riel, B. J. Dahl, Synthesis of dilactone bridged terphenyls with crankshaft architectures, *Tetrahedron*, **2015**, *71*, 283–292.

[174] C. Guardigli, R. liantonio, M. lorenza mele, P. metrangolo, G. resnati, T. pilati, Design and Synthesis of New Tectons for Halogen Bonding-driven Crystal Engineering, *Supramolecular Chemistry*, **2003**, *15*, 177–188.

[175] N. A. Senger, B. Bo, Q. Cheng, J. R. Keeffe, S. Gronert, W. Wu, The element effect revisited: factors determining leaving group ability in activated nucleophilic aromatic substitution reactions, *The Journal of organic chemistry*, **2012**, *77*, 9535–9540.

[176] S. Rohrbach, A. J. Smith, J. H. Pang, D. L. Poole, T. Tuttle, S. Chiba, J. A. Murphy, Concerted Nucleophilic Aromatic Substitution Reactions, *Angewandte Chemie (International ed. in English)*, **2019**, *58*, 16368–16388.

[177] L. A. Wall, W. J. Pummer, J. E. Fearn, J. M. Antonucci, Reactions of Polyfluorobenzenes With Nucleophilic Reagents, *Journal of research of the National Bureau of Standards. Section A, Physics and chemistry*, **1963**, *67A*, 481–497.

[178] M. Kobayashi, Y. Gotoh, M. Goto, Polymerizable Compound, Polymerizable Composition, and Liquid Crystal Display Element. Publication date: 02.03.2016. EP 2990424 A1.

[179] R. W. Holman, Strategic Applications of Named Reactions in Organic Synthesis: Background and Detailed Mechanisms (Kürti, László; Czakó, Barbara), *Journal of Chemical Education*, **2005**, *82*, 1780.

[180] R. Dorel, C. P. Grugel, A. M. Haydl, The Buchwald-Hartwig Amination After 25 Years, *Angewandte Chemie*, **2019**, *58*, 17118–17129.

[181] P. Blencowe, M. Charles, A. Cridland, T. Ekwuru, R. Heald, E. Macdonald, H. Mccarron, L. Rigoreau, Heterocyclic Substituted Ureas, for Use against Cancer. Publication date: 13.02.2020. WO 2020/030925 A1.

[182] R. Chinchilla, C. Najera, The Sonogashira reaction: a booming methodology in synthetic organic chemistry, *Chemical reviews*, **2007**, *107*, 874–922.

[183] G. Larson, Some Aspects of the Chemistry of Alkynylsilanes, *Synthesis*, **2018**, *50*, 2433–2462.

[184] T. Inouchi, T. Nakashima, M. Toba, T. Kawai, Preparation and acid-responsive photophysical properties of T-shaped π-conjugated molecules containing a benzimidazole junction, *Chemistry, an Asian journal*, **2011**, *6*, 3020–3027.

[185] Y. Lin, Q. Song, Cleavage of the Carbon–Carbon Triple Bonds of Arylacetylenes for the Synthesis of Arylnitriles without a Metal Catalyst, *Eur J Org Chem*, **2016**, *2016*, 3056–3059.

[186] Y. Yang, L. Cao, H. Gao, Y. Wu, Y. Wang, F. Fang, T. Lan, Z. Lou, Y. Rao, Discovery, Optimization, and Target Identification of Novel Potent Broad-Spectrum Antiviral Inhibitors, *Journal of medicinal chemistry*, **2019**, *62*, 4056–4073.

[187] M. Gong, Y. Yang, Y. Huang, T. Gan, Y. Wu, H. Gao, Q. Li, J. Nie, W. Huang, Y. Wang et al., Novel quinolone derivatives targeting human dihydroorotate dehydrogenase suppress Ebola virus infection in vitro, *Antiviral research*, **2021**, *194*, 105161.

[188] R. Xiong, L. Zhang, S. Li, Y. Sun, M. Ding, Y. Wang, Y. Zhao, Y. Wu, W. Shang, X. Jiang et al., Novel and potent inhibitors targeting DHODH are broad-spectrum antivirals against RNA viruses including newly-emerged coronavirus SARS-CoV-2, *Protein & cell*, **2020**, *11*, 723–739.

[189] S. Sainas, A. C. Pippione, E. Lupino, M. Giorgis, P. Circosta, V. Gaidano, P. Goyal, D. Bonanni, B. Rolando, A. Cignetti et al., Targeting Myeloid Differentiation Using Potent 2-Hydroxypyrazolo1,5- apyridine Scaffold-Based Human Dihydroorotate Dehydrogenase Inhibitors, *Journal of medicinal chemistry*, **2018**, *61*, 6034–6055.

[190] A. Luganini, G. Sibille, B. Mognetti, S. Sainas, A. C. Pippione, M. Giorgis, D. Boschi, M. L. Lolli, G. Gribaudo, Effective deploying of a novel DHODH inhibitor against herpes simplex type 1 and type 2 replication, *Antiviral research*, **2021**, *189*, 105057.

[191] F. Hahn, C. Wangen, S. Häge, A. S. Peter, G. Dobler, B. Hurst, J. Julander, J. Fuchs, Z. Ruzsics, K. Überla et al., IMU-838, a Developmental DHODH Inhibitor in Phase II for

Autoimmune Disease, Shows Anti-SARS-CoV-2 and Broad-Spectrum Antiviral Efficacy In Vitro, *Viruses*, **2020**, *12*, 1394.

[192] D. C. Schultz, R. M. Johnson, K. Ayyanathan, J. Miller, K. Whig, B. Kamalia, M. Dittmar, S. Weston, H. L. Hammond, C. Dillen et al., Pyrimidine inhibitors synergize with nucleoside analogues to block SARS-CoV-2, *Nature*, **2022**, *604*, 134–140.

[193] K. M. Stegmann, A. Dickmanns, N. Heinen, C. Blaurock, T. Karrasch, A. Breithaupt, R. Klopfleisch, N. Uhlig, V. Eberlein, L. Issmail et al., Inhibitors of dihydroorotate dehydrogenase cooperate with molnupiravir and N4-hydroxycytidine to suppress SARS-CoV-2 replication, *iScience*, **2022**, *25*, 104293.

[194] G. Sibille, A. Luganini, S. Sainas, D. Boschi, M. L. Lolli, G. Gribaudo, The Novel hDHODH Inhibitor MEDS433 Prevents Influenza Virus Replication by Blocking Pyrimidine Biosynthesis, *Viruses*, **2022**, *14*, 2281.

[195] L. Schrell, H. L. Fuchs, A. Dickmanns, D. Scheibner, J. Olejnik, A. J. Hume, W. Reineking, T. Störk, M. Müller, A. Graaf-Rau et al., Inhibitors of dihydroorotate dehydrogenase synergize with the broad antiviral activity of 4'-fluorouridine, *Antiviral research*, **2025**, *233*, 106046.

[196] X. Jia, D. Schols, C. Meier, Lipophilic Triphosphate Prodrugs of Various Nucleoside Analogues, *Journal of medicinal chemistry*, **2020**, *63*, 6991–7007.

[197] N. Matsuda, K. Hirano, T. Satoh, M. Miura, Copper-catalyzed amination of arylboronates with N,N-dialkylhydroxylamines, *Angewandte Chemie (International ed. in English)*, **2012**, *51*, 3642–3645.

[198] E. Watanabe, Y. Chen, O. May, S. V. Ley, A Practical Method for Continuous Production of sp3-Rich Compounds from (Hetero)Aryl Halides and Redox-Active Esters, *Chemistry*, **2020**, *26*, 186–191.

[199] M. H. Keylor, Z. L. Niemeyer, M. S. Sigman, K. L. Tan, Inverting Conventional Chemoselectivity in Pd-Catalyzed Amine Arylations with Multiply Halogenated Pyridines, *Journal of the American Chemical Society*, **2017**, *139*, 10613–10616.

Hazardous substance register

All hazardous substances, including those classified as CMR, are detailed in the tables below. The GHS pictograms, along with the H- and P-statements, have been sourced from the GESTIS, Sigma Aldrich, abcr, TCI and BLDpharm catalogs.

GHS-code legend:

GHS01 GHS02 GHS03 GHS04 GHS05 GHS06 GHS07 GHS08 GHS09

Substance	GHS-code	H-statements	P-statements
Acetic acid	02, 05	226, 314	280, 305+351+338, 310
Acetone	02, 07	225, 319, 336	210, 233, 240, 241, 242, 305+351+338
Acetonitrile	02, 07	225, 302+312+332	210, 280, 301+312, 303+361+353, 304+340+312, 305+351+338
Boric acid	08	360FD	201, 202, 280, 308+313, 405, 501
2‘-Bromoacetophenone	07	315, 319	264, 280, 302+352, 337+313, 362+354, 332+313
5-Bromo-1H-benz[d]-imidazole	07	302, 315, 319, 335	261, 305+351+338
1-Bromo-2-fluoro-4-iodobenzene	07	302	280, 305+351+338
4-Bromo-2-fluoro-1-iodobenzene	07	315, 319, 335	261, 305+351+338

5-Bromoindole	07	315, 319, 335	261, 305+351+338
1-Bromo-4-iodobenzene	07	315, 319	264, 280, 302+352, 305+351+338, 332+313, 337+313
1-Bromo-4-iodo-2-(trifluoromethyl)benzene	07	315, 319, 335	261, 305+351+338
5-Bromo-2-iodophenol	07	302, 315, 319, 335	261, 305, 338, 351
5-Bromo-2-iodopyridine	07	315, 319, 335	261, 264, 271, 280, 302+352, 305+351+338
1-Bromopropane	02, 07, 08	225, 315, 319, 335, 336, 351, 360FD, 373, 412, 420	210, 273, 303+361+353, 305+351+338, 308+313, 502
n-Butyllithium solution (1.6 M in hexanes)	02, 05, 07, 08, 09	225, 250, 260, 304, 314, 336, 361F, 411	210, 231+232, 280, 301+330+331, 303+361+353, 304+340+310, 305+351+338, 370+378
Caffeine	07	302	264, 270, 301+312, 501
Cesium carbonate	05, 08	318, 361F, 373	202, 260, 280, 305+351+338, 308+313, 405
Copper iodide	05, 07, 09	302, 315, 317, 318, 410	273, 280, 301+312+330, 302+353, 305+351+338+310
Dichloromethane	06, 07	315, 319, 336, 351	201, 302+352, 305+351+338, 308+313
2,6-Dichlorophenolindophenol sodium salt	07	302, 315, 319, 335	261, 280, 301+312 302+352, 305+351+338
Diethyl ether	02, 07	224, 302, 336	210, 233, 240, 241, 301+312, 403+233

4,4-Difluoropiperidine hydrochloride	07	319	264, 280, 305+351+338, 337+313
L-Dihydroorotic acid	07	315, 319, 335	261, 264, 271,280, 302+352, 305+351+338
1,4-Diiodobenzene	07	315, 319, 335	261, 305+351+338
Dimethylformamide	02, 07, 08	226, 312+332, 319, 360D	201, 210, 302+353, 305+351+338, 308+313
Dimethyl sulfoxide	Not a hazardous substance or mixture according to CLP (Regulation (EC) 1272/2008)		
Divinyl sulfone	05, 06	300+310, 315, 318, 335, 412	262, 264, 273, 280, 301+310, 305+351+338
7-Ethoxycoumarin	Not a hazardous substance or mixture according to CLP (Regulation (EC) 1272/2008)		
Ethyl acetate	02, 07	225, 319, 336	210, 233, 240, 241, 242, 305+351+338
Ethyl iodide	02, 07, 08	226, 302, 315, 317, 319, 334, 335, 341	210, 280, 301+312, 303+361+353, 305+351+338, 308+313
3-Fluoro-4-iodoanaline	07	302, 315, 319, 335	261, 305+351+338
Glycerol	Not a hazardous substance according to CLP (Regulation (EC) 1272/2008)		
4-Iodoaniline	07	302, 315, 319, 335	261, 264, 271, 301+312, 302+352, 305+351+338
4-Iodo-3(trifluoromethyl)aniline	07	302, 312, 332, 315, 319, 335	261, 280, 305+351+338, 304+340, 405, 501
N-Iodosuccinimide	07, 08, 09	315, 317, 319, 341, 410	202, 273, 280, 302+352, 305+351+338, 308+313
Isopropyl iodide	02, 07	226, 315, 319, 335	210, 233, 240, 241, 303+361+353, 305+351+338

Methanol	02, 06, 08	225, 301+311+331, 370	210, 233, 280, 301+310, 303+361+353, 304+340+311
Methyl-2-amino-5-iodobenzoate	07	315, 319	264, 280, 302+352+332+362+364, 305+351+338+337+313
Methyl-2,3-diamino-5-bromobenzoate	07	302, 315, 319, 335	261, 305+351+338
Methyl iodide	02, 06, 08, 09	226, 301+331, 312, 315, 319, 335, 351, 410	210, 273, 280, 301+310, 303+361+353, 304+340+311
1-Methylpiperazine	02, 05, 07	226, 312+332, 314	210, 280, 301+330+331, 302+352, 304+340, 305+351+338+310
Morpholine	02, 05, 06, 08	226, 302, 311, 314, 331, 361FD	210, 280, 301+312, 303+361+353, 304+340+310, 305+351+338
1-Octanol	07	319, 412	264, 273, 280, 305+351+338, 337+313, 501
2,3,4,5,6-Pentafluoro-iodobenzene	07	315, 319, 335	261, 264, 271, 280, 302+352, 305+351+338
3-Phenylpropionic acid	Not a hazardous substance or mixture according to CLP (Regulation (EC) 1272/2008)		
Phosphate buffered saline	Not a hazardous substance or mixture according to CLP (Regulation (EC) 1272/2008)		
Piperidine	02, 05, 06	225, 302, 311+331, 314	210, 280, 301+312, 303+361+353, 304+340+310, 305+351+338

Potassium carbonate	07	315, 319, 335	261, 264, 271, 280, 302+352, 305+351+338
Potassium hydroxide	05, 07	290, 302, 314	234, 260, 280, 301+312, 303+361+353, 305+351+338
L-Proline	Not a hazardous substance or mixture according to CLP (Regulation (EC) 1272/2008)		
Propionaldehyde	02, 05, 07	225, 302+332, 315, 318, 335	210, 280, 301+312, 303+361+353, 304+340+312. 305+351+338, 403+235
Propionyl chloride	02, 05, 06	225, 302, 331, 314	210, 240, 280, 301+330+331, 305+351+338, 310, 402+404
S9 from Liver, pooled	Not a hazardous substance or mixture according to CLP (Regulation (EC) 1272/2008)		
Sodium hydroxide	05	290, 314	234, 260, 280, 303+361+353, 304+340+310, 305+351+338
Sodium sulfate	Not a hazardous substance or mixture according to CLP (Regulation (EC) 1272/2008)		
Sodium tert-butoxide	05, 07	228, 251, 314	210, 280, 303+361+353, 305+351+338, 310
Sodium triacetoxyborohydride	02, 05, 07, 08	228, 260, 302, 318, 360FD	210, 231+232, 280, 301+312, 305+351+338, 308+313
Sulfuric acid	05	290, 314	234, 280, 303+361+353, 304+340+310, 305+351+338, 363

Tetrahydrofuran	02, 07, 08	225, 302, 319, 335, 336, 351	210, 280, 301+312+330, 305+351+338, 370+378, 403+235
Tetrahydro-4*H*-pyran-4-one	02	226	210
Tetrakis(triphenylphosphine)palladium(0)	07	302	264, 270, 301+312, 501
Thiomorpholine	05	314	280, 301+330+331, 303+361+353, 304+340+310, 305+351+338+310, 501
Thiomorpholine-1,1-dioxide	07	302, 315, 319, 332, 335	261, 280, 305+351+338
Toluene	02, 07, 08	225, 315, 361D, 336, 373, 304, 412	202, 210, 273, 301+310, 303+361+353, 331
Triethylamine	02, 05, 06	225, 301+311+331, 314, 335	210, 280, 301+312, 303+361+353, 304+340+310, 305+351+338+310
Triethylsilane	02, 07	225, 315, 319, 335	210, 233, 240, 241, 393+361+353, 305+351+338
Trifluoroacetic acid	05, 07	314, 332, 412	261, 273, 280, 303+361+353, 304+340+310, 305+351+338
2,2,2-Trifluoroethanol	02, 05, 06, 08	226, 301+331, 318, 360F, 373	202, 210, 280, 301+310, 304+340+311, 305+351+338
3,3,3-Trifluoropropionaldehyde	02	225, 315, 319	210, 240, 241, 242, 243, 261, 264, 271, 280, 302+352, 303+361+353,

			304+340, 305+351+338, 312, 332+313, 337+313, 362, 370+378, 403+233, 403+235, 405, 501
Trimethyl orthoformate	02, 07	225, 319	210, 233, 240, 241, 242, 305+351+338
Trimethylsilylacetylene	02, 07	225, 315, 319	210, 233, 240, 241, 303+361+353, 305+351+338
Tris(dibenzylideneacetone)dipalladium(0)	07, 09	317, 411	261, 272, 273, 280, 302+352, 333+313
Triton™ X-100	05, 07, 09	302, 315, 318, 410	264, 273, 280, 301+312, 302+352, 305+351+338
Trizma® hydrochloride	Not a hazardous substance or mixture according to CLP (Regulation (EC) 1272/2008)		
Ubiquinone-1	Not a hazardous substance or mixture according to CLP (Regulation (EC) 1272/2008)		
Xantphos	07	315, 319, 335	261, 264, 271, 280, 302+352, 305+351+338

Acknowledgements

Mein Dank gilt…

Herrn Prof. Dr. Chris Meier für die interessante und zugleich anspruchsvolle Themenstellung, die wertvolle Unterstützung während der gesamten Promotionszeit sowie das entgegengebrachte Vertrauen und den gewährten Freiraum bei der Bearbeitung des Themas.

Herrn Prof. Dr. Ralph Holl für die freundliche Übernahme des Zweitgutachtens, sowie Frau Prof. Dr. Bianka Siewert und Dr. Thomas Hackl für die Teilnahme am Disputationskolloquium.

Allen Mitarbeitenden des Fachbereichs Chemie der Universität Hamburg, die auf unterschiedliche Weise zum Gelingen meiner Arbeit beigetragen haben, allen voran den Teams der NMR- und MS-Abteilungen unter der Leitung von Dr. Thomas Hackl bzw. Dr. Jennifer Menzel (zuvor Leitung durch Dr. Maria Riedner). Ein besonderer Dank gilt auch Ali Yilmaz und Amir R. M. Zadeh, die zu einem reibungslosen Arbeiten am Fachbereich beitragen, sowie R. Wieczorek für die lustigen und aufmunternden Sprüche beim Vorbeigehen am Pförtnerhäuschen.

Prof. Dr. Johan Neyts, Dr. Lisa Oestereich, Prof. Dr. Ralf Bartenschlager und Dr. Heeyoung Kim, Dr. Thomas Hoenen, und Dr. Allison Groseth sowie Dr. Beate Kümmerer für die Kollaborationen zur antiviralen Testung meiner Zielverbindungen.

Dem ehemaligen DHODH Team, bestehend aus Matze, Kathi und Conny die mit ihrer hervorragenden Vorarbeit die Grundlage für meine Forschung geschaffen haben. Conny danke ich zudem für die geduldige Einführung und Unterstützung bei den für meine Forschung wichtigen Testverfahren.

Meinen Praktikanten Federica, Max, Elmar, Lucas, Jan, Duc und Philipp für die experimentelle Unterstützung.

Den momentanen aber auch einigen ehemaligen Mitgliedern des AK Meier. Die angenehme und positive Atmosphäre hat das Arbeiten hier echt zu einer tollen Zeit gemacht. Besonders möchte ich mich bei Matze, Simon, Stefan, Bene und Vani bedanken, die mich sowohl fachlich als auch emotional unterstützt haben. Mit euch habe ich die witzigsten Momente erlebt, die mir immer in Erinnerung bleiben werden. Simon danke ich zudem für die gründliche Durchsicht meiner Arbeit und die hilfreichen Korrekturen.

Meiner WG und der Gäng! Ihr habt mir abseits der Chemie eine großartige Zeit beschert. Mit euch konnte ich den Stress während des Studiums vergessen und immer wieder neue Energie tanken. Auch die Musik von Bizzarro Universe hat mir immer wieder neuen Antrieb gegeben. Ich freue mich auf viele weitere unvergessliche Momente. Ein besonderer Dank gilt Olaf

für seine liebevolle Unterstützung während der finalen Schreibphase sowie für die Unterhaltung durch seine humorvolle Art.

Meiner Familie für die bedingungslose Unterstützung während meines gesamten Chemiestudiums.

Declaration on Oath

Hiermit versichere ich an Eides statt, die vorliegende Dissertationsschrift selbst verfasst und keine anderen als die angegebenen Quellen und Hilfsmittel benutzt zu haben. Sofern im Zuge der Erstellung der vorliegenden Dissertationsschrift generative Künstliche Intelligenz (gKI) basierte elektronische Hilfsmittel verwendet wurden, versichere ich, dass meine eigene Leistung im Vordergrund stand und dass eine vollständige Dokumentation aller verwendeten Hilfsmittel gemäß der Guten wissenschaftlichen Praxis vorliegt. Ich trage die Verantwortung für eventuell durch die gKI generierte fehlerhafte oder verzerrte Inhalte, fehlerhafte Referenzen, Verstöße gegen das Datenschutz- und Urheberrecht oder Plagiate.

Hamburg, 12.02.2026

Ort, Datum

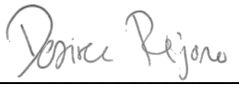

Unterschrift